

การผลิตแก๊สไฮโดรเจนจากกระบวนการรีฟอร์มมิงของกลีเซอรอลในน้ำวิกฤตยิ่งยวด

นายธีรศักดิ์ ไพโรจน์พิริยะกุล

วิทยานิพนธ์นี้เป็นส่วนหนึ่งของการศึกษาตามหลักสูตรปริญญาวิศวกรรมศาสตรดุษฎีบัณฑิต

สาขาวิชาวิศวกรรมเคมี ภาควิชาวิศวกรรมเคมี

คณะวิศวกรรมศาสตร์ จุฬาลงกรณ์มหาวิทยาลัย

ปีการศึกษา 2554

ลิขสิทธิ์ของจุฬาลงกรณ์มหาวิทยาลัย

บทคัดย่อและแฟ้มข้อมูลฉบับเต็มของวิทยานิพนธ์ตั้งแต่ปีการศึกษา 2554 ที่ให้บริการในคลังปัญญาจุฬาฯ (CUIR)

เป็นแฟ้มข้อมูลของนิสิตเจ้าของวิทยานิพนธ์ที่ส่งผ่านทางบัณฑิตวิทยาลัย

The abstract and full text of theses from the academic year 2011 in Chulalongkorn University Intellectual Repository (CUIR)

are the thesis authors' files submitted through the Graduate School.

HYDROGEN PRODUCTION FROM REFORMING OF GLYCEROL  
IN SUPERCRITICAL WATER

Mr. Thirasak Pairojpiriyakul

A Dissertation Submitted in Partial Fulfillment of the Requirements  
for the Degree of Doctor of Engineering Program in Chemical Engineering

Department of Chemical Engineering

Faculty of Engineering

Chulalongkorn University

Academic Year 2011

Copyright of Chulalongkorn University

Thesis Title                                   HYDROGEN PRODUCTION FROM REFORMING OF  
  GLYCEROL IN SUPERCRITICAL WATER  
By   Mr. Thirasak Pairojpiriyakul  
Field of Study                                 Chemical Engineering  
Thesis Advisor                                Professor Suttichai Assabumrungrat, Ph.D.

---

Accepted by the Faculty of Engineering, Chulalongkorn University in Partial  
Fulfillment of the Requirements for the Doctoral Degree

.....Dean of the Faculty of Engineering  
(Associate Professor Boonsom Lerdkhirunwong, Dr.Ing.)

THESIS COMMITTEE

..... Chairman  
(Associate Professor Muenduen Phisalaphong, Ph.D.)

..... Thesis Advisor  
(Professor Suttichai Assabumrungrat, Ph.D.)

..... Examiner  
(Associate Professor ML Supakanok Thongyai, Ph.D.)

..... Examiner  
(Associate Professor Bunjerd Jongsomjit, Ph.D.)

..... Examiner  
(Assistant Professor Soorathep Khewhom, Ph.D.)

..... External Examiner  
(Assistant Professor Waraporn Tanakulrungsank, D.Eng)

ธีรศักดิ์ ไพโรจน์พิริยะกุล : การผลิตแก๊สไฮโดรเจนจากกระบวนการรีฟอร์มมิงของกลีเซอรอลในน้ำวิกฤตยิ่งยวด (HYDROGEN PRODUCTION FROM REFORMING OF GLYCEROL IN SUPERCRITICAL WATER) อ.ที่ปรึกษาวิทยานิพนธ์หลัก : ศ.ดร.สุทธิชัย อัสสะบำรุงรัตน์, 278 หน้า.

งานวิจัยนี้ศึกษาเทคโนโลยีการรีฟอร์มมิงของกลีเซอรอล สำหรับการผลิตแก๊สไฮโดรเจน ซึ่งแบ่งออกเป็น 2 ส่วน คือ 1) การวิเคราะห์ทางอุณหพลศาสตร์ ภายใต้การรีฟอร์มมิงในเฟสแก๊สโดยมีค่าพลังงานความร้อนเป็นศูนย์ ( $Q=0$ ) และ การรีฟอร์มมิงในน้ำวิกฤตยิ่งยวด 2) การทดลองภายใต้การรีฟอร์มมิงในน้ำวิกฤตยิ่งยวดในเตาปฏิริยาอินคอบเนล (Inconel) 625 ทั้งแบบที่ใช้และไม่ใช้ตัวเร่งปฏิริยา การวิเคราะห์ทางอุณหพลศาสตร์ตามสมการของกิบส์สามารถบ่งบอกสถานะที่  $Q=0$  ได้ เมื่อเปลี่ยนค่าอัตราส่วนของน้ำต่อกลีเซอรอล ( $WGR$ ) ออกซิเจนต่อกลีเซอรอล ( $OGR$ ) และอุณหภูมิของระบบ ในระดับรีฟอร์มเมอร์พบว่าปริมาณ  $OGR$  เพียงเล็กน้อยสามารถเกิดสถานะดังกล่าวได้ อย่างไรก็ตาม  $OGR$  ที่มากขึ้นสัมพันธ์กับการให้พลังงานความร้อนกับสารตั้งต้นในการพิจารณาทั้งระบบ การศึกษารูปแบบการป้อนอากาศในการพิจารณาทั้งระบบพบว่าการป้อนแบบรวมมีข้อดีในด้านขยับยั้งการเกิดคาร์บอน ส่วนการป้อนแบบแยกจะให้ผลดีกับค่าสัดส่วนโมลของแก๊สไฮโดรเจน ซึ่งปราศจากแก๊สไนโตรเจนและคาร์บอนไดออกไซด์ในสายผลิตภัณฑ์ การใช้แก๊สออกซิเจนแทนอากาศในระบบแบบรวมสามารถเพิ่มสัดส่วนโมลและผลได้ของแก๊สไฮโดรเจนได้ดี อีกทั้งการใช้ประโยชน์จากสายผลิตภัณฑ์หลังการเผาไหม้มาให้ความร้อนในระบบการป้อนแบบรวม จะช่วยเพิ่มผลได้ของแก๊สไฮโดรเจนจากการลดปริมาณความต้องการเชื้อเพลิง ในระบบการรีฟอร์มมิงในน้ำวิกฤตยิ่งยวด พบว่า อุณหภูมิสูง ความดันต่ำ และความเข้มข้นของกลีเซอรอลป้อนต่ำ จะช่วยส่งเสริมการผลิตแก๊สไฮโดรเจน ส่วนแก๊สคาร์บอนมอนอกไซด์จะถูกขยับยั้งโดยตลอดเนื่องจากความดันของระบบมีค่าสูง (สัดส่วนโมล < 0.01) และองค์ประกอบของผลิตภัณฑ์เปลี่ยนแปลงเพียงเล็กน้อยที่อุณหภูมิมากกว่า 1048 เคลวิน ในส่วนการทดลองภายใต้สภาวะน้ำวิกฤตยิ่งยวด เริ่มจากการใช้เตาปฏิริยาอินคอบเนล 625 แบบไม่ใช้ตัวเร่งปฏิริยา พบว่าค่าการเปลี่ยนแปลงของกลีเซอรอลและผลได้ของแก๊สไฮโดรเจนเพิ่มขึ้นตามการเพิ่มขึ้นของอุณหภูมิ อย่างไรก็ตาม ปัญหาการเกิดคาร์บอนถูกพบเมื่อใช้อัตราการป้อนแบบต่ำและปานกลางที่อุณหภูมิสูง ความเข้มข้นกลีเซอรอลในสายป้อนที่ต่ำลงจะส่งเสริมการผลิตแก๊สไฮโดรเจนโดยปราศจากการเกิดคาร์บอน การรีฟอร์มมิงโดยใช้ตัวเร่งปฏิริยา โลหะโคบอลต์ (Co) และนิกเกิล (Ni) บนตัวรองรับ แลนทานัมออกไซด์ ( $La_2O_3$ ) แกมมา-อะลูมินา ( $\gamma-Al_2O_3$ ) แอลฟา-อะลูมินา ( $\alpha-Al_2O_3$ ) เซอร์โคเนีย ( $ZrO_2$ ) และ ยิเทรียสเดออบิไลต์ เซอร์โคเนีย (YSZ) ถูกเลือกมาใช้ในการศึกษาครั้งนี้ ซึ่งพบว่า Co/YSZ และ Ni/ $La_2O_3$  เป็นตัวแทนของตัวเร่งปฏิริยาที่ดี เมื่อพิจารณาค่าการเปลี่ยนแปลงกลีเซอรอล ผลได้ของแก๊สไฮโดรเจน และขยับยั้งการเกิดคาร์บอน ที่อุณหภูมิ 773 และ 798 เคลวิน กับ 10 และ 15 เปอร์เซ็นต์โดยน้ำหนักของโลหะโคบอลต์และนิกเกิลให้ประสิทธิภาพที่ดีที่สุด ตามลำดับ

ภาควิชา..... วิศวกรรมเคมี.....ลายมือชื่อนิสิต.....

สาขาวิชา..... วิศวกรรมเคมี.....ลายมือชื่อ อ. ที่ปรึกษาวิทยานิพนธ์หลัก.....

ปีการศึกษา..... 2554.....

## 5071811721 : MAJOR CHEMICAL ENGINEERING

KEYWORDS : GLYCEROL REFORMING / HYDROGEN PRODUCTION / THERMODYNAMIC ANALYSIS / THERMAL NEUTRAL / SUPERCRITICAL WATER

THIRASAK PAIROJPIRIYAKUL : HYDROGEN PRODUCTION FROM REFORMING OF GLYCEROL IN SUPERCRITICAL WATER.

ADVISOR : PROF. SUTTICHAJ ASSABUMRUNGRAT, Ph.D., 278 pp.

This dissertation investigates different glycerol reforming technologies for hydrogen production. The studies are divided into two parts including i) thermodynamic analysis under thermal neutral gas phase reforming and supercritical water reforming conditions, and ii) experimental studies under supercritical water reforming condition in an Inconel 625 reactor with and without catalysts. Thermodynamic analysis by Gibbs minimization indicates that the thermal neutral condition can be achieved when water to glycerol ratio (*WGR*), oxygen to glycerol ratio (*OGR*), and operating temperature are carefully selected. The reformer level shows that only a small amount of *OGR* is required in the operation. Much higher *OGR* is required to provide sufficient energy especially for the feed preheating in the system level. Considering two modes of air feeding in the *System* level, the *Single-feed* mode is a superior mode in term of suppressing carbon formation - no carbon formation is observed when operating at temperature above 900 K. The *Split-feed* mode offers higher H<sub>2</sub> mole fraction in the product gas because N<sub>2</sub> from air and part of CO<sub>2</sub> are not present in the gas product in the *Split-feed* mode unlike in the *Single-feed* mode. Use of pure O<sub>2</sub> in the *Single-feed* mode can increase the H<sub>2</sub> mole fraction in the product and H<sub>2</sub> yield. In addition, using the afterburner products stream to supply heat is beneficial to increase the H<sub>2</sub> yield in the *Split-feed* mode as it decreases the fuel requirement (glycerol and air). Thermodynamic calculations of the supercritical water reforming indicates that higher operating temperature, lower pressure, and lower glycerol feed concentration promote hydrogen production. CO is almost inhibited at high pressure, achieving less than 0.01 of mole fraction. Above 1048 K, only slight change of components is found by increasing of operating temperature. The experimental results in the empty Inconel 625 reactor show that conversion of glycerol and hydrogen yield increases when increasing the operating temperature. However, carbon formation is found as a serious problem for low and medium feed rates at high operating temperatures. Lower feed glycerol concentration supports the hydrogen production without carbon formation. For the catalytic supercritical water reforming, cobalt and nickel metals with the La<sub>2</sub>O<sub>3</sub>,  $\gamma$ -Al<sub>2</sub>O<sub>3</sub>,  $\alpha$ -Al<sub>2</sub>O<sub>3</sub>, ZrO<sub>2</sub>, and YSZ supports are chosen. Co/YSZ and Ni/La<sub>2</sub>O<sub>3</sub> catalysts are found to be suitable catalysts in terms of glycerol conversion, hydrogen yield, and carbon formation at 773 and 798 K, respectively. The metal loading is an important parameter to enhance the hydrogen production. The optimum cobalt and nickel loadings are 10 and 15 wt.%, respectively.

Department : ...Chemical Engineering.. Student's Signature .....

Field of Study : Chemical Engineering.. Advisor's Signature .....

Academic Year .....2011.....

## ACKNOWLEDGEMENTS

First of all, I would like to express my highly gratitude to my thesis advisor, Professor Suttichai Assabumrungrat for his guidance, encouragement, kindness, and inspiration during my thesis study and life attitude in non-thesis area. Good experiences from working with him are the great advantages which I can apply and use them in the near future. I also would like to acknowledge Professor Eric Croiset for his kind assistance and encouragement as he allowed me to use his equipments to run the supercritical water conditions in Canada for one year and four months.

As the publication requirement, I would like to thank Assistant Professor Worapon Kiatkittipong, Assistant Professor Amornchai Arpornwichanop, Assistant Professor Apinan Soottitantawat, Associate Professor Navadol Laosiripojana, and Assistant Professor Wisitsree Wiyaratn for their cooperation in successfully published papers. Moreover, I also would like to thank to my members of thesis committee, Associate Professor Muenduen Phisalaphong, Associate Professor ML Supakanok Thongyai, Associate Professor Bunjerd Jongsomjit, Assistant Professor Soorathep Khewhom, and Assistant Professor Waraporn Tanakulrungsan for useful comments.

I would like to acknowledge Thailand Research Fund (TRF) especially the Royal Golden Jubilee PhD Program for financial supports and offering me an opportunity to study abroad. I had learnt so many things during one year and four months such as practicing English language skills, living in different culture. Another one was the Higher Education Research Promotion and National Research University Project of Thailand, Office of the Higher Education Commission (EN278A).

I would like to give special thanks to my senior friend in Canada, Tuan Amran Tuan Abdullah for his helps especially when problems happened with the equipments as same as an analytical chemist, Ralph Dickout, and a technician, Bert Habicher.

Finally, I would like to thank my beloved parent including mom, dad, and younger sister. They always work hard for me, give me many convenient things, and support me when I faced the problem. I can say that I could not achieve my degree on time without their encouragements.

# CONTENTS

	PAGE
ABSTRACT (THAI).....	iv
ABSTRACT (ENGLISH).....	v
ACKNOWLEDGEMENTS.....	vi
CONTENTS.....	vii
LIST OF TABLES.....	xiv
LIST OF FIGURES.....	xvii
NOMENCLATURES.....	xxvii
CHAPTER	
I INTRODUCTION.....	1
1.1 Introduction .....	1
1.2 Objectives.....	4
1.3 Scope of works.....	5
1.4 Dissertation overviews.....	5
II THEORY.....	8
2.1 Glycerol.....	8
2.1.1 Properties.....	8
2.1.2 Applications.....	8
2.1.3 Crude glycerol.....	13
2.2 Reactions of glycerol conversion.....	16
2.2.1 Reactions to produce gas products.....	16
2.2.2 Reactions to produce solid product.....	18
2.2.3 Reactions to produce liquid products.....	18
2.3 Thermodynamic analysis.....	20
2.4 Supercritical water.....	24

CHAPTER	PAGE
III LITERATURE REVIEWS.....	28
3.1 Steam reforming.....	28
3.2 Partial oxidation and autothermal reforming.....	30
3.3 Reforming in supercritical water.....	33
3.4 Glycerol reforming catalyst development and operating parameters.....	46
3.4.1 Steam reforming.....	46
3.4.2 Aqueous phase reforming.....	49
3.4.3 Autothermal reforming.....	50
3.4.4 Supercritical water reforming.....	51
3.5 Mechanism pathways in glycerol reforming.....	53
IV EXPERIMENTAL.....	59
4.1 Material and chemicals.....	59
4.2 Catalyst preparation.....	60
4.3 Catalyst characterization technique.....	60
4.3.1 X-ray Diffraction (XRD).....	60
4.3.2 N <sub>2</sub> physisorption (BET surface area).....	61
4.3.3 Thermal Gravimetric Analysis (TGA).....	61
4.3.4 Scanning Electron Microscope (SEM).....	61
4.3.5 Transmission Electron Microscopy (TEM).....	61
4.4 Experimental setup.....	61
4.4.1 Process diagram.....	62
4.4.2 Equipment detail.....	62
4.4.2.1 High pressure pump (P-1).....	62
4.4.2.2 Syringe pump (P-2).....	64
4.4.2.3 Preheater (H-1).....	64
4.4.2.4 Reactor (R-1).....	64
4.4.2.5 Cooling unit (H-2).....	66



CHAPTER	PAGE
4.4.2.6	Main mass flow controller and mass flow controllers..... 66
4.4.2.7	Back pressure regulator (BPR-1)..... 67
4.4.2.8	Gas-liquid separator (GLS-1)..... 67
4.4.2.9	Gas chromatography..... 67
4.4.2.9.1	Gas analysis (GC-1)..... 67
4.4.2.9.2	Liquid analysis (GC-2)..... 68
V	THERMODYNAMIC ANALYSIS OF HYDROGEN PRODUCTION FROM GLYCEROL AT ENERGY-SELF-SUFFICIENT CONDITIONS..... 72
5.1	Introduction..... 72
5.2	Boundary for calculation..... 73
5.3	Results and discussion..... 75
5.3.1	Hydrogen production from glycerol under isothermal operation..... 75
5.3.1.1	Yield of hydrogen..... 75
5.3.1.2	Carbon formation..... 78
5.3.1.3	Net heat energy..... 79
5.3.2	Hydrogen production from glycerol under energy self-sufficient condition..... 81
5.3.3	Maximum hydrogen production..... 84
5.4	Conclusion..... 86
VI	EFFECT OF MODE OF OPERATION ON HYDROGEN PRODUCTION FROM GLYCEROL AT THERMAL NEUTRAL CONDITIONS: THERMODYNAMIC ANALYSIS..... 87
6.1	Introduction..... 87
6.2	Boundary for calculation..... 89
6.3	Results and discussion..... 92

CHAPTER	PAGE
6.3.1	Effect of operating conditions on the energy requirement..... 92
6.3.2	Effect of operating conditions at the thermal neutral conditions..... 99
6.3.2.1	Carbon formation..... 99
6.3.2.2	Hydrogen production..... 103
6.3.2.2.1	Hydrogen yield..... 103
6.3.2.2.2	Hydrogen mole fraction..... 108
6.3.2.3	By-products..... 110
6.3.3	Effect of oxidizing agent at thermal neutral conditions... 113
6.3.4	Effect of using afterburner products as heat supply..... 116
6.4	Conclusion..... 119
VII	HYDROGEN PRODUCTION FROM GLYCEROL REFORMING IN SUPERCRITICAL WATER: THERMODYNAMIC ANALYSIS..... 120
7.1	Equation of state review..... 120
7.1.1	Soave-Redlich-Kwong (SRK) EOS..... 120
7.1.2	Peng-Robinson (PENG-ROB) EOS..... 121
7.1.3	Others..... 121
7.2	Thermodynamic analysis conditions..... 122
7.3	Results and discussion..... 124
7.3.1	Effect of operating temperature..... 124
7.3.2	Effect of pressure..... 127
7.3.3	Effect of feed glycerol concentration..... 128
7.4	Conclusion..... 130
VIII	HYDROGEN PRODUCTION FROM SUPERCRITICAL WATER REFORMING OF GLYCEROL IN EMPTY INCONEL 625 REACTOR..... 132
8.1	Introduction..... 132

CHAPTER	PAGE
8.2	Material and methods..... 134
8.3	Results and discussion..... 135
8.3.1	Effect of feed rate and operating temperature..... 135
8.3.2	Effect of feed glycerol concentration..... 148
8.3.3	Comparison between “Conventional steam reforming” and “Supercritical water reforming”..... 154
8.4	Conclusion..... 156
IX	HYDROGEN PRODUCTION FROM CATALYTIC SUPERCRITI- CAL WATER REFORMING OF GLYCEROL WITH COBALT BASED CATALYSTS..... 158
9.1	Introduction..... 158
9.2	Results and discussion..... 162
9.2.1	Effect of support and operating temperature..... 163
9.2.2	Effect of feed rate..... 178
9.2.3	Effect of metal loading..... 181
9.3	Conclusion..... 185
X	HYDROGEN PRODUCTION FROM CATALYTIC SUPERCRITI- CAL WATER REFORMING OF GLYCEROL WITH NICKEL BASED CATALYSTS..... 186
10.1	Introduction..... 186
10.2	Results and discussion..... 187
10.2.1	Effect of support and operating temperature..... 187
10.2.2	Effect of feed rate..... 199
10.2.3	Effect of metal loading..... 201
10.2.4	Effect of feed glycerol concentration..... 208
10.3	Conclusion..... 215
XI	CONCLUSION AND RECOMMENDATIONS..... 216
11.1	Conclusion..... 216

CHAPTER	PAGE
11.1.1 Comparison of all processes.....	216
11.1.2 Selection of the suitable catalyst.....	222
11.2 Recommendation for future works.....	222
REFERENCES.....	224
APPENDICES.....	244
APPENDIX A GAS CHROMATROGRAPHY CALIBRATION CURVES.....	245
A.1 Gas calibration curves for gas chromatography (GC, Varian CP-3800).....	245
A.2 Liquid calibration curves for gas chromatography (GC, Agilent 6890).....	251
APPENDIX B MASS FLOW CONTROLLER VS GAS FLOW RATE.....	261
B.1 UFC-1200A (range: 12 SCCM).....	261
B.2 UFC-1100A (range: 125 SCCM).....	261
APPENDIX C CALCULATION FOR CATALYST PREPARA- TION.....	264
C.1 The calculation for the preparation of cobalt based catalyst.....	264
C.2 The calculation for the preparation of nickel based catalyst.....	265
APPENDIX D THERMAL GRAVIMETRIC ANALYSIS DATA.....	266
APPENDIX E SCANNING ELECTRON MICROSCOPE DATA.....	268
APPENDIX F TRANSMISSION ELECTRON MICROSCOPY DATA.....	270

APPENDICES	PAGE
APPENDIX G SUPERCRITICAL WATER OPERATING PROCEDURE.....	272
G.1 Loading the Reactor.....	272
G.2 Removing and Opening the reactor.....	273
G.3 The experiment procedure.....	274
G.4 Shutdown procedure.....	275
APPENDIX H LIST OF PUBLICATIONS.....	276
H.1 International publications.....	276
H.2 International conferences.....	276
H.3 National conferences.....	277
VITAE.....	278

# LIST OF TABLES

TABLE	PAGE
2.1 Physical properties of Glycerol (Perry and Green, seventh edition, 1997; <a href="http://en.wikipedia.org/wiki/Glycerol">http://en.wikipedia.org/wiki/Glycerol</a> ).....	9
2.2 List of compounds which can be produced from glycerol (Johnson et al., 2007).....	10
2.3 Components of analysis of crude glycerin (Douette et al., 2007).....	14
2.4 Composition of crude glycerol in wt% obtained from biodiesel industry (Dasari, 2006).....	16
2.5 Evolution of themophysical properties of pure water as a function of temperature and pressure (Serani et al. 2008).....	25
2.6 Physicochemical properties of water as a function of temperature and pressure (Broll et al., 1999).....	26
2.7 Caparison of gases, supercritical fluids, and liquids (Székely, 2007).....	27
2.8 Dielectric constants for water and some general organic solvents (Loppinet-Serani et al. 2008).....	27
3.1 Comparison of reforming technologies (Holladay et al., 2009).....	32
3.2 History of hydrogen production from organic feedstock under sub, supercritical water conditions.....	36
3.3 The proposed reactions in the free radical reaction part of reaction mechanism (Buhler et al., 2002).....	54
3.4 The proposed reactions in the ionic reaction part of reaction mechanism (Buhler et al., 2002).....	55
4.1 The gas chromatography conditions (TCD and FID).....	69
4.2 Temperature program of the gas analysis.....	69
4.3 Number of rinsing for preinjection, and postinjection.....	70
4.4 The gas chromatography conditions (FID).....	70
4.5 Temperature program of the liquid analysis.....	71

TABLE	PAGE
6.1 Summary of operating conditions at maximum H <sub>2</sub> yields, product yields and product distribution for different cases ( $Q_{\text{net}}=0$ , $P=0.101325$ MPa)..	118
8.1 Total gas products flow rate as a function of feed glycerol concentration (medium feed rate of 2.15 g/min, $P = 25$ MPa, $T = 798$ K).....	152
8.2 Liquid yields as a function of feed glycerol concentration (medium feed rate of 2.15 g/min, $P = 25$ MPa, $T = 798$ K).....	153
8.3 Gas yields as a function of pressure (medium feed rate of 2.15 g/min, 5 wt.% of feed glycerol concentration, $T = 798$ K).....	156
8.4 Liquid yields as a function of pressure (medium feed rate of 2.15 g/min, 5 wt.% of feed glycerol concentration, $T = 798$ K).....	156
9.1 Physical properties of commercial supports.....	163
9.2 Physical properties of 10 wt.% of cobalt based catalysts.....	164
9.3 Glycerol conversion, total gas products flow rate, and gas yields as a function of feed rates (low feed rate=1.05 g/min, medium feed rate=2.50 g/min, and high feed rate=3.60 g/min) by using of 10 wt.% Co/YSZ catalyst ( $T=798$ K, $P = 25$ MPa, medium feed rate of 2.15 g/min, 5 wt.% of feed glycerol concentration).....	179
9.4 Liquid yields as a function of feed rates (low feed rate=1.05 g/min, medium feed rate=2.50 g/min, and high feed rate=3.60 g/min) by using of 10 wt.% Co/YSZ catalyst ( $T=798$ K, $P = 25$ MPa, medium feed rate of 2.15 g/min, 5 wt.% of feed glycerol concentration).....	180
9.5 Physical properties of YSZ support and different cobalt loading for Co/YSZ catalysts.....	182
9.6 Glycerol conversion, and gas yields as a function of cobalt loading for Co/YSZ catalysts ( $T=773$ K, $P = 25$ MPa, medium feed rate of 2.15 g/min, 5 wt.% of feed glycerol concentration).....	183
9.7 Liquid yields as a function of cobalt loading for Co/YSZ catalysts ( $T=773$ K, $P = 25$ MPa, medium feed rate of 2.15 g/min, 5 wt.% of feed glycerol concentration).....	183

TABLE	PAGE
10.1 Physical properties of 10 wt.% of nickel based catalysts.....	189
10.2 Glycerol conversion, total gas products flow rate, and gas yields as a function of feed rates (low feed rate=1.05 g/min, medium feed rate =2.50 g/min, and high feed rate=3.60 g/min) by using of 10 wt.% Ni/La <sub>2</sub> O <sub>3</sub> ( $T=798$ K, $P = 25$ MPa, medium feed rate of 2.15 g/min, 5 wt.% of feed glycerol concentration).....	200
10.3 Liquid yields as a function of feed rates (low feed rate=1.05 g/min, medium feed rate=2.50 g/min, and high feed rate=3.60 g/min) by using of 10 wt.% Ni/La <sub>2</sub> O <sub>3</sub> ( $T=798$ K, $P = 25$ MPa, medium feed rate of 2.15 g/min, 5 wt.% of feed glycerol concentration).....	200
10.4 Physical properties of La <sub>2</sub> O <sub>3</sub> support and different nickel loading for Ni/La <sub>2</sub> O <sub>3</sub> catalysts.....	202
10.5 Glycerol conversion, and gas yields as a function of nickel loading for Ni/La <sub>2</sub> O <sub>3</sub> catalysts ( $T=798$ K, $P = 25$ MPa, medium feed rate of 2.15 g/min, 5 wt.% of feed glycerol concentration).....	203
10.6 Liquid yields as a function of nickel loading for Ni/La <sub>2</sub> O <sub>3</sub> catalysts ( $T=773$ K, $P = 25$ MPa, medium feed rate of 2.15 g/min, 5 wt.% of feed glycerol concentration).....	204
10.7 Glycerol conversion, and gas yields as a function of feed glycerol concentration for Ni/La <sub>2</sub> O <sub>3</sub> catalysts ( $T=798$ K, $P = 25$ MPa, medium feed rate of 2.15 g/min, 5 wt.% of feed glycerol concentration, 5 wt.% of nickel loading).....	210
10.8 Liquid yields as a function of feed glycerol concentration for Ni/La <sub>2</sub> O <sub>3</sub> catalysts ( $T=798$ K, $P = 25$ MPa, medium feed rate of 2.15 g/min, 5 wt.% of feed glycerol concentration, 5 wt.% of nickel loading).....	211
A.1 Retention time of gas components in gas chromatographic analysis.....	250
A.2 Retention time of liquid components in gas chromatographic analysis....	260



# LIST OF FIGURES

FIGURE	PAGE
2.1	Distribution of glycerol consumption in different products and industries (Bondioli, 2003)..... 10
2.2	Applications of glycerol (www.chemistryinnovation.co.uk)..... 13
2.3	Phase diagram for water (Cansell et al., 1998)..... 25
3.1	Different operating conditions for fuel reforming (Rabenstein and Hacker, 2008)..... 31
3.2	(a) free radical reaction, (b) ionic reaction pathways for the formation of acetaldehyde, acrolein, and formaldehyde (Buhler et al., 2002)..... 56
3.3	Pathways to products in glycerol aqueous phase reforming process (Luo et al., 2008)..... 57
3.4	Reaction pathways during glycerol reforming process (Adhikari et al., 2009)..... 58
3.5	Proposed reaction pathways for glycerol reforming in supercritical water to gaseous products (Bennekom et al., 2011)..... 58
4.1	Schematic diagram of supercritical water glycerol reforming set up..... 63
4.2	Schematic diagram of the reactor..... 65
5.1	The schematic of energy boundary conditions - - - Reformer, — System, and - · - · Heat transfer in system case. (If isothermal condition is considered In reformer level, $T_{in}$ , $T_r$ , and $T_{out}$ will be equivalent). 74
5.2	(a) Yield of $H_2$ (b) Yield of carbon at different values of $WGR$ and $OGR$ at $P=0.101325$ MPa, $T = 940$ K; ♦ at $OGR=0$ (Adhikari et al., 2007a); ▲ at $OGR=0$ (Wang et al., 2008); ■ at $OGR=0$ (Rossi et al., 2009)..... 77
5.3	Boundary of carbon formation as a function of $WGR$ , $OGR$ , and $T$ at $P=0.101325$ MPa ..... 79
5.4	Net heat energies ( $Q_{net}$ ) of Reformer and System as a function of $WGR$ and $OGR$ at $P=0.101325$ MPa, $T_r=940$ K..... 80

FIGURE	PAGE
5.5 (a) Yield of H <sub>2</sub> (b) <i>OGR</i> of reformer and system as a function of <i>WGR</i> and operating temperature at energy self-sufficient condition; ----- Reformer, —— System.....	82
5.6 Yield of H <sub>2</sub> and <i>OGR</i> of Reformer ( <i>WGR</i> =10) and System ( <i>WGR</i> =7) as a function of operating temperature at energy self-sufficient condition; ----- Reformer, —— System.....	84
5.7 Maximum of yield of H <sub>2</sub> , <i>OGR</i> and operating temperature of reformer and system levels as a function of <i>WGR</i> at energy self-sufficient condition; ----- Reformer, —— System.....	85
6.1 Schematic diagram of energy balances in <i>Single-feed</i> mode for <i>Reformer</i> and <i>System</i> levels ( $P=P_0=0.101325$ MPa, for isothermal condition in <i>Reformer</i> level, $T_{in}$ , $T_r$ , and $T_{out}$ are equal).....	89
6.2 Schematic diagram of energy balances in <i>Split-feed</i> mode for <i>Reformer</i> and <i>System</i> levels ( $P=P_0=0.101325$ MPa, for isothermal condition in <i>Reformer</i> level, $T_{in}$ , $T_r$ , and $T_{out}$ are equal).....	90
6.3 Net heat energies ( $Q_{net}$ ) of <i>Reformer</i> level in <i>Single-feed</i> mode at different values of <i>WGR</i> and <i>OGR</i> ( $P=0.101325$ MPa, $T_r=900$ K).....	93
6.4 Net heat energies ( $Q_{net}$ ) of <i>Reformer</i> level in <i>Single-feed</i> mode at different values of <i>WGR</i> and $T$ ( $OGR=0.35$ , $P=0.101325$ MPa).....	94
6.5 Heat energy (in the reformer and combustor) and <i>OGR</i> of <i>Reformer</i> level in <i>Split-feed</i> mode at different values of Mole of glycerol to the reformer and <i>WGR</i> ( $P=0.101325$ MPa, $T_r=900$ K).....	96
6.6 Net heat energies ( $Q_{net}$ ) of <i>System</i> level in <i>Single-feed</i> mode at different values of <i>WGR</i> and <i>OGR</i> ( $P=0.101325$ MPa, $T_r=900$ K).....	96
6.7 Net heat energies ( $Q_{net}$ ) of <i>System</i> level in <i>Single-feed</i> mode at different values of <i>WGR</i> and $T$ ( $OGR=1.80$ , $P=0.101325$ MPa).....	98
6.8 Heat energy (in the reformer and combustor) and <i>OGR</i> of <i>System</i> level in <i>Split-feed</i> mode at different values of Mole of glycerol to the reformer and <i>WGR</i> ( $P=0.101325$ MPa, $T_r=900$ K).....	99

FIGURE	PAGE
6.9 Carbon yield of <i>Reformer</i> level at different values of <i>WGR</i> and operating temperature ( $Q_{\text{net}}=0$ , $P=0.101325$ MPa).....	100
6.10 Carbon yield of <i>System</i> level at different values of <i>WGR</i> and operating temperature ( $Q_{\text{net}}=0$ , $P=0.101325$ MPa).....	102
6.11 (a) $H_2$ yield and (b) <i>OGR</i> of <i>Reformer</i> level at different values of <i>WGR</i> and operating temperature ( $Q_{\text{net}}=0$ , $P=0.101325$ MPa).....	106
6.12 (a) $H_2$ yield, and (b) <i>OGR</i> of <i>System</i> level at different values of <i>WGR</i> and operating temperature ( $Q_{\text{net}}=0$ , $P=0.101325$ MPa).....	107
6.13 $H_2$ mole fraction (dry basis) of <i>Reformer</i> level at different values of <i>WGR</i> and operating temperature ( $Q_{\text{net}}=0$ , $P=0.101325$ MPa).....	109
6.14 $H_2$ mole fraction (dry basis) of <i>System</i> level at different values of <i>WGR</i> and operating temperature ( $Q_{\text{net}}=0$ , $P=0.101325$ MPa).....	109
6.15 By-product yields including $CO_2$ , $CO$ , $CH_4$ and non reacted substance $N_2$ of <i>Reformer</i> level as a function of <i>WGR</i> ( $Q_{\text{net}}=0$ , $T_r=900$ K, $P=0.101325$ MPa).....	111
6.16 By-product yields including $CO_2$ , $CO$ , $CH_4$ and non reacted substance $N_2$ of <i>System</i> level as a function of <i>WGR</i> ( $Q_{\text{net}}=0$ , $T_r=900$ K, $P=0.101325$ MPa).....	112
6.17 (a) $H_2$ yield and fraction of glycerol to reformer, (b) $H_2$ mole fraction (dry basis) of <i>System</i> level as a function of <i>WGR</i> for cases with different oxidizing agents (air or pure $O_2$ ) and operation modes ( <i>Co-feed</i> or <i>Split-feed</i> ) ( $Q_{\text{net}}=0$ , $T_r=900$ K, $P=0.101325$ MPa).....	114
6.18 $H_2$ yield and <i>OGR</i> of <i>Split-feed</i> mode in <i>System</i> level as a function of <i>WGR</i> for cases with/without utilizing heat energy from Afterburner products (ABP) stream ( $Q_{\text{net}}=0$ , $T_r=900$ K, $P=0.101325$ MPa).....	117
7.1 Mole fractions of gas products ( $H_2$ , $CO_2$ , $CO$ , and $CH_4$ ) during (a) 673-1273 K (b) 723-848 K and (c) gas product yields as function of operating temperatures ( $P=25$ MPa, 5 wt.% of feed glycerol concentration)..	125

FIGURE	PAGE
7.2 (a) mole fractions of gas products (H <sub>2</sub> , CO <sub>2</sub> , CO, and CH <sub>4</sub> ) (b) gas product yields as a function of pressure ( $T=798$ K, 5 wt.% of feed glycerol concentration).....	128
7.3 (a) mole fractions of gas products (H <sub>2</sub> , CO <sub>2</sub> , CO, and CH <sub>4</sub> ) (b) gas product yields as a function of feed glycerol concentration ( $T=798$ K, $P=25$ MPa).....	129
8.1 Glycerol conversion at different feed rates and operating temperatures ( $P=25$ MPa, 5 wt.% of feed glycerol concentration) $\blacklozenge$ Low feed rate (1.05 g/min), $\blacksquare$ Medium feed rate (2.15 g/min), $\blacktriangle$ High feed rate (3.60 g/min).....	136
8.2 Compositions and flow rate of gas products (H <sub>2</sub> , CO, CO <sub>2</sub> , and CH <sub>4</sub> ) function of operating temperature (a) feed rate=1.05 g/min, (b) feed rate=2.15 g/min, (c) feed rate=3.60 g/min ( $P=25$ MPa, 5 wt.% of feed glycerol concentration).....	138
8.3 Gas yields of (a) H <sub>2</sub> , (b) CO, (c) CO <sub>2</sub> , (d) CH <sub>4</sub> , (e) C <sub>2</sub> H <sub>6</sub> , (f) C <sub>2</sub> H <sub>4</sub> , (g) C <sub>3</sub> H <sub>8</sub> , (h) C <sub>3</sub> H <sub>6</sub> at different feed rates and operating temperatures ( $P=25$ MPa, 5 wt.% of feed glycerol concentration) $\blacklozenge$ Low feed rate (1.05 g/min), $\blacksquare$ Medium feed rate (2.15 g/min), $\blacktriangle$ High feed rate (3.60 g/min).....	139
8.4 Liquid yields of (a) acetaldehyde (b) acetol (c) methanol (d) acetic acid (e) propionaldehyde (f) allyl alcohol at different values of feed rate and operating temperature ( $P=25$ MPa, 5 wt.% of feed glycerol concentration) $\blacklozenge$ Low feed rate (1.05 g/min), $\blacksquare$ Medium feed rate (2.15 g/min), $\blacktriangle$ High feed rate (3.60 g/min).....	144
8.5 (a) Conversion of glycerol, compositions of gas products (H <sub>2</sub> , CO, CO <sub>2</sub> , and CH <sub>4</sub> ), (b) Compositions of gas products (C <sub>2</sub> H <sub>6</sub> , C <sub>2</sub> H <sub>4</sub> , C <sub>3</sub> H <sub>8</sub> , and C <sub>3</sub> H <sub>6</sub> ) as a function of feed glycerol concentration (medium feed rate of 2.15 g/min, $P=25$ MPa, $T=798$ K).....	149

FIGURE	PAGE
8.6 Gas yields of (a) H <sub>2</sub> , CO, CO <sub>2</sub> , and CH <sub>4</sub> , (b) C <sub>2</sub> H <sub>6</sub> , C <sub>2</sub> H <sub>4</sub> , C <sub>3</sub> H <sub>8</sub> , and C <sub>3</sub> H <sub>6</sub> as a function of feed glycerol concentration (medium feed rate of 2.15 g/min, $P = 25$ MPa, $T = 798$ K).....	151
8.7 Effect of pressure on glycerol conversion, composition of main gas products (H <sub>2</sub> , CO, CO <sub>2</sub> , and CH <sub>4</sub> ), total flow rate and H <sub>2</sub> flow rate (medium feed rate of 2.15 g/min, 5 wt.% of feed glycerol concentration, $T = 798$ K).....	155
9.1 XRD patterns of commercial supports and 10 wt.% of cobalt based catalysts.....	165
9.2 Glycerol conversion at different cobalt based catalysts and operating temperature ( $P = 25$ MPa, medium feed rate of 2.15 g/min, 5 wt.% of feed glycerol concentration, 10 wt.% of cobalt loading).....	166
9.3 (a) liquid product sample from the supercritical water reforming of glycerol with 10 wt.% Co/ $\gamma$ -Al <sub>2</sub> O <sub>3</sub> catalyst at 748 K (b) solid products after filtration.....	167
9.4 Carbon plugging at the back pressure regulator seat (left) and nut (right).....	168
9.5 Gas yields of (a) H <sub>2</sub> , (b) CO <sub>2</sub> , (c) CH <sub>4</sub> , (d) CO at different cobalt based catalysts and operating temperatures ( $P = 25$ MPa, medium feed rate of 2.15 g/min, 5 wt.% of feed glycerol concentration, 10 wt.% of cobalt loading).....	172
9.6 Liquid yields of (a) acetaldehyde, (b) acetone, (c) methanol, (d) acetic acid at different cobalt based catalysts and operating temperatures ( $P = 25$ MPa, medium feed rate of 2.15 g/min, 5 wt.% of feed glycerol concentration, 10 wt.% of cobalt loading).....	174
9.7 Yield of (a) H <sub>2</sub> , (b) acetaldehyde as a function of time on stream and operating temperature by using of 10 wt.% Co/YSZ catalyst ( $P = 25$ MPa, medium feed rate of 2.15 g/min, 5 wt.% of feed glycerol concentration).....	176

FIGURE	PAGE
9.8 Compositions of gas products (a) H <sub>2</sub> , CO <sub>2</sub> , CH <sub>4</sub> , and CO (b) C <sub>2</sub> H <sub>6</sub> , C <sub>2</sub> H <sub>4</sub> , C <sub>3</sub> H <sub>8</sub> , C <sub>3</sub> H <sub>6</sub> as a function of operating temperature by using of 10 wt.% Co/YSZ ( $P = 25$ MPa, medium feed rate of 2.15 g/min, 5 wt.% of feed glycerol concentration).....	177
9.9 Yield of (a) H <sub>2</sub> , (b) acetaldehyde as a function of time on stream and feed rate by using of 10 wt.% Co/YSZ catalyst ( $T=798$ K, $P = 25$ MPa, medium feed rate of 2.15 g/min, 5 wt.% of feed glycerol concentration).....	180
9.10 XRD patterns of YSZ support and different cobalt loading for Co/YSZ catalysts.....	182
9.9 Compositions of gas products (a) H <sub>2</sub> , CO <sub>2</sub> , CH <sub>4</sub> , and CO (b) C <sub>2</sub> H <sub>6</sub> , C <sub>2</sub> H <sub>4</sub> , C <sub>3</sub> H <sub>8</sub> , C <sub>3</sub> H <sub>6</sub> as a function of cobalt loading for Co/YSZ catalysts ( $T=773$ K, $P = 25$ MPa, medium feed rate of 2.15 g/min, 5 wt.% of feed glycerol concentration).....	184
10.1 XRD patterns of commercial supports and 10 wt.% of nickel based catalysts.....	188
10.2 Glycerol conversion at different nickel based catalysts and operating temperatures ( $P=25$ MPa, medium feed rate of 2.15 g/min, 5 wt.% of feed glycerol concentration, 10 wt.% of nickel loading).....	189
10.3 Gas yields of (a) H <sub>2</sub> , (b) CO <sub>2</sub> , (c) CH <sub>4</sub> , (d) CO at different nickel based catalysts and operating temperatures ( $P=25$ MPa, medium feed rate of 2.15 g/min, 5 wt.% of feed glycerol concentration, 10 wt.% of nickel loading).....	193
10.4 Liquid yields of (a) acetaldehyde, (b) acetic acid, (c) methanol, (d) acetol, (e) ethanol at different nickel based catalysts and operating temperatures ( $P=25$ MPa, medium feed rate of 2.15 g/min, 5 wt.% of feed glycerol concentration, 10 wt.% of nickel loading).....	195

FIGURE	PAGE
10.5 Compositions of gas products (a) H <sub>2</sub> , CO <sub>2</sub> , CH <sub>4</sub> , and CO (b) C <sub>2</sub> H <sub>6</sub> , C <sub>2</sub> H <sub>4</sub> , C <sub>3</sub> H <sub>8</sub> , C <sub>3</sub> H <sub>6</sub> as a function of operating temperature by using of 10 wt.% Ni/La <sub>2</sub> O <sub>3</sub> catalyst ( <i>P</i> = 25 MPa, medium feed rate of 2.15 g/min, 5 wt.% of feed glycerol concentration).....	198
10.6 Compositions of gas products as a function of feed rates (low feed rate=1.05 g/min, medium feed rate=2.50 g/min, and high feed rate=3.60 g/min) by using of 10 wt.% Ni/La <sub>2</sub> O <sub>3</sub> catalyst ( <i>T</i> =798 K, <i>P</i> = 25 MPa, medium feed rate of 2.15 g/min, 5 wt.% of feed glycerol concentration) .....	201
10.7 XRD patterns of La <sub>2</sub> O <sub>3</sub> support and different nickel loading for Ni/La <sub>2</sub> O <sub>3</sub> catalysts.....	202
10.8 Compositions of gas products (a) H <sub>2</sub> , CO <sub>2</sub> , CH <sub>4</sub> , and CO (b) C <sub>2</sub> H <sub>6</sub> , C <sub>2</sub> H <sub>4</sub> , C <sub>3</sub> H <sub>8</sub> , C <sub>3</sub> H <sub>6</sub> as a function of nickel loading for Ni/La <sub>2</sub> O <sub>3</sub> catalysts ( <i>T</i> =798 K, <i>P</i> = 25 MPa, medium feed rate of 2.15 g/min, 5 wt.% of feed glycerol concentration).....	204
10.9 Gas yields of (a) H <sub>2</sub> , (b) CO <sub>2</sub> , (c) CH <sub>4</sub> , (d) CO and liquid yield of (e) acetaldehyde at different percent nickel loading for Ni/La <sub>2</sub> O <sub>3</sub> catalysts and time on stream ( <i>T</i> = 708 K, <i>P</i> =25 MPa, medium feed rate of 2.15 g/min, 5 wt.% of feed glycerol concentration).....	206
10.10 Compositions of gas products (a) H <sub>2</sub> , CO <sub>2</sub> , CH <sub>4</sub> , CO, and total gas products flow rate (b) C <sub>2</sub> H <sub>6</sub> , C <sub>2</sub> H <sub>4</sub> , C <sub>3</sub> H <sub>8</sub> , C <sub>3</sub> H <sub>6</sub> as a function of feed glycerol concentration for Ni/La <sub>2</sub> O <sub>3</sub> catalysts ( <i>T</i> =798 K, <i>P</i> = 25 MPa, medium feed rate of 2.15 g/min, 5 wt.% of feed glycerol concentration, 5 wt.% of nickel loading).....	209
10.11 Gas yields of (a) H <sub>2</sub> , (b) CO <sub>2</sub> , (c) CH <sub>4</sub> , (d) CO, (e) C <sub>2</sub> H <sub>6</sub> , and liquid yields of (f) acetaldehyde as a function of feed glycerol concentration and time on stream for Ni/La <sub>2</sub> O <sub>3</sub> catalysts ( <i>T</i> =798 K, <i>P</i> = 25 MPa, medium feed rate of 2.15 g/min, 5 wt.% of feed glycerol concentration, 5 wt.% of nickel loading).....	212

FIGURE	PAGE
11.1 Comparison of <i>Reformer</i> (880 K) and <i>System</i> (875 K) levels by providing of <i>WGR</i> , <i>OGR</i> , and maximum H <sub>2</sub> yield at thermal neutral condition ( $Q_{\text{net}}=0$ , $P=0.101325$ MPa).....	216
11.2 Effect of mode at maximum H <sub>2</sub> yield condition in the <i>Reformer</i> level (a) gas product yields (b) mole fraction of gas products ( $Q_{\text{net}}=0$ , $P=0.101325$ MPa).....	218
11.3 Effect of mode and using of pure O <sub>2</sub> , and ABP at maximum H <sub>2</sub> yield condition in the <i>System</i> level (a) <i>WGR</i> , <i>OGR</i> , H <sub>2</sub> yield (b) gas product yields (c) mole fraction of gas products ( $Q_{\text{net}}=0$ , $P=0.101325$ MPa).....	219
11.4 Comparison of thermodynamic analysis, empty reactor (0.1 MPa), empty reactor (25 MPa), Co/YSZ catalyst, and Ni/La <sub>2</sub> O <sub>3</sub> catalyst in the supercritical water reforming of glycerol (a) H <sub>2</sub> yield (b) glycerol conversion, gas product yields.....	221
A.1 N <sub>2</sub> calibration curve in the range of 0-100 vol.%.....	245
A.2 H <sub>2</sub> calibration curves in the range of (a) 0-50 vol.% (b) 50-90 vol.%.....	245
A.3 CO calibration curve in the range of 0-40 vol.%.....	246
A.4 CO <sub>2</sub> calibration curve in the range of 0-45 vol.%.....	247
A.5 CH <sub>4</sub> calibration curve in the range of 0-25 vol.%.....	247
A.6 C <sub>2</sub> H <sub>6</sub> calibration curve in the range of 0-8 vol.%.....	248
A.7 C <sub>2</sub> H <sub>4</sub> calibration curve in the range of 0-80 vol.%.....	248
A.8 Gas products diagram (TCD, 15' x 1/8" stainless steel 60/80 mesh Carboxen- 1000 column) of gas chromatographic analysis for empty reactor studying (2.15 g/min, $T=848$ K (575°C), $P=25$ MPa).....	249
A.9 Gas products diagram (FID, 50 m x 0.53 mm Al <sub>2</sub> O <sub>3</sub> /KCl fused silica PCOT column) of gas chromatographic analysis for empty reactor studying (2.15 g/min, $T=848$ K (575°C), $P=25$ MPa).....	249
A.10 Glycerol calibration curve in the range of 0-11 wt.%.....	251
A.11 Acetaldehyde calibration curve in the range of 0-1.1 wt.%.....	251
A.12 Propionaldehyde calibration curve in the range of 0-1.0 wt.%.....	252



FIGURE	PAGE
A.13 Acetone calibration curve in the range of 0-1.0 wt.%.....	252
A.14 Acrolein calibration curve in the range of 0-1.1 wt.%.....	253
A.15 Methanol calibration curve in the range of 0-1.1 wt.%.....	253
A.16 Ethanol calibration curve in the range of 0-0.5 wt.%.....	254
A.17 Allyl alcohol calibration curve in the range of 0-0.9 wt.%.....	254
A.18 Acetol calibration curve in the range of 0-1.2 wt.%.....	255
A.19 Acetic acid calibration curve in the range of 0-0.9 wt.%.....	255
A.20 Ethylene glycol calibration curve in the range of 0-0.8 wt.%.....	256
A.21 Acrylic acid calibration curve in the range of 0-0.9 wt.%.....	256
A.22 Isopropanol calibration curve in the range of 0-0.9 wt.%.....	257
A.23 Propanol calibration curve in the range of 0-0.9 wt.%.....	257
A.24 1,2 propanediol calibration curve in the range of 0-1.0 wt.%.....	258
A.25 Formaldehyde calibration curve in the range of 0-0.4 wt.%.....	258
A.26 Diagram of gas chromatographic analysis (FID, DB-WAX column) For empty reactor studying (2.15 g/min, $T=823$ K (550°C), $P=25$ MPa).....	259
A.27 Diagram of gas chromatographic analysis (FID, DB-WAX column) for catalyst studying (10 wt.% Co/ $\alpha$ -Al <sub>2</sub> O <sub>3</sub> , 2.15 g/min, $T=773$ K (500°C), $P=25$ MPa).....	259
B.1 Volume metric flow rate of N <sub>2</sub> (3.1-14.5 mL/min) as a function of signal.....	261
B.2 Volume metric flow rate of H <sub>2</sub> (30-190 mL/min) as a function of signal.....	262
B.3 Volume metric flow rate of CO <sub>2</sub> (15-140 mL/min) as a function of signal.....	262
B.4 Volume metric flow rate of CO (15-190 mL/min) as a function of signal.....	263
B.5 Volume metric flow rate of mixed gas (30 vol%. CO <sub>2</sub> , 30 vol.% CO, 25 vol%. CH <sub>4</sub> , 10 vol.% C <sub>2</sub> H <sub>4</sub> , and 5 vol.% C <sub>2</sub> H <sub>6</sub> ) (20-140 mL/min) as a function of signal.....	263

FIGURE	PAGE
D.1 TGA curves for spent 10 wt.% Co/ $\gamma$ -Al <sub>2</sub> O <sub>3</sub> catalyst with 2.15 g/min, $T=748$ K, $P=25$ MPa, 5 wt.% feed glycerol concentration.....	266
D.2 TGA curves for spent 10 wt.% Ni/La <sub>2</sub> O <sub>3</sub> catalyst with 1.05 g/min, $T=798$ K, $P=25$ MPa, 5 wt.% feed glycerol concentration.....	267
E.1 SEM photos for 10 wt.% Co/YSZ catalysts (a) fresh (b) spent at $T=773$ K (c) 798 K (d) 823 K with 2.15 g/min, $P=25$ MPa, 5 wt.% feed glycerol concentration.....	268
E.2 SEM photos for 10 wt.% Co/ $\alpha$ -Al <sub>2</sub> O <sub>3</sub> catalysts (a) fresh (b) spent at $T=798$ K with 2.15 g/min, $P=25$ MPa, 5 wt.% feed glycerol concentration.....	269
E.3 SEM photos for 10 wt.% Co/ZrO <sub>2</sub> catalysts (a) fresh (b) spent at $T=823$ K with 2.15 g/min, $P=25$ MPa, 5 wt.% feed glycerol concentration.....	269
F.1 TEM photos for 10 wt.% Co/ $\alpha$ -Al <sub>2</sub> O <sub>3</sub> catalysts (a) fresh (b) spent at $T=798$ K with 2.15 g/min, $P=25$ MPa, 5 wt.% feed glycerol concentration.....	270
F.2 TEM photos for 10 wt.% Ni/ $\gamma$ -Al <sub>2</sub> O <sub>3</sub> catalysts (a) fresh (b) spent at $T=798$ K with 2.15 g/min, $P=25$ MPa, 5 wt.% feed glycerol concentration.....	271

# NOMENCLATURE

$A_j$	total number of atoms of $j$ -th element in the reaction mixture [-]
$a_{ij}$	number of atoms of the $j$ -th element present in each molecule of $i$ -th species [-]
$F_i$	molar flow rate of product $i$ [mol min <sup>-1</sup> ]
$F_{\text{Glycerol}}$	molar flow rate of glycerol [mol min <sup>-1</sup> ]
$f_i^0$	standard-state fugacity of the $i$ -th species [-]
$\hat{f}_i$	fugacity of the $i$ -th species [-]
$G^t$	total Gibbs free energy [Jmol <sup>-1</sup> ]
$G_i^0$	standard-state Gibbs free energy of the $i$ -th species [Jmol <sup>-1</sup> ]
$\Delta G_{f_i}^0$	standard Gibbs function of formation of the $i$ -th species [Jmol <sup>-1</sup> ]
$G_{\text{C(s)}}$	molar Gibbs free energy of solid carbon [Jmol <sup>-1</sup> ]
$H_i$	enthalpy of the $i$ -th species [Jmol <sup>-1</sup> ]
$M$	total number of elements [-]
$m_0$	mass flow rate of the mixture to the reactor [g min <sup>-1</sup> ]
$N$	total species [-]
$n_i$	mole of the $i$ -th species [mol]
$n_j$	mole of the $j$ -th species except $i$ -th specie [mol]

$n_C$	mole of solid carbon [mol]
$n_{\text{Glycerol}}$	mole of glycerol [mol]
$n_{\text{H}_2\text{O}}$	mole of water in products [mol]
$OGR$	oxygen/glycerol ratio [-]
$P$	pressure [Pa]
$P^0$	standard-state pressure [Pa]
$Q_{\text{combustor}}$	heat energy of combustor [ $\text{kJmol}^{-1}$ ]
$Q_{\text{cooler (ABP)}}$	heat energy of cooler from afterburner products stream [ $\text{kJmol}^{-1}$ ]
$Q_{\text{evaporator}}$	heat energy of evaporator [ $\text{kJmol}^{-1}$ ]
$Q_{\text{heater (net)}}$	net heat energy of heaters [ $\text{kJmol}^{-1}$ ]
$Q_{\text{Reformer level (net)}}$	net heat energy of the <i>Reformer</i> level [ $\text{kJmol}^{-1}$ ]
$Q_{\text{reformer}}$	heat energy of reformer [ $\text{kJmol}^{-1}$ ]
$Q_{\text{System level (net)}}$	net heat energy of the <i>System</i> level [ $\text{kJmol}^{-1}$ ]
$R$	ideal gas constant $8.314472 \text{ [Jmol}^{-1}\text{K}^{-1}\text{]}$
$T, T_r$	operating temperature [K]
$WGR$	water/glycerol ratio [-]
$X_{\text{Glycerol}}$	glycerol conversion [-]
$x$	mole of glycerol for feeding to the reformer [mol]
$V_R$	volume of reactor [ $\text{cm}^3$ ]

$y_i$  mole fraction of each substance in gas products [-]

### Greek letters

$\lambda_j$  Lagrange multiplier [-]

$\mu_i$  chemical potential of species  $i$  [ $\text{Jmol}^{-1}$ ]

$\hat{\phi}_i$  fugacity coefficient of species  $i$  [-]

$\phi$  void fraction of bed [-]

$\rho_R$  density of pure water at the reactor conditions of  $P$  and  $T$  [ $\text{g cm}^{-3}$ ]

$\tau$  residence time in the reactor [s]

### Subscripts

0 inlet stream to the *System* level

gas product in gas phase

in inlet stream to the reformer

liquid product in liquid phase

out outlet stream from the reformer

# CHAPTER I

## INTRODUCTION

### 1.1 Introduction

At present, energies have become essential for the prosperity of mankind. However, humans are using an extravagant amount of energy carelessly. Energy sources such as crude petroleum, natural gas and coal are quickly diminishing. In the future, substitutes such as renewable and sustainable energy will replace the present energy sources.

Alternative energies include solar, nuclear, geothermal (steam dominated, hot water dominated, hot dry rock), wind, water, and biomass. Biodiesel has been a superior option as it is produced from biomass and developed into the one of the more promising carbon neutral biofuels (Iriando et al., 2008). Production of biodiesel in the world has rapidly increased from 2 million tons/year in 2004 to 11.1 million tons/year in 2008 - an increase of more than 500% in only four years (Biodiesel 2020: Global Market Survey, Feedstock Trends and Forecasts, 2008). Moreover, biodiesel is environmentally friendly because of its low sulfur level and no petroleum residual. However, there are some concerns on using biodiesel in old engines of vehicles because biodiesel corrodes seals or rubbers. Nowadays, Thailand has been using biodiesel in B2, B5, etc. for solving the corrosion problem. In the near future, B100 is expected to be promising biodiesel energy.

Biodiesel cost is the main concern for commercial use of this product because it is expensive compared to the current price of diesel. Conversely, the price of biodiesel may not fluctuate as drastically as diesel because biodiesel is more readily available. It is known that when biodiesel is produced, a by-product is subsequently formed via transesterification. The cost of biodiesel can decrease drastically by distributing its by-products. One of the main by-products is glycerol ( $C_3H_8O_3$ ), it is a colorless, odorless, viscous liquid, form of chemical storage of hydrogen, and highly

oxygenated with a hydroxyl group on each carbon atom and an internal carbon-to-oxygen ratio (C/O) equal to 1 (Dauenhauer et al., 2006). Currently, glycerol is widely used in many applications including drugs/pharmaceuticals, personal cares, polymers, foods, and resins. From the increased production of biodiesel, a glut of glycerol (approximate 0.11 ton of crude glycerol from 1 ton of biodiesel yield (Wang, et al. 2008)) is expected in the world market. Glycerol from the biodiesel process often contains up to 50% impurities such as biodiesel & methanol (Slinn et al. 2008). Accordingly, the recent works have been attracted to use glycerol as a by-product from biodiesel manufacturing in many potential applications. Two major approaches are as follows: i) purifying crude biodiesel glycerol (Mink, 2008) for later applications in drug/pharmaceutical industries, and ii) converting glycerol to other high-valued chemicals via different reactions such as hydrogenolysis for producing ethylene glycol, propylene glycol, lactic acid (Dasari et al., 2005; Deutsch et al., 2007; Maris et al., 2007; Rennard et al., 2009), condensation for producing [1,3]dioxan-5-ols that are potential precursors for production of “green” platform chemicals 1,3-dihydroxyacetone and 1,3-propanediol (Deutsch et al., 2007), oxidation for producing glyceric acid, tartronic acid, glycolic acid and oxalic acid (Ketchie et al., 2007; Yang et al., 2008; Rennard et al., 2009), etherification for producing higher glycerol ethers used as oxygenates to diesel fuel, biodiesel or their mixture (Klepacova et al., 2007) and dehydration for synthesis of acrolein (Yang et al., 2008; Rennard et al., 2009). Nevertheless, the economic analysis of the process needs to take into account the purification of glycerol from biodiesel production because the impurities in the mixture can easily deactivate catalysts or produce other undesired products.

Hydrogen production is another promising choice to manage the large excess of glycerol because the impurities content in glycerol always include methanol and water, both being reactants in the reforming process (Slinn et al., 2008; Valliyappan et al., 2008). Hydrogen, a main fuel in most fuel cell applications, can always be produced via steam reforming reaction (SR) (Fishtik et al., 2000; Hirai et al., 2005; Zhang et al., 2007; Cui et al., 2009; Adhikari et al., 2009). SR is actually the most commonly used process, providing high yields of H<sub>2</sub> production (theoretically seven

moles of H<sub>2</sub> per mole of glycerol reacted) which can be continuously enhanced by improving catalysts, operating conditions and heat transfer to achieve better performance (Yanbing et al., 2007). However, it requires a large amount of external heat source, especially at high water to glycerol ratio (*WGR*). Currently, some alternative processes such as autothermal reforming (ATR) process are considered to decrease the demand for external heat source (Dauenhauer et al., 2006; Wang et al., 2009). ATR combines steam reforming and partial oxidation reactions to operate at thermal neutral point, that is with a net reactor heat duty of zero ( $Q = 0$ ).

Most of the research works in hydrogen production from glycerol feedstock can be classified into two major areas which include catalysts development and thermodynamic analysis. A number of catalysts have been developed and tested to enhance hydrogen production and also to suppress undesired by-products in the reforming process, for examples, Ni/Al<sub>2</sub>O<sub>3</sub> (Czernik et al., 2002; Adhikari et al., 2007; Zhang et al., 2007; Valliyappan et al., 2008), Ni/MgO (Hirai et al., 2005; Adhikari et al., 2007; Adhikari et al., 2008), Ni/CeO<sub>2</sub> (Zhang et al., 2007; Adhikari et al., 2008), Ni/TiO<sub>2</sub> (Zhang et al., 2007; Adhikari et al., 2008), Pd/Ni/Cu/K (Swami et al., 2006; Sharma et al., 2008), Ni/CeO<sub>2</sub>/Al<sub>2</sub>O<sub>3</sub> (Adhikari et al., 2007; Adhikari et al., 2008; Profeti et al., 2009), La<sub>1-x</sub>Ce<sub>x</sub>NiO<sub>3</sub> (Cui et al., 2009), Ru/Y<sub>2</sub>O<sub>3</sub> (Hirai et al., 2005), Ir, Co/CeO<sub>2</sub> (Zhang et al., 2007), Rh, Pt, Pd, Ir, Ru, Ce/Al<sub>2</sub>O<sub>3</sub> (Adhikari et al., 2007) for steam reforming (SR), Raney-NiSn (Shabaker et al., 2004), Pt/Al<sub>2</sub>O<sub>3</sub> (Shabaker et al., 2004; Lehnert et al., 2008; Wen et al., 2008), Ni/Al<sub>2</sub>O<sub>3</sub> (Wen et al., 2008; Iriundo et al., 2008) for aqueous phase reforming (APR), RhCeWc/Al<sub>2</sub>O<sub>3</sub> (Dauenhauer et al., 2006), Pd/Ni/Cu/K (Swami et al., 2006; Sharma et al., 2008) for autothermal reforming (ATR), and Ru/Al<sub>2</sub>O<sub>3</sub> (Byrd et al., 2008) for supercritical water reforming (SCWR).

In recent years, SCWR has attracted more and more interest (Boukis et al., 2003a; Boukis et al., 2003b; Gadhe and Gupta, 2005; Tang and Kitagawa, 2005; Byrd et al., 2007) due to its high reaction efficiency and H<sub>2</sub> selectivity (Guo et al., 2010). Because its unique properties, supercritical water offers higher space-time yield, reduces mass transfer limitations, and favors endothermic reforming reactions (Byrd et al., 2007; Gadhe and Gupta, 2007; Loppinet-Serani et al., 2008; Bennekom et al.,



2011). Moreover, hydrogen is produced at high pressure, which can be stored directly without large energy penalty from compression (Gadhe and Gupta, 2005; Boukis et al., 2006; Byrd et al., 2007; Bennekoum et al., 2011). On the other hand, carbon formation has been found to be a severe problem in this technology by plugging in the reactor and pipe lines particularly found in biomass gasification (Matsumura et al., 2005; Xu et al., 2009). From many advantages from supercritical reforming, glycerol reforming in supercritical water would be a good choice to produce hydrogen that has been studied in few catalysts.

For this work, thermodynamic analysis of hydrogen production via various reactions (i.e., steam reforming, partial oxidation, autothermal reforming, and supercritical water) is firstly investigated to find the effects of major operating parameters on the reaction performances and to determine suitable operating conditions for the hydrogen production from glycerol. Then, the study will focus on the hydrogen production from the reforming of glycerol in supercritical water by experiments. From the literatures, there are only a few works studying this reaction system. It is still of great challenge for this study to find a suitable catalyst and understand effects of operating parameters on the hydrogen production.

## **1.2 Objectives**

- To determine the effect of operating conditions for hydrogen production from reforming of glycerol under different reactions: i.e., steam reforming, partial oxidation, autothermal reforming, and supercritical water reforming by thermodynamic analysis and to determine appropriate operating conditions for hydrogen production.
- To select a suitable catalyst and to investigate the effect of operating parameters for hydrogen production from reforming of glycerol in supercritical water.

### **1.3 Scope of works**

1. Based on thermodynamic analysis, the effect of operating parameters including operating temperature, water to glycerol ratio, oxygen to glycerol ratio (in cases of steam reforming, partial oxidation and autothermal reforming) on reaction performances such as hydrogen production, hydrogen concentration, boundary of carbon formation are determined under isothermal condition.
2. Operating conditions which offer thermal neutral operation in which no external heat sources are required for operating the system of autothermal reforming of glycerol are calculated and its suitable operating condition which gives the highest hydrogen production is determined.
3. Thermodynamic study of the glycerol reforming in supercritical water is carried out to investigate effects of operating parameters including operating temperature, pressure and feed glycerol concentration on reaction performances and determined suitable operating conditions for experiments.
4. Catalysts suitable for hydrogen production from glycerol reforming in supercritical water are prepared based on available information of suitable catalysts from previous works on reforming of glycerol.
5. In experiments, the effects of operating conditions include feed rate, operating temperature, pressure, glycerol feed concentration and metal loading are investigated.

### **1.4 Dissertation overview**

This dissertation is organized as the list below.

Chapter II shows all theories relevant to this study. First, glycerol is described in term of properties, applications and, then crude glycerol from biodiesel production is also presented as the glycerol mixed with various impurities. Possible glycerol reactions to valuable gas, solid and liquid products are included. Thermodynamic

analysis is explained from derived equations based on Gibbs minimization method. Finally, the definition of supercritical water is explained and compared its properties with liquid and gas phases.

Chapter III reviews about steam reforming, partial oxidation and autothermal reforming processes. Reforming under supercritical water condition is reviewed as the next part with the history of supercritical water works since 1987 to present. Glycerol reforming catalyst development and operating parameters are reviewed to enhance the hydrogen production. Lastly, the glycerol mechanisms are also reviewed to explain how to reach these various products.

Chapter IV describes the catalyst preparation, catalyst characterization techniques (i.e. XRD, BET, TGA, SEM, and TEM), experimental set up. Equipment details are also explained including high pressure pump, syringe pump, preheater, reactor, cooling unit, mass flow controller, back pressure regulator, gas-liquid separator, and gas chromatography.

Chapter V presents the thermodynamic analysis of hydrogen production from glycerol at energy self-sufficient conditions. The hydrogen production includes steam reforming, partial oxidation, and autothermal reforming (reformer, and overall system level). The effect of operating parameters, i.e. *WGR*, *OGR* and temperature on the hydrogen production, carbon formation, and net energy are investigated.

Chapter VI studies the effect of mode i.e. *Single-feed* and *Split-feed* modes of operation on hydrogen production from glycerol at thermal neutral conditions using thermodynamic analysis. Two levels of system of interest (reformer and overall system) are considered. The results in term of yield of H<sub>2</sub>, by-products, and carbon formation are compared.

Chapter VII presents the hydrogen production from glycerol reforming in supercritical water by thermodynamic analysis. Equations of states are reviewed including SRK, PENG-ROB, SAFT, Duan, and others. The effect of operating temperature, pressure, and feed glycerol concentration are studied by using of PENG-ROB equation of state.

Chapter VIII discusses the hydrogen production from supercritical water reforming of glycerol in empty inconel 625 reactor without addition of catalyst. The effect of operating temperature, feed rate, and feed glycerol concentration are studied. Comparison between supercritical water reforming and conventional steam reforming is also examined in the similar reactor.

Chapter IX presents the catalytic supercritical water reforming of glycerol with cobalt based catalysts i.e. Co/La<sub>2</sub>O<sub>3</sub>, Co/ $\gamma$ -Al<sub>2</sub>O<sub>3</sub>, Co/ $\alpha$ -Al<sub>2</sub>O<sub>3</sub>, Co/La<sub>2</sub>O<sub>3</sub>, and Co/YSZ. The effect of operating temperature is studied for all catalyst. Then, the suitable catalyst for enhancing of hydrogen production is chosen to study the effects of feed rate, and the percents of cobalt loading.

Chapter X provides the experimental results of catalytic supercritical water reforming of glycerol using nickel based catalysts i.e. Ni/La<sub>2</sub>O<sub>3</sub>, Ni/ $\gamma$ -Al<sub>2</sub>O<sub>3</sub>, Ni/ $\alpha$ -Al<sub>2</sub>O<sub>3</sub>, Ni/La<sub>2</sub>O<sub>3</sub>, and Ni/YSZ. The effect of operating temperature is studied for all catalyst. Then, the suitable catalyst for enhancing of hydrogen production is chosen to study the effects of feed rate, the percents of nickel loading, and feed glycerol concentration.

Chapter XI presents the conclusion of this dissertation which comparison of all studied processes is given based on the H<sub>2</sub> yield as well as recommendations for future works.

# CHAPTER II

## THEORY

This chapter presents essential data about glycerol, a major by-product from biodiesel production. Components of crude glycerol from different biodiesel sources were provided. The possible value-added chemical products were presented from conversion of glycerol. Next, the various reactions of glycerol to produce gas, solid, and liquid products were summarized based on the previous literature reviews. Gibbs minimization is the calculation method employed in thermodynamic analysis part. Finally, supercritical water condition was explained by means of different properties from vapor, and liquid waters.

### 2.1 Glycerol

#### 2.1.1 Properties

Glycerol (or glycerin or glycerine or 1,2,3-propanedial) is a liquid organic substance at room temperature. The main physical properties include colorless, odorless, viscous liquid, non-toxic, non-volatile, and non-flammable (Table 2.1). Glycerol is also one kind of alcohol which has a high energy density (Xuan et al., 2008). When compared with other recent substances used in reforming processes, most substances are smaller in molecule size and have amount of carbon less than glycerol (C3) including methane (C1), methanol (C1), ethanol (C2), ethylene glycol (C2), dimethyl ether (C3). This fact might make some problems such as feeding difficulty due to its high viscosity, carbon formation problem from the ratio of C:H:O, high energy requirement for preheating and vaporization from boiling point.

#### 2.1.2 Applications

Glycerol has been utilized in many applications such as production of humectants in food industry, polyol based flexible foams, and to a lesser extent rigid polyurethane foams in foam and polymer industries, nitroglycerin in weapon industry,

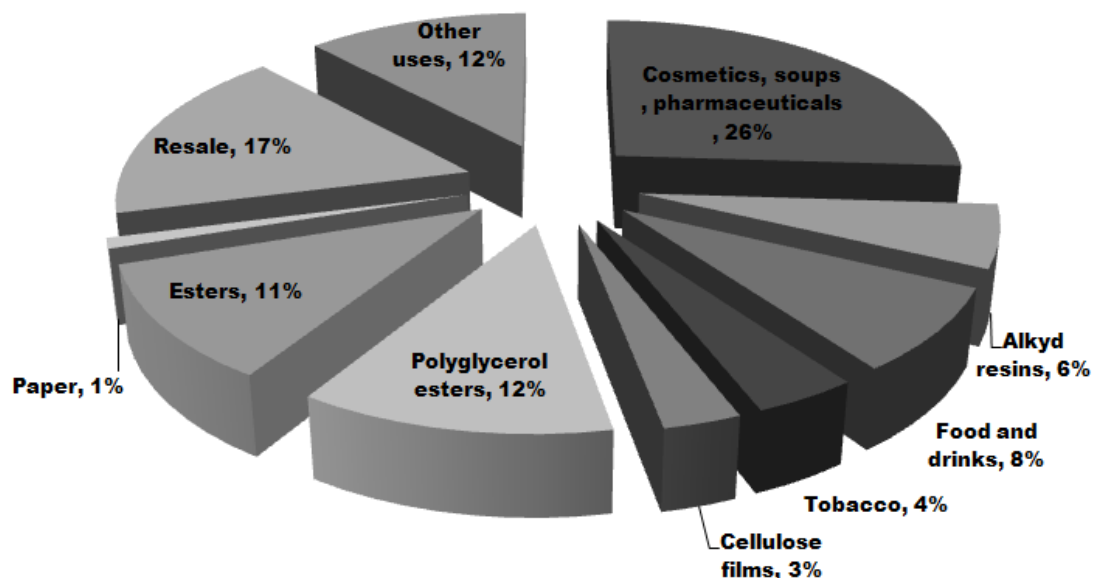
etc. (<http://en.wikipedia.org/wiki/Glycerol>). The main applications (about 26%) are for cosmetics, soaps and pharmaceuticals as shown in Figure 2.1. Considering the glycerol world market, glycerol had the high price of \$0.60-0.90/lb and then, over the past decade, the rapid growth of biodiesel production affected to the lowest price of \$0.05/lb (Dasari, 2006) and the old epichlorohydrin process for glycerol synthesis is no longer economical (<http://en.wikipedia.org/wiki/Glycerol>). Thus, the use of crude glycerol for other potential applications has been widely studied.

**Table 2.1** Physical properties of Glycerol (Perry and Green, seventh edition, 1997; <http://en.wikipedia.org/wiki/Glycerol>).

<b>Formula</b>	<b>CH<sub>2</sub>OH·CHOH·CH<sub>2</sub>OH, C<sub>3</sub>H<sub>5</sub>(OH)<sub>3</sub>, and C<sub>3</sub>H<sub>8</sub>O<sub>3</sub></b>	
<b>Formula weight</b>		92.09
<b>Form and color</b>		Colorless/liquid
<b>Specific gravity</b>		1.260 at 323 K (50°C) referred to water at 277 K(4°C)
<b>Melting point (K)</b>		290.9 (17.9°C)
<b>Boiling point (K)</b>		563 (290°C)
<b>Viscosity (Pa·S)</b>		1.5
	Water	∞
<b>Solubility in</b>	Alcohol	∞
<b>100 parts</b>	Ether	Insoluble

Normally, the conversion of glycerol can be broken down into two classes: i) oxidation or reduction of the glycerol into other three carbon compounds as shown in Table 2.2 or ii) reaction of glycerol with other molecules to form new species as shown in Figure 2.2 (Johnson et al., 2007). A recently significant advance is the improvement of a synthetic route to propylene glycol (1,2-propanediol) from glycerol,

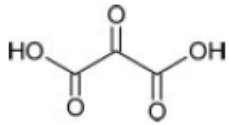
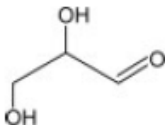
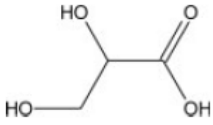
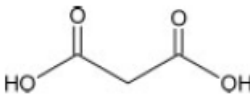
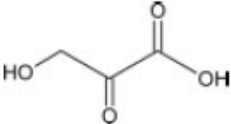
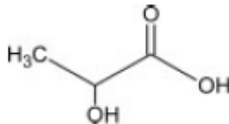
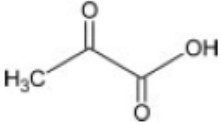
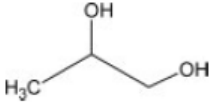
which represents a viable alternative to the classic petrochemical route from propylene (Moser, 2009).



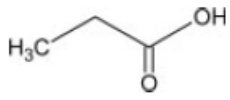
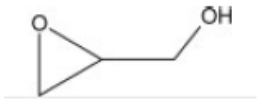
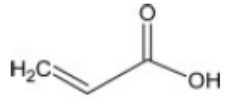
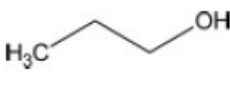
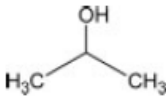
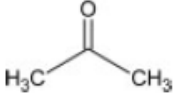
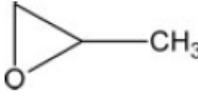

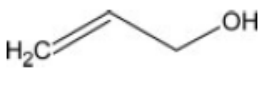
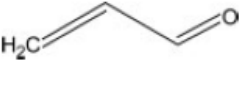
**Figure 2.1** Distribution of glycerol consumption in different products and industries (Bondioli, 2003)

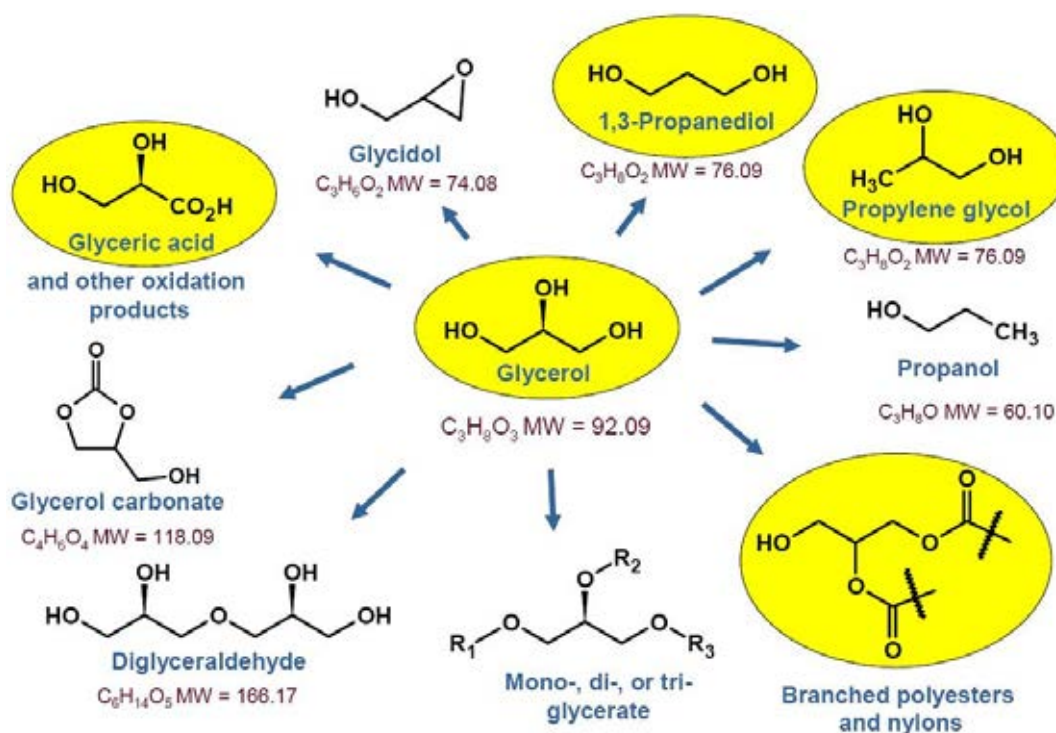
**Table 2.2** List of compounds which can be produced from glycerol (Johnson et al., 2007)

Name	Chemical formula	Chemical structure	Price (\$/lbs)	US capacity (MMlbs)
Glycerol	$C_3H_8O_3$		0.05-0.45	250
Tartronic acid	$C_3H_3O_5$		N/A	N/A
Dihydroxyacetone	$C_3H_6O_3$		2.00	N/A

Name	Chemical formula	Chemical structure	Price (\$/lbs)	US capacity (MMlbs)
Mesoxalic acid (Ketomalonic acid)	$C_3H_2O_5$		Likely high	N/A
Glyceraldehydes	$C_3H_5O_3$		N/A	N/A
Glyceric acid	$C_3H_6O_4$		Likely high	N/A
Malonic acid	$C_3H_4O_4$		14	<1
Hydroxypyruvic acid	$C_3H_4O_4$		High	N/A
Lactic acid	$C_3H_6O_3$		0.70-0.85	<5
Pyruvic acid	$C_3H_4O_3$		High	Small
Propylene glycol	$C_3H_8O_2$		0.44-1.00	1410



Name	Chemical formula	Chemical structure	Price (\$/lbs)	US capacity (MMlbs)
Propionic acid	$C_3H_6O_2$		0.46-0.62	440
Glycidol	$C_3H_6O_2$		>\$11,000	N/A
Acrylic acid	$C_3H_5O_2$		0.45-1.01	2880
Propanol	$C_3H_8O$		0.52	260
Isopropanol	$C_3H_8O$		0.28-0.49	1965
Acetone	$C_3H_6O$		0.1325-0.4225	3441
Propylene oxide	$C_3H_6O$		0.64-0.795	5190
Propionaldehyde	$C_3H_6O$		0.40	400
Allyl alcohol	$C_3H_5O$		1.00	60
Acrolein	$C_3H_4O$		0.64	>250



**Figure 2.2** Applications of glycerol ([www.chemistryinnovation.co.uk](http://www.chemistryinnovation.co.uk))

### 2.1.3 Crude glycerol

Crude glycerol is also called bio-glycerol that is a by-product from biodiesel production via tranesterification. Slinn et al. (2007) reported that glycerol by-products consist of 40% fatty matter, 33% glycerol, 23% methanol, 3.8% ash and 3.2% water. The main impurities including methanol and fatty matters can also react with steam but are not expected to give the same yield as pure glycerol. Moreover, ash and sulphur would cause problems with fouling of catalyst surfaces. However, the impurities of crude glycerol depend on many variables such as sort of vegetable oil, alcohol, catalyst, and temperature in biodiesel production. Thus, analysis of crude glycerol might be essential before studying of crude glycerol applications. Tables 2.3 and 2.4 show the components of crude glycerol and compositions of crude glycerol from biodiesel industries.

**Table 2.3** Components of crude glycerin (Douette et al., 2007)

<b>Proximate analysis (% dry basis)</b>	
<b>Ash</b>	1.20
<b>Volatile matter</b>	96.57
<b>Fixed carbon</b>	2.23
<b>Heating value (MJ/kg)</b>	28.8
<b>Ultimate analysis (% dry basis)</b>	
<b>C</b>	58.20
<b>H</b>	10.58
<b>N</b>	0.19
<b>S</b>	0.01
<b>Ash</b>	1.20
<b>O</b>	29.82
<b>Ash components (% of fuel, dry basis)</b>	
<b>Si</b>	0.065
<b>Al</b>	0.0141
<b>Ti</b>	<0.0001
<b>Fe</b>	0.0022
<b>Ca</b>	0.0012

---

<b>Mg</b>	0.0008
<b>Na</b>	0.0062
<b>K</b>	0.5445
<b>P</b>	0.0037

**Metals (mg/kg fuel)**

---

<b>As</b>	0.0204
<b>B</b>	<0.4
<b>Cd</b>	<0.06
<b>Pb</b>	<0.6
<b>Mn</b>	0.2398
<b>Hg</b>	<0.0001
<b>Mo</b>	<0.06
<b>Se</b>	<0.01
<b>Zn</b>	0.0177

---

**Table 2.4** Compositions of crude glycerol in wt% obtained from biodiesel industry (Dasari, 2006)

<b>Component</b>	<b>Analysis method</b>	<b>Crude glycerol-1<sup>a</sup></b>	<b>Crude glycerol-2<sup>b</sup></b>	<b>Treated glycerol<sup>c</sup></b>
<b>Glycerol</b>	ISO 2879-1975	58.25	72.86	80.8
<b>Ash</b>	ISO 2098-1972	9.86		6.71
<b>MONG<sup>d</sup></b>	ISO 2464-1973	8.36		1.47
<b>Water</b>	Karl Fischer	1.20	0.925	10.3
<b>Methanol</b>	GC	22.33	0	0.72
<b>pH</b>	pH meter	12.73		3.93
<b>Yield (%)</b>		59.47	53.58	3.23

<sup>a</sup>Crude glycerol obtained just after biodiesel production

<sup>b</sup>Crude glycerol from which methanol and some water was stripped out

<sup>c</sup>Crude glycerol in which the excess base catalyst is neutralized with hydrochloric acid and methanol is striped out

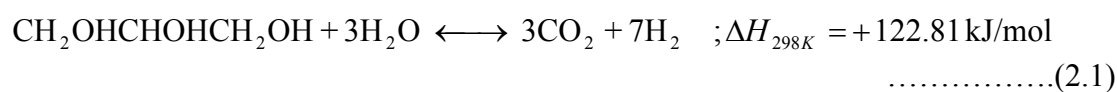
<sup>d</sup>Matter Organic Non-Glycerol

## 2.2 Reactions of glycerol conversion

As we have known that glycerol is an organic liquid compound which has three carbons in the molecule. Various reactions from glycerol conversion would be classified based on the phase of products as follows.

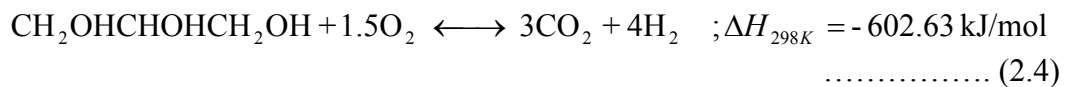
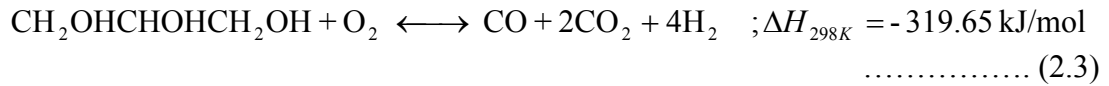
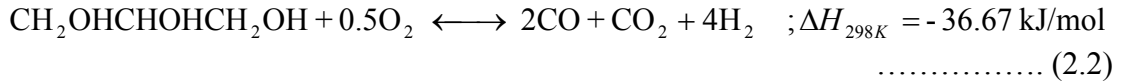
### 2.2.1 Reactions to produce gas products

The overall reaction of glycerol Steam Reforming (SR):

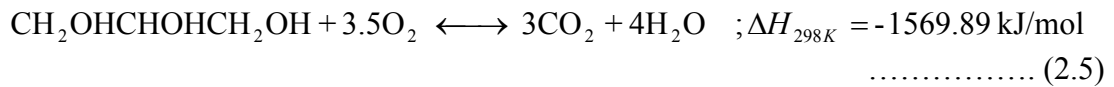


Glycerol oxidations are divided to Partial Oxidation (POX) and Oxidation (OX):

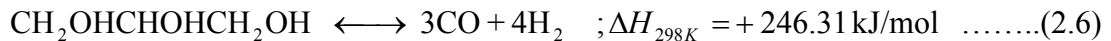
Partial Oxidations (POX):



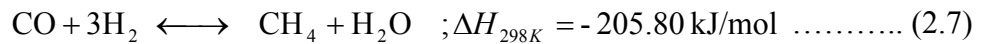
Oxidation or Combustion (OX):



Decomposition Reaction (DR):



Methanation (MET):



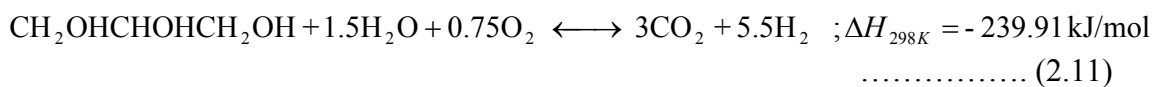
Methane CO<sub>2</sub> Reforming (MCR):



Water Gas Shift (WGR or reverse of this is called RWGS):



Glycerol Autothermal Steam Reforming (ATSR) :

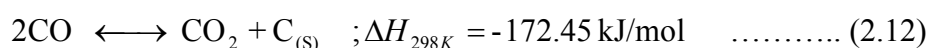


Dauenhauer et al., 2006 reported that Reaction (2.11) is exothermic, and the thermal neutral ( $\Delta H = 0$ ) would occur when temperature changed. However,  $\Delta H$  strongly depends on the temperature which Equation (2.11) could have the other stoichiometric numbers at that temperature for adjusting to be at the thermal neutral condition.

### 2.2.2 Reactions to produce solid products

Solid product means carbon which was possibly occurred in five reactions (Equations (2.12)-(2.16)). All reaction should be avoided in the process because of carbon plugging.

Boudouard reaction:



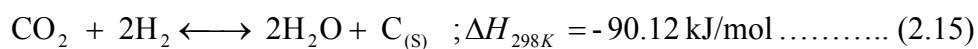
Methane cracking:



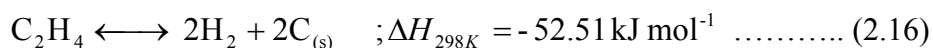
Reduction of CO:



Reduction of CO<sub>2</sub>:

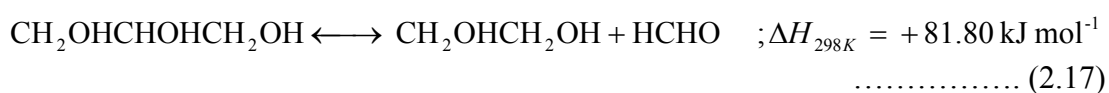


C<sub>2</sub>H<sub>4</sub> cracking:

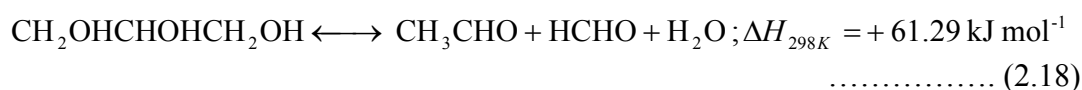


### 2.2.3 Reactions to produce liquid products

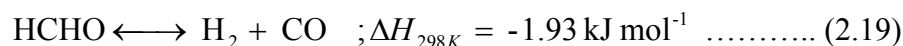
Fragmentation reaction of glycerol



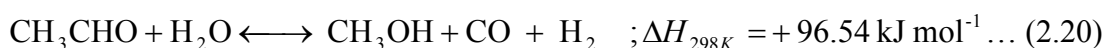
Decomposition of glycerol:



Decomposition of formaldehyde:



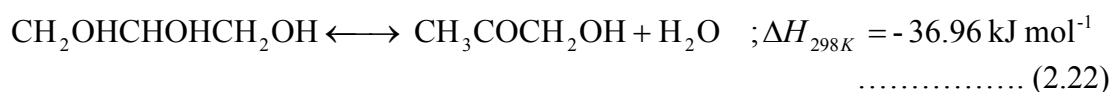
Acetaldehyde steam reforming:



Methanol steam reforming:



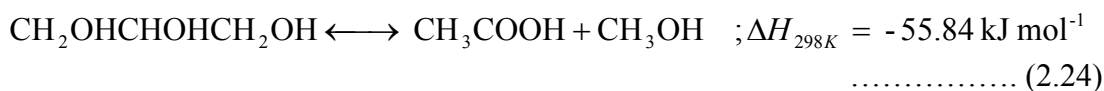
Dehydration of glycerol:



Dehydration of glycerol:



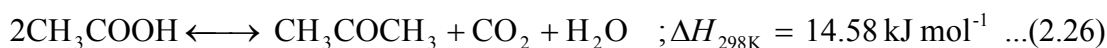
Decomposition of glycerol:



Decomposition of acetaldehyde:

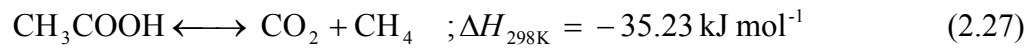


Decarboxylation of acetic acid:





Decomposition of acetic acid:



### 2.3 Thermodynamic analysis

The composition of any reacting system is the equilibrium of the composition which can be calculated by Gibbs free energy equation (Adhikari et al., 2007a). Gibbs free energy reaction values would predict the chance for a reaction to occur by the Minimization of total Gibbs free energy method. At the steady state, pressure and temperature of the system are constant, so the equations are given as follows:

$$dG = \sum_{i=1}^N \mu_i dn_i \quad (2.28)$$

$$G = \sum_{i=1}^N \mu_i n_i \quad (2.29)$$

The total Gibbs function can be written as follows:

$$\min_{n_i} (G^t)_{T,P} = \sum_{i=1}^N n_i G_i^0 + RT \sum_{i=1}^N n_i \ln \frac{\hat{f}_i}{f_i^0} \quad (2.30)$$

For reaction equilibrium in gas phase:

$$\hat{f}_i = \hat{\phi}_i y_i P \quad (2.31)$$

$$f_i^0 = P^0 \quad (2.32)$$

From  $G_i^0$  is set to zero for each chemical element in its standard state:

$$\Delta G^0 = \Delta G_{f_i}^0 \quad (2.33)$$

From the equations,  $N$  is the total number of components in the system;  $n_i$  is the variable that minimizes the value of Gibbs free energy. It can be solved two ways including i) the stoichiometric thermodynamic approach which is determined by a set

of stoichiometrically independent reactions, then typically chosen arbitrarily from a set of possible reactions, and ii) A non-stoichiometric thermodynamic approach value is set up by the direct minimization of the Gibbs free energy for a given set of species (Adhikari et al., 2007a). The advantages of non-stoichiometric thermodynamic approach included i) a selection of the possible set of reactions in that system is not necessary ii) no divergence occurs during the consumption, and iii) an accurate estimation of the initial equilibrium composition is not necessary (Garcia and Laborde, 1991). This research would calculate the equilibrium by using a non-stoichiometric thermodynamic approach. Lagrange's undetermined multiplier method was expressed as:

$$\Delta G_{f_i}^0 + RT \ln \frac{\hat{f}_i}{f_i^0} + \sum_k \lambda_k a_{ik} = 0 \quad (2.34)$$

$$\sum_{i=1}^N n_i \left( \Delta G_{f_i}^0 + RT \ln \frac{\hat{f}_i}{f_i^0} + \sum_k \lambda_k a_{ik} \right) = 0 \quad (2.35)$$

From the constraints of elemental balances:

$$\sum_{i=1}^N n_i a_{ik} = A_k \quad (2.36)$$

where  $a_{ik}$  is the number of atoms of element  $k$  in component  $i$ ,  $A_k$  is the total number of atoms of element  $k$  in the reaction mixture, and  $M$  is the total number of elements.

When solid carbon (graphite) is considered in the system, Gibbs energy of carbon is usually considered (Wang et al., 2008):

$$\bar{G}_{C(g)} = \bar{G}_{C(s)} = G_{C(s)} \cong \Delta G_{f_{C(s)}}^0 = 0 \quad (2.37)$$

However, for a temperature-steady process:

$$dG_{C(s)} = V_C dP \quad (2.38)$$

$V_C$  is the mole volume of solid carbon, and it can be regarded as a constant because it is less affected by temperature and pressure then, Equation (2.38) can be expressed as Equation (2.39):

$$G_{C(s)}(T, P) - G_{C(s)}(T, P^0) = V_C(P - P^0) \quad (2.39)$$

where  $G_{C(s)}(T, P^0)$  is assumed to be zero and  $V_C = 4.58 \times 10^{-6} \text{ m}^3/\text{mol}$ . Equation (2.39) is further expressed as Equation (2.40)

$$G_{C(s)}(T, P) = 4.58 \times 10^{-6}(P - P^0) \quad (2.40)$$

The minimization function of Gibbs energy as following Equation (2.41) is obtained by substituting Equation (2.30) by Equation (2.34) for gaseous species and by Equation (2.28) for solid species

$$\sum_{i=1}^{N-1} n_i \left( \Delta G_{f_i}^0 + RT \ln \frac{\hat{\phi}_i y_i P}{P^0} + \sum_k \lambda_k a_{ik} \right) + n_C G_{C(s)}(T, P) = 0 \quad (2.41)$$

The fugacity coefficient  $\hat{\phi}_i$  of each component in the gas mixture can be calculated according to the Soave-Redlich-Kwong equation of state; that is

$$P = \frac{RT}{V - b} - \frac{a(T)}{V(V + b)} \quad (2.42)$$

$$a(T) = a\alpha(T) = 0.42748 \frac{R^2 T_c^2}{P_c \alpha(T)} \quad (2.43)$$

$$b = 0.08664 \frac{RT_c}{P_c} \quad (2.44)$$

$$\alpha(T) = [1 + m(1 - T_r^{0.5})]^2 \quad (2.45)$$

$$T_r = \frac{T}{T_c} \quad (2.46)$$

$$m = 0.480 + 1.574\omega - 0.176\omega^2 \quad (2.47)$$

Accordingly, the fugacity coefficient  $\hat{\phi}_i$  can be calculated from the following equation:

$$\ln \hat{\phi} = \frac{b_i}{b_m} (Z - 1) - \ln \frac{P(V - b_m)}{RT} + \frac{a_m}{b_m RT} \left( \frac{b_i}{b_m} - \frac{2}{a_m} \sum_{j=1}^N y_j a_{ij} \right) \ln \left( 1 + \frac{b_m}{V} \right) \quad (2.48)$$

The mixture parameters used above in Equation (2.48) are defined by the mixture rules

$$a_m = \sum_i \sum_j y_i y_j a_{ij} \quad (2.49)$$

$$b_m = \sum_i y_i b_i \quad (2.50)$$

$$a_{ij} = (a_i a_j)^{0.5} (1 - k_{ij}) \quad (2.51)$$

The processes of simulation were operated by Aspen Plus software. It is a software program designed to build a process model and then simulate the model without tedious calculations for conceptual design, optimization, and performance monitoring. It can be also used for a wide variety of chemical engineering tasks. This program was used for all calculations consisting of material balances, energy balances, net of energy equals zero, and minimization of total Gibbs free energy for studying the effects of variables at each condition of the system. The RGibbs model was chosen in this analysis in order to minimize Gibbs free energy.

The conditions for glycerol reforming were given:

*Input:* Temperature: 298-1200 K, Pressure: 0.101325 MPa; for Supercritical water offers pressure: 19-30 MPa

*Reactants:* Glycerol (C<sub>3</sub>H<sub>8</sub>O<sub>3</sub>), Water (H<sub>2</sub>O), Oxygen (O<sub>2</sub>), Nitrogen (N<sub>2</sub>),.

*Flow rates:* Glycerol (1 mol/s), WGR = 0-12 (Water = 0-12 mol/s), OGR = 0-3 (Oxygen = 0-3 mol/s); for Supercritical water offers >>12 that means around 0-30 wt.% glycerol.

*Operating conditions:* Temperature: 600-1200 K, this range temperature is higher than boiling temperature of glycerol (563 K) at atmospheric pressure, Pressure: 0.101325 MPa.

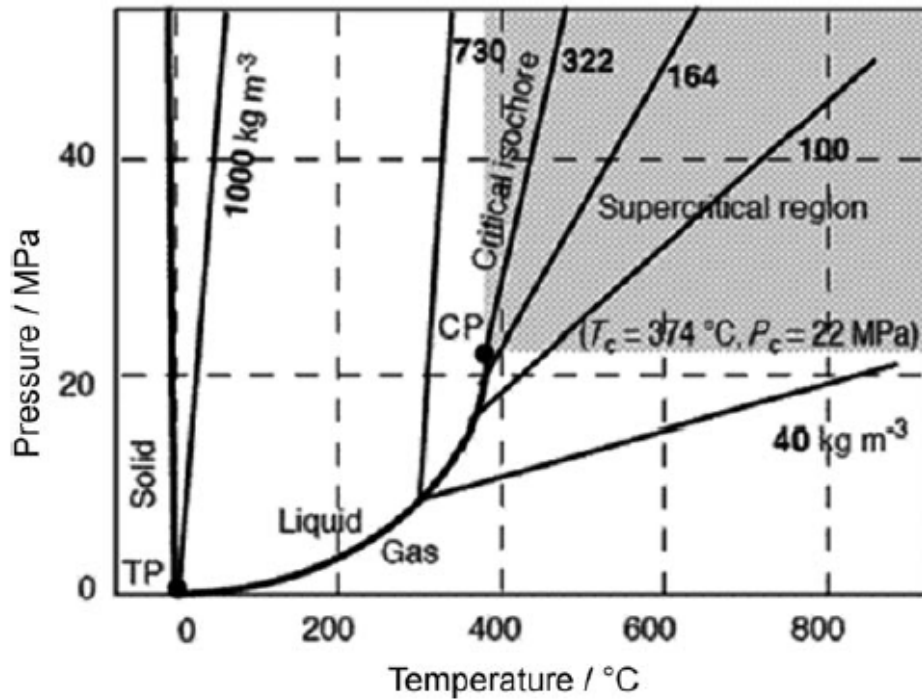
*Identify possible products:* Unreacted glycerol ( $C_3H_8O_3$ ), Water( $H_2O$ ), Hydrogen ( $H_2$ ), Carbon monoxide (CO), Carbon dioxide ( $CO_2$ ), Methane ( $CH_4$ ), Carbon (C(s)), Oxygen ( $O_2$ ), Unreacted Nitrogen ( $N_2$ ). Only unreacted glycerol in liquid phase, all gas products, and carbon formation were identified as possible products.

*Property method and Base method:* SRK (Soave-Redlich-Kwong equation) (Wang et al., 2008; Li et al., 2008); for Supercritical water offers SRK (Lu et al., 2007) and Peng Robinson (PR) (Tang and Kitigawa, 2005)

## **2.4 Supercritical water**

Supercritical water is defined as water that is compressed and heated to its critical pressure and temperature, respectively, namely above 221 bar (22.1 MPa) and 647 K (374°C) from Figure 2.3. Supercritical fluids are distinguished by properties such as densities, viscosities and other properties that are intermediate between gas and liquid. Moreover, they also exhibit diffusivity and good heat transporting properties (Tables 2.5, 2.6, and 2.7) (Broll et al., 1999; Székely, 2007; Loppinet-Serani et al., 2008)

The structure and properties of water change dramatically when its temperature rises because hydrogen bonds are broken. Viscosity of water is one of properties that decrease drastically with increasing temperature. This low viscosity provides high diffusion coefficients, making supercritical water a very good medium to support very fast reactions.



**Figure 2.3** Phase diagram for water (Cansell et al., 1998)

**Table 2.5** Evolution of themophysical properties of pure water as a function of temperature and pressure (Loppinet-Serani et al., 2008).

Property		Liquid	Supercritical	Gas
<b><i>T</i> (K)</b>	Temperature	298 (25°C)	673 (400°C)	423 (150°C)
<b><i>P</i> (MPa)</b>	Pressure	10	30	0.1
<b><i>ρ</i> (kg/m<sup>3</sup>)</b>	Density	999	353	0.52
<b><i>η</i> (Pa.s)</b>	Dynamic viscosity	90 x 10 <sup>-5</sup>	4.5 x 10 <sup>-5</sup>	1 x 10 <sup>-5</sup>
<b><i>D</i> (m<sup>2</sup>s<sup>-1</sup>)</b>	Diffusion coefficient for small particles	≈ 1 x 10 <sup>-9</sup>	≈ 1 x 10 <sup>-8</sup>	1 x 10 <sup>-5</sup>
<b><i>ε<sub>r</sub></i></b>	Relative static permittivity	78.9	5.9	1.5

Under ambient conditions, liquid water has a high dielectric constant and polar compounds are very soluble, but water is a poor solvent for substances of low dielectric constants such as hydrocarbons. As the temperature rises, the dielectric constant of water decreases. Accordingly, supercritical water has a very low dielectric constant (Table 2.8), which changes its behavior as a solvent. Hence, supercritical water is able to dissolve nonpolar compounds (hydrocarbons). As an example, at 298 K the solubility of benzene in water is very low (0.07 wt.%), even as under supercritical conditions, benzene and water are miscible in all proportions. By contrast, supercritical water is a poor solvent for salts.

**Table 2.6** Physicochemical properties of water as a function of temperature and pressure (Broll et al., 1999)

<b>Properties</b>	<b>Normal water</b>	<b>Subcritical water</b>	<b>Supercritical water</b>		<b>Superheated steam</b>
<b><math>T</math> [K]</b>	298 (25°C)	523 (250°C)	673 (400°C)	673 (400°C)	673 (400°C)
<b><math>P</math> [MPa]</b>	0.1	5	25	50	0.1
<b><math>\rho</math> [g cm<sup>-1</sup>]</b>	0.997	0.80	0.17	0.58	0.0003
<b><math>\varepsilon</math></b>	78.5	27.1	5.9	10.5	1
<b><math>pK_w</math></b>	14.0	11.2	19.4	11.9	-
<b><math>c_p</math> [kJ kg<sup>-1</sup> K<sup>-1</sup>]</b>	4.22	4.86	13	6.8	2.1
<b><math>\eta</math> [mPa s]</b>	0.89	0.11	0.03	0.07	0.02
<b><math>\lambda</math> [mW m<sup>-1</sup> K<sup>-1</sup>]</b>	608	620	160	438	55

**Table 2.7** Comparison of gases, supercritical fluids, and liquids (Székely, 2007).

	Density (kg/m <sup>3</sup> )	Viscosity (μPa's)	Diffusivity (mm <sup>2</sup> /s)
<b>Gases</b>	1	10	1-10
<b>Supercritical Fluids</b>	100-1000	50-100	0.01-0.1
<b>Liquids</b>	1000	500-1000	0.001

**Table 2.8** Dielectric constants for water and some general organic solvents (Loppinet-Serani et al., 2008)

Solvent	Dielectric constant
<b>Liquid water (298 K)</b>	78.5
<b>Ethanol (298 K)</b>	24.5
<b>Haxane (298 K)</b>	1.9
<b>Supercritical water (773 K, 24 MPa)</b>	1.2



# CHAPTER III

## LITERATURE REVIEWS

In this chapter, the literature reviews involving glycerol reforming are provided. It is divided into five topics. Firstly, previous works on steam reforming are presented. Next, partial oxidation and autothermal reforming are reviewed and compared with steam reforming. Then, the reforming in supercritical water is described and made a list of previous works from the past up to now by observing in feedstock, reactor type, reactor material, operating conditions, glycerol conversion, and products. Glycerol reforming catalyst for enhancing the hydrogen production is summarized in the next part including steam reforming, aqueous reforming, autothermal reforming and supercritical water reforming. Finally, the mechanism of glycerol reforming is reviewed.

### 3.1 Steam reforming

Steam reforming is a conventional catalytic process for hydrogen production by separating hydrogen from carbon with the presence of steam at high temperature (Tsolakis et al., 2003). It is highly endothermic so the large extent of external heat source is required. This process can be continuously enhanced by improving the catalysts, operating conditions and heat transfer to achieve better performance (Yanbing et al., 2007). Normally, this process has been extensively used for the fuel reforming of natural gas (Dicks, 1996), methane (Takeguchi et al., 2002), methanol (Qia et al., 2007), and ethanol (Rossi et al., 2009). The recent works started to use glycerol that is a by-product from biodiesel production by glycerol steam reforming (Equation (2.1)). The equation shows the maximum hydrogen production from a theoretical value of 7 mol of H<sub>2</sub> per mol of glycerol. It can be also implied that low pressure, high temperature, and high steam ratio are favorable conditions for the glycerol steam reforming.

The side reactions can also be occurred as shown in Equations (2.6)-(2.10), (2.12)-(2.16), depending on variable conditions. Decomposition reaction (Equation (2.6)) is a highly endothermic reaction which converts glycerol to synthesis gas, because of high oxygen content in glycerol molecule (Dauenhauer et al., 2006). Methanations (Equations (2.7)-(2.9)) produce methane which is an unflavored product. Methane always competes against  $H_2$ , especially during low temperatures and water conditions (Adhikari et al., 2007a). Water gas shift reaction (Equation (2.10)) results in slight decrease of hydrogen production at high temperature conditions or more than 960 K (Adhikari et al., 2007a). For carbon formations (Equations (2.12)-(2.16)) there are several undesirable reactions that produce solid carbon due to the decomposition  $CO$ , and/or  $CH_4$ , and/or  $C_2H_4$  and/or the reaction of  $CO_2$ , and/or  $CO$  with  $H_2$ . When they occur, they cause blockage of catalyst pores, plugging at the outlet tubing and in severe cases breakdown of the reactor (Slinn et al., 2008). In general, excess water, oxygen and catalyst are utilized to prevent the coke formation at high temperatures.

Wang et al. (2008) calculated thermodynamic analysis of glycerol steam reforming using direct minimization of total Gibbs free energy method with the Soave-Redlich-Kwong equation of state for calculating the fugacity coefficient of each component in the gas mixture. They found the optimum conditions at a temperature of 925-975 K, atmospheric pressure and water/glycerol ratios of 9-12 under which no carbon formation occurs.

Adhikari et al. (2007b) simulated a thermodynamic analysis coupled with experimentation for the glycerol steam reforming process by Ni/MgO catalyst. The equilibrium concentrations of different compounds were calculated by the direct minimization of total Gibbs free energy method. The best conditions for producing hydrogen were found at a temperature of  $> 900$  K, atmospheric pressure, and water/glycerol ratio of 9 for which methane production is minimized and carbon formation is thermodynamically inhibited. However, experimental results are still far from thermodynamic equilibrium.

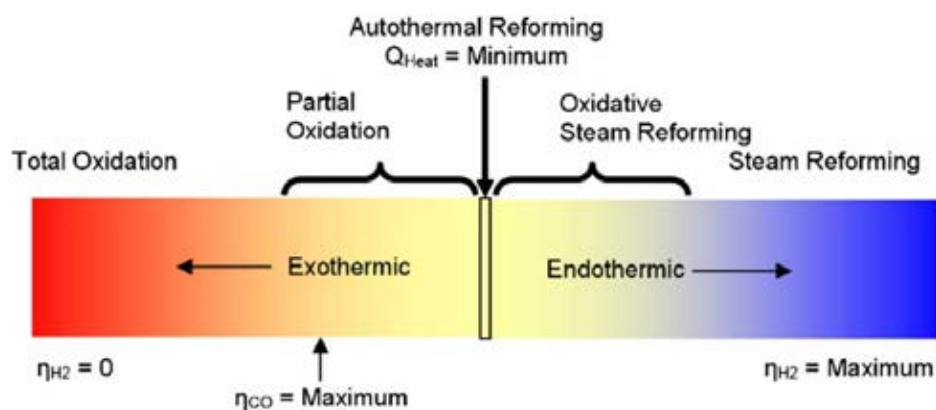
Slinn et al. (2008) studied the steam reforming of glycerol and biodiesel by-product to make hydrogen production with a platinum alumina catalyst. The results showed that thermodynamic theory can be used to predict reformer performance. The optimum conditions for glycerol reforming were 1133 K, 0.12 mol/min glycerol flow per kg of catalyst Pt/Al<sub>2</sub>O<sub>3</sub>, and 2.5 steam/carbon ratio that offered hydrogen selectivity of 70% and glycerol conversion to gas of 100%. By-product glycerol performed slightly worse with a lower yield (around 70% but selectivity was the same) and more carbon deposition.

### **3.2 Partial oxidation and autothermal reforming**

Partial oxidation is an exothermic reaction, as the incomplete oxidation of the fuel stream or partially burns a fuel stream with a sub-stoichiometric amount of air (Adams et al., 2004). This incomplete oxidation generates heat and fractionates the feed to smaller molecules (Rabenstein and Hacker, 2008). The use of oxygen in the feedstock reduces the need of energy extensively owing to the exothermic heat taking place in a reformer (Ahmed et al., 2001). This reaction can also be carried out at high temperature without the use of catalyst (Docter and Lamm, 1999). On the other hand, from Equations (2.2)-(2.4), 4 mol of H<sub>2</sub> is theoretically generated per mol of glycerol that is less than the hydrogen production from steam reforming reaction. It can imply that oxygen suppresses the hydrogen production; however the energy requirement from external heat sources would be decreased also. Generally speaking, partial oxidation processes cause relatively the most significant CO<sub>2</sub> emissions (Turpeinen et al., 2008). Conversely, catalyst has also brought for studying in this reaction which is called Catalytic partial oxidation. It provides sufficient heat internally to maintain a temperature of 873-1473 K (600-1200°C) capable of achieving equilibrium product concentrations at millisecond residence times (Dauenhauer et al., 2006). Auxiliary improvements in hydrogen production need steam addition to the reactant mixture. With appropriate adjustment of air (O<sub>2</sub>) and steam, an adiabatically point, or thermally neutral point (net heat energy of the reformer equals zero) can be occurred that is called Autothermal reforming (see Figure 3.1). It combines endothermic steam reforming and exothermic partial oxidation. Fuel conversion can occur faster and

without an external heat source applied to the catalyst in the process. Nevertheless, for the real operation, it might be difficult to continue at adiabatic condition without external heat source. It should be controlled to keep under slightly exothermic reaction (Xuan et al., 2008). In addition, excess steam (water), oxygen and catalyst can be also utilized to prevent the carbon formation at high temperature.

Wang et al. (2009) calculated thermodynamic analysis of hydrogen production from glycerol autothermal reforming by the Gibbs free energy minimization. The range of conditions included temperature of 700-1000 K (427-727°C), steam to glycerol ratio of 1-12 and oxygen to glycerol ratio of 0.0-3.0. They found the thermal neutral conditions that can be obtained at oxygen to glycerol ratios of around 0.36 at 900 K and 0.38–0.39 at 1000 K. Under these thermo neutral conditions, the highest mol of hydrogen produced are 5.62 (900 K) and 5.43 (1000 K) with a steam to glycerol ratio of 12. In addition, methane and carbon formation can be effectively eliminated at this condition.



**Figure 3.1** Different operating conditions for fuel reforming (Rabenstein and Hacker, 2008)

Dauenhauer et al. (2006) examined the autothermal steam reforming of glycerol and calculated all equilibrium calculations by HSC software. The optimum conditions were found with RhCeWc catalyst (2.5 wt.% Rhodium, 2.5 wt.% Ceria on a 5 wt.%  $\gamma$ -Al<sub>2</sub>O<sub>3</sub> washcoat supported on 80 ppi  $\alpha$ -Al<sub>2</sub>O<sub>3</sub> monoliths) at steam/carbon of 4.5, carbon/oxygen of 0.9, temperature of 1135 K (862°C), GHSV of 10<sup>5</sup> h<sup>-1</sup> by

glycerol conversion of 100% and hydrogen selectivity of 79%. The results are interpreted for the mechanism as occurring primarily through surface reactions initiated by adsorption on metals through hydroxyl oxygen lone pairs to form surface alkoxides, which decompose almost exclusively to H<sub>2</sub> and C<sub>1</sub> carbon compounds. Finally, comparison of reforming technologies is shown in Table 3.1.

**Table 3.1** Comparison of reforming technologies (Holladay et al., 2009)

<b>Technology</b>	<b>Advantages</b>	<b>Disadvantages</b>
<b>Steam reforming</b>	<ul style="list-style-type: none"> <li>• Most extensive industrial experience.</li> <li>• Oxygen not required.</li> <li>• Lowest process temperature.</li> <li>• Best H<sub>2</sub>/CO ratio for H<sub>2</sub> production.</li> </ul>	<ul style="list-style-type: none"> <li>• Highest air emission.</li> </ul>
<b>Autothermal reforming</b>	<ul style="list-style-type: none"> <li>• Lower process temperature than POX.</li> <li>• Lower methane slip.</li> </ul>	<ul style="list-style-type: none"> <li>• Limited commercial experience.</li> <li>• Require air or oxygen.</li> </ul>
<b>Partial oxidation</b>	<ul style="list-style-type: none"> <li>• Decreased desulfurization requirement.</li> <li>• No catalyst required.</li> <li>• Low methane slip.</li> </ul>	<ul style="list-style-type: none"> <li>• Low H<sub>2</sub>/CO ratio.</li> <li>• Very high processing temperature.</li> <li>• Soot formation / handling add process complexity.</li> </ul>

### 3.3 Reforming in Supercritical water

Supercritical fluid has many advantages to be used in various reactions as a reaction medium due to fast heat and mass transfer. Supercritical water (SCW) is an environmentally friendly fluid and possesses properties quite different from liquid water at ambient conditions especially, the dielectric constant of supercritical water. It is much less than that of ambient water and hydrogen bonding is much weaker (Byrd et al., 2007; Loppinet-Serani et al. 2008). Therefore, supercritical water behaves like an organic solvent and is completely miscible with organic materials. Accordingly with supercritical water, it is possible to conduct reactions with organic compounds in a single fluid phase which would otherwise occur in a multiphase system under conventional conditions (Byrd et al., 2007). The hydrocarbons reforming can be carried out in the presence of supercritical water instead of steam, as used in conventional technologies, to produce hydrogen at a very high pressure (Gadhe and Gupta, 2005). The density of supercritical water is higher than that of steam, resulting in a higher space time yield, and higher thermal conductivity and specific heat that are supportive in accomplishing of the endothermic reforming reactions (Byrd et al., 2008). Hydrogen is produced at a high pressure that can be stored directly, hence avoiding the problems associated with its compression. The process becomes economical as the compression work is reduced due to the low compressibility of liquid feed compared to that of gaseous hydrogen (Boukis et al., 2003a). Supercritical water can reduce carbon formation on the catalyst as it is a good solvent for the intermediate carbon precursors (Williams and Onwudili, 2006). Gadhe and Gupta. (2005) reported that the metals catalyzing methanation reactions were arranged in the reducing order of methanation activity as  $Ru > Ni > Co > Fe > Mo$  thus the tubular reactor that was made from Inconel 600 (an alloy of Ni, Cr, and Fe), which has an important methanation activity.

Tang and Kitigawa (2005) calculated thermodynamic analysis with direct Gibbs free energy minimization of supercritical water gasification of biomass process. The algorithm based on Peng–Robinson EoS formulations and direct Gibbs free energy minimization can guarantee the convergence to the correct solution. For the supercritical water reforming of methanol, it was observed that an increase in feed

methanol concentration causes a decrease of hydrogen composition. By contrast, it favored the formation of methane. ( $T$ : 973 K;  $P$ : 27.6 MPa; residence time: 6 s). An increase of temperature caused an increase of hydrogen composition while a decrease of methane composition (feed concentration of methanol 15 wt.%). However, the calculations were in poor agreement with the experimental measurements. When they ignored methane as a gas product in their calculations, the model predictions could fit the experiment measurements quite well, indicating that methanation reaction was a very slow step in supercritical water methanol reforming. The hydrogen in dry gas (mole fraction) was around 0.75.

Gadhe and Gupta (2005) studied hydrogen production by methanol reforming. Suppression of methane formation was considered. The reforming of methanol was carried out in supercritical water in a tubular reactor made of Inconel 600. The factors favoring the methanation reactions are high pressure, high residence time, and low steam-to-carbon ratio. Methanation can be reduced greatly by lowering the residence time so that the equilibrium is not allowed to be reached. The reactor made of Ni-Cu tubing minimizes the formation of methane. Methanation can also be reduced with the addition of  $K_2CO_3$  or KOH in the aqueous methanol feed.

Lu et al. (2007) studied thermodynamic modeling and analysis of biomass gasification for hydrogen production in supercritical water. Chemical equilibrium model is based on minimizing Gibbs free energy. A high-pressure gas-liquid equilibrium model was proposed based on modified universal functional activity coefficient (UNIFAC) model, Soave-Redlich-Kwong (SRK) equation of state and modified Huron-Vidal second-order (MHV2) mixing rule. The highest  $H_2$  yield of 88.623 mol/kg dry biomass is obtained at 923 K, 25MPa with 5 wt.% dry biomass content.

Byrd et al. (2007) studied hydrogen production from ethanol by reforming in supercritical water using Ru/ $Al_2O_3$  catalyst. Hydrogen formation was favored at high temperature and at high water-to-ethanol ratio. The formation of methane can be suppressed by operating at an optimal residence time, high reactor temperature, and a low feed concentration of ethanol. Excellent conversion in reaction time as short as 4

s is achieved. Pressure has a negligible effect on hydrogen yield above the critical pressure, and for less than 10 wt.% ethanol concentration in the feed, there was negligible coke formation. On the basis of the products obtained, a reaction mechanism is discussed. An activation energy of  $65.3 \text{ kJ mol}^{-1}$  was observed.

Consequently the studying about reforming in supercritical water can be concluded on the lists below.



**Table 3.2** History of hydrogen production from organic feedstock under sub, supercritical water conditions

Year	Feedstock	Reactor	Catalyst	Conditions	Conversion, (-)	Main gas products	Liquid products	Reference
1987	ethanol, propanol, ethylene glycol, glycerol, acetaldehyde, formaldehyde	annulus reactor (Hastelloy C276)	no catalyst, H <sub>2</sub> SO <sub>4</sub> , HCl, NaOH	<i>T</i> : 573-773 K <i>P</i> : 34.5 MPa $\tau$ : 8-183 s <i>C</i> <sub>0</sub> : 0.5-1 M <i>C</i> <sub>cat</sub> : 0.005-0.05 M	0.02-0.85	H <sub>2</sub> , CO <sub>2</sub> , CH <sub>4</sub> , CO, C <sub>2</sub> H <sub>4</sub> , C <sub>2</sub> H <sub>6</sub> , C <sub>3</sub> H <sub>6</sub> , C <sub>3</sub> H <sub>8</sub>	ethyl ether, acetaldehyde, acrolein, crotonaldehyde	Rameyya et al. (1987)
1993	glucose, formic acid, acetic acid	9.94 cm <sup>3</sup> coiled Hastelloy C276, Inconel 625 capillary tubes	no catalyst	<i>T</i> : 873 K <i>P</i> : 34.5 MPa $\tau$ : 34 s <i>C</i> <sub>0</sub> : 0.1-1 M	NA	H <sub>2</sub> , CO <sub>2</sub> , CO, CH <sub>4</sub>	NA	Yu et al. (1993)
1996	glycerol, glucose, cellobiose, biomass, waste (methanol, methyl ethyl ketone, ethylene glycol, acetic acid, phenol)	tubular reactor with 9.53 mm o.d. and 4.75 mm i.d. (Inconel 625)	activated carbons	<i>T</i> : 873 K <i>P</i> : 34.5 MPa $\tau$ : 27.7-44 s <i>C</i> <sub>0</sub> : 1.2 M	0.48-1	H <sub>2</sub> , CO <sub>2</sub> , CH <sub>4</sub> , CO	NA	Xu et al. (1996)
1998	sewadge sludge, saw dust, corb starch gel	30.88 cm <sup>3</sup> flow reactor (Hastelloy C276)	no catalyst	<i>T</i> : 923 K <i>P</i> : 28 MPa <i>C</i> <sub>0</sub> : 2-12 wt% <i>F</i> : 1-4 g/min WHSV: 0.96-3.81 hr <sup>-1</sup>	NA	H <sub>2</sub> , CO <sub>2</sub> , CH <sub>4</sub> , CO	NA	Xu et al. (1998)

Year	Feedstock	Reactor	Catalyst	Conditions	Conversion, (-)	Main gas products	Liquid products	Reference
2000	corn, potato starch gels, wood sawdust	30.88 cm <sup>3</sup> flow reactor (Hastelloy C276)	no catalyst	<i>T</i> : 973-1078 K <i>P</i> : 28 MPa <i>C</i> <sub>0</sub> : 3-23 wt% <i>F</i> : 2 g/min	NA	CO <sub>2</sub> , H <sub>2</sub> , CH <sub>4</sub> , CO	NA	Antal et al. (2000)
2000	glucose, vanillin, glycine	754 cm <sup>3</sup> tubular flow reactor (Inconel 625) (also batch studies with 2 autoclaves)	KOH, K <sub>2</sub> CO <sub>3</sub>	<i>T</i> : 673-873 K <i>P</i> : 10.-45 MPa $\tau$ : 30-140 s <i>C</i> <sub>0</sub> : 0.067-0.6 M <i>C</i> <sub>cat</sub> : 1-5 x 10 <sup>-3</sup> M	NA	H <sub>2</sub> , CO <sub>2</sub> , CO, CH <sub>4</sub> , C <sub>2</sub> -C <sub>4</sub> hydrocarbons	NA	Schmieder et al. (2000)
2001	acetic acid	6 cm <sup>3</sup> stainless steel tube bomb batch reactor (SS 316)	alkali (KOH), ZrO <sub>2</sub>	<i>T</i> : 673 K <i>P</i> : 25-40 MPa <i>C</i> <sub>0</sub> : 0.3 g/1.0 g w <i>t</i> : 10-60 min <i>C</i> <sub>cat</sub> : 1 M	NA	CO <sub>2</sub> , CO, H <sub>2</sub> , CH <sub>4</sub>	acetone	Watanabe et al. (2001)
2002	glycerol	horizontal tubular reactor	no catalyst	<i>T</i> : 621.5-747.5 K <i>P</i> : 25,35,45 MPa $\tau$ : 32-165 s <i>C</i> <sub>0</sub> : 0.19-0.57 M	0-0.31	H <sub>2</sub> , CO, CO <sub>2</sub>	acetaldehyde, formaldehyd, acrolein, methanol, allyl alcohol, propionaldehyde	Buhler et al. (2002)

Year	Feedstock	Reactor	Catalyst	Conditions	Conversion, (-)	Main gas products	Liquid products	Reference
2002	glucose	20.37 cm <sup>3</sup> horizontal tubular reactor (Hastelloy C276)	no catalyst	<i>T</i> : 753-1023 K <i>P</i> : 28 MPa $\tau$ : 10-50 s <i>C</i> <sub>0</sub> : 0.6 M	NA (GE%)	H <sub>2</sub> , CO, CO <sub>2</sub> , CH <sub>4</sub>	NA	Lee et al. (2002)
2002	glucose, cellulose	6 cm <sup>3</sup> stainless steel tube bomb batch reactor (SS 316)	ZrO <sub>2</sub> , NaOH	<i>T</i> : 400-440 °C <i>P</i> : 30-35 MPa <i>C</i> <sub>0</sub> : 0.1 g/ 1.2 g (w) <i>t</i> : 10-15 min <i>C</i> <sub>cat</sub> : 1 M	NA	CO <sub>2</sub> , CO, H <sub>2</sub> , CH <sub>4</sub> and C <sub>2</sub> -C <sub>4</sub> hydrocarbons	NA	Watanabe et al. (2002)
2003	glucose	special stainless steel with 6 or 9 mm inner diameter	no catalyst, KOH, Na <sub>2</sub> CO <sub>3</sub>	<i>T</i> : 773-923 K <i>P</i> : 17.5-32.5 MPa $\tau$ : 0.4-7.1 min <i>C</i> <sub>0</sub> : 0.1-0.8 M <i>C</i> <sub>cat</sub> : 0.01 M	NA (GE%)	H <sub>2</sub> , CO <sub>2</sub> , CO, CH <sub>4</sub>	NA	Hao et al. (2003)
2003	biomass	stirred batch reactor device (nickel base alloy Nimonic 90)	no catalyst	<i>T</i> : 603-683 K <i>P</i> : 30-50 MPa <i>t</i> : 15 min <i>C</i> <sub>0</sub> : 10.8% dry matter	NA	H <sub>2</sub> , CO <sub>2</sub> , CO, CH <sub>4</sub>	phenol, cresols, furfurals, acetic acid, formic acid, lactic acid, leyulinic acid, etc.	Kruse et al. (2003)

Year	Feedstock	Reactor	Catalyst	Conditions	Conversion, (-)	Main gas products	Liquid products	Reference
2003	ethanol	frame-sealed small quartz tube, stainless steel (SUS 316)	no catalyst, copper wires	$T$ : 723-773 K $C_0$ : 1 M	NA	H <sub>2</sub> , CH <sub>4</sub> , CO <sub>2</sub> , CO	acetaldehyde, acetic acid	Arita et al. (2003)
2003	methanol	54.1 cm <sup>3</sup> tubular reactor (Inconel 625)	no catalyst	$T$ : 673-873 K $P$ : 25-45 MPa $\tau$ : 3-100 s $C_0$ : 5-64 wt.%	0.86-1	H <sub>2</sub> , CO <sub>2</sub> , CO, CH <sub>4</sub>	NA	Boukis et al. (2003a)
2003	methanol	56.8 cm <sup>3</sup> horizontal tubular reactor (Inconel 625)	no catalyst	$T$ : 873 K $P$ : 25 MPa $\tau$ : 100 s $C_0$ : 50000 ppm	1	H <sub>2</sub> , CO <sub>2</sub> , CO, CH <sub>4</sub>	NA	Boukis et al. (2003b)
2003	methanol, ethane, ethylene glycol, acetone, diesel fuel	tubular reactor (Inconel 625)	no catalyst	$T$ : 823-973 K $P$ : 27.6 MPa $\tau$ : 3,6 s $C_0$ : 15-45 wt% $F_0$ : 0.6, 1.2 mL/min	0.27-1	H <sub>2</sub> , CO <sub>2</sub> , CO, CH <sub>4</sub>	NA	Taylor et al. (2003)
2003	formaldehyde	6 cm <sup>3</sup> stainless steel tube bomb batch reactor (SS 316)	no catalyst, H <sub>2</sub> SO <sub>4</sub> , NaOH, CeO <sub>2</sub> , MoO <sub>3</sub> , TiO <sub>2</sub> , ZrO <sub>2</sub>	$T$ : 673 K $P$ : 25-40 MPa $t$ : 3-30 min	NA	CO <sub>2</sub> , H <sub>2</sub> , CO	methanol	Watanabe et al. (2003a)

Year	Feedstock	Reactor	Catalyst	Conditions	Conversion, (-)	Main gas products	Liquid products	Reference
2003	formaldehyde, acetic acid, 2-propanol, glucose	6 cm <sup>3</sup> stainless steel tube bomb batch reactor (SS 316)	H <sub>2</sub> SO <sub>4</sub> , NaOH, CeO <sub>2</sub> , MoO <sub>3</sub> , TiO <sub>2</sub> , ZrO <sub>2</sub>	<i>T</i> : 673 K <i>P</i> : 25-35 MPa <i>C</i> <sub>0</sub> : 0.1-0.3 g/1-2.1 g (w) <i>t</i> : 15-60 min	NA	H <sub>2</sub> , CO, CO <sub>2</sub>	acetone	Watanabe et al. (2003b)
2004	carbon monoxide	13.2 cm <sup>3</sup> coiled reactor (SS 316)	no catalyst	<i>T</i> : 653-713 K <i>P</i> : 10-30 MPa $\tau$ : 57-414 s CO/H <sub>2</sub> O molar ratio: 0.03±0.0065	0.02-0.11	CO <sub>2</sub> , H <sub>2</sub> , CO	NA	Sato et al. (2004)
2004	n-decane, diesel	NA	no catalyst, NiO, MgO, K <sub>2</sub> O, CaO, SiO <sub>2</sub> , Al <sub>2</sub> O <sub>3</sub>	<i>T</i> : 823 K <i>P</i> : 25 MPa $\tau$ : 10-40 s <i>C</i> <sub>0</sub> : 10-20 vol%	0-0.80	H <sub>2</sub> , CH <sub>4</sub> , C <sub>2</sub> H <sub>6</sub> , C <sub>3</sub> H <sub>8</sub> , C <sub>3</sub> H <sub>6</sub>	NA	Pinkwart et al. (2004)
2005	methanol	tubular reactor (Inconel 600, i.d. 0.085 in) reactor length: 0.5, 1, 2 m	no catalyst, K <sub>2</sub> CO <sub>3</sub> , KOH	<i>T</i> : 973 K <i>P</i> : 3.4, 6.9, 13.8, 20.7, 27.6 MPa $\tau$ : 2-59 s S/C: 4-35 <i>F</i> <sub>0</sub> : 0.5, 1, 2 mL/min <i>C</i> <sub>cat</sub> : 0.68, 0.83 wt%	NA	H <sub>2</sub> , CO <sub>2</sub> , CH <sub>4</sub> , CO	NA	Gadhe et al. (2005)

Year	Feedstock	Reactor	Catalyst	Conditions	Conversion, (-)	Main gas products	Liquid products	Reference
2006	cellulose, starch, glucose, biomass waste	500 cm <sup>3</sup> batch reactor	H <sub>2</sub> O <sub>2</sub>	<i>T</i> : 603-653 K <i>P</i> : 9.5-22.5 MPa Water: 5 g <i>t</i> : 0-120 min	NA	H <sub>2</sub> , CO <sub>2</sub> , CO	oil	Williams and Onwudili et al. (2006)
2006	methanol	54.1 cm <sup>3</sup> tubular reactor (Inconel 625)	no catalyst	<i>T</i> : 673-873 K <i>P</i> : 25-45 MPa $\tau$ : 3-100 s <i>C</i> <sub>0</sub> : 5-64 wt%	reach to 1	H <sub>2</sub> , CO <sub>2</sub> , CO, CH <sub>4</sub>	NA	Boukis et al. (2006)
2006	glycerol	1.6 cm <sup>3</sup> stainless steel reactor	no catalyst, zinc sulfate (0-790 ppm)	<i>T</i> : 573-663 K <i>P</i> : 25-34 MPa $\tau$ : 10-60 s <i>C</i> <sub>0</sub> : 1 wt.%	reach to 0.80	NA	acrolein	Ott et al. (2006)
2006	methanol	batch reactor (quartz-homogeneous study)	no catalyst, nickel wire	<i>T</i> : 773-823 K <i>P</i> : 23.4 MPa <i>t</i> : 1-150 min	reach to 0.90	H <sub>2</sub> , CO, CO <sub>2</sub>	NA	DiLeo et al. (2006)
2007	ethanol	3.65 cm <sup>3</sup> fixed bed tubular reactor (Inconel 600)	5 wt.% Ru/Al <sub>2</sub> O <sub>3</sub>	<i>T</i> : 873-1073 K <i>P</i> : 22.1,24.3,27.6 MPa $\tau$ : 0.5-10 s <i>C</i> <sub>0</sub> : 5-20 wt.%	1	H <sub>2</sub> , CO <sub>2</sub> , CH <sub>4</sub> , CO	NA	Byrd et al. (2007a)

Year	Feedstock	Reactor	Catalyst	Conditions	Conversion, (-)	Main gas Products	Liquid products	Reference
2007	methanol	¼" SS 316 tubing, 46 cm length (12%Ni,17%Cr,2%Mo,69%Fe)	0.1 wt.% cupric acetate (nanoparticles)	$T$ : 773-973 K $P$ : 6.9-27.6 MPa $\tau$ : < 1 min $F_0$ : 0.13, 0.83 mL/min Sulfur concentration: 0.133, 0.633, 1.326 ppmw (thianaphthene)	NA	H <sub>2</sub> , CO <sub>2</sub> , CO, CH <sub>4</sub>	NA	Gadhe et al. (2007)
2007	glycerol	1/16 inch tubular reactor (SS316) and its length ranged 10-50 m (depends on residence time)	no catalyst, H <sub>2</sub> SO <sub>4</sub>	$T$ : 573-673 K $P$ : 25-34.5 MPa $\tau$ : 5-83 s $C_0$ : 0.05-0.25 M $C_{cat}$ : 1,5 M	0.02-0.96	NA	acrolein, acetaldehyde, formaldehyde, acetol, allyl alcohol	Watanabe et al. (2007)
2007	lignin	6 cm <sup>3</sup> stainless steel reactor	10 wt.% Ni/MgO, Co/MgO	$T$ : 773-1173 K $C_0$ : 5.26 wt.%	NA	H <sub>2</sub> , CH <sub>4</sub> , CO <sub>2</sub> , C <sub>2</sub> H <sub>6</sub>	NA	Furusawa et al. (2007)
2008	glycerol	3.65 cm <sup>3</sup> fixed bed tubular reactor (Inconel 600)	5 wt.% Ru/Al <sub>2</sub> O <sub>3</sub>	$T$ : 973-1073 K $P$ : 24.1 MPa $\tau$ : 1-4 s $C_0$ :2.5-40 wt%	1	H <sub>2</sub> , CO <sub>2</sub> , CH <sub>4</sub> , CO	NA	Byrd et al. (2008)

Year	Feedstock	Reactor	Catalyst	Conditions	Conversion, (-)	Main gas products	Liquid products	Reference
2009	glycine, glycerol	202 cm <sup>3</sup> tubular flow reactor	no catalyst and Na <sub>2</sub> CO <sub>3</sub> adding	<i>T</i> : 653-773 K <i>P</i> : 25 MPa <i>C</i> <sub>0</sub> : 1 wt% <i>C</i> <sub>cat</sub> : 0.1, 0.2 wt. %	NA (GE%)	H <sub>2</sub> , CO <sub>2</sub> , CH <sub>4</sub> , CO	formaldehyde, ethylene glycol	Xu et al. (2009)
2009	xylose, xylose-phenol mixtures	0.405 cm <sup>3</sup> stainless steel micro-tube reactor (SS 316), 0.912 cm <sup>3</sup> Hastelloy micro-tube reactor (Hastelloy C276)	no catalyst	<i>T</i> : 923-1023 K <i>P</i> : 25 MPa $\tau$ : 0.8-27 s <i>C</i> <sub>0</sub> : 20 g/L	NA	H <sub>2</sub> , CO <sub>2</sub> , CH <sub>4</sub> , CO	acetic acid, propenoic acid, benzene	Goodwin and Rorrer (2009)
2010	microalgae, glycerol	2.24 cm <sup>3</sup> tubular reactor (Inconel 600), 0.5 cm <sup>3</sup> quartz capillaries	no catalyst, Ru/TiO <sub>2</sub> , NiMo/Al <sub>2</sub> O <sub>3</sub> , PtPd/Al <sub>2</sub> O <sub>3</sub> , inconel powder, Ni wire, amino acids, K <sub>2</sub> CO <sub>3</sub>	<i>T</i> : 673-973 K <i>P</i> : 25 MPa $\tau$ : 5 s <i>C</i> <sub>0</sub> : 7.3, 10 wt%	NA	H <sub>2</sub> , CO, CO <sub>2</sub> , CH <sub>4</sub>	NA	Chakinala et al. (2010)
2010	- (Stability studying)	3.65 cm <sup>3</sup> fixed bed tubular reactor (Inconel 600)	1-10 wt.% Ce/ $\gamma$ -Al <sub>2</sub> O <sub>3</sub>	<i>T</i> : 773-973 K <i>P</i> : 24.6 MPa <i>F</i> <sub>w</sub> : 2 mL/min	-	-	-	Byrd et al. (2010)



Year	Feedstock	Reactor	Catalyst	Conditions	Conversion, (-)	Main gas products	Liquid products	Reference
2010	glycerol	2.75 cm <sup>3</sup> fixed bed reactor	1 wt.% Ru/ZrO <sub>2</sub>	<i>T</i> : 783-823 K <i>P</i> : 35 MPa $\tau$ : 2-10 s <i>C</i> <sub>0</sub> : 5 wt%	0-1	H <sub>2</sub> , CO <sub>2</sub> , CO, CH <sub>4</sub>	acetaldehyde, acetic acid, hydroxyl-acetone, allyl alcohol, propionaldehyde, acrolein, acrylic acid	May et al. (2010)
2011	bioethanol	50 cm <sup>3</sup> packed bed (Inconel 625)	no catalyst and H <sub>2</sub> O <sub>2</sub>	<i>T</i> : 773-873 K <i>P</i> : 25 MPa W/F : 3, 20, 30 O <sub>2</sub> /F: 0-0.156	0.20-1	H <sub>2</sub> , CO, CO <sub>2</sub> , CH <sub>4</sub>	acetaldehyde	Therdthianwong et al. (2011)
2011	bioethanol	50 cm <sup>3</sup> packed bed (Inconel 625)	no catalyst, Ni/Al <sub>2</sub> O <sub>3</sub> , Ni/CeZrO <sub>2</sub> /Al <sub>2</sub> O <sub>3</sub>	<i>T</i> : 773 K <i>P</i> : 25 MPa W/F : 20	0.24-1	H <sub>2</sub> , CH <sub>4</sub> , CO <sub>2</sub> , CO	acetaldehyde, methanol	Therdthianwong et al. (2011)
2011	glycerol	8.8 cm <sup>3</sup> batch reactor (SUS 304)	no catalyst	<i>T</i> : 473-673 K <i>P</i> : 30 MPa <i>t</i> : 20-60 min <i>C</i> <sub>0</sub> : 6.89-16.86 wt. %	1	NA	acrolein, acetaldehyde, allyl alcohol	Qadariyah et al. (2011)

Year	Feedstock	Reactor	Catalyst	Conditions	Conversion, (-)	Main gas products	Liquid products	Reference
2011	methanol, glycerol	2,618 cm <sup>3</sup> reactor (Incoloy 825): pilot plant	No catalyst (soda methanol, crude glycerol), alkali salt	$T$ : 723-923 K $\tau$ : 6-173 s $C_0$ : 3-20 wt%	NA	methanol: H <sub>2</sub> , CO <sub>2</sub> , CO glycerol: H <sub>2</sub> , CO, CO <sub>2</sub> , CH <sub>4</sub>	acetic acid, acetol, acetaldehyde, propionaldehyde, allyl alcohol, methanol, formaldehyde, acrolein	Bennekom et al. (2011)
2011	switchgrass	4.02 cm <sup>3</sup> horizontal packed bed reactor (Inconel 600)	Ru, Ni, Co catalysts supported on ZrO <sub>2</sub> , TiO <sub>2</sub> , MgAl <sub>2</sub> O <sub>4</sub>	$T$ : 923 K $P$ : 250 bar WHSV: 9 h <sup>-1</sup>	NA (GE%)	H <sub>2</sub> , CO <sub>2</sub> , CH <sub>4</sub> , CO	NA	Byrd et al. (2011)
2011	glucose	140 cm <sup>3</sup> autoclave (stainless steel)	bimetallic Ni-M/ $\gamma$ -Al <sub>2</sub> O <sub>3</sub> catalysts (M=Cu, Co and Sn)	$T$ : 673 K $C_0$ : 9.09 wt. %	NA	H <sub>2</sub> , CH <sub>4</sub> , CO <sub>2</sub> , CO	NA	Li et al. (2011)

### 3.4 Glycerol reforming catalyst development and operating parameters

In glycerol reforming, glycerol reacts with the other substance including steam (water) or/and air (oxygen) to produce hydrogen. Catalyst is essential for these processes in order to activate the target reaction, decrease by-products, increase hydrogen production, and decrease retention time. Glycerol reforming can be divided to four parts including aqueous phase glycerol reforming (liquid phase), steam glycerol reforming (gas phase), autothermal glycerol steam reforming (gas phase) and glycerol reforming in supercritical water (fluid phase; between liquid and gas phase). The history of catalyst using in the reforming and mostly in glycerol reforming field are listed below.

#### 3.4.1 Steam reforming

Trimm (1997) reviewed that catalysts for steam reforming of hydrocarbons are mostly based on Ni as active component supported on oxides with high thermal stability. Even though noble metals (Ru, Rh, Pt) are more effective than Ni and less susceptible to carbon formation, such catalysts are not common in industrial applications because of their high cost.

Czernik et al. (2002) used crude glycerol that was received as a high-viscosity liquid in the steam reforming process by a commercial nickel-based naphtha reforming catalyst (C11-NK). It had to be preheated to facilitate pumping and atomizing for studying the steam reforming of biomass-derived liquids at 1123 K (850°C) with S/C = 2.1 and 2.6, GHSV=1400 and 1440 h<sup>-1</sup>. At S/C=2.6, the H<sub>2</sub> yield was around 77% of the stoichiometric potential, which equaled 23.6 g/100 g of glycerol.

Hirai et al. (2005) studied catalysts loaded with Group 8-10 metals in glycerol steam reforming using Y<sub>2</sub>O<sub>3</sub>, ZrO<sub>2</sub>, CeO<sub>2</sub>, La<sub>2</sub>O<sub>3</sub>, SiO<sub>2</sub>, MgO, and Al<sub>2</sub>O<sub>3</sub> as supports. The experiments were carried out at a temperature of 773-873 K (500-600°C), atmospheric pressure, a steam-to-carbon molar ratio of S/C = 3.3, and a W/F (contact time) of glycerin of 13.4 g-cat h/mol. From all catalysts studied, Ruthenium on Y<sub>2</sub>O<sub>3</sub>

(Ru/Y<sub>2</sub>O<sub>3</sub>) was found to be the best catalyst by loading of 3 wt%. It was performed at 873 K (600°C) and gave the complete conversion (100%) with H<sub>2</sub> yield of 87%.

Soares et al. (2006) reported the studying of Pt supported on Al<sub>2</sub>O<sub>3</sub>, ZrO<sub>2</sub>, CeO<sub>2</sub>/ZrO<sub>2</sub>, MgO/ZrO<sub>2</sub>, and Carbon in glycerol steam reforming. The conditions included temperature of 623 K (350 °C), pressure of 1 bar with aqueous glycerol feed solution (30 wt.%) over oxide supported Pt catalysts (1.0 g) or Pt/C catalyst (0.060 g) and a feed flow rate of 0.32 cm<sup>3</sup>min<sup>-1</sup>. Pt/C catalyst was tested at various feed rates and temperatures. Other catalysts tested were Pt–Ru and Pt–Re. Pt/C catalysts showed the superior performance. At 673 K (400 °C), and pressure = 0.1 MPa, 100% glycerol conversion was achieved at feed rate of 0.32 cm<sup>3</sup>min<sup>-1</sup>.

Zhang et al. (2007) studied the glycerol steam reforming over ceria-supported Ir, Co and Ni catalysts (Ir/CeO<sub>2</sub>, Co/CeO<sub>2</sub> and Ni/CeO<sub>2</sub>). The process was conducted in a continuous flow fixed-bed quartz micro-reactor under atmospheric pressure within the temperature range of 523-873 K (250-600°C). 0.2 g of catalyst (grain size of 40–60 mesh) were loaded and sandwiched by two quartz wool layers. The ratio of glycerol/H<sub>2</sub>O/He equaled 2:18:80 vol.% and gas hourly space velocity (GHSV) was 11,000 ml/g-cat.h. The Ir/CeO<sub>2</sub> catalyst was also significantly more active and selective toward hydrogen production. Complete conversion of glycerol (100%) with hydrogen selectivity of more than 85% was obtained at temperature as low as 673 K (400°C). However, the complete conversion over Co/CeO<sub>2</sub> and Ni/CeO<sub>2</sub> occurred at 698 and 723 K (425 and 450 °C) with hydrogen selectivities of 88% and 75%, respectively.

Adhikari et al. (2007c) investigated the performance of Ni and Pt group metal-based on Al<sub>2</sub>O<sub>3</sub> and CeO<sub>2</sub>/Al<sub>2</sub>O<sub>3</sub> supports about 14 catalysts including Al<sub>2</sub>O<sub>3</sub>, Rh/Al<sub>2</sub>O<sub>3</sub>, Pt/Al<sub>2</sub>O<sub>3</sub>, Pd/Al<sub>2</sub>O<sub>3</sub>, Ir/Al<sub>2</sub>O<sub>3</sub>, Ru/Al<sub>2</sub>O<sub>3</sub>, Ni/Al<sub>2</sub>O<sub>3</sub>, CeO<sub>2</sub>/Al<sub>2</sub>O<sub>3</sub>, Rh/CeO<sub>2</sub>/Al<sub>2</sub>O<sub>3</sub>, Pt/CeO<sub>2</sub>/Al<sub>2</sub>O<sub>3</sub>, Pd/CeO<sub>2</sub>/Al<sub>2</sub>O<sub>3</sub>, Ir/CeO<sub>2</sub>/Al<sub>2</sub>O<sub>3</sub>, Ru/CeO<sub>2</sub>/Al<sub>2</sub>O<sub>3</sub>, and Ni/CeO<sub>2</sub>/Al<sub>2</sub>O<sub>3</sub>. The experiments were conducted at a constant flow rate of 0.15-0.5 ml/min at furnace temperatures from 873 to 1123 K (600 to 900°C) and steam/carbon molar ratio (S/C) = 1/3–3.0. The reactor was made of alumina (99.8%) tube with 19 mm inner diameter. About 80% of hydrogen selectivity was achieved only with

Ni/Al<sub>2</sub>O<sub>3</sub>, whereas the selectivity was 71% with Rh/CeO<sub>2</sub>/Al<sub>2</sub>O<sub>3</sub> at a S/C = 3, 1123 K, and feed flow rate of 0.15 mL/min. The hydrogen selectivity and glycerol conversion for the reaction at 1123 K were in the order: Ni > Ir > Ru > Pt > Rh, Pd, and Ni > Ir > Pd > Rh > Pt > Ru, respectively.

Douette et al. (2007) studied the crude glycerol steam reforming by using Ni-based catalyst (G-91 EW steam reforming catalyst, Süd-Chemie Inc., Louisville, KY). The reforming reaction took place in a stainless steel pipe, 294 mm in length with an internal diameter of 25 mm. The reactor was placed inside a furnace to provide temperature control. A 4.5 mol of hydrogen was produced per mol of glycerin at experimental conditions of steam to carbon ratio of 2.2, and temperature of 1077 K (804°C). This is 65% of the maximum theoretical H<sub>2</sub> yield, and 90% of the H<sub>2</sub> yield predicted by thermochemical equilibrium. A 1.4 mol quantity of CO was also produced per mol of glycerin.

Cui et al. (2009) studied the activity of La<sub>1-x</sub>Ce<sub>x</sub>NiO<sub>3</sub> catalyst in comparison to the thermodynamic reaction equilibrium for glycerol steam reforming process. It was investigated with non-substituted and partially Ce substituted La<sub>1-x</sub>Ce<sub>x</sub>NiO<sub>3</sub> mixed oxides where x = 0, 0.1, 0.3 or 0.7, and the activities were compared with Pt metal catalysts. Tubular quartz microreactor (i.d. 10 mm, 300 mm length) was used in this process. The mixed oxide catalyst (100 mg) having particle size between 280 and 560 nm was packed between layers of quartz wool and was located in the reactor at a position 2/3 of the whole length, whereas the last 1/3 part of the reactor was filled with inert aluminium oxide ( $\alpha$ -Al<sub>2</sub>O<sub>3</sub>). The reactor was placed in an electric furnace equipped with K-type thermocouples. The Ni was easily reduced in the La<sub>0.3</sub>Ce<sub>0.7</sub>NiO<sub>3</sub> structure. The experimental results were compared with the thermodynamic equilibrium concentrations, which were calculated for the system with non-stoichiometric method. The La<sub>0.3</sub>Ce<sub>0.7</sub>NiO<sub>3</sub> catalyst was highly active in the glycerol steam reforming with conversions approaching to the equilibrium at temperatures of 773 to 973 K (500 to 700°C). The formation of carbonaceous deposits on the La<sub>0.3</sub>Ce<sub>0.7</sub>NiO<sub>3</sub> was smallest among all the investigated La<sub>0.3</sub>Ce<sub>0.7</sub>NiO<sub>3</sub> catalysts. Unchanged catalyst surface area (BET) during operation and low carbon deposition

after reaction confirm the efficient operation and high stability of the non-noble, inexpensive catalyst of  $\text{La}_{0.3}\text{Ce}_{0.7}\text{NiO}_3$ .

### 3.4.2 Aqueous phase reforming

Cortright et al. (2002) studied hydrogen from catalytic reforming of biomass-derived hydrocarbons in liquid water by using  $\text{Pt}/\gamma\text{-Al}_2\text{O}_3$  catalyst. The one of reactants was glycerol that operated in temperature of 498-538 K (225-265°C), pressure of 2.9-5.6 MPa and weight hourly specific velocity (WHSV) = 0.008 g of glycerol/g-cat.h. The lower temperature and pressure offered higher mol (%) of  $\text{H}_2$  in gas phase composition equaled 64.8% and higher  $\text{H}_2$  selectivity equaled 75% but lower Alkane selectivity equaled 19% at 498 K (225 °C) and 2.9 MPa. (APR)

Davda et al. (2003) concluded that silica-supported Pt and Pd catalysts exhibited relatively high selectivities for  $\text{H}_2$  production, with low rates of alkane production. It appears that catalysts based on Pt and Pd may be promising materials for the selective production of hydrogen by aqueous-phase reforming of oxygenated hydrocarbons, such as ethylene glycol.

Iriondo et al. (2008) reviewed that effective catalyst for production of hydrogen by aqueous phase reforming of oxygenated hydrocarbons must break C–C, O–H and C–H bonds in the oxygenated hydrocarbon reactant and facilitate the water–gas shift reaction to remove adsorbed CO from the surface. They also studied the catalyst of  $\text{Ni}/\gamma\text{-Al}_2\text{O}_3$  modified with Mg, Ce, La and Zr in glycerol aqueous phase reforming and steam reforming. They were conducted in a bench-scale unit equipped with a stainless steel fixed-bed catalytic reactor. The feed was 1 wt.% of glycerol in water. Aqueous reforming conditions included at 3 MPa of total pressure, at 498 K (225°C) and with a WHSV equal to  $1.25\text{ h}^{-1}$ . This process showed that all the catalysts exhibited severe deactivation phenomena. The initial glycerol conversions were found to decrease following the sequence:  $\text{Ni}/\text{La}_2\text{O}_3/\text{Al}_2\text{O}_3 > \text{Ni}/\text{CeO}_2/\text{Al}_2\text{O}_3 = \text{Ni}/\text{ZrO}_2/\text{Al}_2\text{O}_3 > \text{Ni}/\text{Al}_2\text{O}_3 = \text{Ni}/\text{MgO}/\text{Al}_2\text{O}_3$ . Steam reforming conditions comprised at atmospheric pressure, at 873 K and with a WHSV equal to  $2.5\text{ h}^{-1}$ . The results showed glycerol conversion was 100% and hydrogen was also the major product in

gas phase. It can be seen that Ni/ZrO<sub>2</sub>/Al<sub>2</sub>O<sub>3</sub> offered the maximum selective with a gas.

Lehnert and Claus (2008) studied the influence of Pt particle size and support type on the aqueous phase reforming of glycerol. Aqueous phase reforming reaction was carried out in a 1/4 in. stainless steel tubular reactor. The catalyst (300 mg) was contained in the centre of the reactor at temperature of 523 K (250°C), pressure of 20 bar, glycerol concentration of 10 wt.%, feed flow rate of 0.5 ml/min and Pt loading of 3 wt.%. In the catalytic reaction selectivity to hydrogen increased with increasing particle size from 78% to 95% while the conversion of glycerol remained nearly constant at 20%. Also, variation of support material from pure  $\gamma$ -alumina to a mixture of  $\alpha$ -,  $\delta$ - and  $\theta$ -phases (Puralox) led to an increase in hydrogen production from  $1.2 \times 10^{-3}$  to  $7.6 \times 10^{-3}$  mol/min.g-cat. The maximum glycerol conversion achieved was around 57%. The production of hydrogen from crude glycerol was significantly lower than from pure (pharma grade) glycerol in steady state. Moreover, after a reaction time of 200 min, considerable loss of catalytic activity could be observed. In addition, the selectivity to hydrogen was found to be higher than 90% at steady state condition. The impurities of crude glycerol, which are mostly inorganic salts (e.g. NaCl) strongly affect catalytic activity, probably because of catalyst poisoning by blocking its active sites. The performance of the catalyst is also affected by metal loading and metal particle size.

### 3.4.3 Autothermal reforming

Swami and Abraham (2006) studied the steam reforming and autothermal reforming of glycerol by using Pd/Ni/Cu/K supported on  $\alpha$ -Al<sub>2</sub>O<sub>3</sub> catalyst. For steam reforming, the range of temperature was 823-1123 K (550-850°C) at an S/C ratio of 3. H<sub>2</sub> yield was at maximum around 42% at 1073 to 1123 K (800-850°C). For autothermal reforming, the conditions were operated with O/C ratio of 0.3. H<sub>2</sub> yield was around 58% at 1123 K (850 °C) and more than the value of H<sub>2</sub> yield from steam reforming.

Luo et al. (2008) studied the effect of catalyst composition and reaction conditions in glycerol aqueous phase reforming for hydrogen production over Pt. The

reactions were performed in a 17 cm (diameter) x 40 cm (height) tubular reactor made of stainless steel, where the catalyst sample was loaded in the middle of the tubular reactor, with filling  $\text{SiO}_2$  in two heads. The operating parameters included temperature = 453–493 K (180–220°C), pressure = 1.1–2.5 MPa; feed flow rate = 0.05–0.1 mL/min; glycerol concentration 5–10 wt.%; catalyst weight = 1–2 g; and Pt loading = 0.3–1.2 wt.%. From the results, 0.9 wt.% Pt/ $\gamma$ - $\text{Al}_2\text{O}_3$  catalysts exhibited the highest reforming activities for hydrogen production, not same as the order of Pt loading. Pt aggregation might be occurred after reduction when higher Pt loading was employed, thus decreasing its reactivity. Temperature of 493 K (220°C) and 2.5 MPa was seen to be the most suitable reaction condition. Lower reaction temperature would decrease the conversion of glycerin and higher temperature leads to more side reactions.

#### **3.4.4 Supercritical water reforming**

Xu et al. (1996) conducted the gasification of 2 M of glycerol in supercritical water at 873 K (600°C), 34.5 MPa with and without coconut shell activated carbon catalyst. A tubular reactor was made of Inconel 625. Glycerol was completely gasified to hydrogen rich gas with only small CO amount in both cases. It was found that activated carbon offered only the small effect by changing of gas composition.

Byrd et al. (2008) studied hydrogen production from glycerol by supercritical water reforming over a Ru/ $\text{Al}_2\text{O}_3$  catalyst in a fixed bed tubular Inconel 600 reactor. The conditions for low  $\text{CH}_4$  and CO formation were considered. Experiments were conducted in a tubular fixed-bed flow reactor over a temperature range of 427–527 K (700–800 °C), feed concentrations up to 40 wt.% glycerol, all at short reaction time of less than 5 s. Glycerol was completely gasified to hydrogen, carbon dioxide, and methane along with small amounts of carbon monoxide. At dilute feed concentrations, near-theoretical yield of 7 mol of hydrogen/mol of glycerol was obtained, which decreases with an increase in the feed concentration. Based on a kinetic model for glycerol reforming, an activation energy of 55.9 kJ/mol was observed.

Xu et al. (2009) found that  $\text{Na}_2\text{CO}_3$  showed a negative effect on glycerol gasification. Note that  $\text{Na}_2\text{CO}_3$  performed a positive effect on some types of organic



matters supercritical water processes. Around 98% of glycerol gasification was observed by feeding of 1 wt.% glycerol solution in a continuous tubular flow reactor at 773 K (500°C), 25 MPa, and residence time of 0.98 min. The hydrogen yield was obtained around 5.08.

Chakinala et al. (2010) examined the effect of amino acids (glycine, alanine, proline), alkali salt ( $K_2CO_3$ ) in supercritical water reforming of glycerol. 10 wt.% of feed glycerol concentration mixed with amino acid, and/or alkali salt at temperature of 773, 873 K (500, 600°C), 25 MPa, and 5 s of residence time in an Inconel 600 reactor. The increasing of operating temperature enhanced the hydrogen yield but offered the similar gas composition (51 mol% of  $H_2$ , 32 mol% of CO, and 10 mol% of  $CO_2$ ). However, the adding of amino acids clearly reached to carbon formation. The presence of  $K_2CO_3$ , and  $K_2CO_3$  with glycine improved the gasification efficiency, but depressed the CO formation and increased in  $CO_2$ , and  $C_{2-3}$  compounds.

May et al. (2010) investigated the catalytic glycerol reforming in supercritical water with 1%Ru/ZrO<sub>2</sub>. The condition consisted of 783-823 K (510-550°C), 35 MPa, residence time of 2 and 10 s, and 5 wt.% of feed glycerol concentration in a continuous isothermal fixed bed reactor. Residence time of 8.5 and 5 s were sufficient to reach the complete glycerol conversion for 783 and 823 K, respectively. Hydrogen and carbon monoxide were the main gases with the smaller amounts of methane and ethylene. Ru/ZrO<sub>2</sub> promoted the formation of acetic acid, gasification of glycerol, but inhibited the formation of acrolein. However, this catalyst could not perform to achieve complete gasification because the primary products including acetaldehyde, and acetic acid were still observed. 3.50 of hydrogen yield were obtained which was around 50% of stoichiometric value.

Bennekom et al. (2011) studied the supercritical water reforming of glycerol in an Incoloy 825 reactor at temperature of 723-923 K (450-650°C), residence time of 6-173 s, and feed glycerol concentration of 3-20 wt.%. The presence of  $Na_2CO_3$  was also studied. The results showed  $H_2$ , CO,  $CO_2$ ,  $CH_4$ , and higher hydrocarbons ( $C_2H_6$ ,  $C_2H_4$ ,  $C_3H_6$  and  $C_3H_8$ ) were produced with 66% of carbon atoms terminated in carbon oxide. They proposed that the mechanism of glycerol decomposition acted as the

dehydration of 1 mol of H<sub>2</sub>O/mol of glycerol. In addition, the addition of Na<sup>+</sup> in the feed was independent of the mechanism pathway.

### **3.5 Mechanism pathways in glycerol reforming**

Glycerol is an organic compound which includes 3 carbons in the molecule. After the reforming, the various products are always occurred as C<sub>1</sub>, C<sub>2</sub>, and C<sub>3</sub> compounds in solid, liquid, and gas phases; however, possible products significantly depend on the operating conditions. For example, Buhler et al. (2002) stated that product distribution depended on the operating temperature by the differences in activation energies. The mechanism pathways of glycerol conversion have been known as very complex. Many possible reactions occurred and led to different intermediate products (Bennekom et al., 2011). A few literatures have proposed the mechanism pathways as follows.

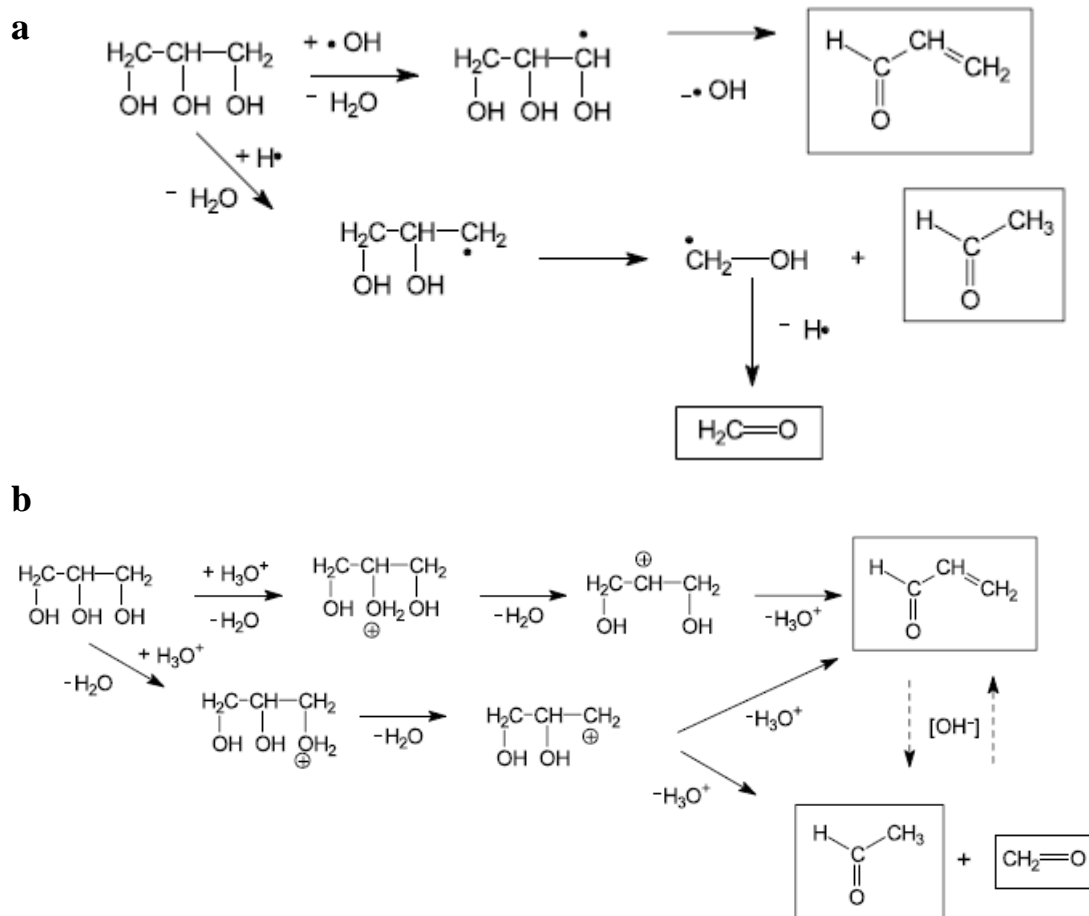
Buhler et al. (2002) conducted the glycerol reforming in sub, and supercritical water. They classified two possible pathways, i) free radical reaction takes a role at lower pressures and/or higher temperature as shown in Table 3.3 and ii) ionic reaction steps that are likely appeared at higher pressure and/or lower temperatures as shown in Table 3.4. The formation of acetaldehyde, acrolein, and formaldehyde were proposed in the free radical, and ionic reaction pathways as shown in Figure 3.2a,b, respectively.

**Table 3.3** The proposed reactions in the free radical reaction part of reaction mechanism (Buhler et al., 2002)

Reaction type	Example
<b>Initiation reaction</b>	$\begin{array}{c} \text{H}_2\text{C}-\text{CH}-\text{CH}_2 \\   \quad   \quad   \\ \text{OH} \quad \text{OH} \quad \text{OH} \end{array} \longrightarrow \begin{array}{c} \text{H}_2\text{C}-\dot{\text{C}}\text{H} \\   \quad   \\ \text{OH} \quad \text{OH} \end{array} + \begin{array}{c} \cdot\text{CH}_2 \\   \\ \text{OH} \end{array} \quad \dots\dots(3.1)$
<b><math>\beta</math>-Scission</b>	$\begin{array}{c} \text{H}_2\text{C}-\text{CH}-\text{CH}_2 \\   \quad   \quad   \\ \text{OH} \quad \text{OH} \quad \text{O}\cdot \end{array} \longrightarrow \text{H}_2\text{C}=\text{O} + \begin{array}{c} \text{H}_2\text{C}-\dot{\text{C}}\text{H} \\   \quad   \\ \text{OH} \quad \text{OH} \end{array} \quad \dots\dots(3.2)$
<b>Hydrogen transfer</b>	$\begin{array}{c} \text{H}_2\text{C}-\text{CH}-\text{CH}_2 \\   \quad   \quad   \\ \text{OH} \quad \text{OH} \quad \text{OH} \end{array} + \text{H}\cdot \longrightarrow \begin{array}{c} \text{H}_2\text{C}-\dot{\text{C}}-\text{CH}_2 \\   \quad   \quad   \\ \text{OH} \quad \text{OH} \quad \text{OH} \end{array} + \text{H}_2 \quad \dots\dots(3.3)$
<b>Radical isomerization</b>	$\dot{\text{C}}\text{H}_2-\text{OH} \longrightarrow \text{CH}_3-\text{O}\cdot \quad \dots\dots(3.4)$
<b>Radical addition</b>	$\text{H}_2\text{C}=\text{CH}_2 + \dot{\text{C}}\text{H}_2-\text{OH} \longrightarrow \begin{array}{c} \text{H}_2\dot{\text{C}}-\text{CH}_2-\text{CH}_2 \\   \\ \text{OH} \end{array} \quad \dots\dots(3.5)$
<b>Radical dehydration</b>	$\begin{array}{c} \text{H}_2\text{C}-\dot{\text{C}}-\text{CH}_2 \\   \quad   \quad   \\ \text{OH} \quad \text{OH} \quad \text{OH} \end{array} \longrightarrow \begin{array}{c} \text{HO} \\   \\ \text{CH}_2-\text{C} \\   \quad   \\ \quad \quad \text{OH} \\ \quad \quad \cdot\text{H} \end{array} + \text{H}_2\text{O} \quad \dots\dots(3.6)$
<b>Radical substitution</b>	$\text{CH}_3-\text{OH} + \text{H}\cdot \longrightarrow \text{H}_3\text{C}\cdot + \text{H}_2\text{O} \quad \dots\dots(3.7)$
<b>Radical termination reaction</b>	$\text{H}\cdot + \text{H}\cdot \longrightarrow \text{H}_2 \quad \dots\dots(3.8)$

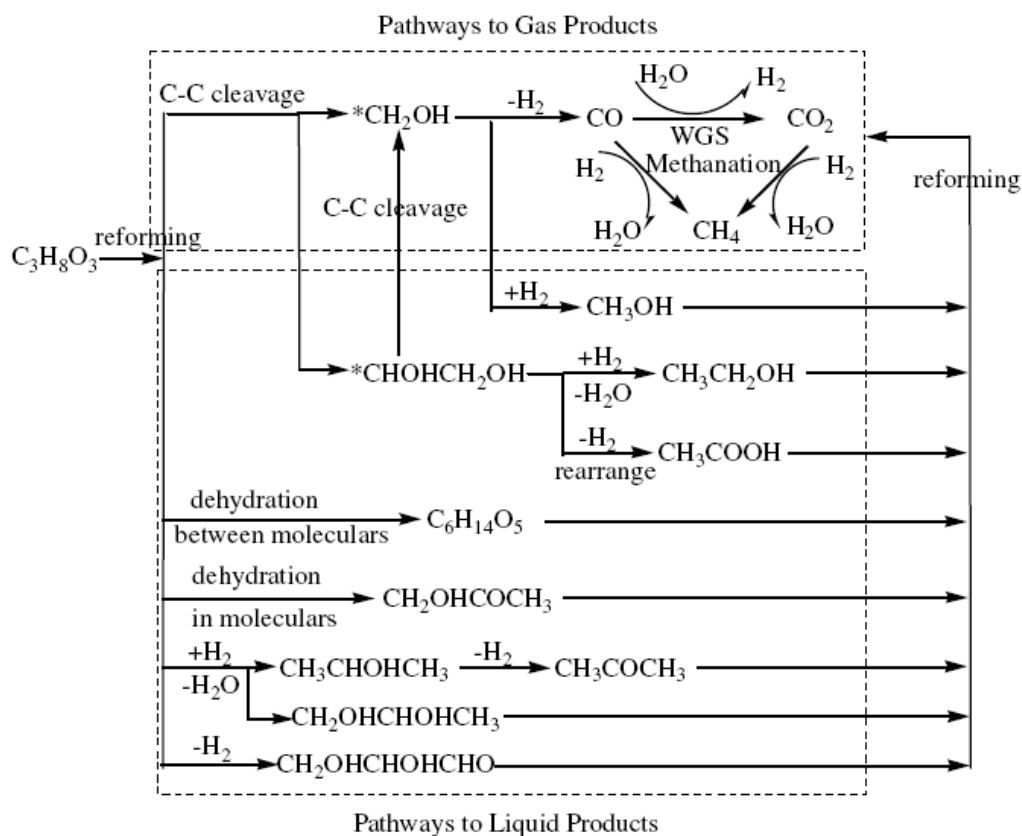
**Table 3.4** The proposed reactions in the ionic reaction part of reaction mechanism (Buhler et al., 2002)

Reaction type	Example
Autoprotolysis	$2\text{H}_2\text{O} \rightleftharpoons \text{H}_3\text{O}^+ + \text{OH}^- \quad \dots\dots(3.9)$
Protonation	$\begin{array}{c} \text{H}_2\text{C}-\text{CH}-\text{CH}_2 \\   \quad   \quad   \\ \text{OH} \quad \text{OH} \quad \text{OH} \end{array} + \text{H}_3\text{O}^+ \rightleftharpoons \begin{array}{c} \text{H}_2\text{C}-\text{CH}-\text{CH}_2 \\   \quad   \quad   \\ \text{OH} \quad \text{OH} \quad \text{OH}_2^+ \end{array} + \text{H}_2\text{O} \quad \dots\dots(3.10)$
Deprotonation by OH <sup>-</sup> ion	$\begin{array}{c} \text{H}_2\text{C}-\text{CH}-\text{CH}_2 \\   \quad   \quad   \\ \text{OH} \quad \text{OH} \quad \text{OH} \end{array} + \text{HO}^- \rightleftharpoons \begin{array}{c} \text{H}_2\text{C}-\text{CH}-\text{CH}_2 \\   \quad   \quad   \\ \text{OH} \quad \text{OH} \quad \text{O}^- \end{array} + \text{H}_2\text{O} \quad \dots\dots(3.11)$
Dehydration	$\begin{array}{c} \text{H}_2\text{C}-\text{CH}-\text{CH}_2 \\   \quad   \quad   \\ \text{OH} \quad \text{OH}_2^+ \quad \text{OH} \end{array} \rightleftharpoons \begin{array}{c} \text{H}_2\text{C}-\text{CH}-\text{CH}_2 \\   \quad   \\ \text{OH} \quad \text{OH} \end{array} + \text{H}_2\text{O} \quad \dots\dots(3.12)$
Keto-enol-tautomerization	$\begin{array}{c} \text{H}_3\text{C}-\text{C}-\text{H} \\ \quad \parallel \\ \quad \text{O} \end{array} \rightleftharpoons \begin{array}{c} \text{H}_2\text{C}=\text{C}-\text{H} \\ \quad   \\ \quad \text{OH} \end{array} \quad \dots\dots(3.13)$
Acetalization	$\begin{array}{c} \text{H}_2\text{C}-\text{CH}-\text{CH}_2 \\   \quad   \quad   \\ \text{OH} \quad \text{OH} \quad \text{OH} \end{array} + \begin{array}{c} \text{H}-\text{C}-\text{H} \\ \quad \parallel \\ \quad \text{O} \end{array} \xrightarrow{\text{H}_3\text{O}^+} \begin{array}{c} \text{O} \\ \diagup \quad \diagdown \\ \text{HO}-\text{C}-\text{C}-\text{C} \\ \diagdown \quad \diagup \quad \diagdown \\ \text{O} \quad \text{O} \end{array} + \text{H}_2\text{O} \quad \dots\dots(3.14)$
Aldol condensation	$\begin{array}{c} \text{H}_3\text{C}-\text{C}-\text{H} \\ \quad \parallel \\ \quad \text{O} \end{array} + \begin{array}{c} \text{H}-\text{C}-\text{H} \\ \quad \parallel \\ \quad \text{O} \end{array} \xrightarrow{\text{HO}^-} \begin{array}{c} \text{CH}_2=\text{C}-\text{C}-\text{H} \\ \quad \parallel \\ \quad \text{O} \end{array} + \text{H}_2\text{O} \quad \dots\dots(3.15)$



**Figure 3.2** (a) free radical reaction, (b) ionic reaction pathways for the formation of acetaldehyde, acrolein, and formaldehyde (Buhler et al., 2002).

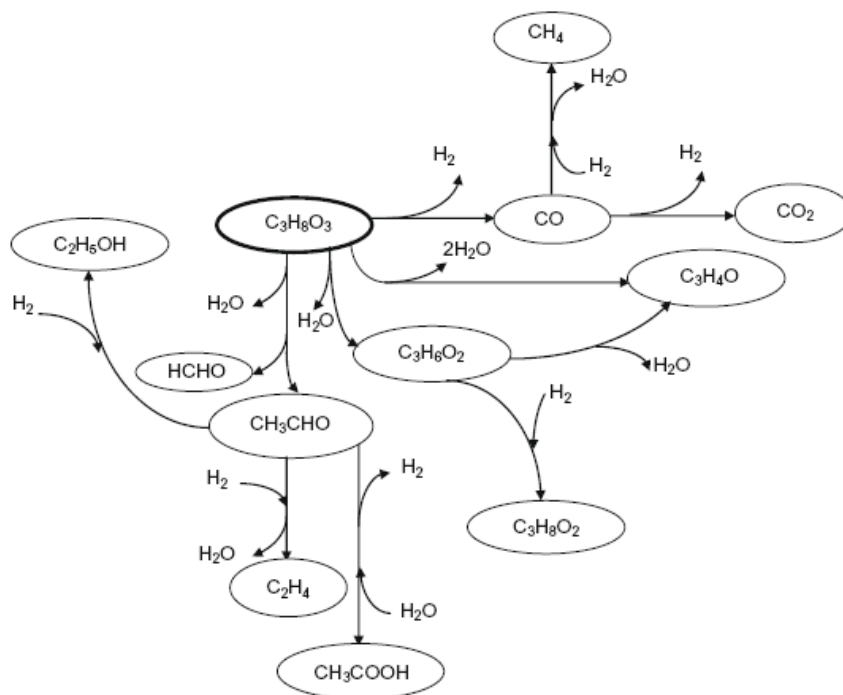
Luo et al. (2008) concluded the glycerol pathways to products in glycerol aqueous phase reforming process by Figure 3.3. They found that hydrogen production was an interesting topic because various parallel reactions in the liquid phase were occurred. Adhikari et al. (2009) also reviewed the reaction pathways i.e. C-C bond cleavage, dehydration, and dehydrogenation in glycerol reforming process as shown in Figure 3.4.



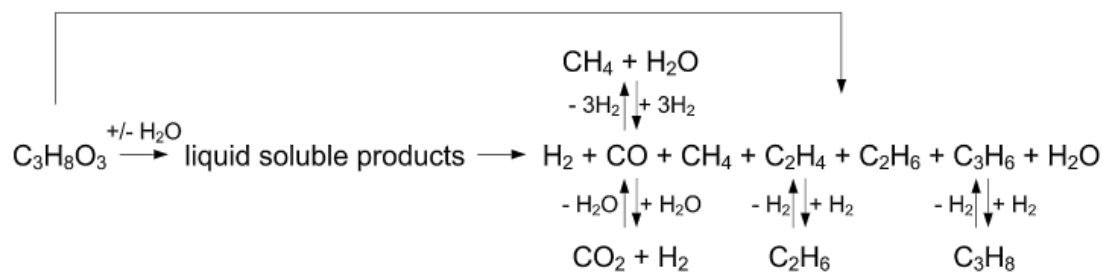
**Figure 3.3** Pathways to products in glycerol aqueous phase reforming process (Luo et al., 2008).

May et al. (2010) conducted the glycerol supercritical water reforming at 783 K and 35 MPa. They concluded that free radical pathway dominated the ionic pathway with occurring of three unstable radicals including  $\bullet\text{CH}_2\text{-CHOH-CH}_2\text{OH}$  (propionaldehyde, ally alcohol),  $\bullet\text{COH-CHOH-CH}_2\text{OH}$  (formaldehyde, acrolein, acrylic acid), and  $\bullet\text{COH-(CH}_2\text{OH)}_2$  (acetaldehyde, acetic acid).

Bennekom et al. (2011) proposed the reaction pathway to gas products from supercritical water reforming of glycerol. The results showed that  $\text{H}_2$ ,  $\text{CO}$ ,  $\text{CH}_4$ ,  $\text{C}_2\text{H}_4$ , and  $\text{C}_3\text{H}_6$  are the primary gas products.  $\text{CO}_2$ , and  $\text{C}_3\text{H}_8$  were formed as the secondary gas products which  $\text{CO}_2$  mostly occurred from WGS reaction (Equation (2.10)). Note that  $\text{C}_2\text{H}_6$  was still unclear whether a primary or secondary gas products.



**Figure 3.4** Reaction pathways during glycerol reforming process (Adhikari et al., 2009)



**Figure 3.5** Proposed reaction pathways for glycerol reforming in supercritical water to gaseous products (Bennekom et al., 2011).

# CHAPTER IV

## EXPERIMENTAL

This chapter presents the overview of the glycerol reforming experiment in the supercritical water conditions. Firstly description about materials and chemicals are provided for the experiments, products analysis, and catalyst preparation. The procedure of the catalyst preparation by the wetness impregnation method was then described. XRD, BET surface area, TGA, SEM, and TEM were conducted as catalyst characterization techniques to determine bulk crystalline phase, surface area, carbon formation on surface, surface morphology, and metal dispersion of catalyst, respectively. Next part, the schematic diagram of supercritical water glycerol reforming set up was shown with the explanation in details of the process. Then the equipment details including high pressure pump, syringe pump, preheater, reactor, cooling unit, mass flow controllers, back pressure regulator, gas-liquid separator, and gas chromatography for determine gas and liquid products are provided.

### 4.1 Material and chemicals

Glycerol (Fisher scientific, USP/FCC) was mixed with deionized water (DI water) at a required weight percent solution as an organic feedstock.  $\text{Ni}(\text{NO}_3)_2 \cdot 6\text{H}_2\text{O}$  (Alfa Aesar, 99.9985%), and  $\text{Co}(\text{NO}_3)_2 \cdot 6\text{H}_2\text{O}$  (Alfa Aesar, 98.0-102.0%) were used as precursors for Nickel and Cobalt loadings, respectively. YSZ (TOSOH, TZ-8Y, powder),  $\text{La}_2\text{O}_3$  (Alfa Aesar, 99.99%, powder),  $\text{ZrO}_2$  (ALDRICH, 99%, powder),  $\gamma\text{-Al}_2\text{O}_3$  (Alfa Aesar, 99.97%, powder),  $\alpha\text{-Al}_2\text{O}_3$  (Alfa Aesar, 99.98%, powder) were commercial supports in this work. Acetaldehyde (Sigma-Aldrich,  $\geq 99.5\%$ ), acetol (Aldrich, 90%), methanol (Caledon,  $\geq 99.8\%$ ), acetic acid (Sigma-Aldrich, 99.7%), propionaldehyde (Sigma-Aldrich, 97%), allyl alcohol (Aldrich, 99%), acetone (Sigma-Aldrich, 99.9%), acrolein (Sigma-Aldrich, 90%), ethanol (Sigma-Aldrich, HPLC grade), ethylene glycol (Acros Organics, 99.5%), formaldehyde (Sigma-Aldrich, 37%) and acrylic acid (Aldrich, 99%) were used as standards for identifying



concentrations in a liquid product solution. 1-4 Butanediol (Sigma-Aldrich, 99%) was used as an internal standard. Mixed gas (Praxair, 30%CO, 30%CO<sub>2</sub>, 25%CH<sub>4</sub>, 10%C<sub>2</sub>H<sub>4</sub>, and 5%C<sub>2</sub>H<sub>6</sub>), hydrogen (Praxair, 99.999%), and nitrogen (Praxair, 99.999%) were mixed to fill a Kynar gas sampling bag (Cole-Parmer, 6''x6'') at different concentrations for making calibration curves in gas analysis.

## 4.2 Catalyst preparation

All catalysts were prepared by wet impregnation method. Start with the beaker was filled with 250 mL of DI water and covered with aluminum foil. Then water was stirred and heated to 363 K (90°C). Carefully open the foil and put the support to the water, then slightly add the metal precursor to the solution in order to make a good dispersion. The solution was stirred at 363 K (90°C) for 5 hours. After that, open the covered foil to dry the solution. Wait until the solution becomes very thick and paste-like. The paste was dried overnight in an oven at 383 K (110°C), and then dry paste was calcined at 973 K (700°C) for 5 hours. Finally, it was crushed and sieved with the 2 screens including 1.4, and 2 mm. Collect the only catalyst size of 1.4-2 mm. In case of the experimental support studies (YSZ, La<sub>2</sub>O<sub>3</sub>), only skip adding the metal precursor to the solution.

## 4.3 Catalyst characterization technique

The catalysts were characterized by various techniques in order to gain more understanding about the catalyst structure, catalytic activity of catalyst, and possibly imply to suggest about the mechanism pathways.

### 4.3.1 X-ray Diffraction (XRD)

XRD was used to determine the bulk crystalline phases of catalyst. SIEMENS D-5000 X-ray diffractometer was its model which connected with a computer with Diffract ZT version 3.3 program for fully control of the XRD analyzer. The analysis were conducted by using CuK<sub>α</sub> ( $\lambda = 1.54439 \text{ \AA}$ ) radiation with Ni filter in the range of  $2\theta = 10-80^\circ$  and resolution of 0.04.

### **4.3.2 N<sub>2</sub> physisorption (BET surface area)**

Surface area analysis was measured by low temperature nitrogen adsorption in a surface area and porosity analyzer from Micromeritics brand model ASAP 2020 (BET multipoint). Before the analysis, 0.2 g of catalyst sample was degassed at 473 K (200°C) and 10<sup>-3</sup> mmHg for 4 hours. Adsorption measurements were carried out using liquid nitrogen at 77 K(-196°C). Specific surface areas were calculated on the basis of the BET isotherm. Pore size, volume distributions were performed by BJH (Barrett-Joyner-Halenda) desorption branch analysis.

### **4.3.3 Thermal Gravimetric Analysis (TGA)**

TGA was performed to determine the soft and hard carbons on the catalyst surface. TA Instrument SDT Q600 analyzer was used in the analysis. Around 10 mg of catalyst sample was required for analysis in air zero (carrier gas) with a temperature ramping 10 K/min from 273 to 1273 K.

### **4.3.4 Scanning Electron Microscope (SEM)**

Surface morphology was observed by using a Hitachi S-3400 N model of SEM. Before the scanning, the catalyst samples were coated by gold. An acceleration voltage of 10 kV was used in this observation.

### **4.3.5 Transmission Electron Microscopy (TEM)**

TEM with a JEM-2010 from JEOL was used to determine the catalyst morphology, size of metal catalyst, metal dispersion, and carbon on the catalyst surface.

## **4.4 Experimental setup**

Because of the high pressure (up to 30 MPa) and temperature (up to 873 K) system, the experiment was carefully set up. During the experiment, observing of the pressure system was very essential in order to avoid the process blow out; even the safety tools had already been installed.

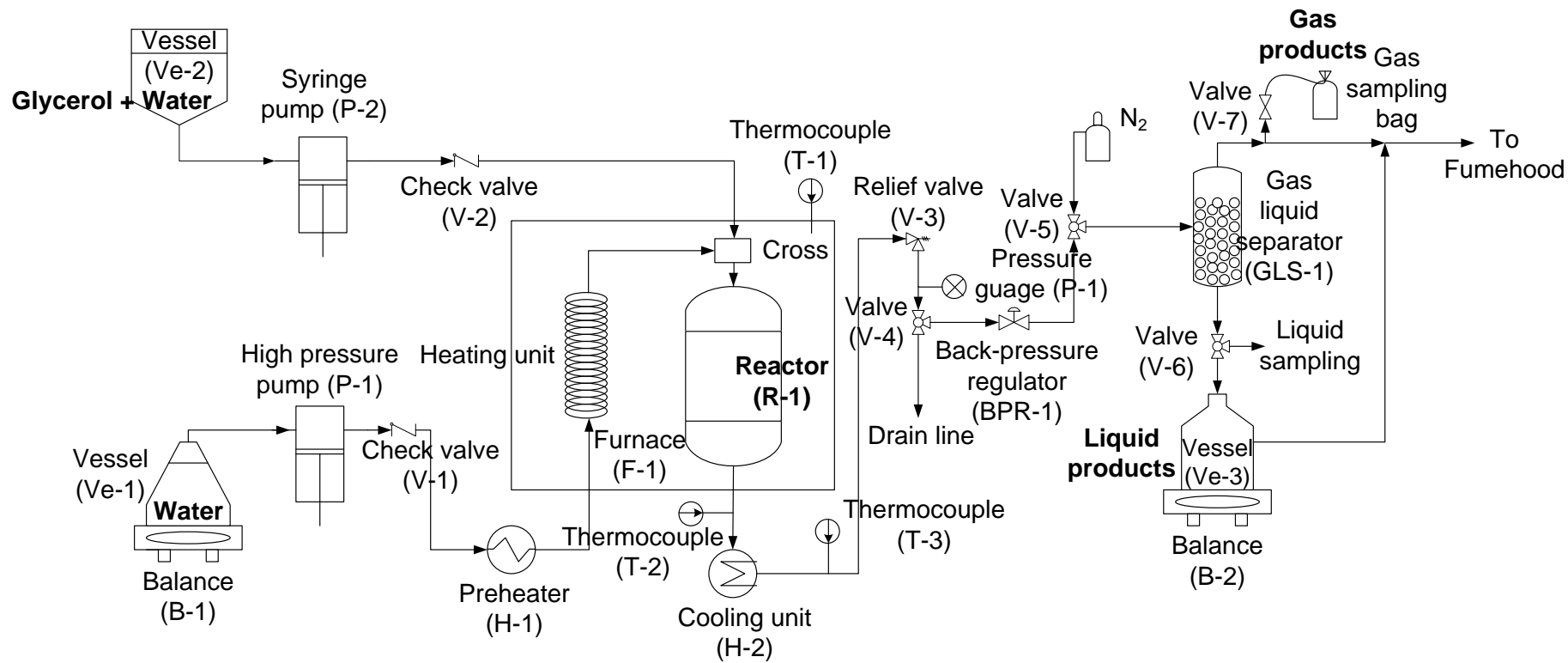
#### 4.4.1 Process diagram

A schematic diagram of the supercritical water reforming system is shown in Figure 4.1. Firstly, DI water was fed to the preheater (H-1, Thar designs) at a set flow rate through a high pressure pump (P-1, Thar designs) where it was heated to 473 K (200°C). It was further heated from 473 K to a desired operating temperature in the main heater inside the furnace (F-1, Fisher scientific). The other feed consisting of a glycerol-water mixture was delivered by a syringe pump (P-2, Teledyne Isco, 260D) to mix with the heated DI water. This was to avoid plugging the glycerol feed tube as a result of carbon formation. The mixture flowed downward through the Inconel 625 reactor (R-1, Autoclave Engineer Inc., 3 in long, 2.13 in o.d., and 0.5 in i.d.), passed the screens and went to the reacting zone. The product stream was cooled down to 283 K (10°C) by a cooling unit (H-2, Polyscience) before entering the back pressure regulator (BPR-1, Thar designs). Subsequently, it was delivered to a gas-liquid separator (GLS-1) where gas product flowed to the top. It was collected in a Kynar gas sampling bag, and then analyzed by gas chromatography (GC, Varian CP-3800). Liquid product at the bottom of separator was periodically sampled for liquid analysis by GC (Agilent 6890). ICM software (Thar designs) was used for controlling the system including the high pressure pump and the preheater.

#### 4.4.2 Equipment details

##### 4.4.2.1 High pressure pump (P-1)

DI water was stored in the Erlenmeyer flask and weighted by using a balance (B-1) model Scout Pro II 2000 g from Ohaus Inc. The ICM software was used to control DI water feed flow rate (e.g. 1, 2, and 3 g/min (actually available for 1-30 g/min)). Software from Ohaus Inc was used to record weight data every 5 s for checking the real time mass flow rate. Sometimes the air bubbles were occurred in the plastic tubes, causing lower DI water feed flow rate especially after operated for 2-3 hours. The high pressure pump was from Thar designs model P-Series P-50. It has four check valves for inlet and outlet of the pump head to ensure only one way flow. The pressure gauge at the pump also measured the real time pressure of DI water feed.



**Figure 4.1** Schematic diagram of supercritical water glycerol reforming set up

#### 4.4.2.2 Syringe pump (P-2)

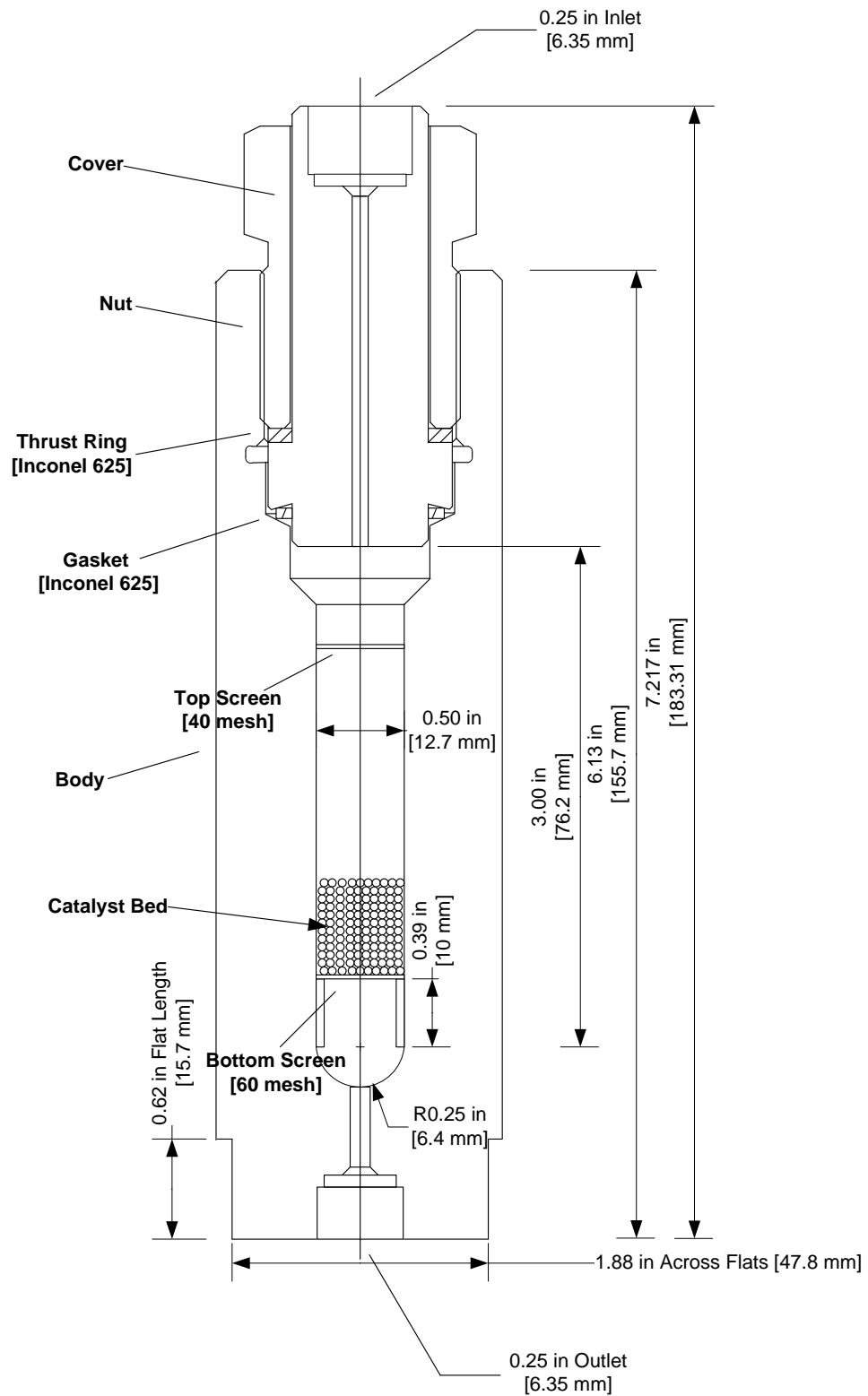
Another feed of glycerol solution (glycerol mixed with water) was delivered by Syringe pump (P-2) from Teledyne model ISCO 260 D D-Series. It was set as the volumetric flow rate (mL/min) and always offered the high precision value. Real time of pressure and liquid in the pump cylinder were also shown on the display screen. Only 266 mL of the liquid reactant was possibly stored in the pump cylinder. This syringe pump was connected to the check valve by 1/8" 316 SS tubing in order to avoid the back liquid flow to the pump. Next, an adaptor was used to change the tubing to the smaller size as 1/16" 316 SS with 0.26 mm of internal diameter tubing. The smaller internal diameter tubing was required for maximizing in velocity at the injection point in order to minimize possible glycerol cracking to graphite carbon before reaching to the reactor. It caused the failure system from its plugging.

#### 4.4.2.3 Preheater (H-1)

It was designed by Thar Technologies specific for heating in high pressure system. It consists of 1/8 inch 316 stainless steel x 0.02 in thickness x 20 ft long (H-1). A six-zone PID temperature controller (CN616 Series, Omega Engineering Inc.) controlled the water temperature to reach the set point, normally 473 K (200°C). The aluminum foil and cotton wool were used to avoid the heat transfer loss before the furnace.

#### 4.4.2.4 Reactor (R-1)

The special reactor was designed to carry out the experiments in supercritical water condition. A Kuentzel closure pressure vessel was made of Inconel 625 which was fabricated by Autoclave Engineers. It has been certified by Autoclave Engineers and the Technical Standards and Safety Authority in Canada (TSSA). The maximum safety working temperature and pressure allowable of the reactor are 923 K and 31 MPa.



**Figure 4.2** Schematic diagram of the reactor

The reactor dimension includes 0.5 inch i.d., 2.13 inch o.d., and 3 inch long as shown in Figure 4.2. A 0.39 inch long stainless steel tube with 0.5 inch o.d. and 0.08 inch thickness was stayed to support the screen. The 1 g of catalyst was packed in the middle of reactor supported on a 60 mesh (SS 316, Sigma-Aldrich). The bottom screen acted as a filter to prevent carbon particles that may be formed and carried over to the back pressure regulator. However, the top screen (40 mesh SS 316, Sigma-Aldrich) was used to protect any small particle flowing back to the equipments and to avoid particle from an anti sieve lubricant compound that might fall and mix with the catalyst during opening the reactor.

#### 4.4.2.5 Cooling unit (H-2)

The hand-made heat exchanger includes a 20 ft long, 1/8 inch 316 stainless steel tube houses in a horizontal copper vessel. The head of vessel was made by brass which was connected from the outlet tube's reactor in order to cool down the product stream after reaction in the reacting zone. The temperature was rapidly decreased to 283 K (10 °C), avoiding the stream to stay in subcritical conditions for a long period. 30 vol.% of ethylene glycol in water was a coolant for removing heat of the product stream. It was circulated in the circulating bath model 910-TH type refrigeration/heat from PolyScience Inc. Note that the temperature of product stream should be around 283 K (set approximately 280 K at the circulating bath) in order to make sure all condensable species in liquid phase especially acetaldehyde (boiling point at 294 K). After the experiments, the liquid samples were collected in the fridge, waiting for analysis.

#### 4.4.2.6 Main mass flow controller and mass flow controllers

Main mass flow controller model is URS-100 from Unit Instruments, Inc. which can possibly connect to five channels. Each channel can be adjusted from 0.0 to 99.9 corresponding to the gas flow rate passing the mass flow controller. Calibration curve was required before the experiment in order to control the gas flow rate (Appendix B). Only two channels were used in this research, one was UFC-1200A (range: 12 SCCM) that controlled nitrogen gas flow rate to the gas-liquid separator as an internal standard in gas analysis. Another one was UFC-1100A (range: 125

SCCM) which controlled the hydrogen gas to the reactor in order to pre-treat the catalyst.

#### 4.4.2.7 Back pressure regulator (BPR-1)

Back pressure regulator model BPR-A 200B from Thar Technologies Inc. was used to control the pressure system with a hand held controller. Back pressure regulator was worked by pushing (increasing the pressure) and drawing (decreasing the pressure) a needle into a seat during the experiment in the range pressure of 0.01 to 35 MPa. A built in pressure sensor provides a close loop feedback for controlling pressure to the set point. The alarm pressure was set at 35 MPa in the ICM software. In case of exceeding the pressure (more than 35 MPa), pump 1 and preheater will be shut down for the safety reason.

#### 4.4.2.8 Gas-liquid separator (GLS-1)

Glass beads of 4 mm diameter fill in around 75% of Gas-Liquid Separator unit which has a dimension of 25 mm internal diameter x 120 mm height. This equipment is connected from the back pressure regulator to separate gas and liquid products at atmospheric pressure. The liquid product bottle is connected to the Gas-Liquid Separator and vent line and also stayed on the balance for online weighting.

#### 4.4.2.9 Gas chromatography

##### 4.4.2.9.1 Gas analysis (GC-1)

The sampling gas product was properly collected in the gas sampling bag to avoid the contamination of gas impurities from outside. Subsequently, the gas sampling bag was connected to the GC Varian CP-3800. The analysis should be within one day after collecting the sample for accuracy reason. During of the stabilization time, it must be pushed by hands to let the gas products flowed to fill the sampling loop until the analysis was started. Two columns including 15 ft long x 1/8 inch stainless steel of 60/80 mesh Carboxen 1000 column (TCD) and 50 m x 0.53 mm of Al<sub>2</sub>O<sub>3</sub>/KCl fused silica PCOT column. The conditions are shown in Tables 4.1 and 4.2. The results for TCD and FID were offered after finishing 20 min of analysis.



#### 4.4.2.9.2 Liquid analysis (GC-2)

After collecting the liquid product samples from the experiment, they would be stored in the fridge at 263 K (-10°C) to avoid product loss from evaporation before analysis. For preparation before the analysis, each sample must be warmed up by the water at room temperature until the liquid product sample was in the liquid phase. Then immediately mixed the sample with the standard solution (1,4 butanedial as an internal standard in water). The amount of standard solution and sample were measured by weight approximately around 1.76 and 0.24 g, respectively. Only small amount of sample in the solution was used reasoning order to avoid the high viscous components content such as glycerol, acetic acid, etc. which could be remained in the column and caused long tailed peaks in the next analysis. Gas Chromatography (6890 Series Agilent) was used in this analysis. It was started after 1  $\mu$ L was injected by Auto sampler (7683 Sereis injector Agilent). The problem was found as the different amount of sample (exactly set the similar volume at the software) was injected to the column. It was explained from the unsmooth syringe causing of the high viscous components stucked to the plunger. Solvent A (methanol), and B (water) were applied to be rinsing solutions. Number of rinsing is shown in Table 4.3. A capillary column (DB-wax, Capillary 30.0 m x 530  $\mu$ m x 1.00  $\mu$ m normal) was set up to the GC for liquid analysis. The GC conditions and temperature program were shown in Table 4.4 and 4.5, respectively.

**Table 4.1** The gas chromatography conditions (TCD and FID)

Flow rate set point	50 mL/min
Pressure	0.32 MPa (47 psi)
Linear velocity	9000 cm/s
Column oven temperature start	308 K (35 °C)
Front valve temperature	423 K (150 °C)
Mid valve temperature	423 K (150 °C)
Rear valve temperature	423 K (150 °C)
Front TCD temperature	423 K (150 °C)
Rear FID temperature	523 K (250 °C)
Stabilization time	1 min
Enable coolant start	323 K (50 °C)
Stabilization time	20 min

**Table 4.2** Temperature program of the gas analysis.

<i>Temperature (K)</i>	<i>Ramp rate (K/min)</i>	<i>Hold (min)</i>	<i>Run time (min)</i>
308 (35 °C)	-	5	5
468 (195°C)	20	7	20

**Table 4.3** Number of rinsing for pre-injection and post-injection.

	<i>Pre-injection (time)</i>	<i>Post-injection (time)</i>
Sample	3	-
Solvent A	7	7
Solvent B	5	3
Pump	3	-

**Table 4.4** The gas chromatography conditions (FID)

Helium flow rate (carrier gas)	4.8 mL/min
Hydrogen flow rate	30 mL/min
Air flow rate	400 mL/min
Gas saver flow rate	20 mL/min for 2 min
Makeup flow rate (Helium)	10.5 mL/min
Average velocity	34 cm/s
Split ratio	10:1
Split flow	48 mL/min
Injection port temperature	523 K (250 °C)
Detector temperature	573 K (300 °C)

**Table 4.5** Temperature program of the liquid analysis.

<i>Temperature (K)</i>	<i>Ramp rate (K/min)</i>	<i>Hold (min)</i>	<i>Run time (min)</i>
313 (40°C)	-	1	1
373 (100°C)	10	0	7
493 (220°C)	20	7	20

# CHAPTER V

## THERMODYNAMIC ANALYSIS OF HYDROGEN PRODUCTION FROM GLYCEROL AT ENERGY SELF- SUFFICIENT CONDITIONS

In this chapter, a thermodynamic analysis based on the principle of minimization of Gibbs free energy was performed for hydrogen production from glycerol from various reaction routes including steam reforming, partial oxidation, and autothermal reforming. The effects of operating parameters, i.e. water/glycerol ratio (*WGR*), oxygen/glycerol ratio (*OGR*) and operating temperature (*T*) on hydrogen production, carbon formation, and net energy were investigated. The operating conditions were carefully chosen to achieve the energy self-sufficient conditions for two system levels, i.e., the reformer level and the overall system level. Finally, the suitable conditions which offer the highest hydrogen production for both system levels are determined and the obtained hydrogen productions are compared.

### 5.1 Introduction

Among all the applications of glycerol, hydrogen production has attracted a number of researches, especially considering the large potential for hydrogen demand in fuel cell applications for stationary power generator, portable power, micro power, and transportation (Youn et al., 2008). Hydrogen production can be carried out via different reactions such as gasification, steam reforming (SR) (Faungnawakij et al., 2006; Adhikari et al., 2007b; Das et al., 2007; Rakib et al., 2008; Hernandez and Kafarov, 2009; Oliveira et al., 2009; Beaver et al., 2010), aqueous-phase reforming (APR) (Luo et al., 2007, 2008; Iriondo et al., 2008), and autothermal reforming (ATR) (Dauenhauer et al., 2006; Li et al., 2008; Reese et al., 2009, 2010). Steam

reforming is currently the most commonly-used process for hydrogen production, which can be developed by investigating suitable operating conditions (pressure, temperature, water to fuel ratios), catalysts, and heat transfer management (Yanbing et al., 2007). However, it requires a large amount of heat from an external heat source. On the other hand, considerably lower energy demand can be achieved when adding some oxygen in the reforming process. Therefore, autothermal reforming is considered as a process with lower demand of external heat sources.

A number of works on hydrogen production from glycerol have recently been studied. Adhikari et al. (2007a) exposed that temperatures higher than 900 K, atmospheric pressure and water/glycerol ratio (*WGR*) of 9 were suitable for hydrogen production via glycerol steam reforming by using of Gibbs minimization method. Under these conditions methane production and solid carbon are thermodynamically diminished. Dauenhauer et al. (2006) examined the autothermal reforming of glycerol. The best condition was found with Rhodium-Ceria-washcoat catalyst at *WGR* of 4.5, carbon to oxygen ratio of 0.9 and temperature of 1135 K, offering hydrogen selectivity of 79%. Furthermore, Slinn et al. (2008) reported the prediction of reformer performance by thermodynamic theory with the optimum conditions for glycerol reforming at 1133 K and *WGR* of 2.5.

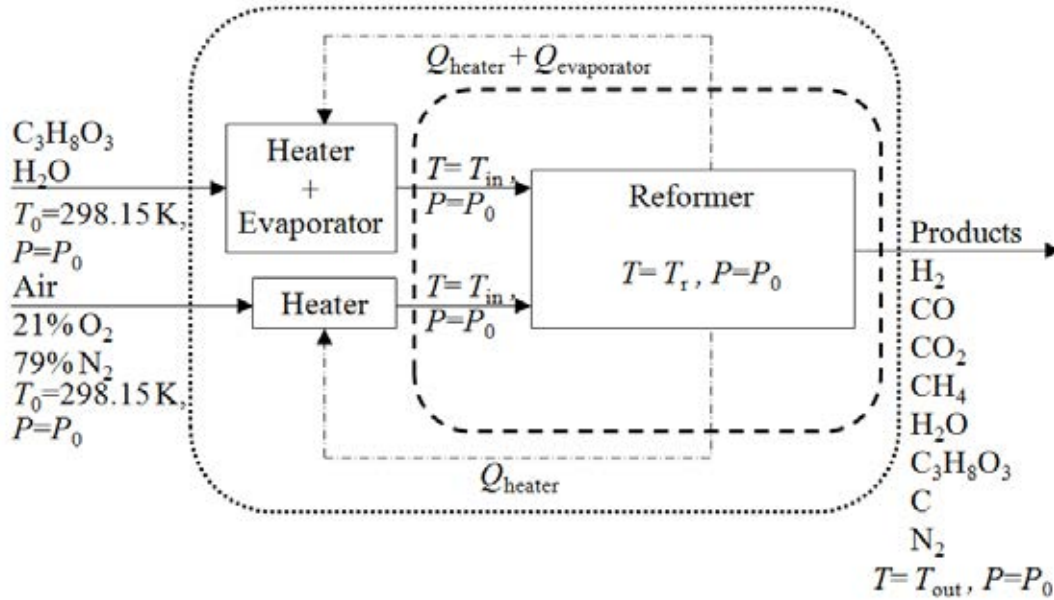
## 5.2 Boundary for calculation

Equation (2.41) is provided for consideration of solid carbon-gas system (Wang et al. 2008).

$$\sum_{i=1}^{N-1} n_i \left( \Delta G_{f_i}^0 + RT \ln \frac{\hat{\phi}_i y_i P}{P^0} + \sum_j \lambda_j a_{ij} \right) + n_C G_{C(s)}(T, P) = 0 \quad (2.41)$$

Aspen Plus program (Aspen Plus<sup>®</sup> Version 2006) was employed for calculating equilibrium compositions and the corresponding overall heat of reactions under the conditions of minimization of Gibbs free energy. Glycerol (C<sub>3</sub>H<sub>8</sub>O<sub>3</sub>), water (H<sub>2</sub>O), hydrogen (H<sub>2</sub>), carbon monoxide (CO), carbon dioxide (CO<sub>2</sub>), methane (CH<sub>4</sub>), carbon (C<sub>(s)</sub>), oxygen (O<sub>2</sub>) and nitrogen (N<sub>2</sub>) are identified as possible species in the equilibrium products. The Soave–Redlich–Kwong equation was selected as the

method for estimating thermodynamic properties of the reaction systems (Li et al., 2008; Wang et al., 2008, 2009).



**Figure 5.1** The schematic of energy boundary conditions – – – Reformer, ..... System, and - · - · - Heat transfer in system case. (If isothermal condition is considered in reformer level,  $T_{in}$ ,  $T_r$ , and  $T_{out}$  will be equivalent).

Figure 5.1 shows the system of energy balance in the hydrogen production from glycerol. Two levels of energy balances; i.e. reformer and overall system levels, are considered. Equation (5.1) shows the energy balance equation around the reformer unit. However, depending on the amount of air supplied, the reformer duty might be relatively small in comparison of the overall system duty. Therefore, in the overall system level analysis, net energy including all heat required in the heater, evaporator, and reformer are taken into account. The energy balance in the system level is shown in Equation (5.2).

$$Q_{\text{reformer (net)}} = \sum_{i=1}^N n_{i,\text{out}} H_{i,\text{out}} - \sum_{i=1}^N n_{i,\text{in}} H_{i,\text{in}} \quad (5.1)$$

$$Q_{\text{system (net)}} = Q_{\text{heater (net)}} + Q_{\text{evaporator}} + Q_{\text{reformer}} = \sum_{i=1}^N n_{i,\text{out}} H_{i,\text{out}} - \sum_{i=1}^N n_{i,0} H_{i,0} \quad (5.2)$$

The total net heat energy can be positive (endothermic), negative (exothermic) and zero (energy self-sufficient). The last one is the condition of interest in this study. The energy self-sufficient condition can be found by setting Equations (5.1) and (5.2) equal to zero for the reformer, and system cases, respectively. It should be noted that the results obtained from the calculations in this work represent the maximum achievable hydrogen production based on the energy self-sufficient system. In a real system, the values will be lower due to deviation from the thermodynamic equilibrium reactions and the presence of heat loss.

The reaction performances are expressed in terms of glycerol conversion (Equation (5.3)), and yield of product H<sub>2</sub> (Equation (5.4)), carbon product *i* (Equation (5.5)). In all simulations the glycerol feed rate and operating pressure are kept at 1 mol s<sup>-1</sup> and 0.101325 MPa, respectively.

$$\text{Glycerol conversion} = \frac{n_{\text{Glycerol},0} - n_{\text{Glycerol},\text{out}}}{n_{\text{Glycerol},0}} \quad (5.3)$$

$$\text{Yield of product H}_2 = \frac{n_{\text{H}_2,\text{out}}}{n_{\text{Glycerol},0}} \quad (5.4)$$

$$\text{Yield of carbon product } i = \frac{n_{i,\text{out}}}{3 \times n_{\text{Glycerol},0}} \quad (5.5)$$

## 5.3 Results and discussion

At the conditions chosen in this work, all simulations showed that the glycerol conversion from Equation (5.3) is 1, which means that no glycerol appears in the products.

### 5.3.1 Hydrogen production from glycerol under isothermal operation

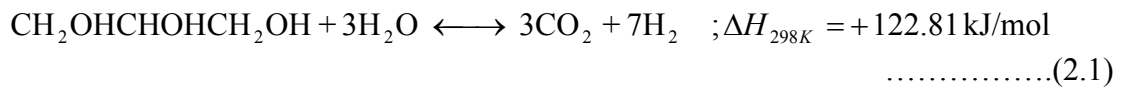
#### 5.3.1.1 Yield of hydrogen

Figure 5.2a shows the yield of H<sub>2</sub> at different values of *WGR* and *OGR*. The calculations are based on isothermal operation at  $T = 940$  K. To verify the



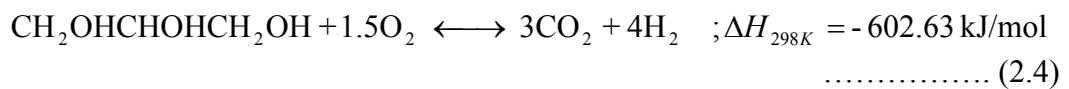
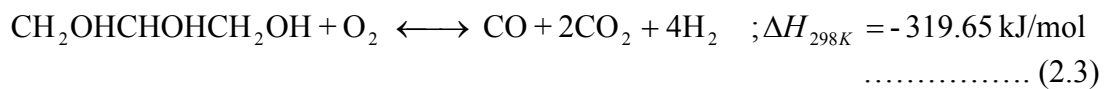
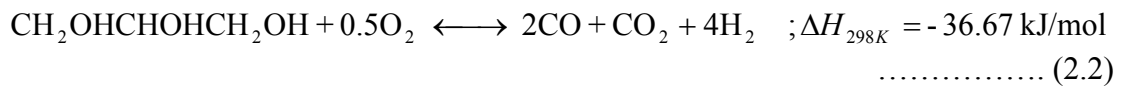
calculations, the results from previous published works (Adhikari et al., 2007a; Wang et al., 2008; Rossi et al., 2009) shown by symbols are compared with those from simulations in this work. The simulation results from this work show very good agreement with those from previous works with discrepancy within  $\pm 1.50\%$ . It is clearly shown that they all are in good agreement.

The overall reaction of glycerol Steam Reforming (SR):

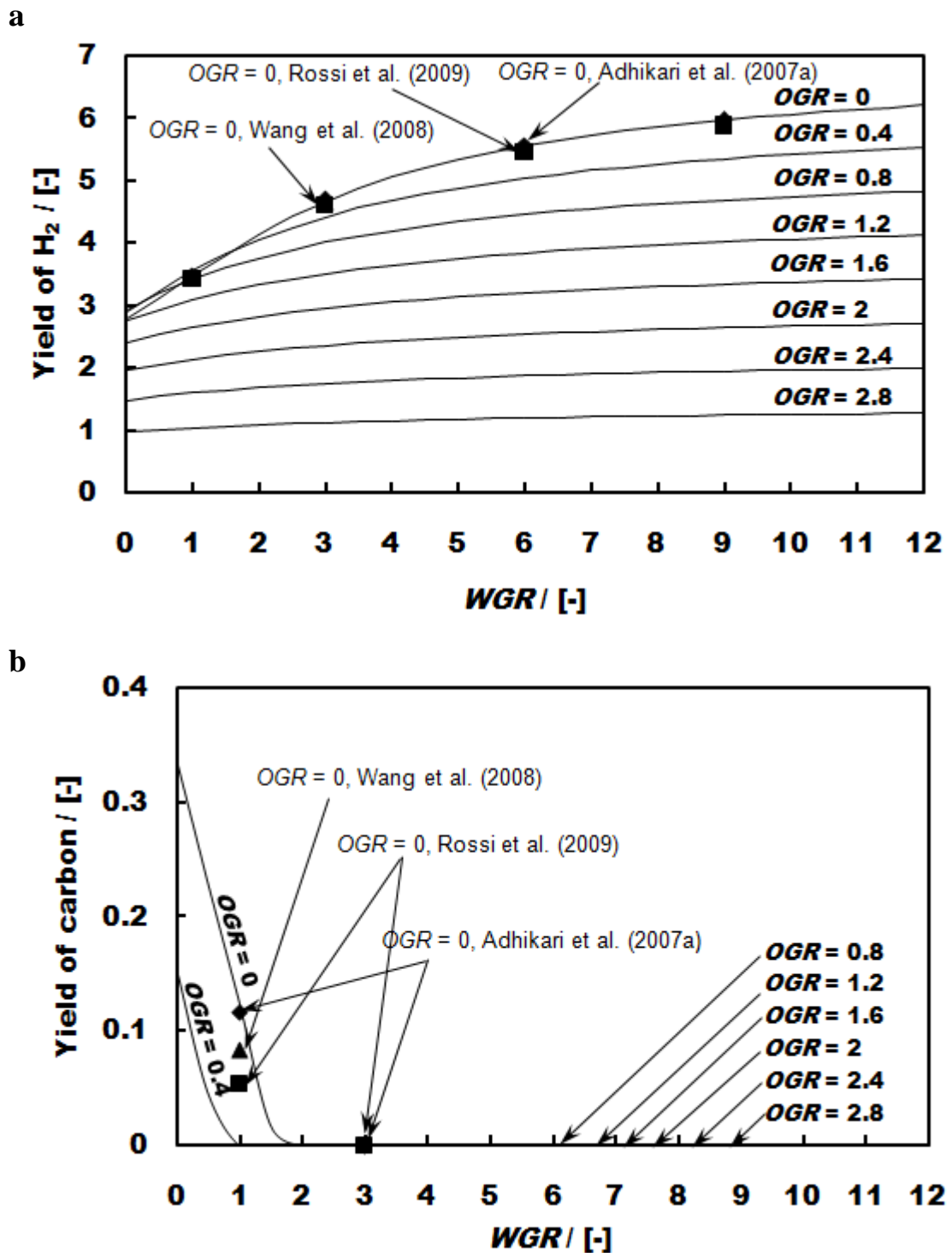


Glycerol oxidations are divided to Partial Oxidation (POX) and Oxidation (OX):

Partial Oxidations (POX):



At  $OGR = 0$ , SR (Equation (2.1)) is the main reaction. According to the reaction stoichiometry, three moles of  $\text{H}_2\text{O}$  ( $WGR = 3$ ) are required to react with one mole of glycerol. It is obvious that the yield of  $\text{H}_2$  increases with increasing  $WGR$  and the value as high as 6.20 could be achieved at  $WGR = 12$  and  $OGR = 0$ . When  $OGR$  is greater than 0, hydrogen is also generated via POXs (Equations (2.2)-(2.4)). The use of oxidant (air) together with steam has been a promising strategy in hydrogen production technology as it can reduce the demand of energy requirement/transfer to the reaction system (Rabenstein et al., 2008). However, the yield of  $\text{H}_2$  obviously decreases with increasing  $OGR$ , and therefore, high levels of  $OGR$  should be avoided. It should be noted that at the same values of  $WGR$ , the yield of  $\text{H}_2$  at  $OGR = 0$  are generally higher than those at  $OGR > 0$  except at  $WGR < 2$ . This is attributed to the presence of carbon formation which will be discussed in the following section.

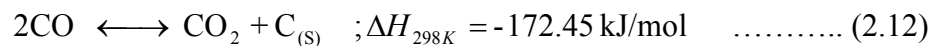


**Figure 5.2** (a) Yield of  $H_2$  (b) Yield of carbon at different values of  $WGR$  and  $OGR$  at  $P=0.101325$  MPa,  $T = 940$  K;  $\diamond$  at  $OGR=0$  (Adhikari et al., 2007a);  $\blacktriangle$  at  $OGR=0$  (Wang et al., 2008);  $\blacksquare$  at  $OGR=0$  (Rossi et al., 2009);

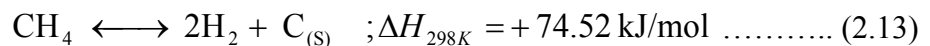
### 5.3.1.2 Carbon formation

A major problem with the reforming processes is the formation of solid carbon or coke. When solid carbon occurs, it causes some disadvantages to the processes including blockage of the catalyst pores, and breakdown of the reactor in severe cases because of plugging (Reese et al., 2010). Solid carbon is an unfavored product in hydrogen production. It can take place via several undesired reactions (Equations (2.12)-(2.14)), e.g. CO disproportionation (Equation (2.12)) or CH<sub>4</sub> cracking (Equation (2.13)) or the reaction of CO with H<sub>2</sub> (Equation (2.14)) (Wang et al., 2008). As shown in Figure 5.2b for  $T = 940$  K, no carbon formation occurs when  $WGR > 2$  or  $OGR > 0.8$ . The highest mole of carbon (0.34) appears at the most severe condition of  $WGR = 0$  and  $OGR = 0$ . Carbon formation can be suppressed by increasing  $WGR$ , which retards the reduction of CO (Equation (2.14)) and/or increasing  $OGR$  which promotes the POXs whose products could subsequently suppress carbon formation. Figure 5.2b also compares the values of the yield of carbon calculated from this work with those from literatures (Adhikari et al., 2007a; Wang et al. 2008; Rossi et al., 2008). Some discrepancy observed among the literatures (Adhikari et al., 2007a; Wang et al., 2008; Rossi et al., 2009) and this work is due to the differences in equation of state and thermodynamic data sources.

Boudouard reaction:

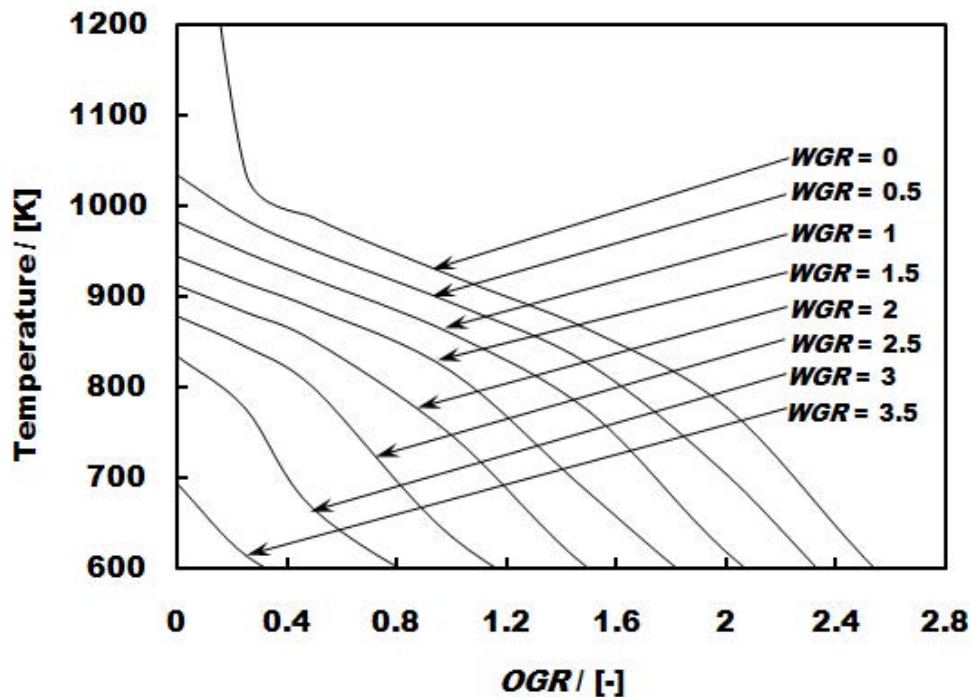


Methane cracking:



Reduction of CO:





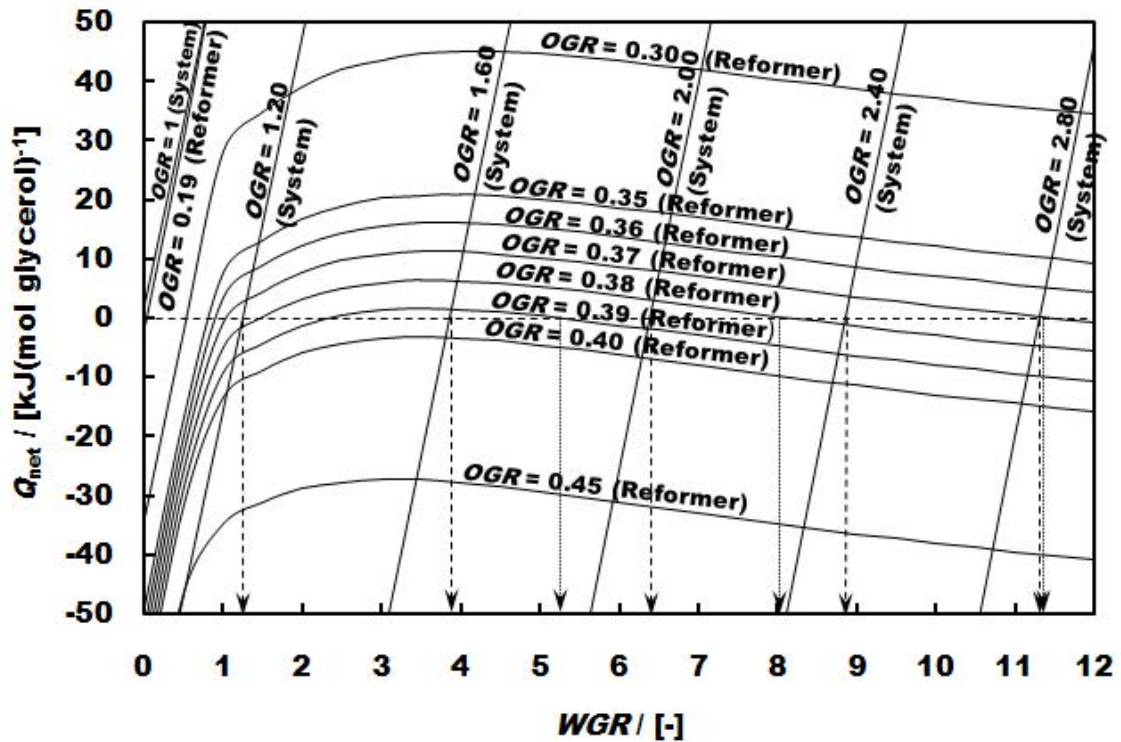
**Figure 5.3** Boundary of carbon formation as a function of  $WGR$ ,  $OGR$ , and  $T$  at  $P=0.101325$  MPa

Figure 5.3 shows the temperatures at boundary of carbon formation for wider ranges of  $WGR$  and  $OGR$ . For example, at  $WGR = 0.5$  and  $OGR = 0$ , carbon formation starts to appear at  $T = 1038.5$  K and a higher temperature than this value ( $T > 1038.5$  K) is required to avoid the carbon formation. Again, it is clear that carbon formation becomes less severe when increasing  $WGR$  or  $OGR$ .

### 5.3.1.3 Net heat energy

Figure 5.4 shows the effects of  $WGR$  and  $OGR$  on the net heat energies of the reformer and the overall system at  $T = 940$  K. For the reformer level, when increasing  $WGR$  from 0 to 1.5, the net heat energy sharply increases until reaching a maximum. After reaching its maximum value, the net heat energy gradually decreases. The increase of the net heat energy is mainly governed by the strong endothermic SR while the decrease of the net heat energy is likely from the exothermic WGS particularly at high excess amount of water. The net heat energy obviously decreases with increasing  $OGR$  as the exothermic POXs play a more important role. There are only some ranges of  $OGR$  (0.19-0.39) which provides the energy self-sufficient

condition ( $Q_{\text{net}} = 0$ , dashed line). It should be noted that although two values of  $WGR$  are observed for a given value of  $OGR$ , the higher value  $WGR$  should be selected as it offers a higher hydrogen production.



**Figure 5.4** Net heat energies ( $Q_{\text{net}}$ ) of Reformer and System as a function of  $WGR$  and  $OGR$  at  $P=0.101325$  MPa,  $T_r=940$  K.

Considering the energy balance on the system level, in contrast, energy self-sufficient condition of the system can occur in a wider range of  $OGR$  (1.0-2.8 for  $T = 940$  K). At  $OGR = 1$ , it is the minimum  $OGR$  value to offer energy self-sufficient condition at  $WGR = 0$ , then increasing  $WGR$  increases energy requirement of the system. The relationship of  $OGR$  and  $WGR$  in the system at energy self-sufficient condition is quite different from that of the reformer case; namely, increasing  $WGR$  always requires higher  $OGR$ . The key reason is the huge energy requirement for heating liquid water at  $T_0 = 298.15$  K to vapor at a high temperature. Thus, a relatively high value of  $OGR$  is necessary to generate sufficient energy for the system. However, hydrogen production greatly reduces when operating at higher values of  $OGR$  (Figure 5.2a). Therefore,  $WGR$  is a significant parameter to be selected for

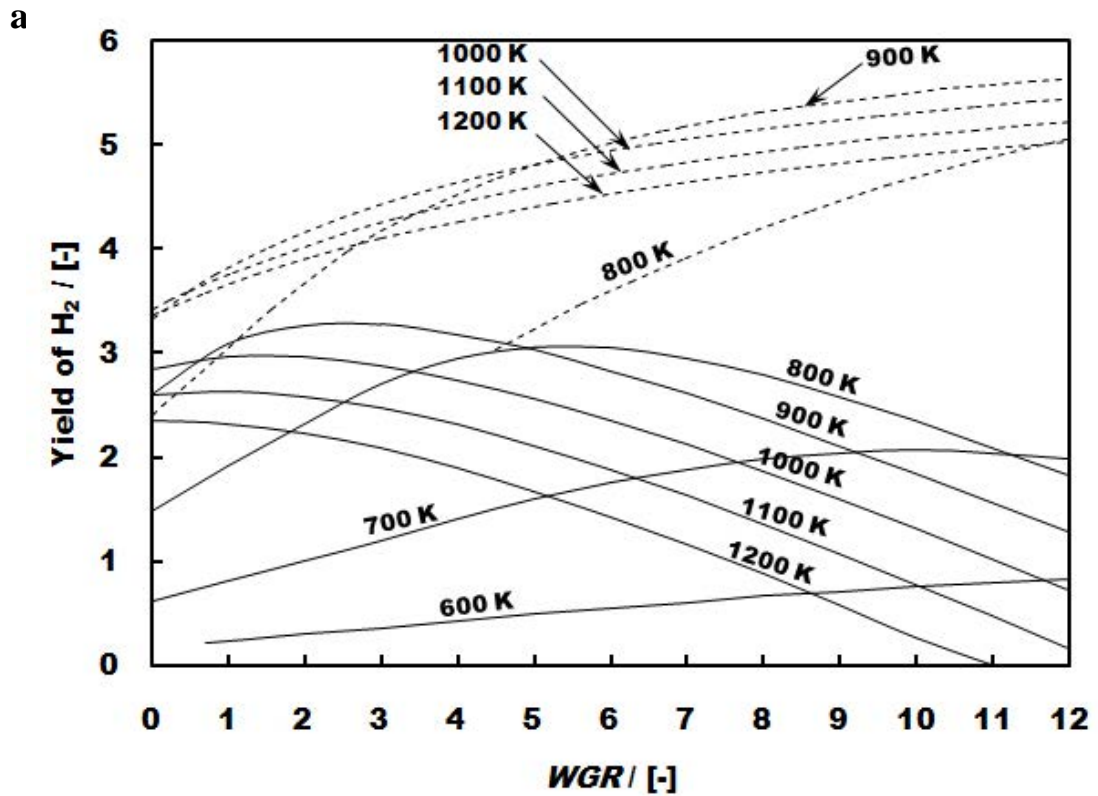
achieving high hydrogen production. In the following sections only the simulation results based on the energy self-sufficient condition will be reported.

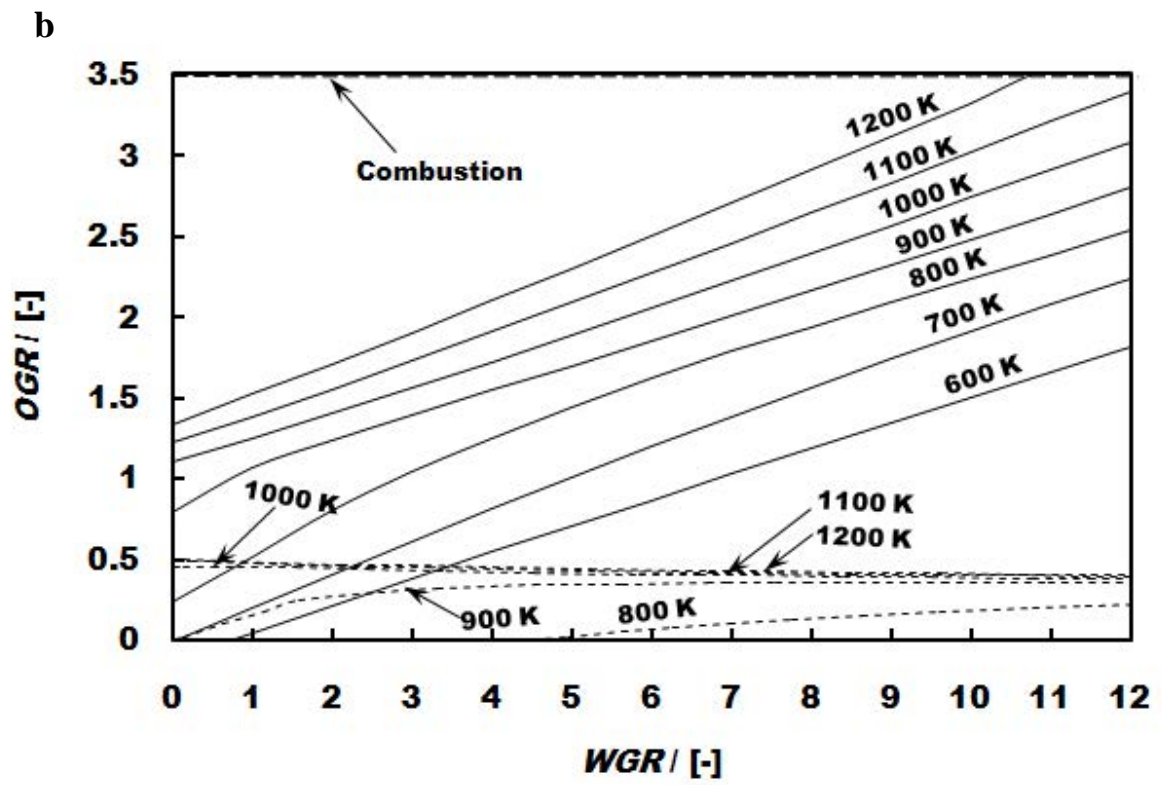
### **5.3.2 Hydrogen production from glycerol under energy self-sufficient condition**

From the previous section, it is demonstrated that energy self-sufficient condition can be achieved by appropriate adjustment of operating parameters including  $WGR$ ,  $OGR$ , and the operating temperature. However, only 2 parameters can be specified and the other is to be determined. For example, when  $WGR$  and  $OGR$  are given, only some values of temperature are possible to offer the energy self-sufficient condition. It should be noted that although operating pressure can also influence the condition, the main SR is favorable at low pressure and therefore only the operation at atmospheric pressure is considered in this study. Figure 5.5a shows the yield of  $H_2$  at different values of  $WGR$  and operating temperatures while their corresponding values of  $OGR$  are given in Figure 5.5b. For the reformer case (shown by dashed lines), the yield of  $H_2$  always increases when increasing  $WGR$ . In contrast, for the system case, there is an optimum  $WGR$  that provides the highest mole of  $H_2$  for each temperature. Figure 5.5b indicates that the corresponding values of  $OGR$  are not quite dependent on  $WGR$  for the reformer case unlike the overall system case (continuous lines). This is obviously because the feed temperature for the reformer case is assumed to be at the operating temperature of interest while it is at  $T_0 = 298.15$  K for the system case. Therefore, the energy change within the reformer only arises from the change in heat of reaction which is quite small relatively to the high energy demanded for preheating the feeds (especially water). For the system case at low values of  $WGR$ , the yield of  $H_2$  increases with increasing  $WGR$  according to the promotion of SR; however, the higher  $OGR$  required for generating sufficient energy for feed heating deteriorates the hydrogen production. It should be noted that for some operating temperatures, minimum values of  $WGR$  to achieve energy self-sufficient condition are observed for both the reformer and the system levels. The values appear at  $OGR = 0$ .

The influence of operating temperature on the yield of  $H_2$  and corresponding  $OGR$  at a specific value of  $WGR$  is demonstrated in Figure 5.6 ( $WGR = 10$  for the reformer case and  $WGR = 7$  for the system case). It is clear that the value of  $OGR$  always increases with increasing operating temperature; however, there is an optimum temperature which provides the highest yield of  $H_2$  for a given  $WGR$ . Because the strong endothermic SR is favorable at high temperatures, the yield of  $H_2$  increases significantly with increasing operating temperature. However, the decrease of  $H_2$  at higher temperatures results from both the reverse of WGS (Equation (2.10)) which is also favorable at high temperatures and from the demand of higher  $OGR$  which results in lowering hydrogen production (Figure 5.2a).

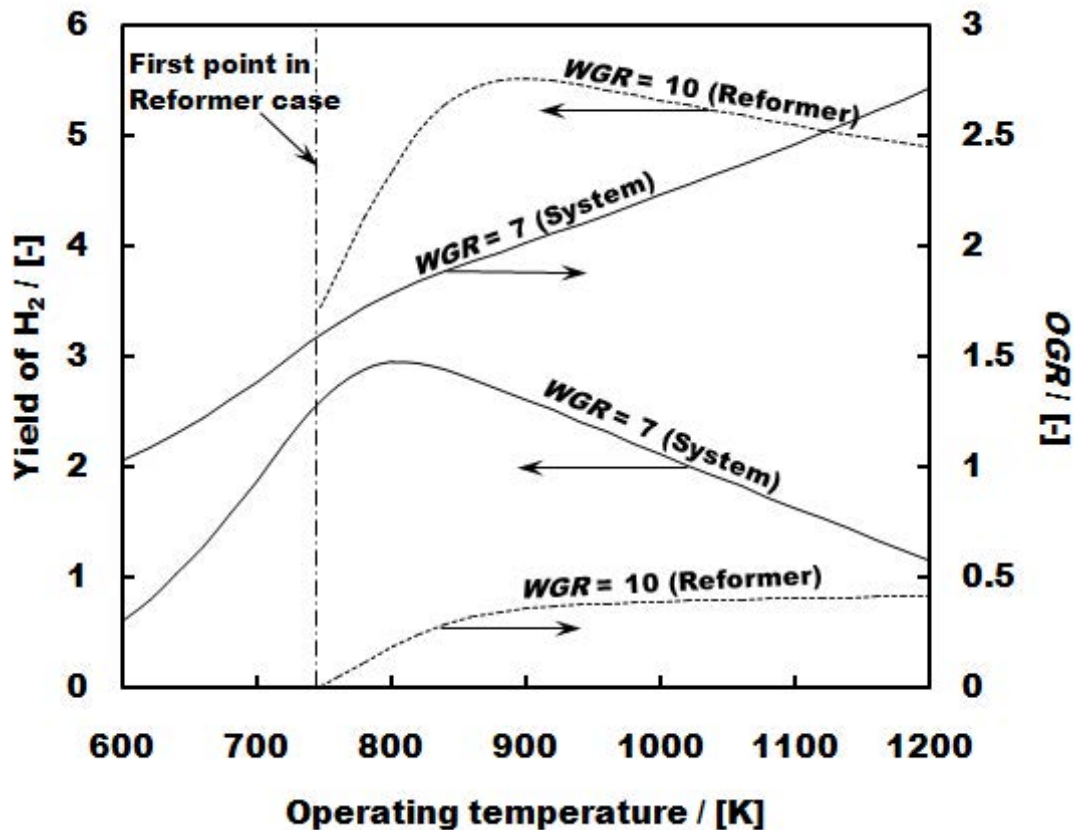
Water Gas Shift (WGR or reverse of this is called RWGS):





**Figure 5.5** (a) Yield of  $H_2$  (b)  $OGR$  of reformer and system as a function of  $WGR$  and operating temperature at energy self-sufficient condition; ----- Reformer, —— System.



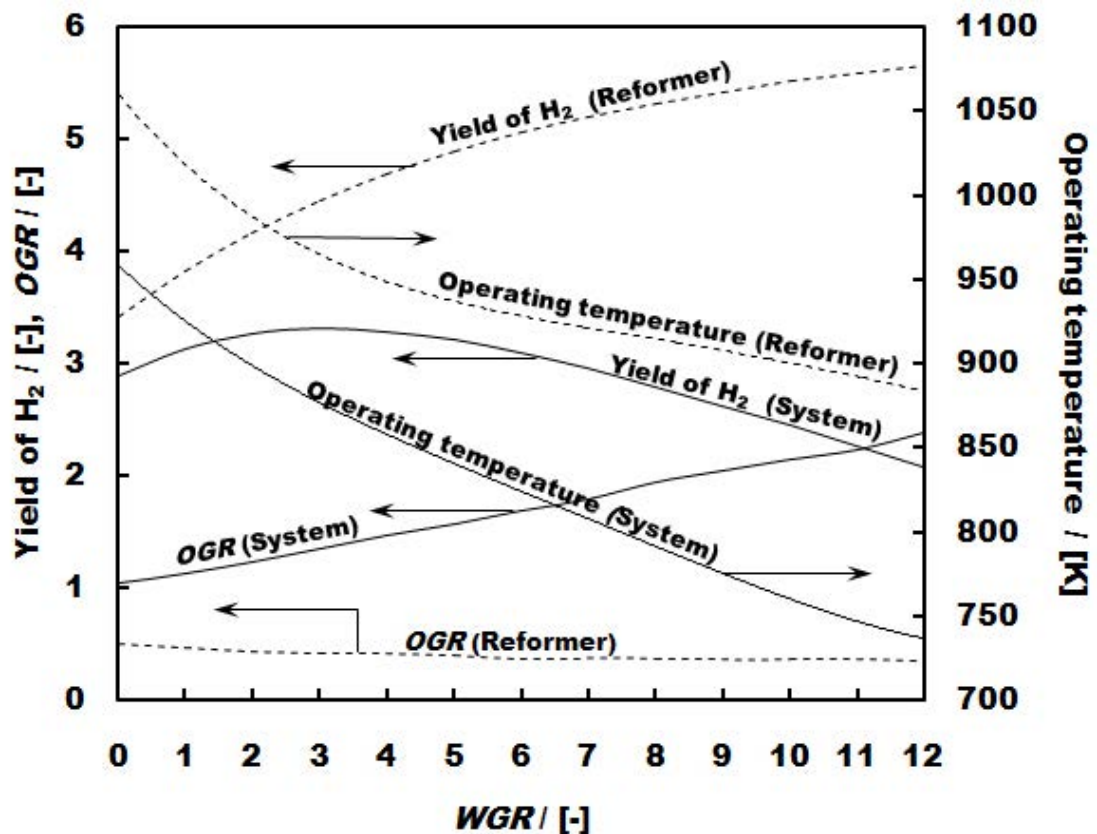


**Figure 5.6** Yield of H<sub>2</sub> and OGR of Reformer ( $WGR=10$ ) and System ( $WGR=7$ ) as a function of operating temperature at energy self-sufficient condition; ----- Reformer, ——— System.

### 5.3.3 Maximum hydrogen production

From the previous section it is clear that there is an optimum operating temperature which provides the highest yield of H<sub>2</sub> for each  $WGR$ . In order to determine the maximum possible hydrogen production, the highest yield of H<sub>2</sub> together with their corresponding OGR and operating temperature are calculated at different values of  $WGR$  (Figure 5.7). In the reformer case, it was observed that the yield of H<sub>2</sub> always increase with increasing  $WGR$ . Within the range of  $WGR = 0-12$ , the maximum yield of H<sub>2</sub> is 5.65 at  $WGR = 12$ ,  $OGR = 0.35$ , and  $T = 880$  K. However, for the system case, the maximum value of 3.31 appears at  $WGR = 3$ ,  $OGR = 1.35$ , and  $T = 875$  K. Although the yield of H<sub>2</sub> increases at the beginning, the use of too much value of  $WGR$  causes detrimental effect on the hydrogen production as the system requires too much energy for heating the excessive water. Figure 5.7 also

indicates that the value of  $OGR$  for the reformer case slightly changes with increasing  $WGR$ . As reported earlier, there is a small range of  $OGR$  which can offer energy self-sufficient condition. However, for the system case the energy requirement changes quite significantly with increasing  $WGR$  and therefore the  $OGR$  becomes more dependent on  $WGR$ . It should be noted that when operating the reformer or the system with higher  $WGR$ , the optimum temperature always decreases. This should be related to the exothermic WGS which becomes more favorable toward hydrogen production at a lower temperature.



**Figure 5.7** Maximum of yield of H<sub>2</sub>,  $OGR$  and operating temperature of reformer and system levels as a function of  $WGR$  at energy self-sufficient condition; ----- Reformer, —— System.

From this study, it is demonstrated that when hydrogen production operates under energy self-sufficient condition, a maximum hydrogen production of 3.31 mol H<sub>2</sub>/mol glycerol is achieved. In practice, the hydrogen production will be lower than this value because of the presence of inevitable heat losses in the system. The reported

value is much lower compared with the case when the production is operated under the energy self-sufficient in the reformer. However, in this case additional heat sources are required for other unit operations.

## 5.4 Conclusion

A thermodynamic analysis of hydrogen production from glycerol reforming was carried out. The results from isothermal operation indicate that increasing  $WGR$  enhances the hydrogen production but also requires large extent of external heat source. However, an increase of  $OGR$  reduces the hydrogen production but decreases the energy requirement. The energy self-sufficient condition can be achieved when  $WGR$ ,  $OGR$ , and operating temperature are carefully selected. The energy self-sufficient for the reformer level shows that only a small amount of  $OGR$  is required in the operation. The maximum mole of  $H_2$  in the range of study is 5.65 at  $WGR = 12$ ,  $OGR = 0.35$ , and  $T = 880$  K. Much higher  $OGR$  is required to provide sufficient energy especially for the feed preheating which is in contrast to the energy self-sufficient for the overall system level. At the system level, the maximum yield of  $H_2$  is achievable under self-sufficient conditions 3.31, which corresponds  $WGR = 3$ ,  $OGR = 1.35$ , and  $T = 875$  K.

# CHAPTER VI

## EFFECT OF MODE OF OPERATION ON HYDROGEN PRODUCTION FROM GLYCEROL AT THERMAL NEUTRAL CONDITIONS: THERMODYNAMIC ANALYSIS

Thermodynamic analysis of hydrogen production from glycerol under thermal neutral conditions is studied in this chapter. Heat requirement from the process can be achieved from the exothermic reaction of glycerol with oxygen in air fed to the system. Two modes of operation for air feeding are considered including (i) *Single-feed* mode in which air is fed in combination with water and glycerol to the reformer, and (ii) *Split-feed* mode in which air and part of glycerol are fed to a combustor in order to generate heat. The thermal neutral conditions are considered for two levels including *Reformer* and *System* levels. The comparisons between the different modes and levels are addressed in terms of yield of H<sub>2</sub>, by-products, and carbon formation.

### 6.1 Introduction

Regarding the autothermal reforming process, all works have always focused only on the “*Reformer level*” (Dauenhauer et al., 2006; Rabenstein et al., 2008; Wang et al., 2009) at which thermal neutral ( $Q=0$ ) occurs around the reformer, but the whole process still needs a significant amount of energy (heat sources), especially for preheating feeds. Wang et al. (2009) reported that the maximum moles of H<sub>2</sub> in ATR of glycerol is always attained at  $WGR=12$  for  $WGR$  in the range 1-12. It is clear that thermal neutral condition occurs around the reformer, but a large amount of energy is still be required for generating steam to reach  $WGR=12$ . So, it might be worth

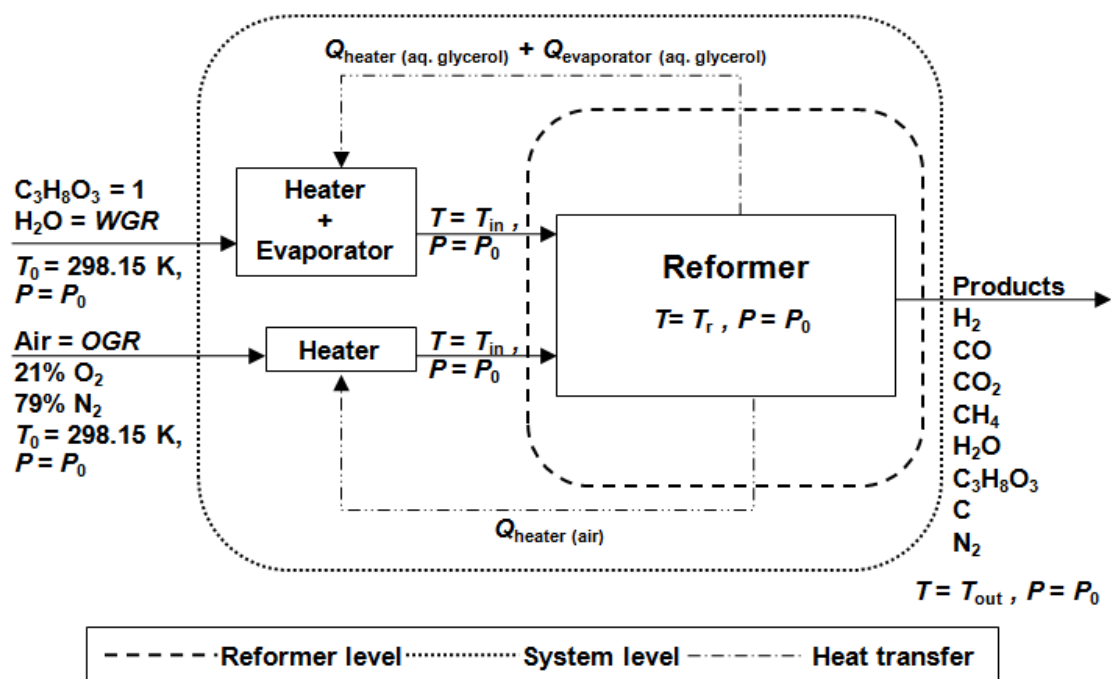
operating at a lower  $WGR$  from an overall energy saving point of view. However, there has been no work that considers the  $H_2$  production at the thermal neutral condition for the “*System level*” where heat requirements in both feeds preheating and reforming are taken into account. Therefore, the scope of this work focuses on glycerol reforming at both levels of consideration (i.e. *Reformer* and *System* levels) at thermal neutral conditions.  $H_2$  concentration in the gas product is another important issue in  $H_2$  production. SR and ATR processes offer different  $H_2$  concentrations (Swami and Abraham, 2006; Wang et al., 2009). Therefore, the mode of supplying heat energy for the endothermic steam reforming becomes important. It is possible to supply oxygen or air directly into the steam reforming feed as ATR operation or to carry out combustion of fuel with oxygen or air in a separate chamber adjacent to the reformer to provide sufficient heat for operating the system at thermal neutral conditions. Hence, this work also investigates the effect of operation modes including i) *Single-feed* mode and ii) *Split-feed* mode for comparison between SR and ATR processes under thermal neutral conditions. The *Single-feed* mode represents an ATR, in which all reactants, consisting of glycerol, water, and air, are fed into the reactor while the *Split-feed* mode involves separated operation of a steam reformer fed by glycerol and water and a combustor fed by part of glycerol and air. It should be noted that both modes at thermal neutral conditions do not require any additional fuel other than glycerol. In order to compare performances between the two modes, the amounts of glycerol feed must be equal so that the comparison is on the same basis.

In this work, the effects of water to glycerol ratio ( $WGR$ ), oxygen to glycerol ratio ( $OGR$ ), and operating temperature ( $T$ ) on the reaction performances are investigated over these two operation modes with two levels of consideration including *Reformer* and *System* levels. Suitable operating conditions for the  $H_2$  production from glycerol of different modes and levels under thermal neutral conditions are determined and the obtained results on  $H_2$  yield and concentrations of  $H_2$  and by-products are compared.

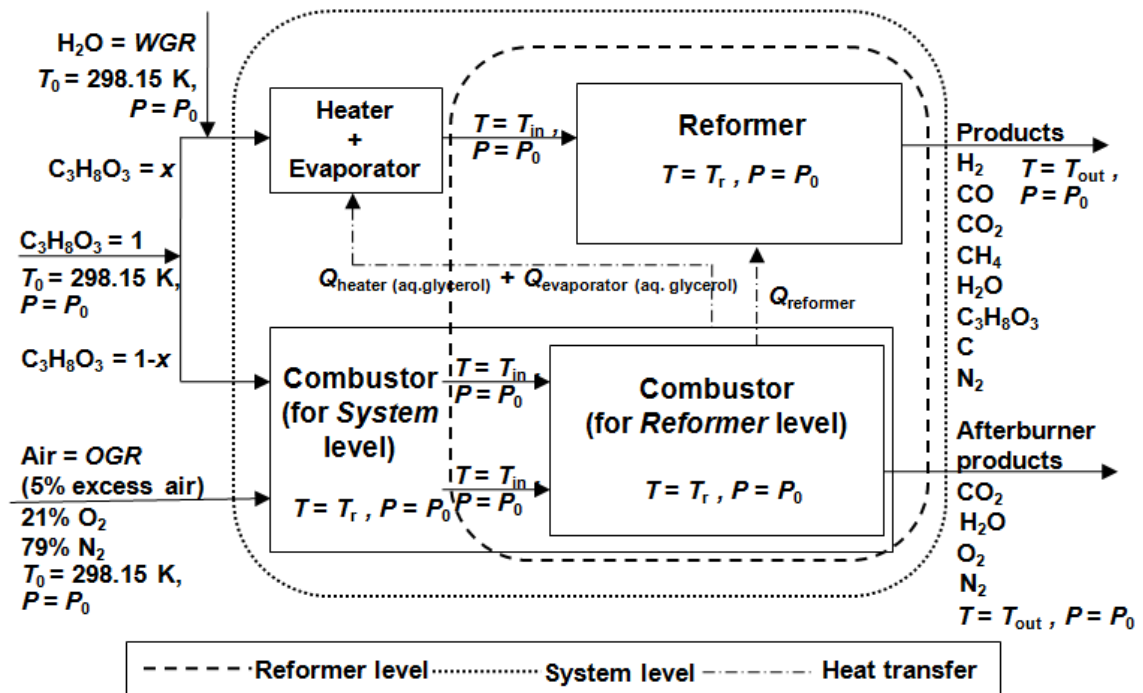
## 6.2 Boundary for calculation

Thermodynamic analysis in this work was done following a non-stoichiometric approach. Possible species in the equilibrium products include glycerol ( $C_3H_8O_3$ ), water ( $H_2O$ ), hydrogen ( $H_2$ ), carbon monoxide ( $CO$ ), carbon dioxide ( $CO_2$ ), methane ( $CH_4$ ), carbon ( $C_{(s)}$ ), oxygen ( $O_2$ ) and nitrogen ( $N_2$ ). Equation (2.41) is provided for consideration of solid carbon-gas system (Wang et al., 2008; Wang et al., 2009).

$$\sum_{i=1}^{N-1} n_i \left( \Delta G_{f_i}^0 + RT \ln \frac{\hat{\phi}_i y_i P}{P^0} + \sum_j \lambda_j a_{ij} \right) + n_C G_{C_{(s)}}(T, P) = 0 \quad (2.41)$$



**Figure 6.1** Schematic diagram of energy balances in *Single-feed* mode for *Reformer* and *System* levels ( $P=P_0=0.101325$  MPa, for isothermal condition in Reformer level,  $T_{in}$ ,  $T_r$ , and  $T_{out}$  are equal).



**Figure 6.2** Schematic diagram of energy balances in *Split-feed* mode for *Reformer* and *System* levels ( $P=P_0=0.101325\text{ MPa}$ , for isothermal condition in *Reformer* level,  $T_{in}$ ,  $T_r$ , and  $T_{out}$  are equal).

Aspen Plus program was employed for calculating equilibrium compositions and the corresponding overall heat of reactions while minimizing the Gibbs free energy. The Soave–Redlich–Kwong equation was selected as the method for estimating thermodynamic properties of the reaction systems (Wang et al., 2008; Li et al., 2008; Wang et al., 2009).

Figure 6.1 shows two levels of energy balance consideration including *Reformer* (dash line around reformer) and *System* levels (outside dash line) for *Single-feed* mode. At the *Reformer* level, the energy balance equation around the reformer unit can be expressed by Equation (6.1) while Equation (6.2) shows the energy balance equation at the *System* level. It should be noted that at the *System* level, apart from the energy involved in the reformer, the heat demands for feeds preheating are also taken into account, and therefore, in order to achieve a thermal neutral operation,

it inevitably requires higher extent of exothermic reactions in order to supply enough energy to the system.

$$Q_{Reformer\ level\ (net)} = \sum_{i=1}^N n_{i,\ out} H_{i,\ out} - \sum_{i=1}^N n_{i,\ in} H_{i,\ in} \quad (6.1)$$

$$Q_{System\ level\ (net)} = Q_{heater\ (net)} + Q_{evaporator} + Q_{reformer} = \sum_{i=1}^N n_{i,\ out} H_{i,\ out} - \sum_{i=1}^N n_{i,0} H_{i,0} \quad (6.2)$$

Figure 6.2 shows two levels of energy balance consideration including *Reformer* level (dash line around reformer) and *System* level (outside dash line) for the *Split-feed* mode of H<sub>2</sub> production from glycerol. Instead of co-feeding air with the reactants as in the *Single-feed* mode, air and part of the glycerol are fed to a combustor which generates heat for the units in the *Split-feed* mode. Glycerol is split into two fractions; first one (*x*) is for H<sub>2</sub> production inside reformer and the other one (1-*x*) is for generating heat under combustion reaction in the combustor. At the *Reformer* level, the heat duty involves only that of the reformer; however, at the *System* level, it involves the duties of the reformer, heater, and evaporator units. Equations. (6.3)-(6.5) and Equation (6.6) show the energy balance equations for the *Reformer* and *System* levels, respectively. It should be noted that comparison between the two operation modes is based on the same amount of glycerol fed to the system.

$$Q_{reformer} = \left( \sum_{i=1}^N n_{i,\ out} H_{i,\ out} - \sum_{i=1}^N n_{i,\ in} H_{i,\ in} \right)_{reformer} \quad : \quad n_{C_3H_8O_3,\ in} = x \text{ mol} \quad (6.3)$$

$$Q_{combustor} = \left( \sum_{i=1}^N n_{i,\ out} H_{i,\ out} - \sum_{i=1}^N n_{i,\ in} H_{i,\ in} \right)_{combustor} \quad : \quad n_{C_3H_8O_3,\ in} = 1-x \text{ mol} \quad (6.4)$$

$$Q_{Reformer\ level\ (net)} = Q_{reformer} + Q_{combustor} \quad (6.5)$$

$$Q_{System\ level\ (net)} = Q_{heater\ (net)} + Q_{evaporator} + Q_{reformer} + Q_{combustor} = \sum_{i=1}^N n_{i,\ out} H_{i,\ out} - \sum_{i=1}^N n_{i,0} H_{i,0} \quad \dots\dots\dots(6.6)$$



The total net heat energy can be positive (endothermic), negative (exothermic) and zero (thermal neutral).  $Q_{\text{combustor (net)}}$  is always negative because of the exothermic combustion reactions, while  $Q_{\text{heater}}$  and  $Q_{\text{evaporator}}$  are always positive. The thermal neutral condition can be found by setting Equations. ((6.1),(6.2)) and Equations. ((6.5),(6.6)) equal to zero for the *Single-feed* and *Split-feed* modes, respectively.

The reaction performances are expressed in terms of yield of product  $i$  (Equation (6.8)), and mole fraction of product  $i$  (dry basis) (Equation (6.9)). In all simulations the glycerol feed rate and operating pressure are kept at  $1 \text{ mol s}^{-1}$  and  $0.101325 \text{ MPa}$ , respectively.

$$\text{Yield of product H}_2 = \frac{n_{\text{H}_2, \text{out}}}{n_{\text{Glycerol}, 0}} \quad (6.7)$$

$$\text{Carbon product } i \text{ yield (-)} = \frac{n_{i, \text{out}}}{3 \times n_{\text{glycerol}, 0}} \quad (6.8)$$

$$\text{Product } i \text{ mol fraction (dry basis)} = \frac{n_{i, \text{out}}}{\sum_{i=1}^N n_{i, \text{out}} - n_{\text{H}_2\text{O}}} \quad (6.9)$$

## 6.3 Results and discussion

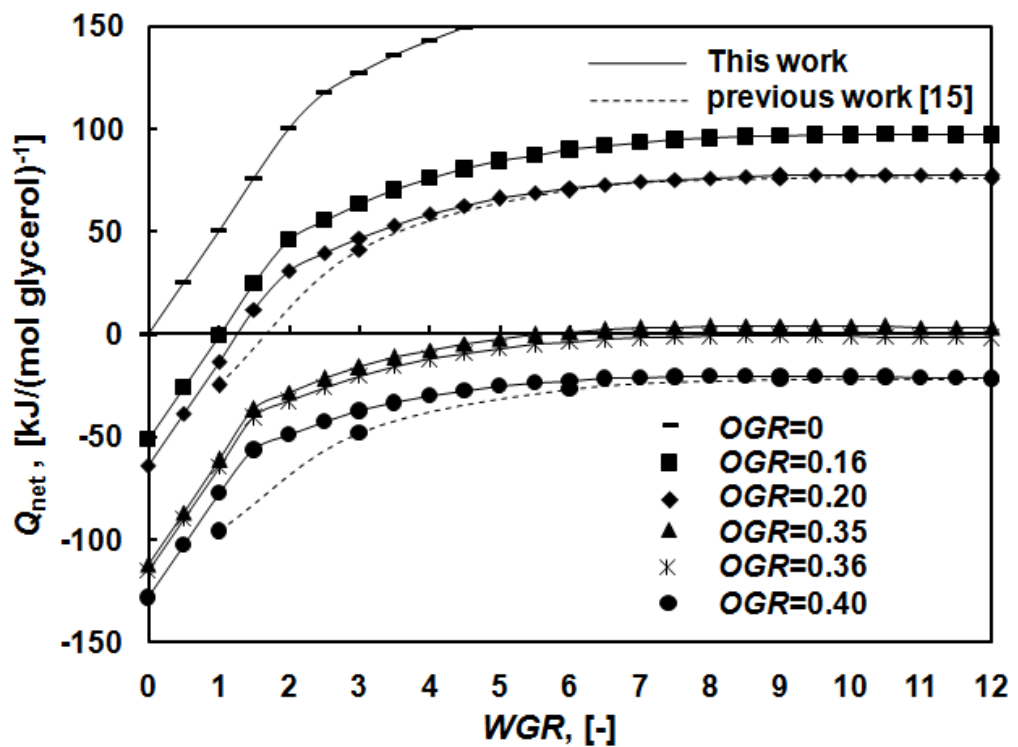
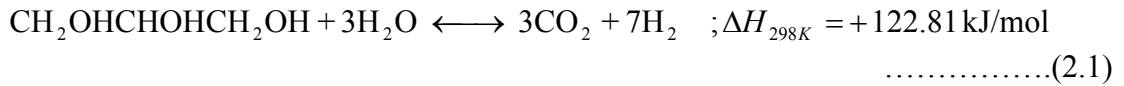
In this study, simulations were carried out at temperatures ranging from 600 to 1200 K. Based on the thermodynamic equilibrium, all of the glycerol was totally consumed in the reactions. This is also reported by other researchers (Adhikari et al., 2007a; Wang et al., 2008; Wang et al., 2009).

### 6.3.1 Effect of operating conditions on the energy requirement

The effect of operating conditions, including temperature ( $T$ ), water to glycerol ratios ( $WGR$ ), and oxygen to glycerol ratios ( $OGR$ ), on the net heat energy requirement ( $Q_{\text{net}}$ ) was first investigated at constant atmospheric pressure ( $P$ ) in order to determine ranges of variables that are possible for thermal neutral conditions. Energies from the two operation modes (*Single-feed* and *Split-feed*) at two levels

(*Reformer* and *System*) were determined in order to determine the effect of all variables. Then, the operating conditions to achieve thermal neutral conditions were considered.

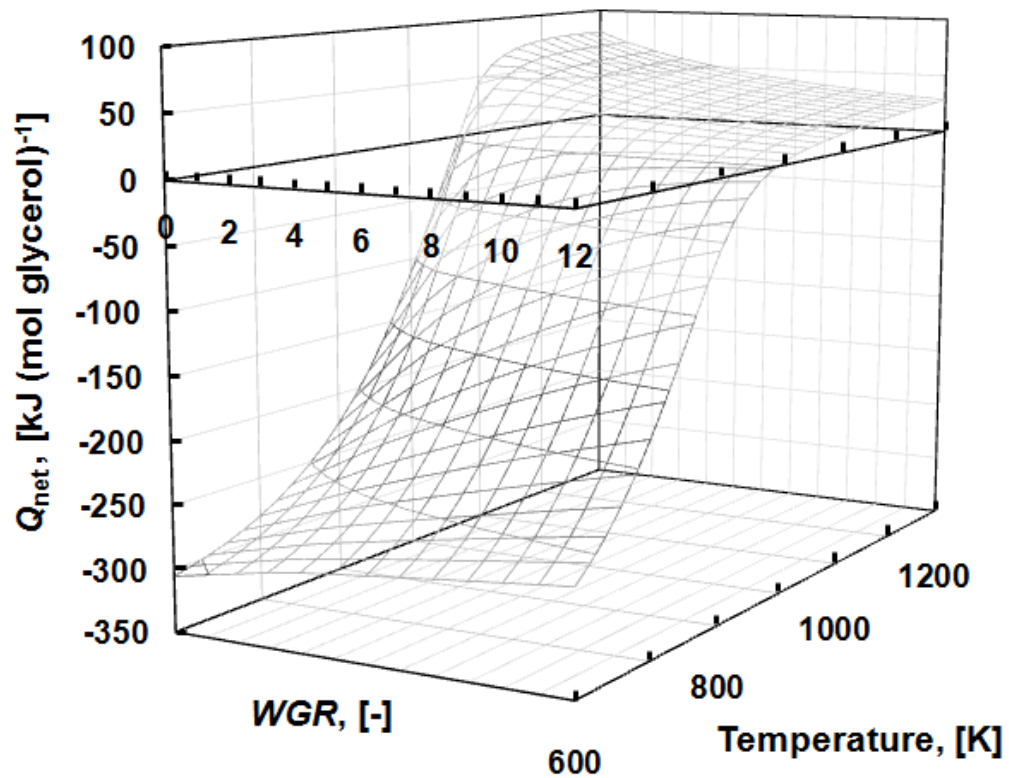
The overall reaction of glycerol Steam Reforming (SR):



**Figure 6.3** Net heat energies ( $Q_{\text{net}}$ ) of *Reformer* level in *Single-feed* mode at different values of  $WGR$  and  $OGR$  ( $P=0.101325 \text{ MPa}$ ,  $T_r=900 \text{ K}$ ).

At the *Reformer* level, the net heat energy only involves heats of reactions. Steam reforming reaction (Equation (2.1)) is an endothermic reaction but it can possibly be at thermal neutral conditions by adding oxygen to the reformer (Dauenhauer et al., 2006; Rabenstein et al., 2008; Adhikari et al., 2009). For the *Single-feed* mode, Figure 6.3 shows that at  $OGR=0-0.36$  the reformer can be operated at thermal neutral conditions for  $WGR=0-12$  and  $T = 900 \text{ K}$ . Increasing  $WGR$  increases the net heat energy until  $WGR$  greater than 8, then it becomes almost

constant until  $WGR=12$ . Dash-lines in Figure 6.3 show the results of previous work (Wang et al., 2009) at similar conditions with  $T=900$  K,  $WGR=1-12$  and  $OGR=0.2$  and  $0.4$ . Our simulation results are in good agreement with them, especially at high  $WGR$ s ( $WGR=6, 9, 12$ ). However, some discrepancies are observed at low  $WGR$ s. This is because their work used pure oxygen as an oxidant while air is considered in our study.

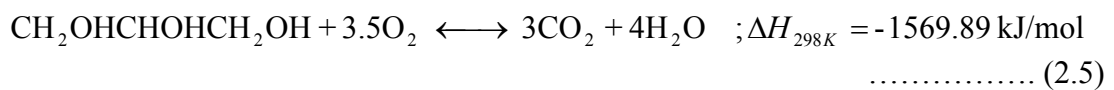


**Figure 6.4** Net heat energies ( $Q_{net}$ ) of *Reformer* level in *Single-feed* mode at different values of  $WGR$  and  $T$  ( $OGR=0.35$ ,  $P=0.101325$  MPa).

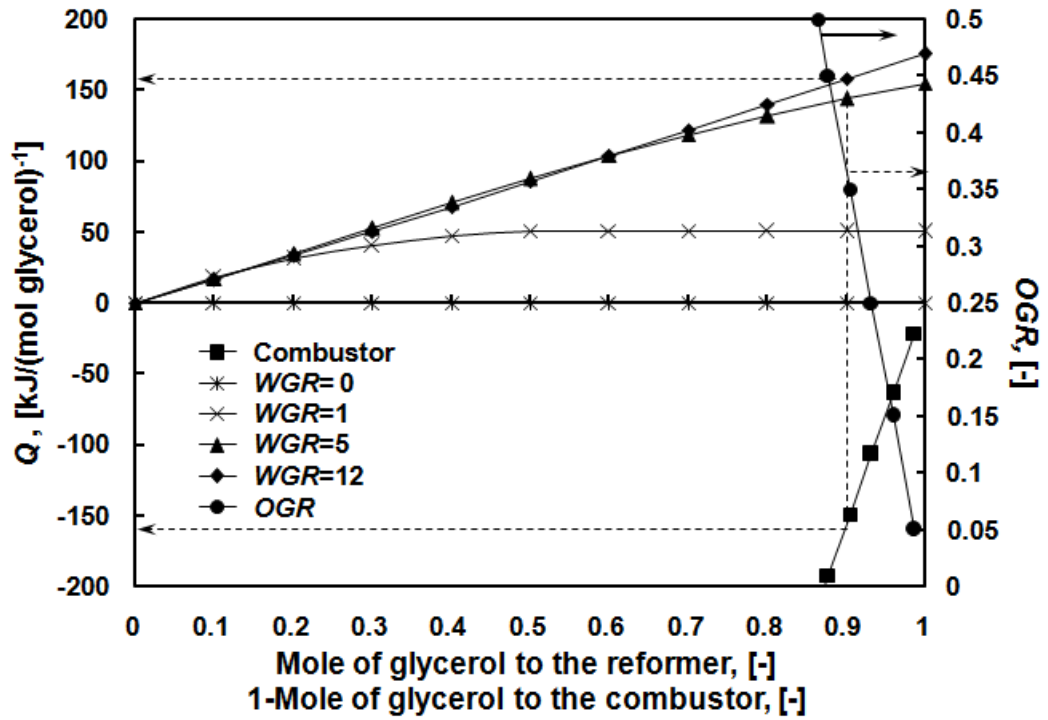
From Figure 6.3, it is clear that at  $T=900$  K,  $OGR=0.35$  offers thermal neutral condition at  $WGR$  around 6. The operating temperature is another variable which influences the net energy. Figure 6.4 indicates that the net heat energy surface is changed for  $WGR$  in the range 0-12 and operating temperature in the range 600-1200 K. From the results, increasing  $WGR$  affects only slightly the net energy. In contrast, operating temperature can significantly change the net heat energy from -300 at 600 K

to 100 kJ/mol-glycerol at 1200 K. Increasing temperature between 600 and 900 K sharply increases the net heat energy but between 900 and 1200 K the change in net heat energy is not as significant. It should be noted that the energy neutral condition occurs only within a certain range of temperature: 900 to 960 for *WGR* between 0 and 12.

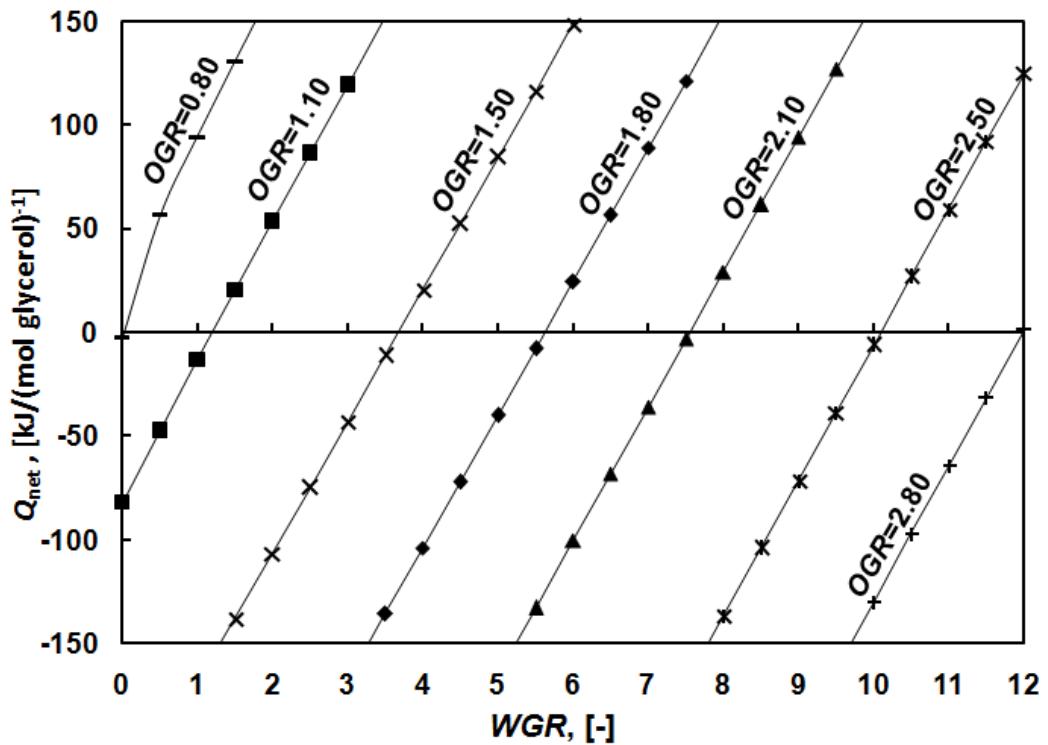
Oxidation or Combustion (OX):



For the *Split-feed* mode, the net energy depends on the fractions of glycerol to be fed to the reformer and the combustor. Figure 6.5 shows that increasing the fraction of glycerol to the reformer increases the net energy. It should be noted that the net energy for the combustor is always negative because of the oxidation reaction (Equation (2.5)) which increases when increasing the number of moles of glycerol to the reformer. In order to provide sufficient heat to the reformer for *WGR* between 0 and 12, the fraction of glycerol to be fed to the combustor is between 0 and 0.11. Hence, more than 0.89 mole of glycerol is still always fed to the reformer. The reformer can be operated at thermal neutral conditions when *OGR* is between 0 and 0.37, which is close to that of the *Single-feed* mode. However one should expect, at least a slightly higher value of *OGR* in the *Split-feed* mode since the combustor operates with 5% excess air. Furthermore,  $\text{O}_2$  disappears in the product stream of the *Single-feed* mode but still appears in afterburner product stream in the *Split-feed* mode.



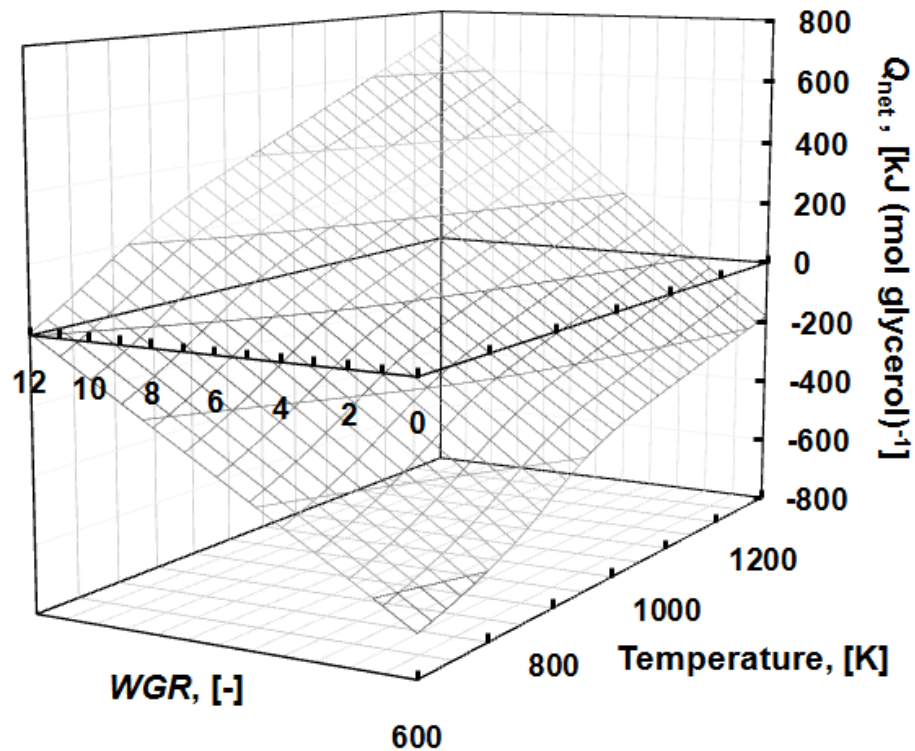
**Figure 6.5** Heat energy (in the reformer and combustor) and  $OGR$  of Reformer level in *Split-feed* mode at different values of Mole of glycerol to the reformer and  $WGR$  ( $P=0.101325$  MPa,  $T_r=900$  K).



**Figure 6.6** Net heat energies ( $Q_{net}$ ) of System level in *Single-feed* mode at different values of  $WGR$  and  $OGR$  ( $P=0.101325$  MPa,  $T_r=900$  K).

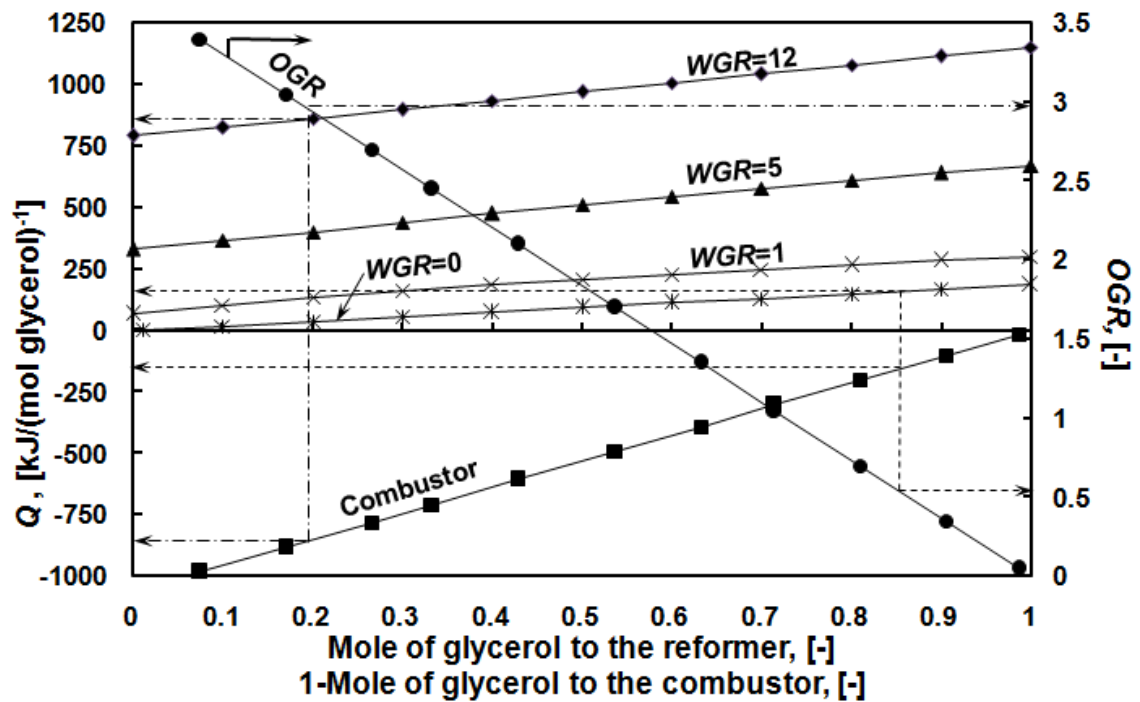
Considering the *System* level, the net energy includes preheating energy for heating up all feeds from room temperature (298.15 K) to the desired temperature, and heat of reactions in the reformer and combustor. For the *Single-feed* mode, Figure 6.6 shows that increasing *WGR* increases the net heat energy for all *OGRs*. For providing thermal neutral conditions for *WGR* between 0 and 12, *OGR* has to be in the range 0.80-2.80. The values of *OGR* at the *System* level are much higher than those at the *Reformer* level. This can be explained by the fact that the heat of reaction inside the reformer is only a small part of the net heat energy at the *System* level. Thus, much higher *OGR* is required to provide sufficient exothermic heat for the system. The high values of *OGR* can directly affect the H<sub>2</sub> production. However, *OGR* at the thermal neutral conditions at the *System* level is more sensitive to *WGR* than at the *Reformer* level; for examples, *OGR*=1.8 with *WGR*=5.60, *OGR*=2.10 with *WGR*=7.60, etc. The value of *WGR* was found to significantly influence the *OGR* requirement. Figure 6.7 shows the net energy surface plot at different *WGR* and operating temperatures for *OGR* = 1.80. The operating temperature at the thermal neutral condition varies as *WGR* changes, for example, at *WGR*=6, *T*=860 K and at *WGR*=7, *T*=800 K. For *OGR* = 1.80 and *T* between 630 and 1120 K, the value of *WGR* to attain the thermal neutral condition will be between 3 and 11, depending on the value of temperature.

For the *Split-feed* mode at the *System* level, Figure 6.8 shows that increasing *WGR* still increases the net heat energy but it is more pronounced than at the *Reformer* level. The fractions of glycerol to the reformer are 0.85 to 0.19 for *WGR* of 0 to 12. Increasing *WGR* rapidly decreases the fraction of glycerol to the reformer because the increase in energy demand requires glycerol fuel to be burnt in the combustor for decreasing the net heat energy from positive to zero via the combustion reaction (Equation (2.5)). From the increase in the fraction of glycerol fed to the combustor, *OGR* has to increase from 0.51 to 3.00 to satisfy the combustion reaction with 5% excess air, when *WGR* increases from 0 to 12.



**Figure 6.7** Net heat energies ( $Q_{net}$ ) of *System* level in *Single-feed* mode at different values of  $WGR$  and  $T$  ( $OGR=1.80$ ,  $P=0.101325$  MPa).

At the *System* level and for the *Single-feed* mode, the value of  $WGR$  strongly influences the value of  $OGR$  and the range of operating temperatures at thermal neutral conditions. However, operating temperature has the most influence at the *Reformer* level. It can be concluded that the net energy at the *System* level is considerably greater than that at the *Reformer* level due to the heat requirement for preheating the feeds. Apart from the selection of suitable conditions for operating the reformer or the system at thermal neutral conditions, the resulting products of  $\text{H}_2$  and other gases as well as  $\text{H}_2$  concentration are important information required to evaluate suitable operation modes for  $\text{H}_2$  production from glycerol.



**Figure 6.8** Heat energy (in the reformer and combustor) and *OGR* of *System* level in *Split-feed* mode at different values of Mole of glycerol to the reformer and *WGR* ( $P=0.101325$  MPa,  $T_r=900$  K).

### 6.3.2 Effect of operating conditions at the thermal neutral conditions

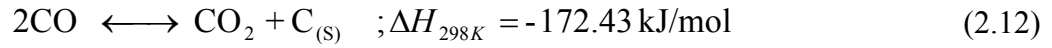
Appropriate operating conditions should be selected to achieve the thermal neutral conditions and to enhance  $H_2$  production as well as to suppress undesired by-products. In the  $H_2$  production process, not only the steam reforming of glycerol (Equation (2.1)) but also other reactions are involved in the reaction system, leading to formation of carbon and other by-products that might directly affect the stability of the system and the concentration of  $H_2$  in the final product. All of them have been investigated from thermodynamic analysis and will be discussed in the following sections.

#### 6.3.2.1 Carbon formation

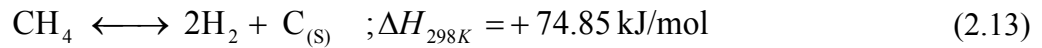
The main reactions leading to carbon formation during reforming are the following reactions:



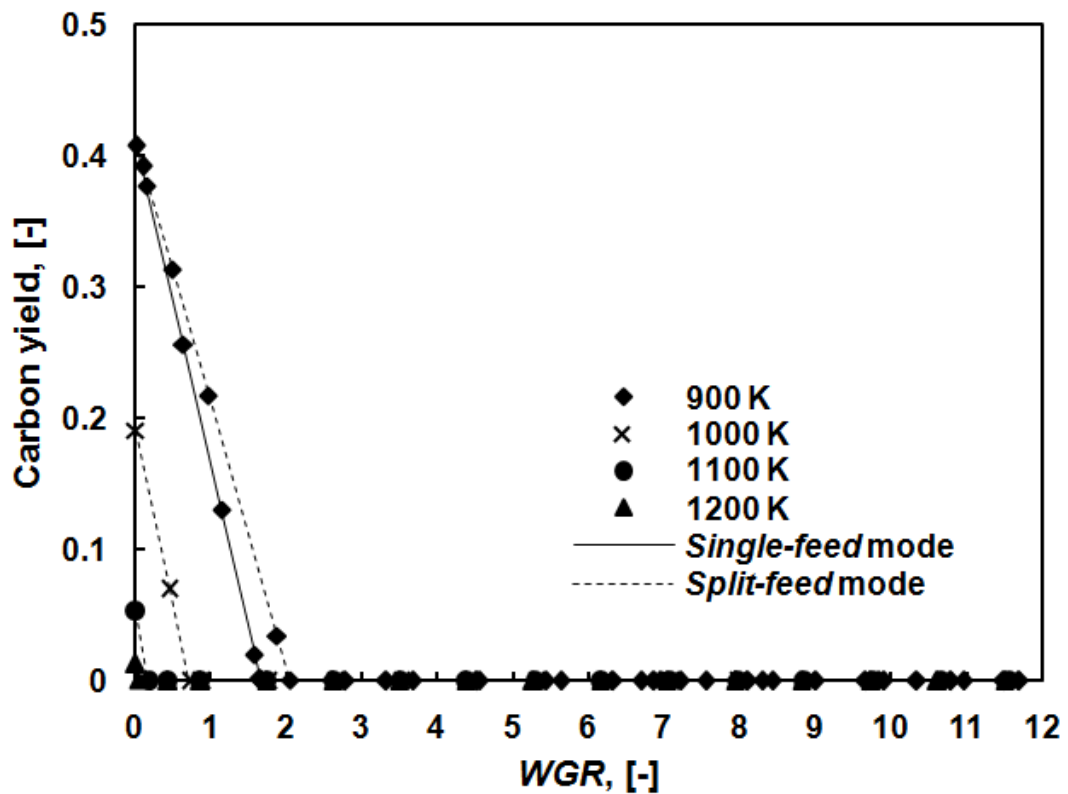
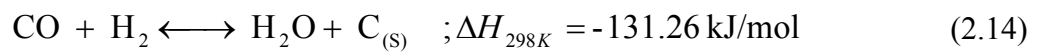
Boudouard reaction:



Methane cracking:



Reduction of CO:

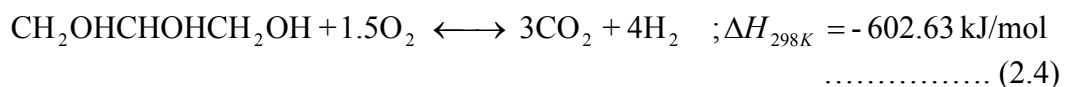
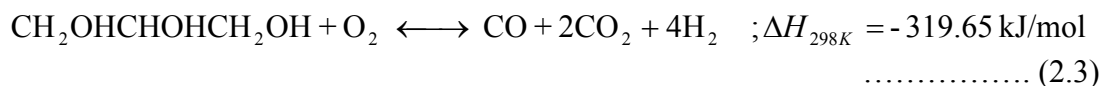
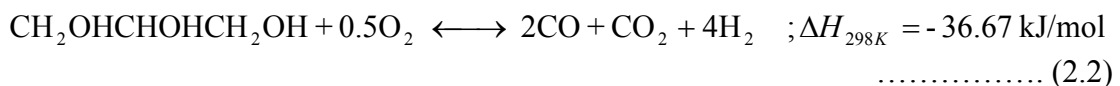


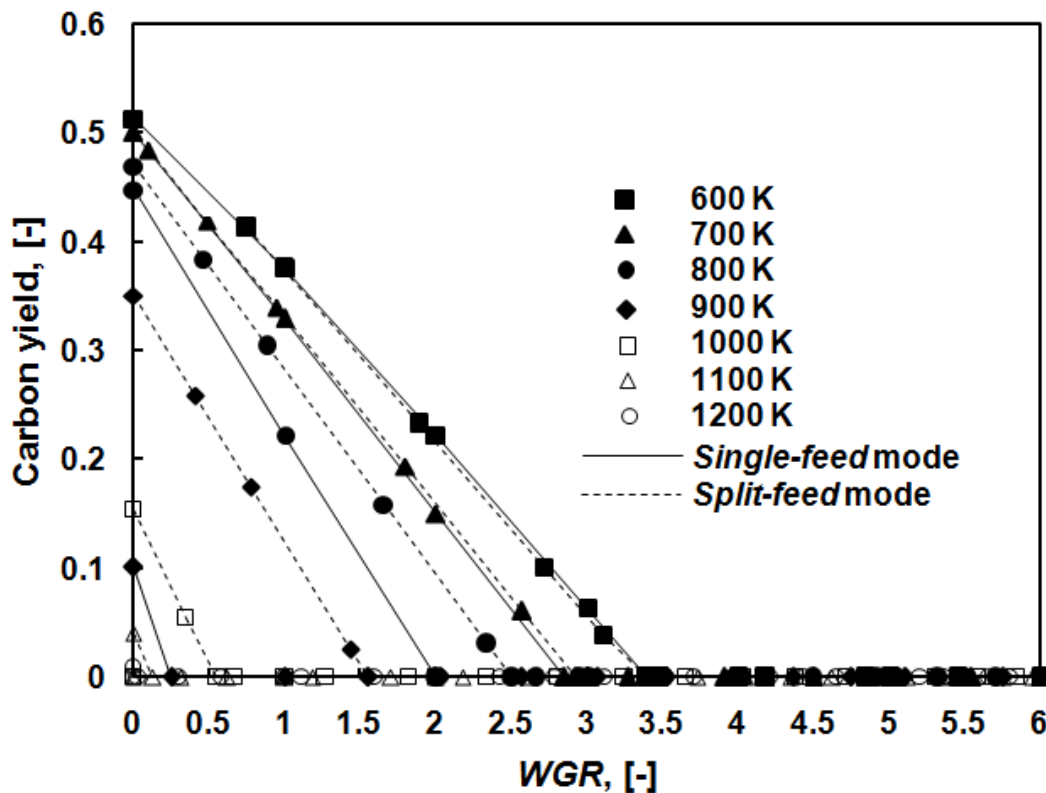
**Figure 6.9** Carbon yield of *Reformer* level at different values of *WGR* and operating temperature ( $Q_{\text{net}}=0$ ,  $P=0.101325$  MPa).

Carbon formation is a major problem that causes blockage of the catalyst pores and that potentially can lead to break down of the reactor [8]. It can occur via several undesired reactions (Equations (2.12)-(2.14)) (Adhikari et al., 2007a; Wang et al., 2009). Wang et al. (2009) reported that the Boudouard reaction (Equation (2.12))

plays a significant role at temperatures below 915 K, whereas CH<sub>4</sub> cracking (Equation (2.13)) becomes predominant at temperatures higher than 915 K. Figure 6.9 shows the yield of solid carbon in two modes for *WGR* between 0 and 12 and *T* between 800 and 1200 K, at the *Reformer* level. It is shown that low *WGR*s tend to form solid carbon (Rabenstein et al., 2008) but it does not appear at 800 K in both modes because a thermal neutral condition cannot occur at *WGR* lower than 4.5 (At 800 K, the thermal neutral condition for both modes start at *WGR*=4.5). *WGR* of 4.5 is high enough to eliminate carbon in the reformer. However, the solid carbon appears in both modes at 900 K but the *Single-feed* mode shows less carbon than the *Split-feed* mode. This is because oxygen in the *Single-feed* mode facilitates operation above carbon boundary condition due to the presence of oxidation reactions (Equations (2.2)-(2.5)). No carbon formation is observed at *T* = 1000, 1100 and 1200 K. In the *Split-feed* mode, solid carbon is still formed even at temperatures higher than 900 K because water (Equation (2.14)) is the only component that suppresses carbon formation unlike the case of *Single-feed* mode where oxygen is also present in the reformer. It can be concluded that carbon formation can be decreased by increasing *WGR*, *OGR*, and operating temperature in the *Single-feed* mode, but only *WGR* and operating temperature in the *Split-feed* mode. However, at *WGR* greater than 2, it is clear that no carbon is formed to the point of breaking down the reactor at the *Reformer* level. This is in agreement with Wang et al. (2009) who reported that no carbon occurred at temperature above 1000 K, and *WGR* higher than 2.

Partial Oxidations (POX):





**Figure 6.10** Carbon yield of *System* level at different values of  $WGR$  and operating temperature ( $Q_{net}=0$ ,  $P=0.101325$  MPa).

At the *System* level, there is a huge energy requirement, requiring higher  $OGR$  for operating at the thermal neutral condition. Figure 6.10 shows the carbon formation from both modes at the *System* level. Clearly, the results are very different than those obtained at the *Reformer* level. Within ranges of operating temperatures of 600-1200 K and  $WGR$  of 0-12, carbon formation is decreased when increasing the operating temperature and  $WGR$ . At 600 and 700 K, carbon formation is nearly equivalent between *Single-feed* and *Split-feed* modes. However, the difference between them starts at 800 K at which the *Split-feed* mode leads to higher carbon formation than the *Single-feed* mode. The *Single-feed* mode can operate without carbon formation at operating temperatures higher than 900 K, similar to the *Reformer* level. In contrast, the *Split-feed* mode still shows carbon formation above 900 K and it requires higher temperature ( $T=1100-1200$  K) to suppress carbon formation. From these results, it is clear that water ( $WGR$ ) and oxygen in air ( $OGR$ ) are the most important variables to manipulate in order to operate the system without carbon formation. However,  $OGR$

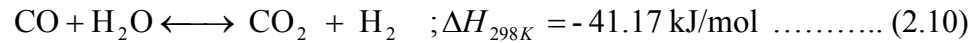
does not directly affect the carbon formation in the *Split-feed* mode because oxygen is only used in the combustor. At thermal neutral conditions,  $WGR$  greater than 3.5 is sufficient to avoid carbon formation at the *System* level for  $T$  between 600 and 1200 K in both modes.

### 6.3.2.2 Hydrogen production

#### 6.3.2.2.1 Hydrogen yield

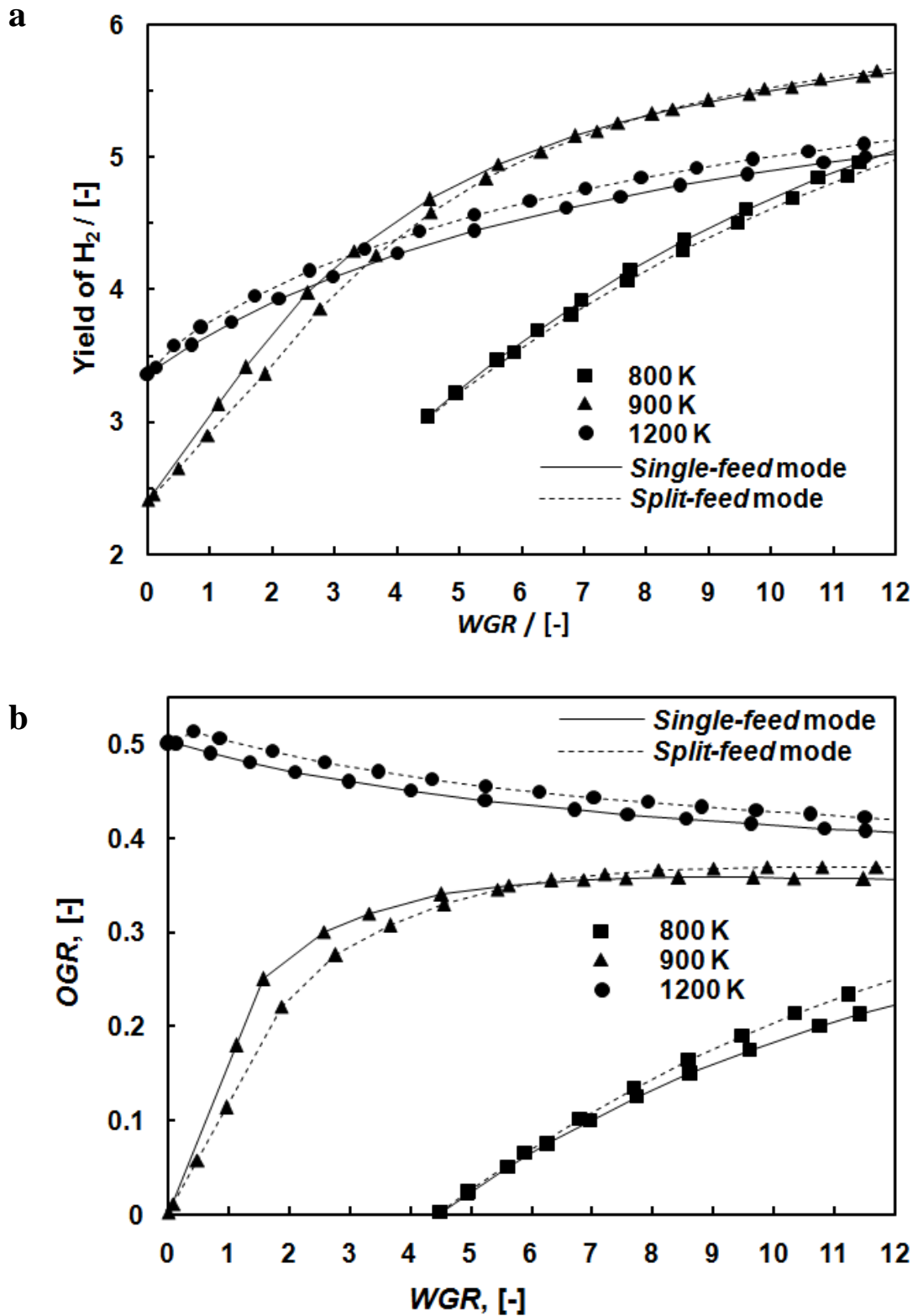
Figure 6.11a shows that the  $H_2$  yield increases with increasing  $WGR$  at the *Reformer* level. The maximum  $H_2$  yield is obtained at an operating temperature around 900 K. An optimum temperature is observed because the endothermic steam reforming is favorable at high temperature but the exothermic WGS reaction (Equation (2.10)) is favorable at low temperature. Optimum temperatures were reported by other researchers to be at 925 K (Wang et al., 2008) and 960 K (Adhikari et al., 2007a). The *Split-feed* mode always offers a slightly higher  $H_2$  yield than the *Single-feed* mode, except at low temperature (800 K) or small  $WGR$ s (0-7). This is because the small amount of oxygen fed to the reformer decreases the  $H_2$  yield in the *Single-feed* mode. Figure 6.11b shows the amount of  $OGR$  in both modes. Increasing  $WGR$  increases  $OGR$  at low temperatures (800, 900 K) but it slightly decreases  $OGR$  at high temperatures (1200 K). Although not shown in Figure 6.11b, the curves at 1000 K and above follow the same trend as that at 1200 K, that continuous decrease of  $OGR$  when increasing  $WGR$ . As seen in the previous section, to suppress carbon formation, increasing of  $OGR$  at small  $WGR$  for all temperatures, especially for the *Split-feed* mode, is required. However, the value of  $OGR$  does not strongly influence the  $H_2$  production at the *Reformer* level because the amount of  $OGR$ s is quite small (0-0.51). It should be noted that the differences between *Single-feed* and *Split-feed* modes are not significant at the reformer level – the maximum  $H_2$  yields at  $WGR$  of 12, and operating temperature of 900 K are 5.67, and 5.64 for *Split-feed* and *Single-feed* modes, respectively. It agrees with the value of 5.62 at  $WGR$  of 12 determined by Wang et al. (2009).

Water Gas Shift (WGR or reverse of this is called RWGS):

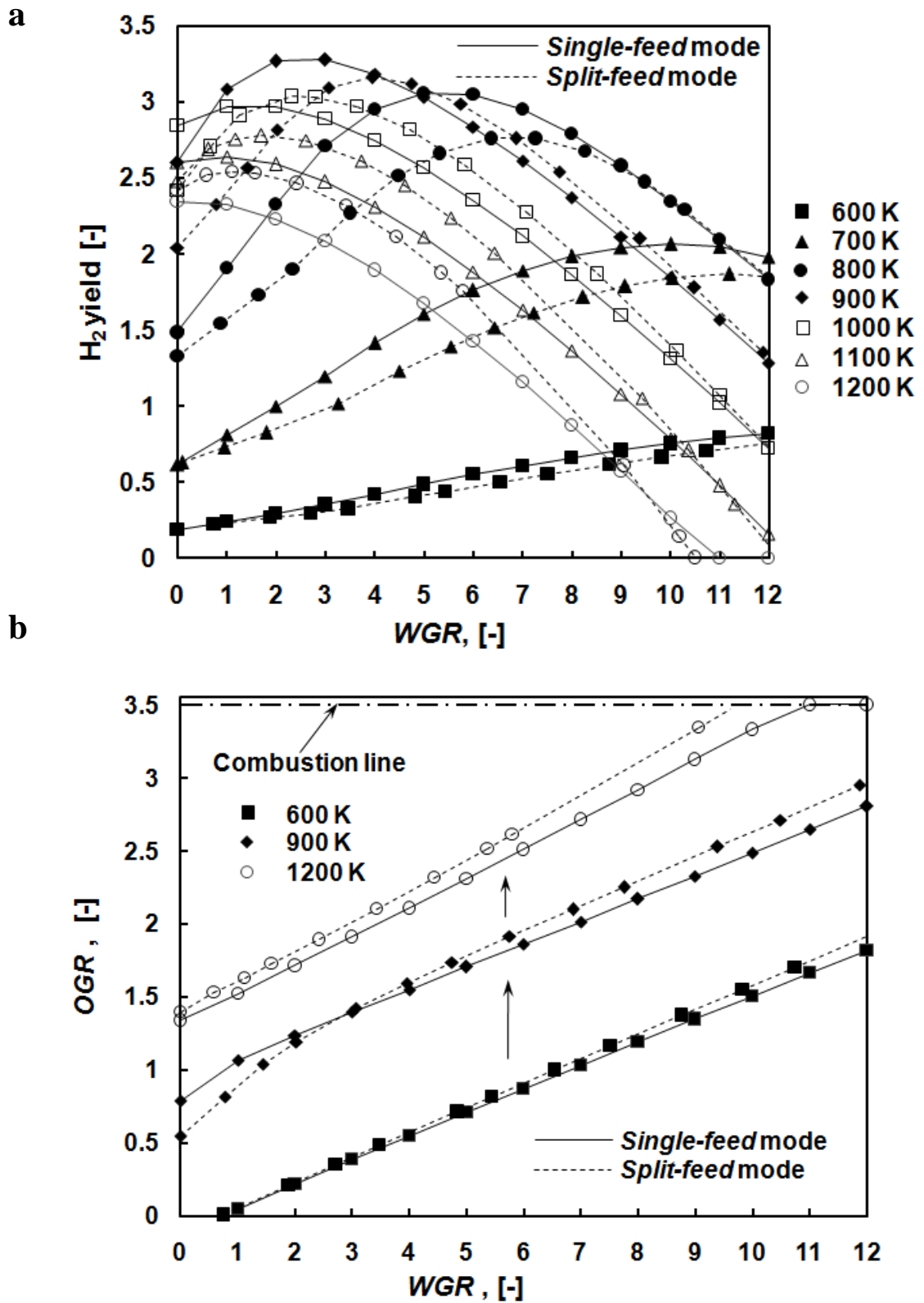


Considering the thermal neutral condition at the *System* level, as more heat requirement is involved, more glycerol is consumed to generate sufficient heat via partial oxidation or combustion for the system. Figure 6.12a shows the H<sub>2</sub> yield at the *System* level for different operating temperatures, *WGRs*, and operation modes. It can be seen that the H<sub>2</sub> yield increases with increasing *WGR* at low operating temperatures (600 and 700 K). On the other hand, at higher operating temperatures (800, 900, 1000, 1100, and 1200 K), the H<sub>2</sub> yield increases only at low range of *WGR*; then it drops at high *WGR*. Moreover, increasing the temperature increases the H<sub>2</sub> yield until 900 K, above which it decreases because of the reverse water gas shift (Reverse WGS) effect (Equation (2.10)), as discussed in the previous section on the *Reformer* level. At low temperatures (600, 700 K) within all ranges of *WGR*, it is observed that the *Single-feed* mode always offers higher H<sub>2</sub> yield than the *Split-feed* mode, likely due to the requirement of lower *OGRs* (Figure 6.12b) which could promote H<sub>2</sub> production. However, at higher temperatures when *WGR* is high enough, it appears that the *Split-feed* mode becomes more favorable than the *Single-feed* mode. The values of *WGR* at this turning point vary with temperature; for examples, *WGR*=9 at 800 K, *WGR*=4 at 900 K, *WGR*=2 at 1000 K, *WGR*=0.5 at 1100 K, and *WGR*=0 at 1200 K. These observations can be explained by the difference in characteristics among the two operation modes. For the *Single-feed* mode, all glycerol in the feed is fed to the reformer and therefore hydrogen atoms in glycerol reacting with oxygen could possibly be converted to additional H<sub>2</sub> unlike in the *Split-feed* mode where part of glycerol is totally combusted to CO<sub>2</sub> and H<sub>2</sub>O which appear in the combustor effluent or afterburner products stream. Consequently, the *Single-feed* mode is likely to offer higher H<sub>2</sub> yield. However, at higher temperatures where the WGS reaction (Equation (2.10)) becomes unfavorable, the presence of additional glycerol and oxygen for generating exothermic heat in the reformer in the *Single-feed* mode becomes less significant for improving H<sub>2</sub> production. The influence of WGS on H<sub>2</sub> production becomes important particularly at high temperature as evidenced by the lower value of transition *WGR* at higher temperature. Based on the simulation results, a maximum H<sub>2</sub> yield of 3.28 can be achieved at *WGR*=3, *OGR*=1.40, *T*= 900

K and *Single-feed* mode. At the same temperature, the *Split-feed* mode offers a slightly lower H<sub>2</sub> yield of 3.16 at a higher *WGR* of 3.96. It should be noted that the large amount of energy requirement at the *System* level decreases the H<sub>2</sub> yield from 5.67 at the *Reformer* level to 3.28 at the *System* level.



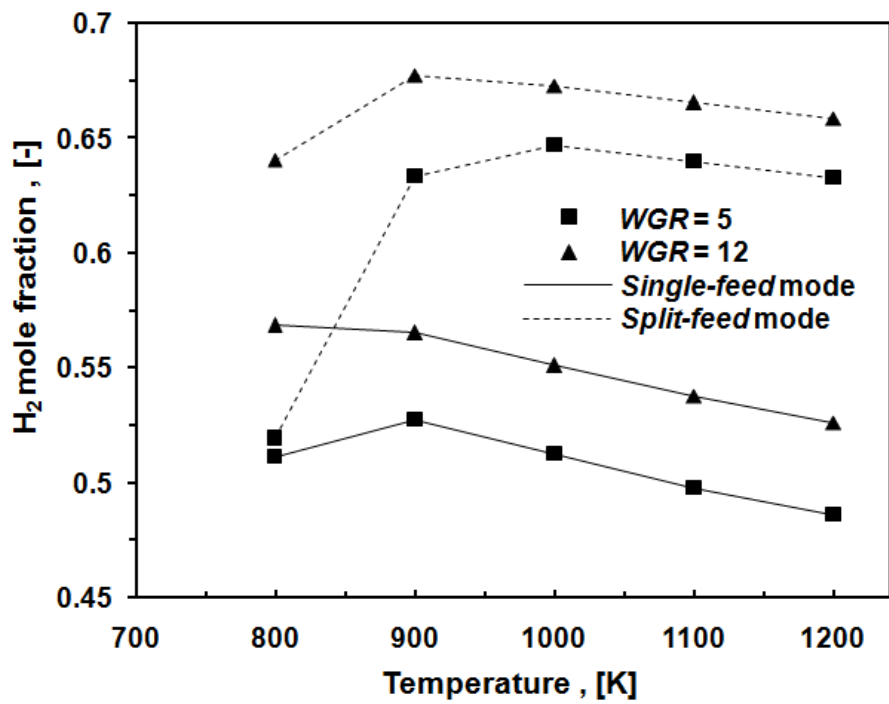
**Figure 6.11** (a)  $H_2$  yield and (b)  $OGR$  of *Reformer* level at different values of  $WGR$  and operating temperature ( $Q_{net}=0$ ,  $P=0.101325$  MPa).



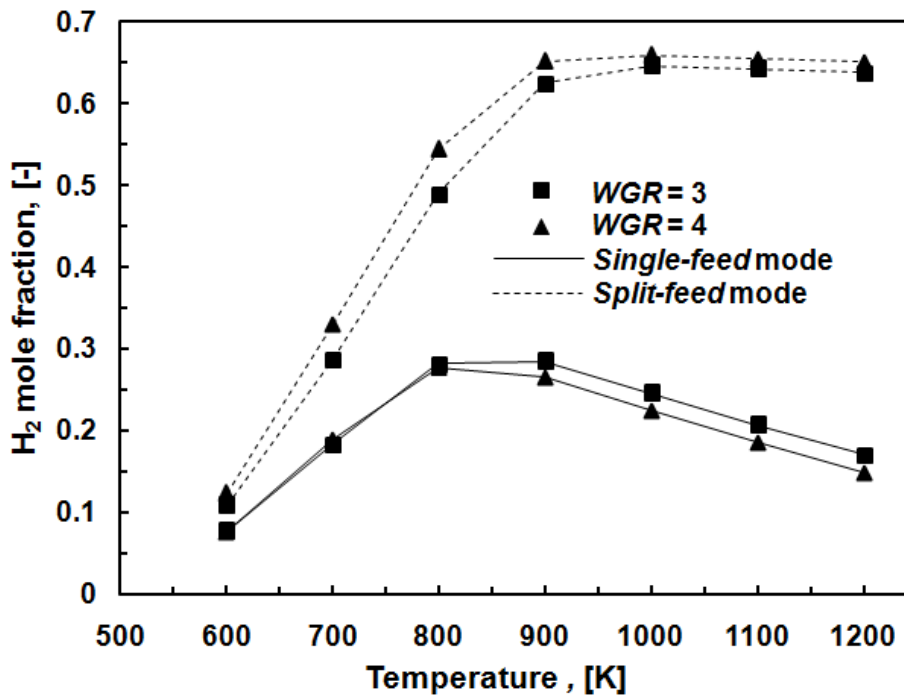


#### 6.3.2.2.2 Hydrogen mole fraction

From the previous part concerning the  $H_2$  yield at the *Reformer* level, it is shown that operation at  $T=900$  K and  $WGR=12$  offers the highest  $H_2$  yield in both modes. Another important issue of concern is the  $H_2$  concentration in the gas product. Figure 6.13 shows the  $H_2$  mole fraction (dry basis) at various operating temperatures for two values of  $WGR$  ( $WGR=5$  and  $12$ ). It is obvious that at the *Reformer* level, the *Split-feed* mode outperforms the *Single-feed* mode in term of  $H_2$  concentration for both values of  $WGR$ s. In the *Split-feed* mode, air and part of glycerol are combusted in the combustor, and thus by-products including  $CO_2$  and  $H_2O$  or  $N_2$  (non-reacted substance) are not mixed with the  $H_2$  product in the reformer unlike in the *Single-feed* mode. This is the main advantage of the *Split-feed* mode.  $WGR=12$  offers higher  $H_2$  mole fraction (dry basis) than  $WGR=5$  in both modes due to the higher  $H_2$  yield. Increasing the operating temperature (800-900 K) increases the  $H_2$  mole fraction initially, and then decreases due to the effect of the reverse WGS (Equation (2.10)), except at  $WGR=12$  in *Single-feed* mode. This is because the effect of  $N_2$  dilution might hide the reverse WGS effect in the *Single-feed* mode. It can be concluded that the *Split-feed* mode is a preferable mode at the *Reformer* level as it offers higher  $H_2$  mole fraction without lowering the  $H_2$  yield compared to the *Single-feed* mode. The maximum  $H_2$  mole fraction is 0.68 at  $WGR=12$  and  $T=900$  K for *Split-feed* mode, at the *Reformer* level.



**Figure 6.13** H<sub>2</sub> mole fraction (dry basis) of *Reformer* level at different values of *WGR* and operating temperature ( $Q_{\text{net}}=0$ ,  $P=0.101325$  MPa).

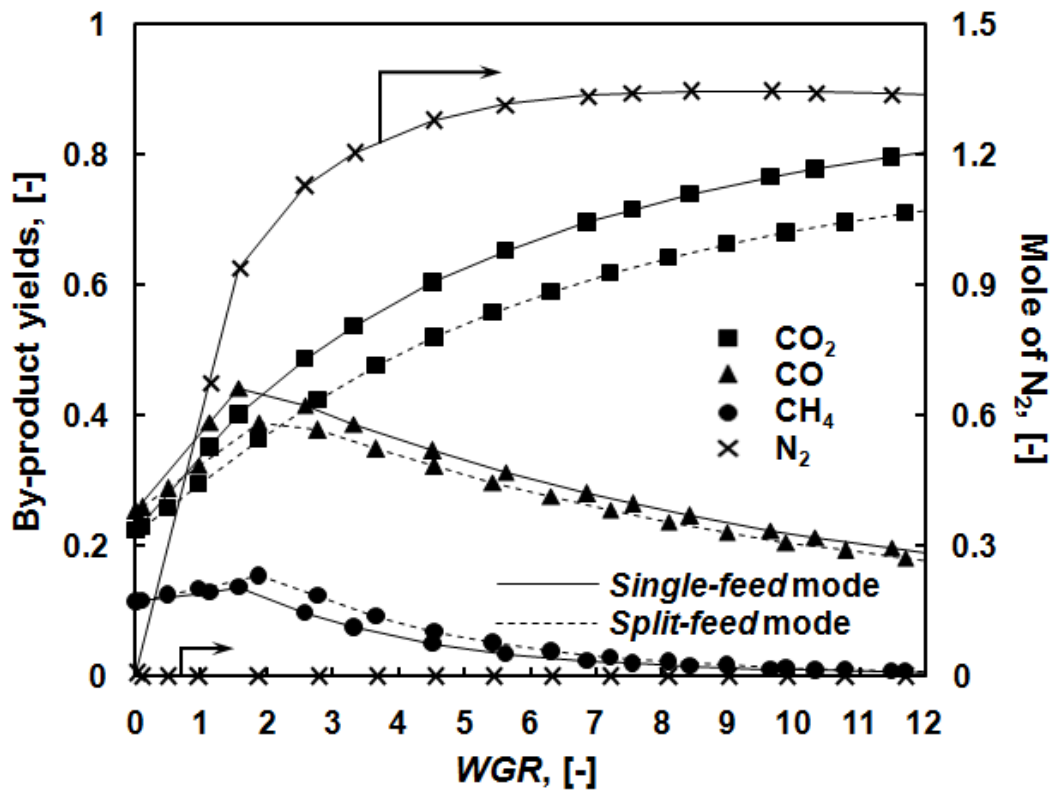


**Figure 6.14** H<sub>2</sub> mole fraction (dry basis) of *System* level at different values of *WGR* and operating temperature ( $Q_{\text{net}}=0$ ,  $P=0.101325$  MPa).

Considering the *System* level,  $WGR=3$  and 4 are the conditions that provide maximum  $H_2$  yields in the *Single-feed* and *Split-feed* modes, respectively. Figure 6.14 shows the  $H_2$  mole fraction at both  $WGR$ s and at various operating temperatures (600-1200 K) for both modes. It is obvious that the *Split-feed* mode is still a superior choice than the *Single-feed* mode at both  $WGR=3$  and 4 because the exothermic reactions occur outside the reformer and the by-products from the reactions do not dilute  $H_2$  in this mode. Increasing the temperature up to around 900 K increases the  $H_2$  mole fraction, which then remains constant for temperatures between 900 and 1200 K, in the *Split-feed* mode. It is the opposite of the  $H_2$  yield case.  $H_2$  production is actually constant in the steam reforming process at high temperatures (Rabenstein et al., 2008). In the *Split-feed* mode, some of the glycerol must be separated and fed to the combustor which causes the  $H_2$  yield to decrease, but it does not affect to the  $H_2$  concentration. Similar to the trend of  $H_2$  yield,  $WGR=4$  offers higher  $H_2$  mole fraction than  $WGR=3$ . In contrast, increasing the temperature up to 850 K increases the  $H_2$  mole fraction; above 850 K, the  $H_2$  mole fraction then decreases when increasing the temperature in the *Single-feed* mode. It is clear that the reverse WGS and nitrogen ( $N_2$ ) from air influence  $H_2$  dilution in the reformer. The maximum  $H_2$  mole fraction is 0.66 at  $WGR = 4$  and temperature of 900-1000 K for the *Split-feed* mode at the *System* level.

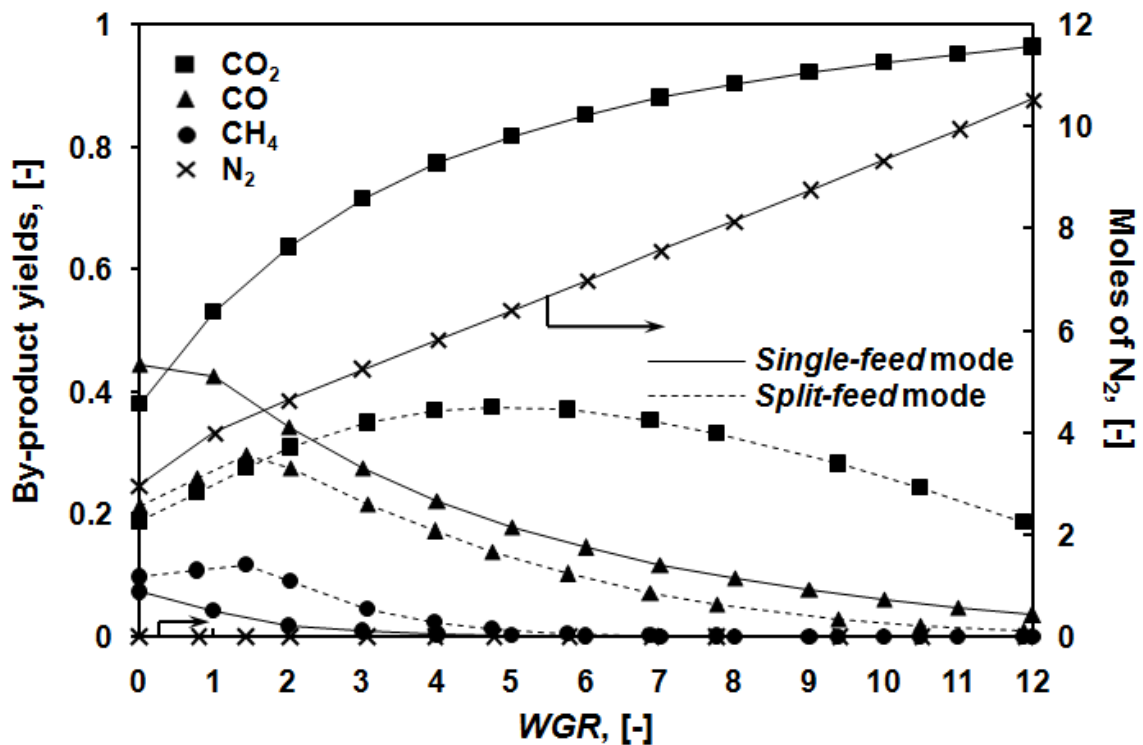
### 6.3.2.3. By-products

From the previous part on  $H_2$  mole fraction (dry basis), it is known that some by-products and unreacted reactants dilute  $H_2$  concentration. Considering all the reactions in this system, the possible by-products include CO,  $CO_2$ , and  $CH_4$ , whereas the unreacted reactants are  $C_3H_8O_3$ ,  $O_2$ . The thermodynamic analysis studies showed that, at all operating conditions chosen here, the glycerol conversion is 100% (Adhikari et al., 2007a; Wang et al., 2008; Wang et al., 2009). Therefore, the main obstruction to dilute  $H_2$  must be  $N_2$ . Figures 6.15 and 6.16 show the by-products and unreacted reactants at  $T=900$  K,  $WGR=0-12$ , and both modes at the *Reformer* and *System* levels, respectively. It is observed that the trends of the by-products are quite similar at both levels, as will be discussed in the following.



**Figure 6.15** By-product yields including CO<sub>2</sub>, CO, CH<sub>4</sub> and non reacted substance N<sub>2</sub> of *Reformer* level as a function of *WGR* ( $Q_{\text{net}}=0$ ,  $T_r=900$  K,  $P=0.101325$  MPa).

The amount of nitrogen gas is the major problem in term of H<sub>2</sub> dilution. It is directly dependent on the value of *OGR* in the *Single-feed* mode. However, N<sub>2</sub> is not present in the reforming product in the *Split-feed* mode. Consequently, it does not affect the mole fraction of H<sub>2</sub>. N<sub>2</sub> at the *Reformer* level is almost constant at *WGR* above 5 as *OGR* is almost constant in this range. In contrast, N<sub>2</sub> at the *System* level varies more significantly due to the strong dependency of *OGR* on *WGR*.

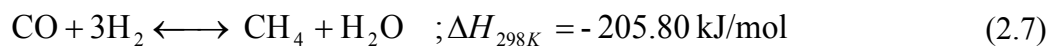


**Figure 6.16** By-product yields including CO<sub>2</sub>, CO, CH<sub>4</sub> and non reacted substance N<sub>2</sub> of *System* level as a function of *WGR* ( $Q_{\text{net}}=0$ ,  $T_r=900$  K,  $P=0.101325$  MPa).

CO and CO<sub>2</sub> are the impurities that do not compete against H<sub>2</sub> production (Adhikari et al., 2007a). At the *Reformer* level, CO<sub>2</sub> increases when increasing *WGR* in both modes; however the *Split-feed* mode offers lower CO<sub>2</sub> yield than the *Single-feed* mode where air is fed outside the reformer. Nevertheless, it is different at the *System* level because CO<sub>2</sub> is lower for *WGR* in the range 6-12 in the case of *Split-feed* mode. This is because a larger amount of glycerol is diverted to the combustor to supply higher heat requirement. It is also the reason why CO<sub>2</sub> in the *Split-feed* mode is always less than in the *Single-feed* mode. Considering CO, the same trends are observed for both modes and levels. CO decreases when increasing *WGR* above 2 (Equation (2.10)) (Adhikari et al., 2007a). The *Split-feed* mode still offers lower CO yield than the *Single-feed* mode, similar to CO<sub>2</sub>. Even though the amount of CO is not large, it remains an issue if the product gas is to be used in low-temperature fuel cells (such as proton exchange membrane fuel cells (PEMFCs), CO being a poison for the platinum electrode of polymer electrolyte fuel cells (PEFCs)) (Wang et al., 2008;

Hernandez et al., 2009). Another undesired by-product is CH<sub>4</sub> (Adhikari et al., 2007a; Wang et al., 2009). CH<sub>4</sub> is almost suppressed when *WGR* is between 0 and 12 at 900 K in both modes and at both levels. The CH<sub>4</sub> yield decreases when increasing *WGR*. It is noted that the CH<sub>4</sub> yield initially increases at small values of *WGR* (0-2) due to the methanation reaction (Equation (2.7)) but the reaction becomes unfavorable in the presence of high H<sub>2</sub>O at higher *WGR*. Moreover, CH<sub>4</sub> is not favor in a system that involves oxygen in feed (*Single-feed* mode) because the products become CO or CO<sub>2</sub> rather than CH<sub>4</sub>. The conditions that favor CH<sub>4</sub> formation are low ranges of temperature and low *WGR* (Adhikari et al., 2007a). It is the reason why CH<sub>4</sub> is always observed in higher amount in *Split-feed* mode than *Single-feed* mode at both levels. However, the CH<sub>4</sub> yield can be neglected in this range.

Methanation:



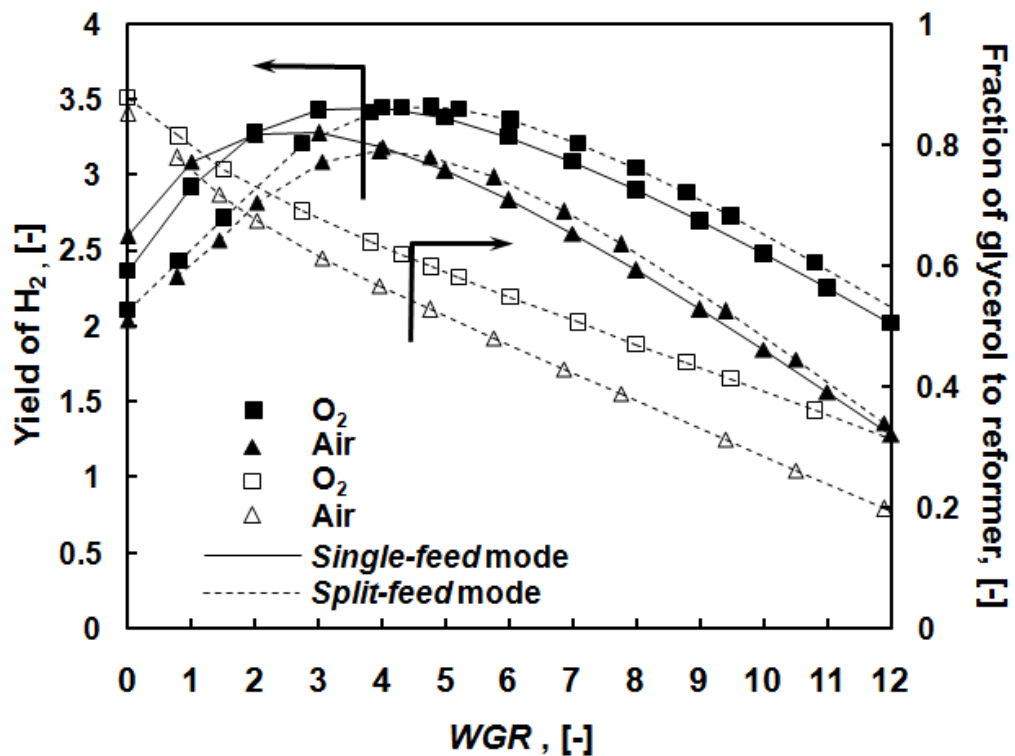
It can be concluded that N<sub>2</sub> and CO<sub>2</sub> are the main impurities to dilute H<sub>2</sub> in the product. *Split-feed* mode is a promising operating mode to avoid this problem by feeding air as oxidizing agent outside the reformer and consequently higher mole fractions of H<sub>2</sub> are achieved in the gas product.

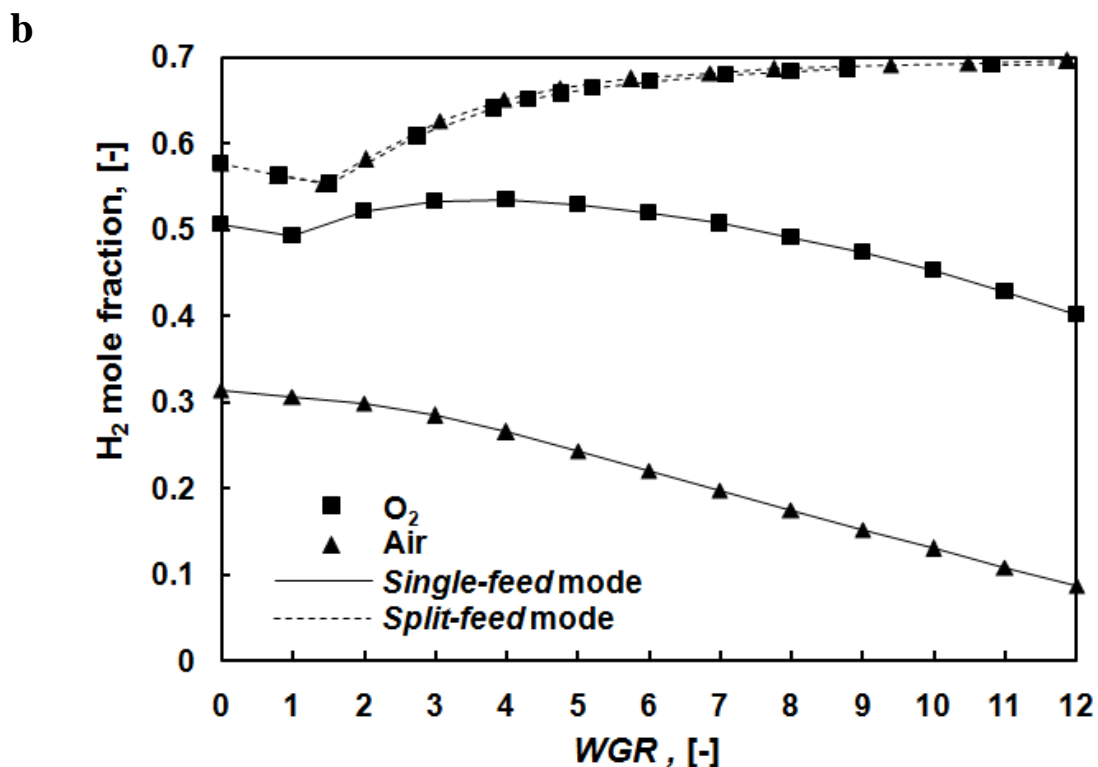
### 6.3.3 Effect of oxidizing agent at thermal neutral conditions

In the previous section, air was the oxidizing agent used in glycerol reforming at thermal neutral conditions; however, air contains significant amount of N<sub>2</sub>. It is an interesting issue to determine whether using pure O<sub>2</sub> instead of air could improve H<sub>2</sub> production although it is well known that pure O<sub>2</sub> increases production costs. As it was concluded that the *Single-feed* and *Split-feed* modes at the *Reformer* level are not significantly different due to the low energy requirement, only the *System* level is investigated for determining the effect of the type of oxidizing agent. The calculations were based on the thermal neutral condition and at a temperature of 900 K which provides the highest H<sub>2</sub> yield. Figure 6.17a compares the H<sub>2</sub> yield and the fraction of glycerol sent to the reformer for the cases using air and O<sub>2</sub> at different *WGR*s. Pure O<sub>2</sub> leads to higher H<sub>2</sub> yield than air for all values of *WGR* (0-12) in the *Split-feed* mode.

This is because using pure O<sub>2</sub> reduces the demand of heat energy for heating N<sub>2</sub>, and therefore, less glycerol is split to the combustor. The use of pure O<sub>2</sub> also increases the highest H<sub>2</sub> yield from 3.15 (air) to 3.45 (pure O<sub>2</sub>) in the *Split-feed* mode at *WGR* of 4.00 (air) to 4.80 (pure O<sub>2</sub>), respectively. However, for the *Single-feed* mode at low values of *WGR* (0-2), the H<sub>2</sub> yield in the air case is higher than that in the pure O<sub>2</sub> case. This can be explained from the fact that the difference of moles in the products and the reactants is positive for glycerol reforming and, therefore, the H<sub>2</sub> yield is favored at low operating pressures according to Le Chatelier's principle (Adhikari et al., 2007a). The presence of N<sub>2</sub> provides similar effects as decreasing the pressure. However, at higher *WGR*s (2-12) the use of pure O<sub>2</sub> offers higher H<sub>2</sub> yield. The H<sub>2</sub> yield can also be improved from 3.28 (air at *WGR* of 3) to 3.45 (O<sub>2</sub> at *WGR* of 4) in the *Single-feed* mode. Considering the maximum H<sub>2</sub> yield, both modes can provide a maximum yield of around 3.45 when using O<sub>2</sub> but at different *WGR*s. It is also observed that the fraction of glycerol to the reformer in the *Split-feed* mode strongly depends on the oxidizing agent. This is the reason that why O<sub>2</sub> also offers a higher H<sub>2</sub> yield than air.

a





**Figure 6.17** (a) H<sub>2</sub> yield and fraction of glycerol to reformer, (b) H<sub>2</sub> mole fraction (dry basis) of *System* level as a function of *WGR* for cases with different oxidizing agents (air or pure O<sub>2</sub>) and operation modes (*Co-feed* or *Split-feed*) ( $Q_{\text{net}}=0$ ,  $T_r=900$  K,  $P=0.101325$  MPa).

Figure 6.17b shows the effect of oxidizing agent on the H<sub>2</sub> mole fraction when increasing *WGR*. The *Split-feed* mode shows much higher mole fractions of H<sub>2</sub> than that of the *Single-feed* mode in both air and pure O<sub>2</sub> cases. For the *Split-feed* mode, air and O<sub>2</sub> are not significantly different. Increasing *WGR* decreases the H<sub>2</sub> mole fraction for *WGR* in the range 0-1.5, and then continuously increases to a H<sub>2</sub> mole fraction of 0.70. In contrast, O<sub>2</sub> in the *Single-feed* mode highly enhances the mole fraction of H<sub>2</sub> because the reformer does not have N<sub>2</sub> to dilute H<sub>2</sub>. However, increasing *WGR* in the range of 1-4 increases the H<sub>2</sub> mole fraction similar to the *Split-feed* mode, and then at *WGR*=4-12 decreases the mole fraction of H<sub>2</sub> similar to using air in *Single-feed* mode.

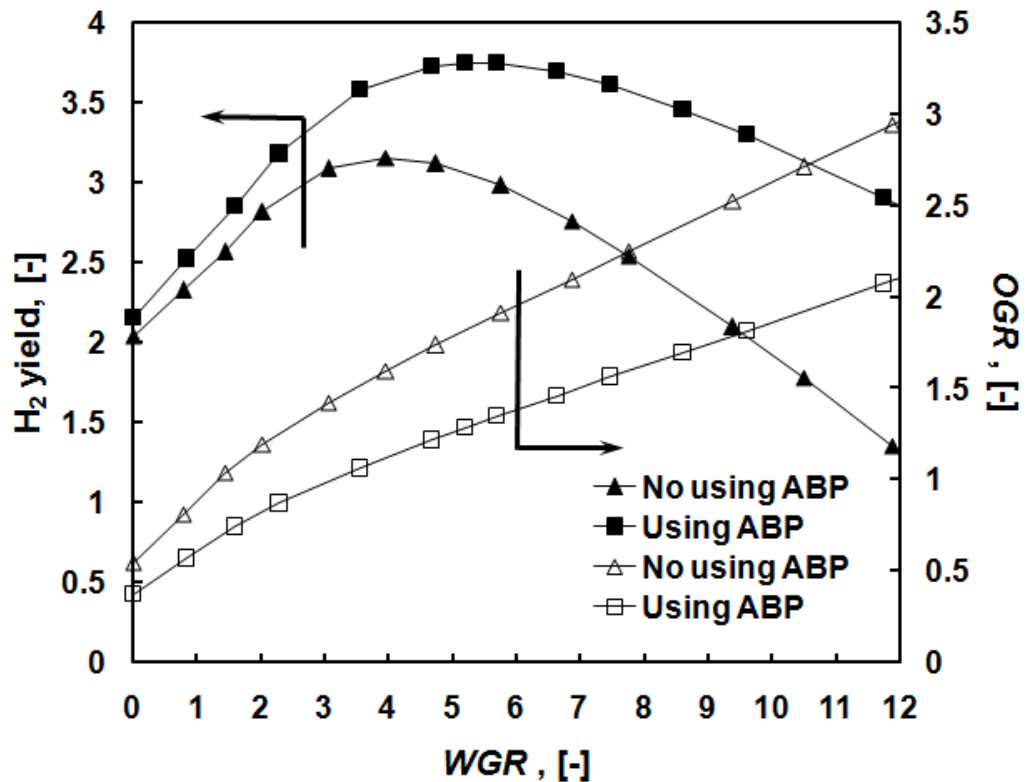


### 6.3.4. Effect of using afterburner products as heat supply

The afterburner products (ABP) stream in the *Split-feed* mode is at a high temperature ( $T_r$ ), and thus is a potential heat source. It should be noted that for the *Split-feed* mode, as part of glycerol is split and combusted to supply heat for the reforming and evaporating processes outside the main reforming zone, the ABP from the combustion are unable to be further contributed on the hydrogen production, resulting in the decrease of  $H_2$  yield from appearing of  $O_2$ . In addition, although it is possible to recycle part of the ABP to the reforming section, the presence of inert  $N_2$  in the ABP stream would decrease the  $H_2$  mole fraction in the final product. When the ABP recycle ratio increases close to 1, the performances of the *Split-feed* mode becomes similar to those of the *Single-feed* mode. Hence, only heat energy from ABP should be transferred to the heat demanding units including heater, evaporator, and reformer. With additional heat from ABP at the *System* level, Equation (6.6) can be modified to Equation (6.10) as shown below.

$$Q_{\text{System level (net)}} = Q_{\text{heater(net)}} + Q_{\text{evaporator}} + Q_{\text{reformer}} + Q_{\text{combustor}} + Q_{\text{cooler(ABP)}} = \sum_{i=1}^N n_{i, \text{out}} H_{i, \text{out}} - \sum_{i=1}^N n_{i, 0} H_{i, 0} \quad (6.6)$$

It should be noted that the use of ABP stream for heat supply is not considered at the *Reformer* level.



**Figure 6.18** H<sub>2</sub> yield and OGR of *Split-feed* mode in *System* level as a function of WGR for cases with/without utilizing heat energy from Afterburner products (ABP) stream ( $Q_{\text{net}}=0$ ,  $T_r=900$  K,  $P=0.101325$  MPa).

As shown in Figure 6.18, the H<sub>2</sub> yield increases from 3.16 ( $WGR=3.96$ ,  $OGR=1.60$ ,  $T=900$  K) to 3.75 ( $WGR=5.21$ ,  $OGR=1.28$ ,  $T=900$  K) when recovering heat from the ABP stream. In addition, the value of OGR also decreases because a lower amount of glycerol has to be split to the combustor. The operating conditions, products yields and products concentrations at maximum H<sub>2</sub> yields are summarized Table 1 for different modes and at different levels. It is clear that the operating mode at the *Reformer* level does not significantly affect the H<sub>2</sub> yield, but the *Split-feed* mode enhances the H<sub>2</sub> mole fraction. At the *System* level, the H<sub>2</sub> yield in the *Single-feed* mode is higher than the *Split-feed* mode, but it leads to a lower H<sub>2</sub> mole fraction in the final products. However, the use of pure O<sub>2</sub> can increase the H<sub>2</sub> mole fraction in the *Single-feed* mode and the use of ABP in the *Split-feed* mode can further improve the H<sub>2</sub> yield while keeping a H<sub>2</sub> concentration. Moreover, no solid carbon is detected at the conditions which offer the highest H<sub>2</sub> yields.

**Table 6.1** Summary of operating conditions at maximum H<sub>2</sub> yields, product yields and product distribution for different cases ( $Q_{\text{net}}=0$ ,  $P=0.101325$  MPa).

Boundary Mode	Reformer		System				
	Single-feed	Split-feed	Single-feed	Single-feed + Pure O <sub>2</sub>	Split-feed	Split-feed + Pure O <sub>2</sub>	Split-feed + ABP
<b>Conditions</b>							
<i>WGR</i> , [-]	12	12	3	4	3.96	4.78	5.21
<i>OGR</i> , [-]	0.36	0.37	1.40	1.32	1.60	1.48	1.28
<i>T</i> , [K]	900	900	900	900	900	900	900
<b>Yield, [-]</b>							
H <sub>2</sub>	5.64	5.67	3.28	3.45	3.16	3.45	3.75
CO	0.19	0.18	0.28	0.25	0.17	0.17	0.18
CO <sub>2</sub>	0.80	0.71	0.71	0.74	0.37	0.41	0.45
CH <sub>4</sub>	0.01	0.01	0.01	0.01	0.02	0.02	0.02
C	-	-	-	-	-	-	-
<b>Mole fraction (dry basis), [-]</b>							
H <sub>2</sub>	0.57	0.68	0.28	0.54	0.65	0.66	0.66
CO	0.06	0.06	0.07	0.11	0.11	0.10	0.10
CO <sub>2</sub>	0.24	0.26	0.19	0.34	0.23	0.23	0.23
CH <sub>4</sub>	≈0	≈0	≈0	0.01	0.01	0.01	0.01

## 6.4 Conclusion

A thermodynamic analysis was performed to investigate H<sub>2</sub> production from glycerol reforming at thermal neutral conditions. This work considers two modes of air feeding; i.e., *Single-feed* and *Split-feed* modes and at two levels, including *Reformer* and *System* levels. The H<sub>2</sub> yield from both modes is not significantly different at the *Reformer* level due to the small energy requirement from the heat of reactions. In contrast, it is observed at the *System* level that the *Single-feed* is favorable to H<sub>2</sub> generation at low temperatures (600-900 K), whereas in the *Split-feed* mode, more H<sub>2</sub> are generated at high temperatures (900-1200 K). The maximum H<sub>2</sub> yields are 5.67 ( $WGR=12$ ,  $OGR=0.37$ ,  $T=900$  K, *Split-feed* mode), and 3.28 ( $WGR=3$ ,  $OGR=1.40$ ,  $T=900$  K, *Single-feed* mode), at the *Reformer* and *System* levels, respectively. The *Single-feed* mode is a superior mode in term of suppressing carbon formation - no carbon formation is observed when operating at temperature above 900 K. However, carbon formation from both modes is totally inhibited at  $WGR$  higher than 2, and 3.5 at *Reformer* and *System* levels, respectively. Other by-products including CO, CO<sub>2</sub> and CH<sub>4</sub> were determined. The *Split-feed* mode offers higher H<sub>2</sub> concentration in the product gas because N<sub>2</sub> from air and part of CO<sub>2</sub> are not present in the gas product in the *Split-feed* mode unlike in the *Single-feed* mode. The use of pure O<sub>2</sub> instead of air is also considered in both modes at the *System* level. Use of pure O<sub>2</sub> in the *Single-feed* mode can increase the H<sub>2</sub> mole fraction in the product and H<sub>2</sub> yield from 0.28 to 0.54 and from 3.28 to 3.45, respectively. Moreover, the H<sub>2</sub> yield in the *Split-feed* mode is also enhanced when replacing air by pure O<sub>2</sub> (from 3.16 with air to 3.45 with O<sub>2</sub>). However, using air or O<sub>2</sub> does not make a significant difference in term of H<sub>2</sub> mole fraction. Using pure O<sub>2</sub> is considered to be a good choice for H<sub>2</sub> production from glycerol at the thermal neutral conditions especially in the *Single-feed* mode. In addition, using the ABP stream to supply heat is beneficial to increase the H<sub>2</sub> yield in the *Split-feed* mode as it decreases the fuel requirement (glycerol and air). The maximum H<sub>2</sub> yield after recovering the ABP heat is 3.75 ( $WGR=5.21$ ,  $OGR=1.28$ ,  $T=900$  K, *Split-feed* mode) at thermal neutral condition.

# **CHAPTER VII**

## **HYDROGEN PRODUCTION FROM GLYCEROL REFORMING IN SUPERCRITICAL WATER: THERMODYNAMIC ANALYSIS**

After the discussions from thermodynamic analysis of Steam reforming (SR), Partial oxidation (POx), and Autothermal reforming (ATR) processes, this chapter shifted to attention to the thermodynamic analysis of supercritical water reforming (SWR) process. Particular focus is on the effect of operating temperature, pressure, and feed glycerol concentration on the reaction performance.

### **7.1 Review on equation of state**

Earlier literatures (Gadhe et al., 2007; Byrd et al., 2007; Serani et al. 2008; Bennekom et al., 2011) reported that properties (i.e. dielectric constant, density, diffusivity, thermal conductivity, and viscosity) of supercritical water were very different from those of steam and liquid water. Hence, the equation of state (EOS) might be different from the previous reforming processes (We used SRK as the EOS in the previous sections). Although there are a number of EOSs proposed in literatures, only a few of them have been employed for predicting thermodynamic properties at supercritical conditions. The followings provide details of previous works which employed different EOSs for different reaction systems.

#### **7.1.1 Soave-Redlich-Kwong (SRK) EOS**

Anikeev et al. (2004) investigated 2-propanol dehydration in supercritical water. SRK EOS was used to calculate the partial molar volumes of the reaction participants including a transition state and activation volume of the reaction. Lu et al.

(2007) investigated biomass gasification in supercritical water. They proposed a high-pressure gas-liquid equilibrium model based on modified universal functional coefficient (UNIFAC) model, SRK EOS, and modified Huron-Vidal second-order (MHV2) mixing rule. Tuan (2009) investigated ethanol reforming in supercritical water. The Gibbs free energy minimization was used to calculate mass and energy balance with SRK EOS. However, the heat capacity of each component was assumed to be dependent only on temperature.

### **7.1.2 Peng-Robinson (PENG-ROB) EOS**

Tang and Kitagawa (2005) investigated biomass gasification i.e. methanol, glucose, cellulose, and real biomass in supercritical water. The model improved with PENG-ROB EOS and global Gibbs free energy minimization strategy. Model predications made generally good agreement with the experiment results. Byrd et al. (2008) investigated glycerol reforming in supercritical water. Minimizing Gibbs free energy was used with PENG-ROB EOS in thermodynamic equilibrium calculations. However it did not predict coke formation in their work. Voll et al. (2009) investigated supercritical water gasification of methanol, ethanol, glycerol, glucose, and cellulose. They used PENG-ROB EOS to calculate fugacity coefficients and it was found that their values were far from ideal conditions. The model predictions expressed as a good agreement with the experimental studies. Letellier et al. (2010) investigated aqueous biomass gasification in supercritical water. PENG-ROB EOS was used to calculate the fugacity coefficient that compressibility factor computed using the third order dimensionless polynomial equation. Castello et al. (2011) investigated biomass gasification in supercritical water. A two-phase non-stoichiometric thermodynamic model was considered based on Gibbs free energy minimization. PENG-ROB was used for fugacity coefficient calculations which offered a capability of dealing effectively with supercritical fluids.

### **7.1.3 Others**

Feng et al. (2004) used statistical association fluid theory (SAFT) EOS to predict the biomass gasification in subcritical and supercritical water conditions. It was applied for the calculations in mass distribution in different phases and to

approximate the enthalpy and entropy values for different mass streams. Yan et al. (2006) used Duan EOS to predict the biomass gasification in supercritical water. They explained that this EOS was based on a corresponding states assumption with only two parameters for each pure component and two additional parameters for each binary mixture. Ortiz et al. (2011) compared four EOSs for glycerol reforming under supercritical water including PENG-ROB, Peng-Robinson with the Boston-Mathias  $\alpha$ -function (PR-BM), SRK, and Predictive Soave-Redlich-Kwong (PSRK) EOS by focusing on the changing of enthalpy with temperature and pressure in liquid and vapor phases. PENG-ROB and PR-BM expressed the similar behaviors as PSRK but their deviations were slightly higher. However, SRK offered the large errors. Finally, they chose PSRK to be an EOS for all calculations.

## 7.2 Thermodynamic analysis conditions

Thermodynamic analysis in this section was done following a non-stoichiometric approach. Aspen Plus program was employed for calculating equilibrium compositions. An RGibbs reactor was used for calculations based on minimizing the Gibbs free energy. Note that the thermodynamic analysis is independent of reaction pathways as the method depends on the pre-defined possible product species. In this study of glycerol reforming in supercritical water, the possible product species reported from literatures (Buhler et al., 2002; Xu et al., 2009; May et al., 2010) including glycerol ( $C_3H_8O_3$ ), water ( $H_2O$ ), hydrogen ( $H_2$ ), carbon monoxide (CO), carbon dioxide ( $CO_2$ ), methane ( $CH_4$ ), ethane ( $C_2H_6$ ), ethylene ( $C_2H_4$ ), propane ( $C_3H_8$ ), propylene ( $C_3H_6$ ), carbon (C(s)), formaldehyde ( $CH_2O$ ), acetaldehyde ( $CH_3CHO$ ), acetol ( $CH_3COCH_2OH$ ), methanol ( $CH_3OH$ ), acetic acid ( $CH_3COOH$ ), propionaldehyde ( $CH_3CH_2CHO$ ), allyl alcohol ( $CH_2CHCH_2OH$ ), acetone ( $CH_3COCH_3$ ), acrolein ( $CH_2CHCHO$ ), ethanol ( $CH_3CH_2OH$ ), ethylene glycol ( $CH_2OHCH_2OH$ ), and acrylic acid ( $CH_2CHCOOH$ ) were specified in the calculations. Three EOSs consisting of SRK, PENG-ROB, and PSRK were compared as the method for estimating thermodynamic properties for the reaction systems. It was found that SRK and PENG-ROB EOSs predicted almost the similar results for all the parameter ranges (results not shown here). However, PSRK showed significant

differences from the other two EOSs especially at high operating temperatures and pressures (CO<sub>2</sub> and CO components). In addition, solid carbon is not available in PSRK EOS. Finally, we chose PENG-ROB EOS to calculate the equilibrium products in this work. This EOS was employed in a number of previous studies (Tang and Kitagawa, 2005; Byrd et al., 2008; Voll et al., 2009; Letellier et al., 2010; Castello et al., 2011). PENG-ROB EOS is written as follows:

$$P = \frac{RT}{V-b} - \frac{a\alpha}{V^2 + 2bV - b^2} \quad (7.1)$$

where  $a = \frac{0.457235R^2T_C^2}{P_C}$ ;  $b = \frac{0.077796RT_C}{P_C}$ ;  $T_r = \frac{T}{T_C}$ ;  $\alpha = (1 + \kappa(1 - \sqrt{T_r}))^2$ ;

$$\kappa = 0.37464 + 1.54226\omega - 0.26992\omega^2$$

$\omega$  is the acentric factor of the species.

$R$  is the ideal gas constant.

In the polynomial form, it is given as follows:

$$Z^3 - (1-B)Z^2 + (A-2B-3B^2)Z - (AB-B^2-B^3) = 0 \quad (7.2)$$

where  $A = \frac{a\alpha P}{R^2T^2}$ ;  $B = \frac{bP}{RT}$ ;

$Z = \frac{PV}{RT}$  is compressibility factor.

The reaction performances are expressed in terms of glycerol conversion (Equation (7.3)), mole fraction in gas phase (Equation (7.4)), yield of H<sub>2</sub> (Equation (7.5)), and yield of carbon containing species  $i$  (Equation (7.6)) are defined as follows.

$$X_{\text{Glycerol}} = \frac{F_{\text{Glycerol,in}} - F_{\text{Glycerol,out}}}{F_{\text{Glycerol,in}}} \quad (7.3)$$



$$\text{Mole fraction in gas phase of species } i = \frac{F_{i,\text{gas}}}{\sum_n F_{i,\text{gas}}} \quad (7.4)$$

$$\text{Yield of H}_2 = \frac{F_{\text{H}_2}}{F_{\text{Glycerol,in}}} \quad (7.5)$$

$$\text{Yield of carbon containing species } i = \frac{F_i}{F_{\text{Glycerol,in}}} \times \frac{\text{number of carbon atom in molecule}}{3} \quad (7.6)$$

where  $F_{\text{Glycerol,in}}$  and  $F_{\text{Glycerol,out}}$  are the inlet and outlet glycerol molar flow rates, respectively, and  $F_i$  is the molar flow rate of species  $i$ .

### 7.3 Results and discussion

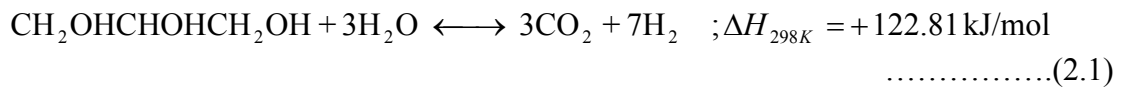
In this study, simulations were carried out at different operating temperature (673-1273 K), pressure (19-30 MPa), and feed glycerol concentration (2.5-40 wt.%). Based on the thermodynamic equilibrium, all of the glycerol was totally consumed in the reactions, therefore the glycerol conversion is always 1.00 which is in good agreement with previous reports (Byrd et al., 2008; Ortiz et al., 2011). C<sub>2</sub>-C<sub>3</sub> hydrocarbon gaseous products and liquid hydrocarbon products were also negligible in all process conditions as the yields were less than 0.01.

#### 7.3.1 Effect of operating temperature

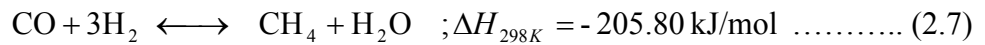
Figure 7.1a indicates that only four components (H<sub>2</sub>, CO<sub>2</sub>, CH<sub>4</sub>, and CO) were observed as the gaseous products within 673 to 1273 K at a pressure of 25 MPa, and 5 wt.% feed glycerol concentration. Increasing operating temperature enhanced the glycerol steam reforming (SR, Equation (2.1)) to promote mole fraction of H<sub>2</sub> up to 0.70 (CO<sub>2</sub> around 0.30). It is clear that CH<sub>4</sub> mole fraction has a drastic decreasing with increasing of operating temperature, according to increasing in H<sub>2</sub> mole fraction. The exothermic methanations of CO (Equation (2.7)) and CO<sub>2</sub> (Equation (2.8)) can explain the trends of H<sub>2</sub>, CO<sub>2</sub>, CH<sub>4</sub>, CO mole fractions. CH<sub>4</sub> was totally inhibited above 1048 K. CO mole fraction was increased by increasing of operating

temperature; however it seems to be suppressed during 673 to 873 K. Reverse water gas shift (RWGS, Equation (2.10)) begins to take a role above 1173 K, resulting in slightly increasing of CO, and decreasing of H<sub>2</sub> and CO<sub>2</sub> mole fractions. However, all components had only slight changing at high operating temperatures (1048-1273 K).

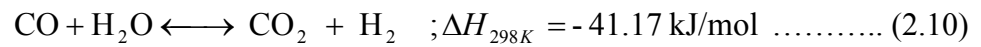
The overall reaction of glycerol Steam Reforming (SR):



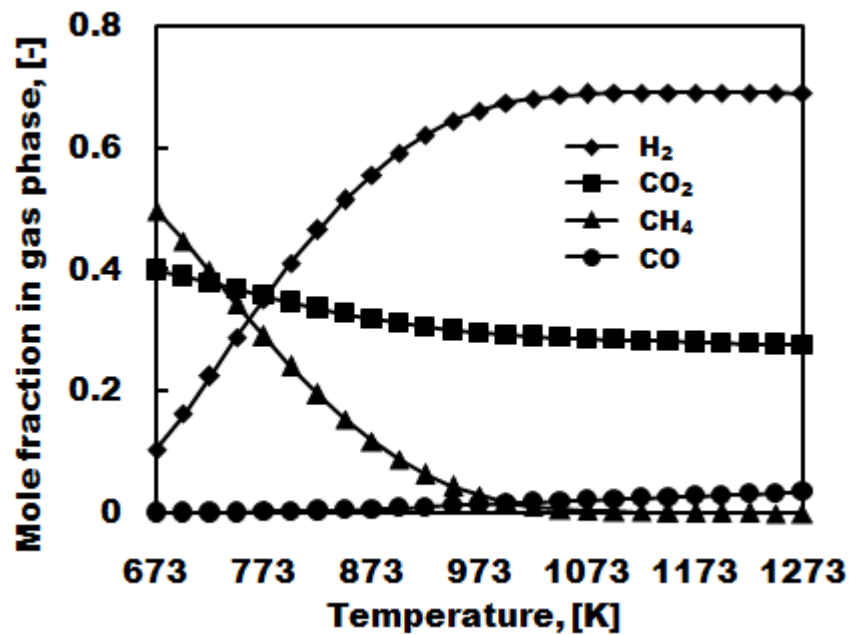
Methanation (MET):



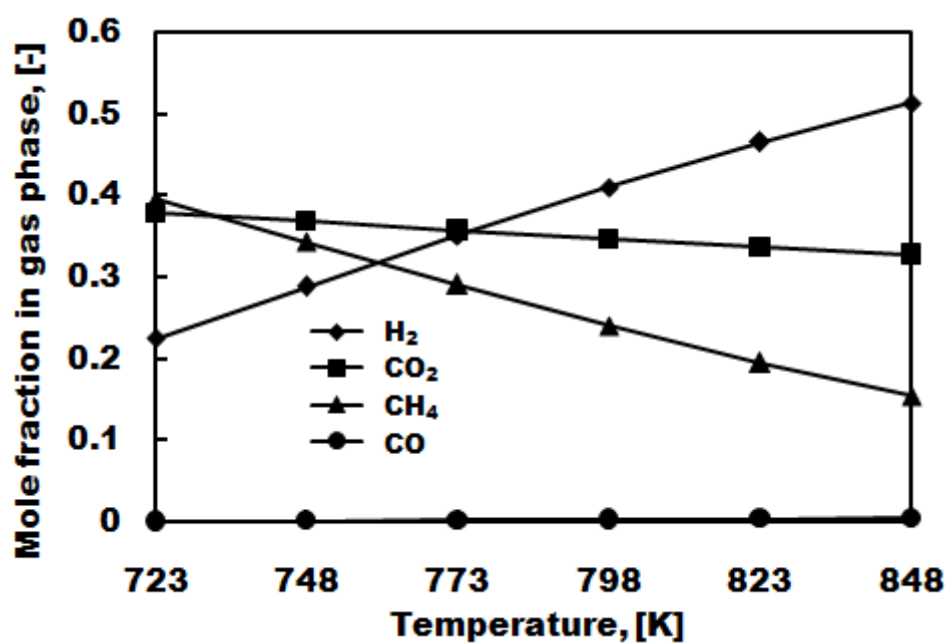
Water Gas Shift (WGR or reverse of this is called RWGS):



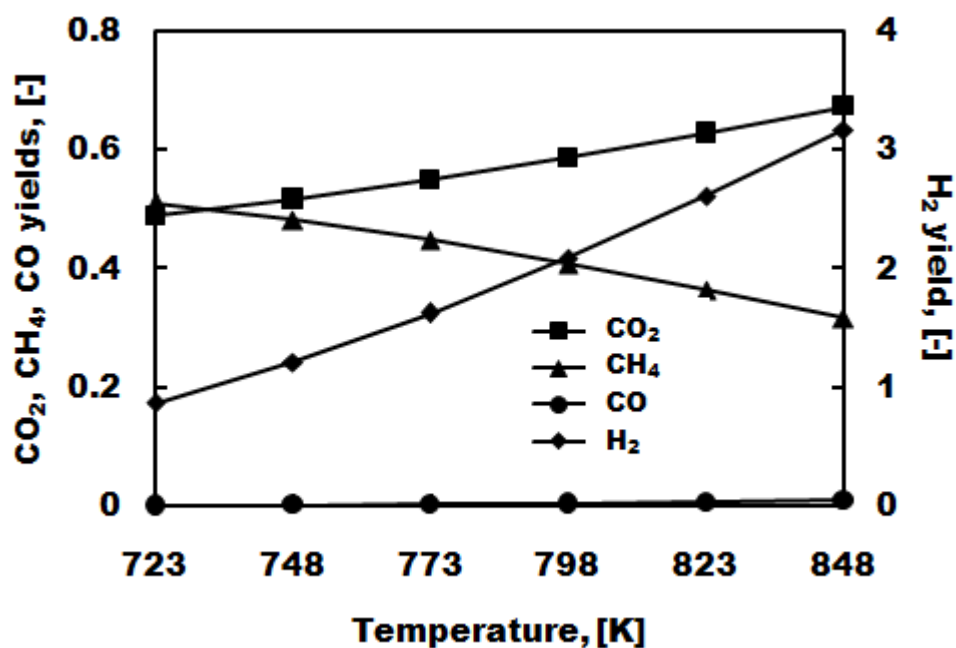
**a**



b



c

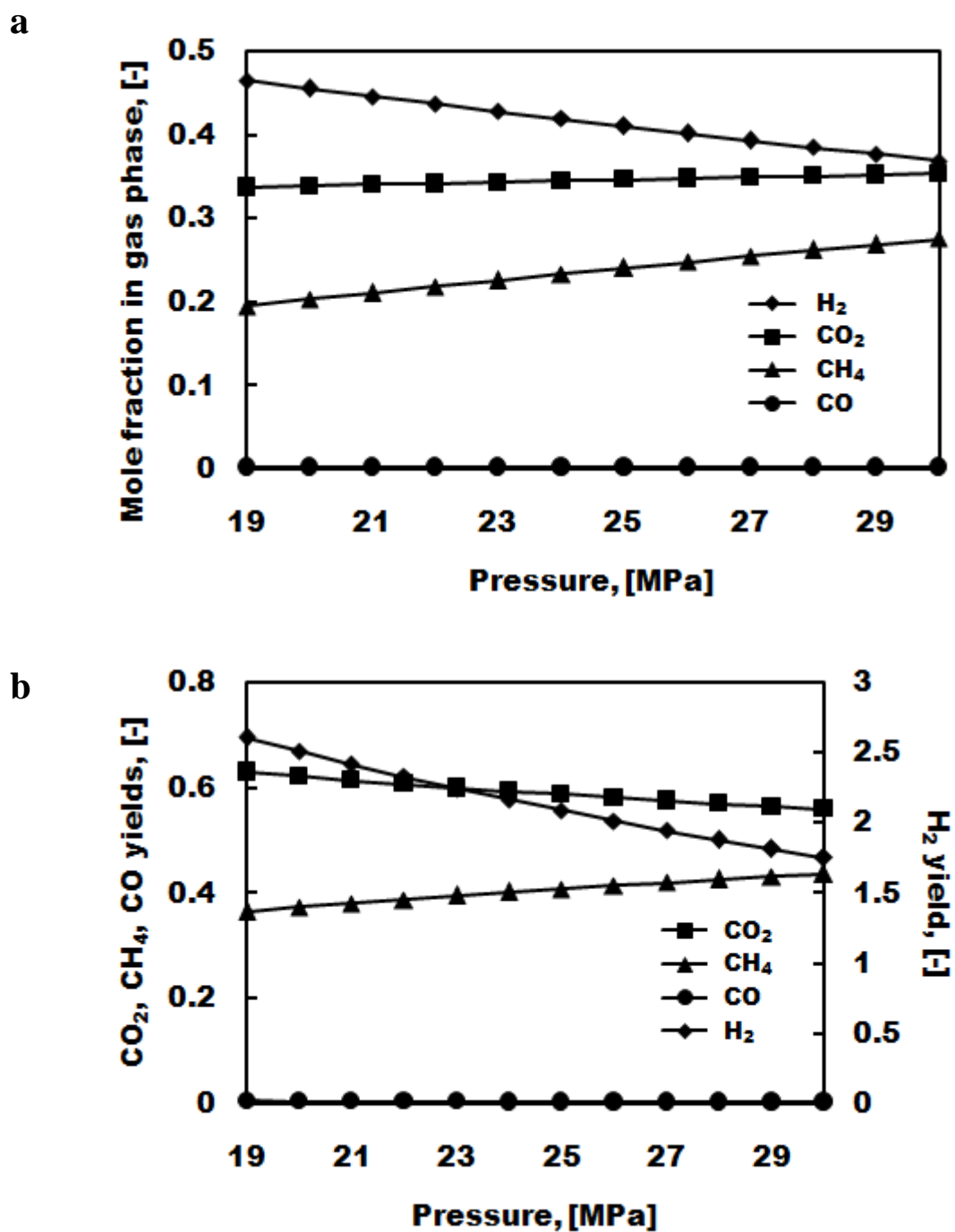


**Figure 7.1** Mole fractions of gas products (H<sub>2</sub>, CO<sub>2</sub>, CO, and CH<sub>4</sub>) during (a) 673-1273 K (b) 723-848 K and (c) gas product yields as function of operating temperatures ( $P=25$  MPa, 5 wt.% of feed glycerol concentration)

Operating temperature of 1048 K was considered as a very high temperature for SCWR process. It causes of large energy requirement to operate the process especially the energy for heating up a large amount of water from room temperature (273 K) to the desired operating temperature. That might be releasing of the unnecessary energies, even though hydrogen production was achieved. Therefore lower operating temperatures in the range of 723 to 848 K were more interesting for the study of this process. Figure 7.1b shows that increasing of H<sub>2</sub> mole fraction opposed to the mole fraction of CH<sub>4</sub> by increasing operating temperature. Only a slight deceasing of CO<sub>2</sub> mole fraction and CO suppression were found within these operating temperatures. It is clear that CO<sub>2</sub> methanation influences the changes of H<sub>2</sub>, CO<sub>2</sub>, CH<sub>4</sub> mole fractions. In addition, H<sub>2</sub>, and CO<sub>2</sub> yields were rising by increasing of operating temperature, according to decreasing of CH<sub>4</sub> yield as shown in Figure 7.1c. At 848 K, mole fraction and yield of H<sub>2</sub> reached the maximum values around 0.51 and 3.17, respectively.

### 7.3.2 Effect of pressure

We have known that pressure is an important parameter to reach the supercritical water condition. This part focuses on the effect of pressure at subcritical (near supercritical water condition: 19-22 MPa), and supercritical water (22-30 MPa) with the operating temperature of 798 K. Figure 7.2a shows only slight changes observed by increasing the pressure. H<sub>2</sub> mole fraction opposed with CH<sub>4</sub> mole fraction but CO<sub>2</sub>, CO mole fractions were almost constant during the range of pressures. It is clear that methanations (Equations (2.7) and (2.8)) were promoted by increasing the pressure especially Equation (2.8). CO<sub>2</sub> reacted with H<sub>2</sub> to produce more CH<sub>4</sub> by the principle of Le Chatelier. Figure 7.2b confirms that the trend of CO<sub>2</sub> yield opposed to CH<sub>4</sub> yield. Note that SR (Equation (2.1)) was independent of increasing pressure because a huge amount of water was added (water to glycerol ratio more than 3). In addition, conversion of glycerol was still 1.00 at all pressure range. It can be concluded that H<sub>2</sub> production is favorable at lower pressure with the thermodynamic study



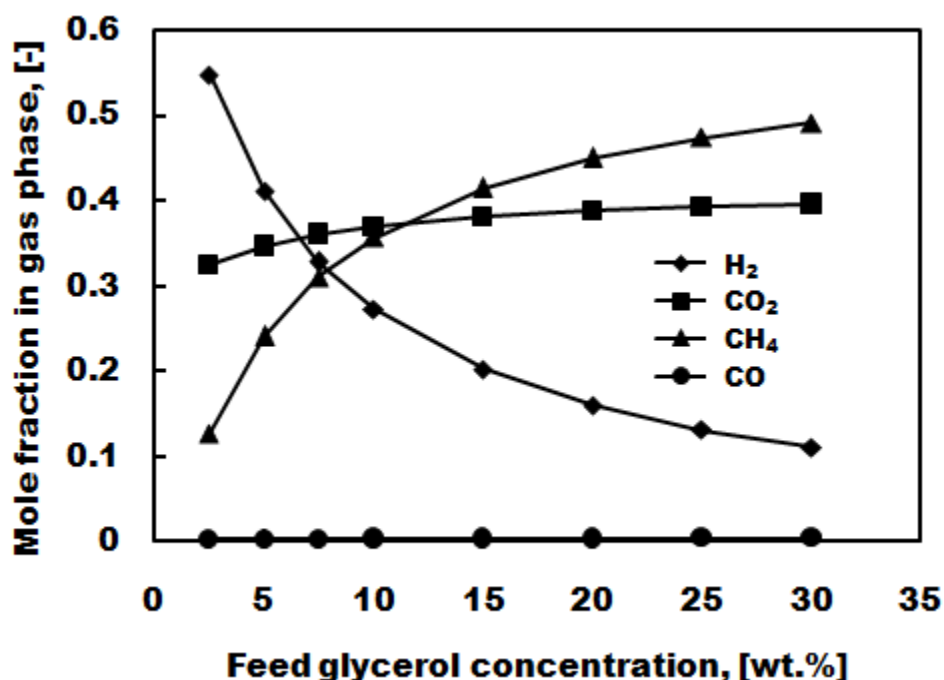
**Figure 7.2** (a) mole fractions of gas products (H<sub>2</sub>, CO<sub>2</sub>, CO, and CH<sub>4</sub>) (b) gas product yields as a function of pressure ( $T=798$  K, 5 wt.% of feed glycerol concentration)

### 7.3.3 Effect of feed glycerol concentration

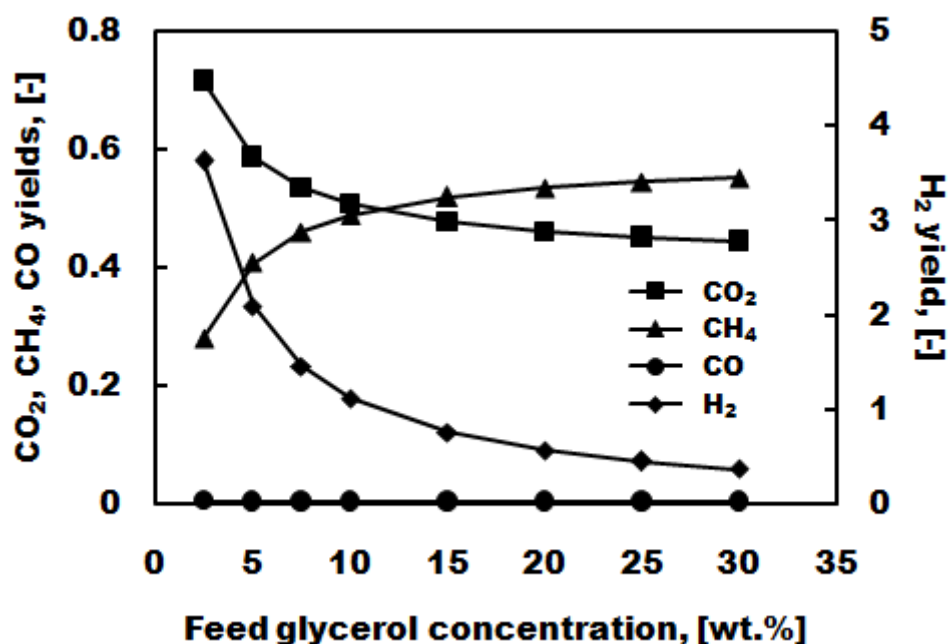
Feed glycerol concentration is another parameter which directly affects the energy requirement of the process. Figures 7.3a,b indicate that the effect of feed

glycerol concentration was observed as same as pressure from the previous part. Increasing of feed glycerol concentration promoted methanations (Equations (2.7),(2.8)) by increasing of  $\text{CH}_4$ , but decreasing of  $\text{H}_2$ .  $\text{CO}_2$  yield was clearly unflavored with the increasing of feed glycerol concentration, according to Equation (2.8). It was found that the changing of feed glycerol concentration at low values (2.5-7.5 wt.%) was a crucial effect to gas products mole fraction and yield. For example,  $\text{H}_2$  yield was dropped around 42% when increasing the feed glycerol concentration from 2.5 to 5 wt.%. It caused 100% of feed glycerol concentration increasing in this range. However, from 5 to 7.5 wt.% there is only 50% increasing, and then was decreased by increasing of feed glycerol concentration at higher values. Thus, the maximum of  $\text{H}_2$  mole fraction and yield were found around 0.55 and 3.63 at 2.5 wt.% of feed glycerol concentration, respectively. The higher energy requirement is concerned as a key parameter to weight with the increasing in  $\text{H}_2$  production, after the economic analysis (not calculated here) was finished.

a



b



**Figure 7.3** (a) mole fractions of gas products (H<sub>2</sub>, CO<sub>2</sub>, CO, and CH<sub>4</sub>) (b) gas product yields as a function of feed glycerol concentration ( $T=798$  K,  $P=25$  MPa)

Note that H<sub>2</sub>, CO<sub>2</sub>, and CH<sub>4</sub> were main gaseous products from glycerol reforming in SCW process by thermodynamic analysis. However, the experimental studies might be different from this analysis as some catalysts would promote more CO and inhibit CH<sub>4</sub>, a lot of solid carbon probably occurred causing of failure system, etc. For highly CO content gaseous product, it has been known that it could not be used for a PEMFC application to avoid catalyst poisoning (CO < 10-50 ppm) (Authayanun et al., 2011). A water gas shift reactor is a necessary choice to be installed after the supercritical water reactor with the purpose of CO conversion to CO<sub>2</sub> (Equation (2.10)), also enhancement of H<sub>2</sub> content in gaseous product.

## 7.4 Conclusion

Glycerol reforming in supercritical water was calculated based on thermodynamic analysis. The Gibbs minimization was used to estimate the product compositions using PENG-ROB as the equation of state. The higher operating temperature, lower pressure, and lower glycerol feed concentration promoted

hydrogen production. Only H<sub>2</sub>, CO<sub>2</sub>, and CH<sub>4</sub> were found as the main components in this study. CO was almost inhibited at high pressure and offered less than 0.01 of mole fraction. Above 1048 K, only the slight changing of components was found by increasing of operating temperature causing methane suppression. However, pressure and the glycerol feed concentration performed as the similar affect to the product trends. Note that the suppression of methane totally enhanced hydrogen production causing of CO inhibition in supercritical water condition.



# **CHAPTER VIII**

## **HYDROGEN PRODUCTION FROM SUPERCRITICAL WATER REFORMING OF GLYCEROL IN EMPTY INCONEL 625 REACTOR**

After glycerol reforming from thermodynamic analysis was studied. In this chapter, glycerol reforming was investigated under supercritical water conditions (723-848 K, 25 MPa) in an Inconel 625 reactor without catalyst. An initial feed containing 5 wt.% of glycerol was continuously fed to the reactor at different feed rates (i.e. 1.05, 2.15, and 3.60 g/min). The effect of feed glycerol concentration (i.e. 2.5, 5, 7.5, and 10 wt.%) on glycerol conversion, yield of H<sub>2</sub> and product distributions was determined. Finally, comparison between supercritical water reforming and conventional steam reforming was also examined.

### **8.1 Introduction**

Without addition of a catalyst in supercritical water reforming, some studies have investigated the impact of reactor wall materials on the production of hydrogen rich gas. Yu et al. (1993) investigated supercritical water gasification of glucose in Inconel 625 and Hastelloy C276 tubular reactors. 0.1 M glucose was gasified at 873 K, 34.5 MPa and 30 s of residence time without carbon formation; however the results were far from thermochemical equilibrium. Gasification efficiency and yield highly depended on the reactor material and feed concentration of glucose. Inconel 625 reactor offered higher selectivity toward hydrogen due to the enhancement in water gas shift reaction, yielding a product gas rich in hydrogen and carbon dioxide; however, Hastelloy C276 reactor produced more carbon monoxide and only catalyzed the decomposition of acetic acid after the reactor wall was corroded by salt solution.

Buhler et al. (2002) reported that the reforming of glycerol at 622-748 K, 25-45 MPa, and residence time of 32-165 s in an empty horizontal tubular reactor (no report on the reactor's material was provided) yielded conversions between 0.4 and 31%. The main products included hydrogen, carbon dioxide, carbon monoxide, formaldehyde, methanol, acetaldehyde, propionaldehyde, ethanol, acrolein, and allyl alcohol. They proposed two pathways, one consisting of ionic reactions (higher pressures and/or lower temperatures) and a second one involving free radical degradation (lower pressures and/or higher temperatures). Arita et al. (2003) reported that the addition of copper wire promoted ethanol reforming in supercritical water. A stainless steel (SUS 316) reactor exhibited small catalytic activity at 723 K, compared to a non-catalytic quartz reactor. Boukis et al. (2003a) reported that Inconel 625 was a promising alloy in supercritical water applications mostly due to its resistance to high temperature and corrosion. Boukis et al. (2003b) investigated supercritical water gasification of methanol in a tubular Inconel 625 reactor at 673-873 K, 25-45 MPa without catalyst. Conversion of 99.9% was reported, yielding a hydrogen rich gas (up to 75 vol.%) with small fractions of carbon monoxide, carbon dioxide, and methane. Residence times as low as 4 s was enough to achieve high conversion; however, higher reaction temperature (873 K) would be necessary. Gadhe et al. (2007) carried out methanol supercritical water reforming in a tubular Inconel 600 reactor at 973 K, 27.6 MPa by focusing on suppression of methane formation. The favorable conditions were low residence time, and high feed methanol concentration. Therdthianwong et al. (2011a) conducted supercritical water reforming of bioethanol without catalyst in an Inconel 625 reactor. Only 23.9% of ethanol conversion was obtained at 773 K, 25 MPa and water/ethanol ratio of 20. The main products included hydrogen, carbon monoxide, carbon dioxide, and methane. Bennekom et al. (2011) performed glycerol reforming at supercritical water conditions (723, 923 K, residence times of 6-173 s, and 3-20 wt.% of glycerol in feed) in an Incoloy 825 reactor. The results showed that gasification efficiency increased with the operating temperature and residence time but it was nearly independent of the feed concentration. They proposed that hydrogen, carbon monoxide, methane, ethylene, and propylene were the primary gas products. The remaining products, including carbon dioxide and propane, were formed due to secondary gas phase reactions. In the case of catalytic supercritical water reforming,

Guo et al. (2010) distinguished 2 types of catalysts: 1) homogeneous catalyst (alkali metals:  $\text{Na}_2\text{CO}_3$ ,  $\text{KHCO}_3$ ,  $\text{K}_2\text{CO}_3$ ,  $\text{NaOH}$ , etc.) which is favorable to water gas shift reaction, and 2) heterogeneous catalyst (metal catalyst: Ni, Ru, Pt, Pd Rh, Ir, etc., and activated carbon catalyst) which offers several advantages such as high selectivity, recyclability and being environmentally friendly.

## 8.2 Material and methods

Material and methods were described in Chapter IV Experimental and procedure of glycerol reforming in supercritical water. The schematic of supercritical water diagram was shown in Figure 4.1.

Three levels of feed rates including low feed rate (1.05 g/min), medium feed rate (2.15 g/min), and high feed rate (3.60 g/min) were considered. As the feed glycerol concentration was about 5 wt.%, it was assumed that the fluid density can be approximated by that of pure water. Wagner and Kruse (1998), May et al. (2010), and Bennekom et al. (2011) calculated the residence time using Equation (8.1).  $V_R$  is the volume of reactor,  $\phi$  is the void fraction of bed (=1 for empty reactor),  $\rho_R$  is the density of pure water at the reactor conditions of  $P$  and  $T$ ,  $m_0$  is the mass flow rate of the mixture to the reactor.

$$\tau = \frac{V_R \cdot \phi \cdot \rho_R}{m_0} \times 60 \quad (8.1)$$

From Equation (1), residence time depends on the density of pure water, and then it implies that residence time is dependent on the operating temperature. With operating temperature between 723-848 K, the residence times for low, medium and high feed rates are in the range of 39-60 s, 19-30 s and 11-18 s, respectively.

The conversion of glycerol (Equation (8.2)), concentration in gas phase (Equation (8.3)), yield of  $\text{H}_2$  (Equation (8.4)), and yield of carbon containing species  $i$  (Equation (8.5)) are defined as follows.

$$X_{\text{Glycerol}} = \frac{F_{\text{Glycerol,in}} - F_{\text{Glycerol,out}}}{F_{\text{Glycerol,in}}} \quad (8.2)$$

$$\text{Concentration in gas phase of species } i \text{ (mol\%)} = \frac{F_{i,\text{gas}}}{\sum_n F_{i,\text{gas}}} \times 100 \quad (8.3)$$

$$\text{Yield of H}_2 = \frac{F_{\text{H}_2}}{F_{\text{Glycerol,in}}} \quad (8.4)$$

$$\text{Yield of carbon containing species } i = \frac{F_i}{F_{\text{Glycerol,in}}} \times \frac{\text{number of carbon atom in molecule}}{3} \quad (8.5)$$

Where  $F_{\text{Glycerol,in}}$  and  $F_{\text{Glycerol,out}}$  are the inlet and outlet glycerol molar flow rates, respectively, and  $F_i$  is the molar flow rate of species  $i$ .

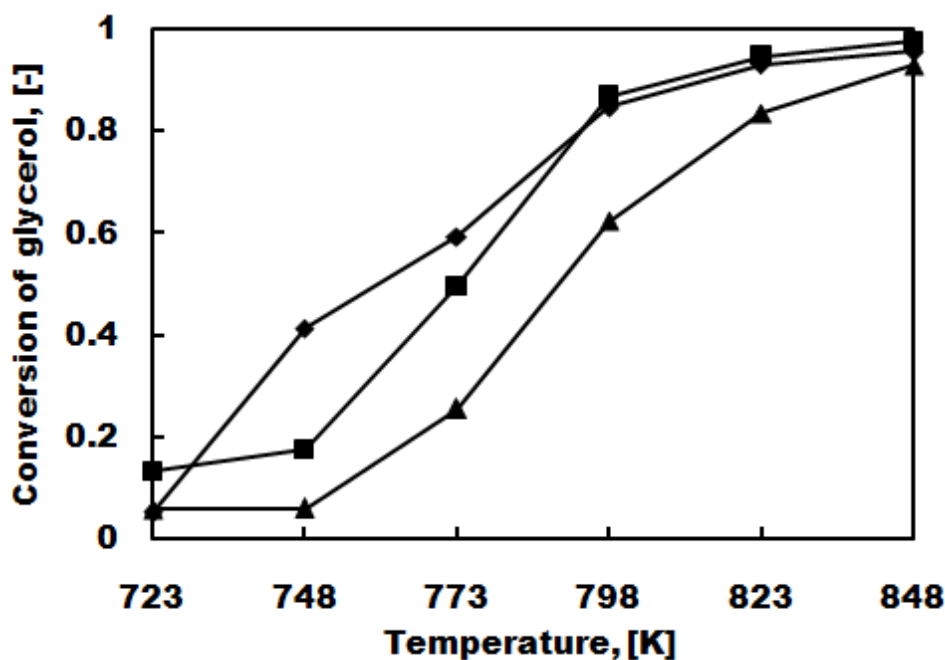
## 8.3 Results and discussion

### 8.3.1 Effect of feed rate and operating temperature

Glycerol conversion is highly dependent on the operating temperature as shown in Figure 8.1. The glycerol conversion at 723 K for all feed rates was less than 0.15. In the temperature range of 748-798 K, increasing the operating temperature linearly increased the glycerol conversion. The low feed rate (high residence time) showed the highest conversion along this temperature range.

At 798-848 K, the low and medium feed rates show the similar trends of glycerol conversion. No significant difference in conversions was observed. The results are in good agreement with Taylor et al. (2003) who conducted the methanol supercritical water reforming in an Inconel 625 reactor. They reported that lower feed rate offered the higher conversion in the temperature range of 823-923 K, and then the conversion of both feed rates became the similar values at the temperature above 923 K. However in this work, carbon formation was pronounced at low and medium feed rates and high operating temperatures - this will be discussed later. Therefore, the

medium feed rate became the most suitable feed rate to reach the highest glycerol conversion; nearly complete conversion was achieved especially at 823 K (0.95) without carbon formation.



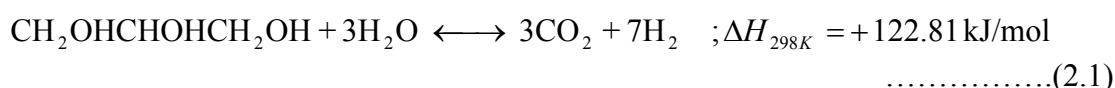
**Figure 8.1** Glycerol conversion at different feed rates and operating temperatures ( $P = 25$  MPa, 5 wt.% of feed glycerol concentration) —◆— Low feed rate (1.05 g/min), —■— Medium feed rate (2.15 g/min), —▲— High feed rate (3.60 g/min).

Figures 8.2a-c show the composition of gas products including  $H_2$ ,  $CO$ ,  $CH_4$ , and  $CO_2$  in cases of low, medium and high feed rates, respectively. Similar trends are observed for all feed rates. It is clear that  $H_2$  is the main component in the gas product with a composition as high as 64 mol%. Theoretically, 70 mol% and 30 mol% of  $H_2$  and  $CO_2$  can be obtained from complete glycerol steam reforming (Equation (2.1)). The concentration of  $H_2$  slightly decreased when the temperature changed from 723 to 798 K but then slightly increased when the temperature increased from 798 to 848 K. Clearly, the total flow rate and  $H_2$  flow rate increased when increasing operating temperature and feed rate. This corresponds to the trend for glycerol conversion shown in Figure 8.1. Increasing the operating temperature increased  $CO$  content in the gas phase until 798 K but subsequently decreased when the temperature was higher

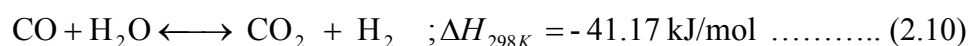
than 798 K. The concentration in the gas phase of CO<sub>2</sub> was the opposite to that of CO. The high content of CO and the decrease in CO mole fraction at high temperature were reported by Lee et al. (2002) who studied supercritical water gasification of glucose in a Hastelloy C276 reactor without catalyst. Water gas shift reaction (WGS, Equation (2.10)) would explain the changing of H<sub>2</sub>, CO, and CO<sub>2</sub> content in gas phase. At the operating temperature higher than 798 K, increasing of H<sub>2</sub> and CO<sub>2</sub>, and decreasing of CO concentrations was observed, indicating that WGS reaction starts to play important role at operating temperature higher than 798 K. It was called a “fast type water gas shift reaction” occurred in this operating temperature range. Holgate et al. (1995) and Lee et al. (2002) reported this type of WGS above the temperature of 848 K and 823 K in supercritical water gasification of glucose. From Figures 8.2a-c, CH<sub>4</sub> is another main gaseous product whose amount was not over 6 mol% in the temperature range of 723-848 K. It slightly increased with increasing operating temperature. For other gas product distributions, all of their concentrations were lower than 3.1 mol% with C<sub>2</sub>H<sub>6</sub> as a main byproduct especially at higher operating temperatures. C<sub>2</sub>H<sub>4</sub>, C<sub>3</sub>H<sub>8</sub>, and C<sub>3</sub>H<sub>6</sub> were not significantly changed when compared to C<sub>2</sub>H<sub>6</sub>. However, the influence becomes more pronounced at lower operating temperature and higher feed rate as shown in Figures 8.2a-c.

Considering the product yields, Figure 8.3a shows that the yield of H<sub>2</sub> increased with increasing operating temperature corresponding to the endothermic steam reforming (Equation (2.1)). Over 773 K, the medium feed rate seems to offer a suitable residence time for enhancing hydrogen production until 848 K. H<sub>2</sub> yield of 0.03 at 723 K continuously increased to reach 3.34 at 848 K (theoretical maximum yield is 7 as per Equation (2.1)).

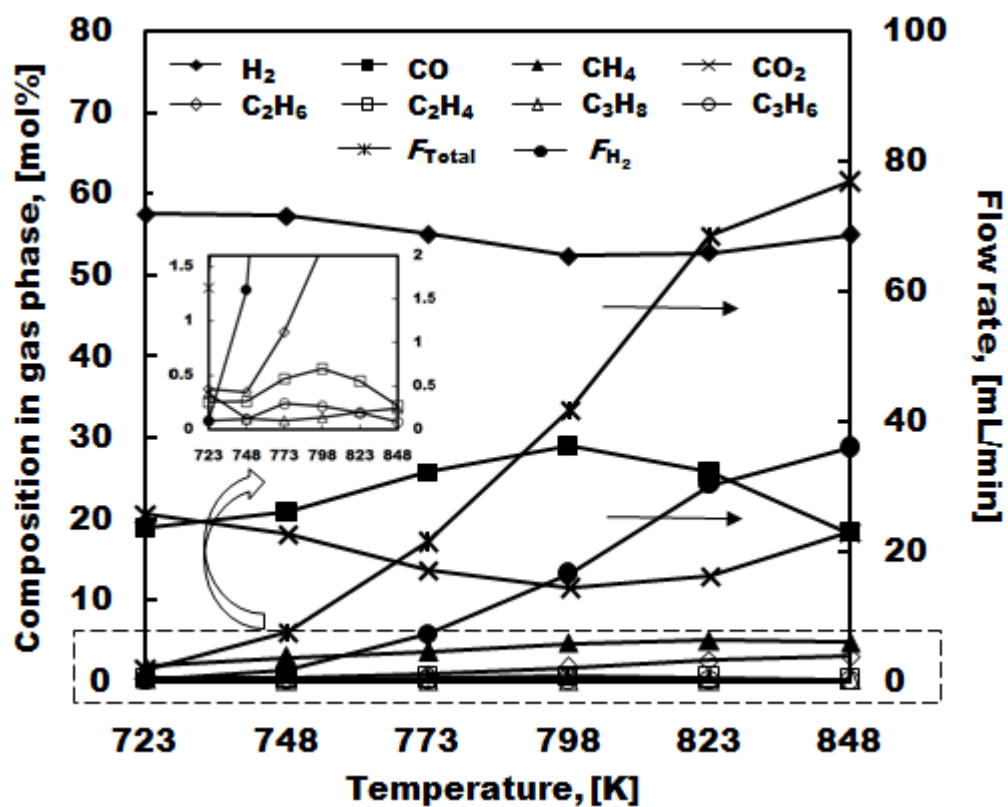
The overall reaction of glycerol Steam Reforming (SR):



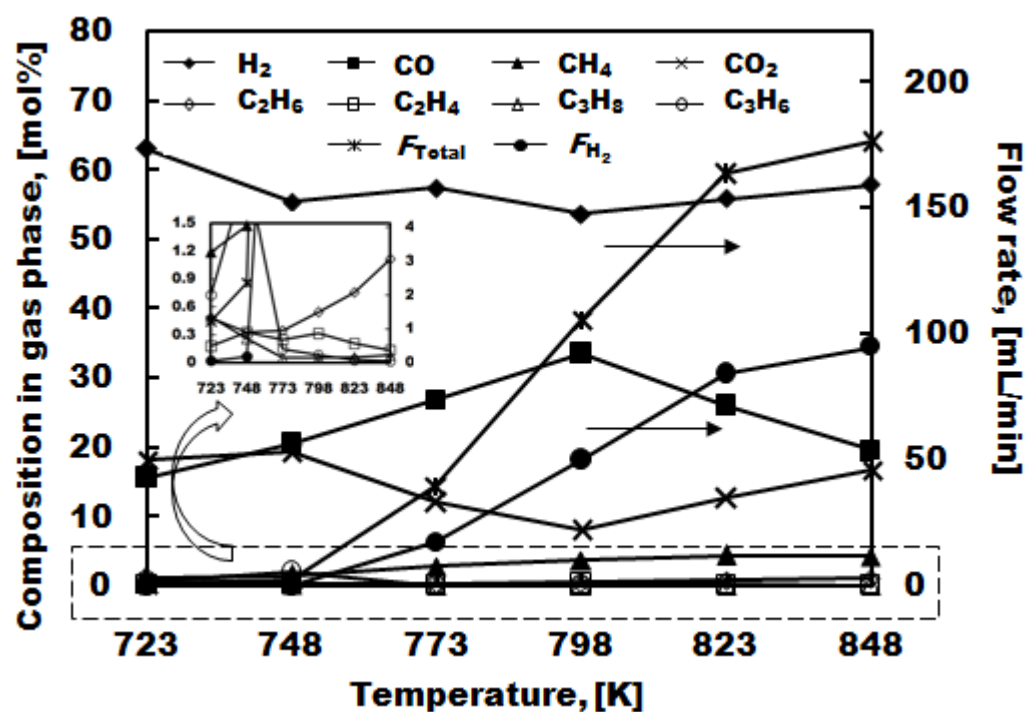
Water Gas Shift (WGR or reverse of this is called RWGS):

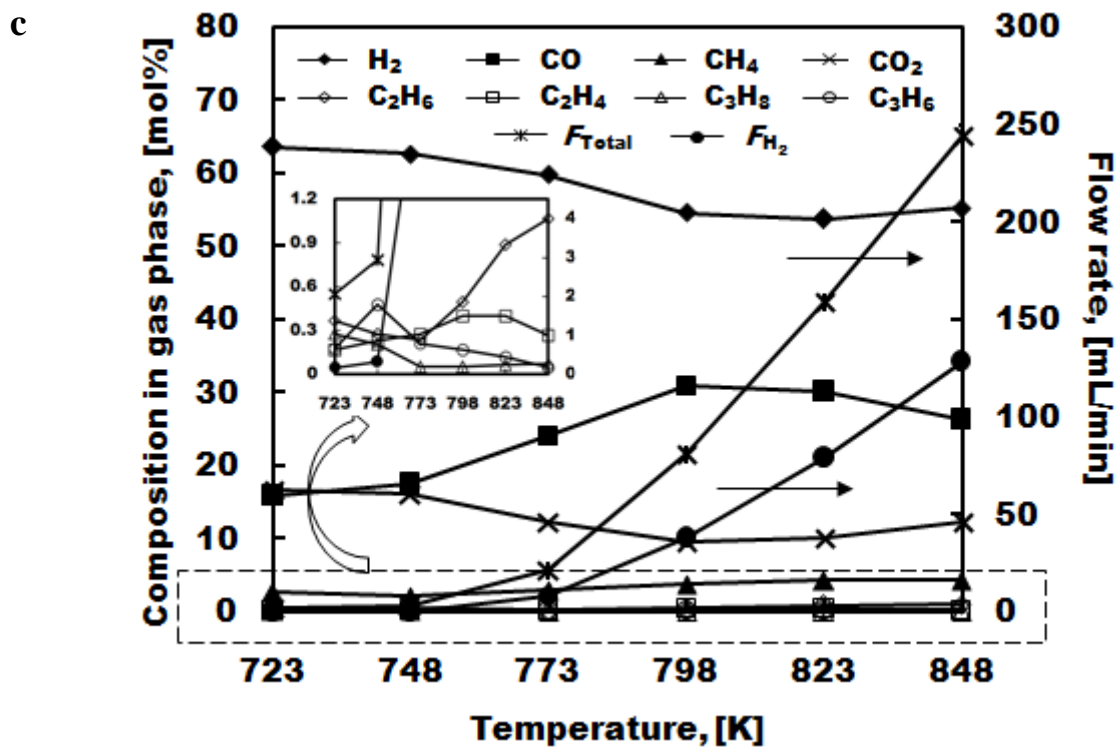


a

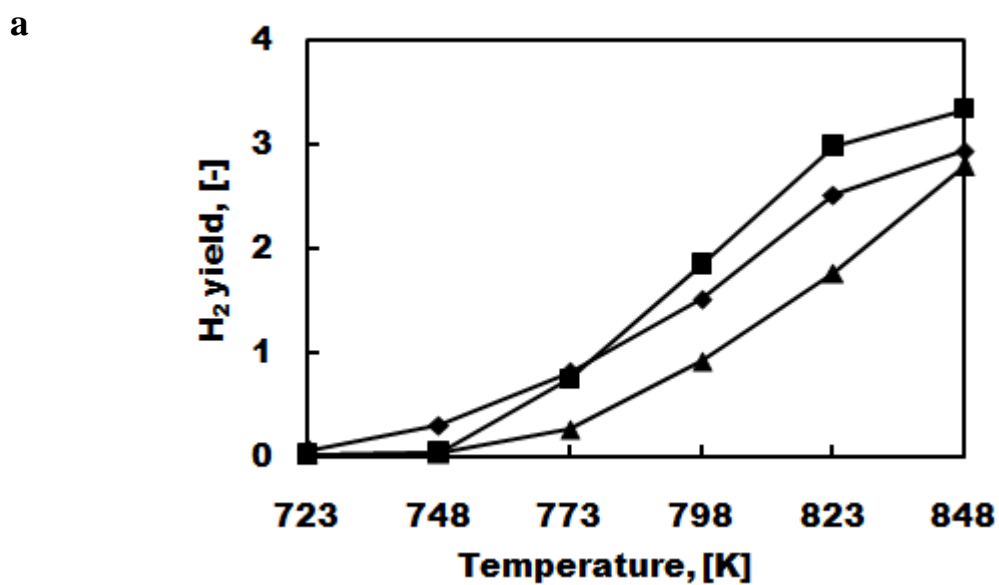


b



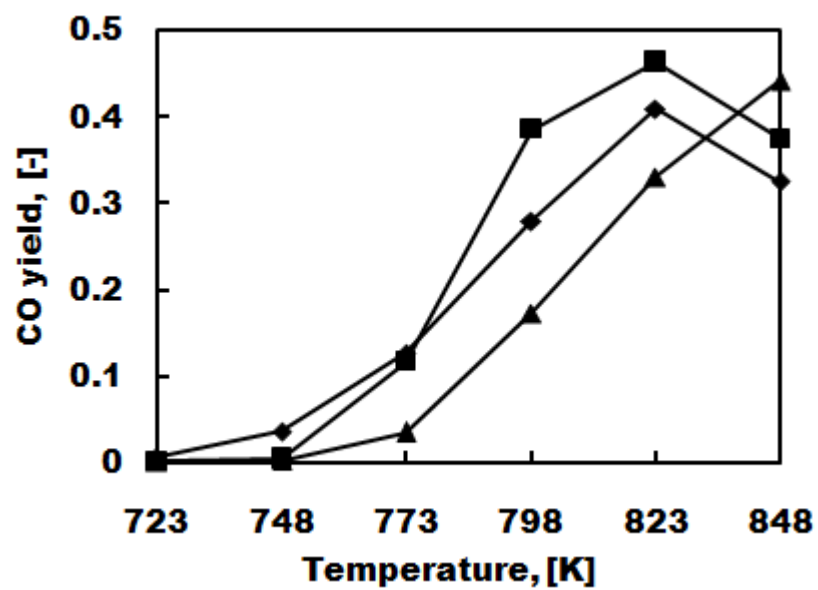


**Figure 8.2** Compositions and flow rate of gas products ( $\text{H}_2$ ,  $\text{CO}$ ,  $\text{CO}_2$ , and  $\text{CH}_4$ ) function of operating temperature (a) feed rate=1.05 g/min, (b) feed rate=2.15 g/min, (c) feed rate=3.60 g/min ( $P = 25$  MPa, 5 wt.% of feed glycerol concentration)

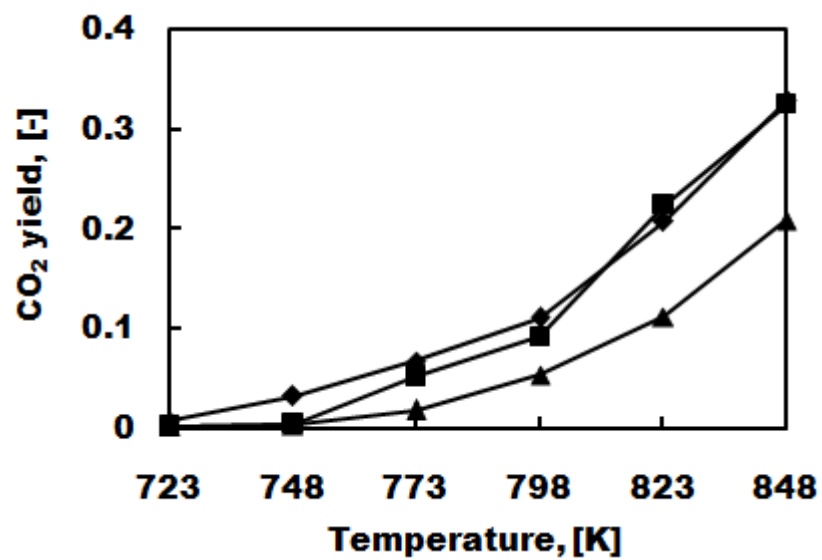




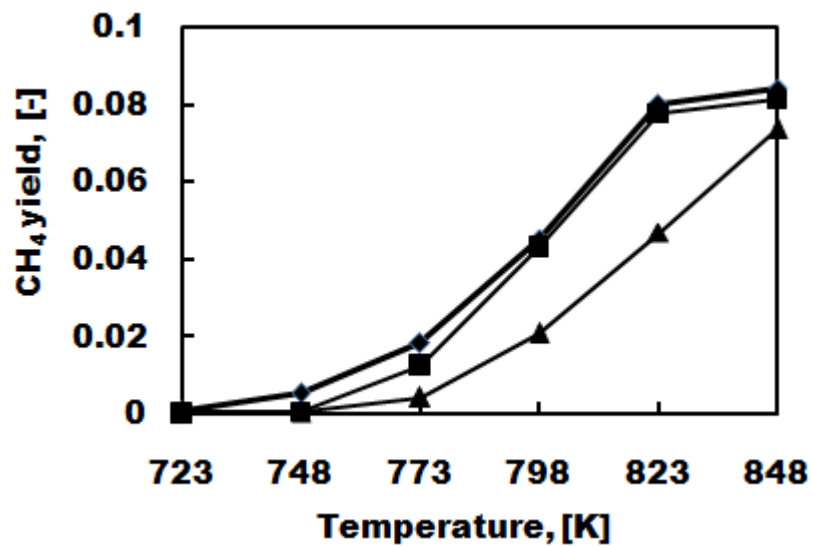
b



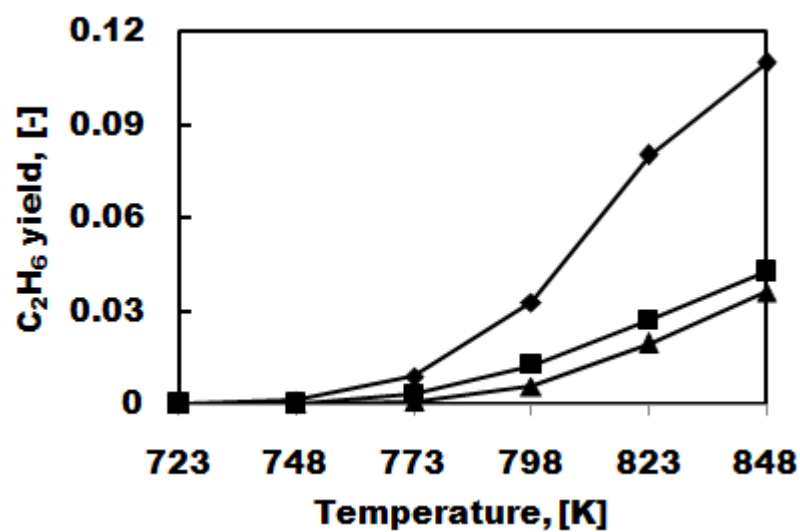
c



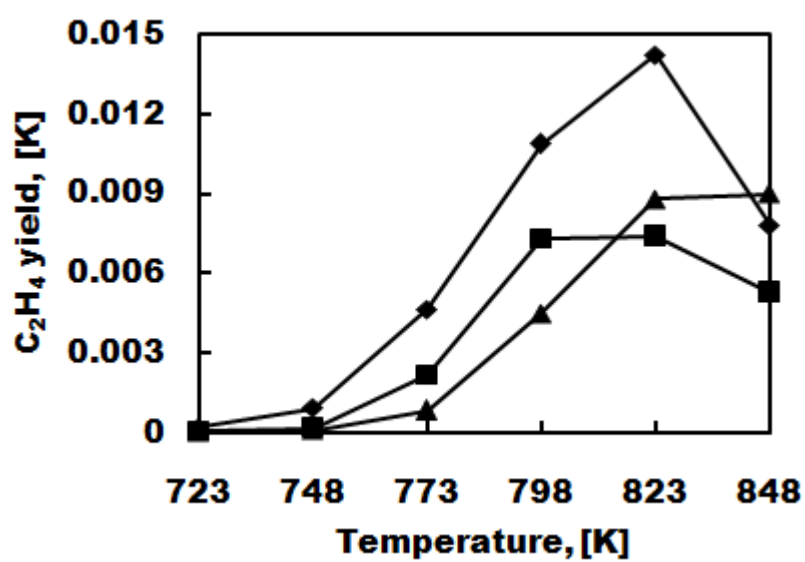
d



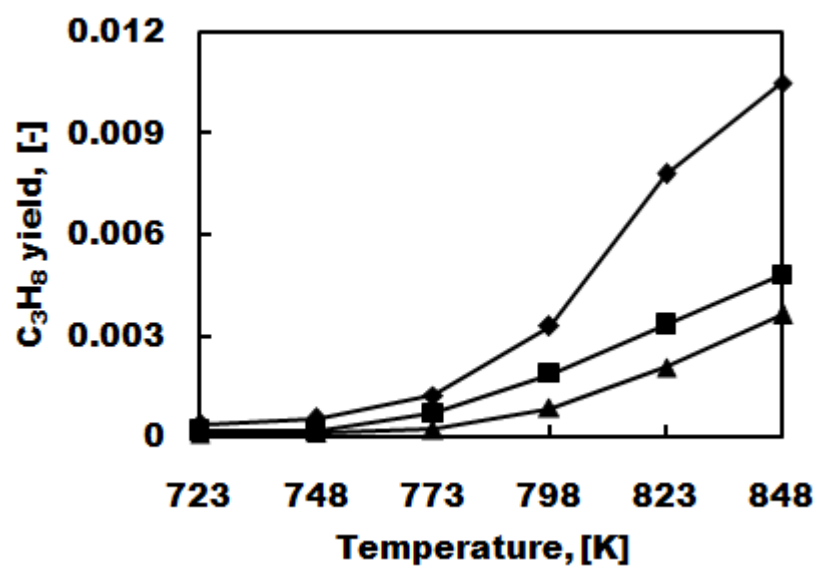
e

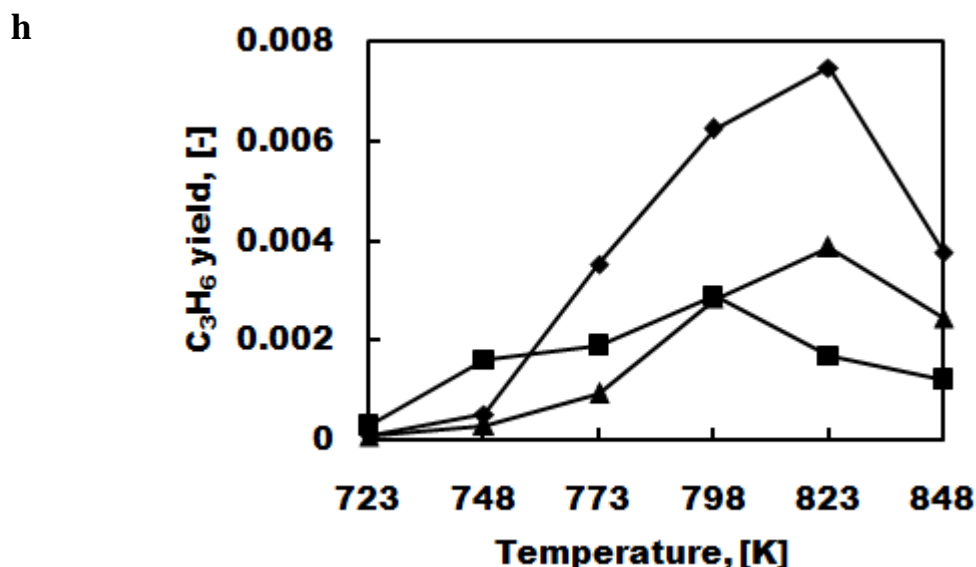


f



g



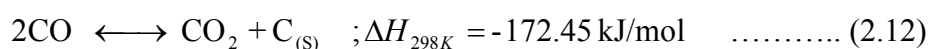


**Figure 8.3** Gas yields of (a) H<sub>2</sub>, (b) CO, (c) CO<sub>2</sub>, (d) CH<sub>4</sub>, (e) C<sub>2</sub>H<sub>6</sub>, (f) C<sub>2</sub>H<sub>4</sub>, (g) C<sub>3</sub>H<sub>8</sub>, (h) C<sub>3</sub>H<sub>6</sub> at different feed rates and operating temperatures ( $P=25$  MPa, 5 wt.% of feed glycerol concentration) —◆— Low feed rate (1.05 g/min), —■— Medium feed rate (2.15 g/min), —▲— High feed rate (3.60 g/min)

Yields of CO, CO<sub>2</sub>, CH<sub>4</sub>, C<sub>2</sub>H<sub>6</sub>, C<sub>2</sub>H<sub>4</sub>, C<sub>3</sub>H<sub>8</sub>, and C<sub>3</sub>H<sub>6</sub> were also increased by increasing operating temperatures as shown in Figures 8.3b-h. The main reason was that the higher operating temperatures promoted more products in the gas phase because of the increase in glycerol conversion. Buhler et al. (2002) and Benenekom et al. (2011) stated that free radical pathways were favored at higher operating temperature which promoted more gaseous products. However, yields of CO, C<sub>2</sub>H<sub>4</sub>, and C<sub>3</sub>H<sub>6</sub> decreased when increasing operating temperature between 823 and 848 K. It should be noted that problems were encountered with low feed rate at high temperature (i.e. 823-848 K) and medium feed rate at 848 K by uncontrollable pressure fluctuation at the back pressure regulator because of the solid plugging the bottom screen. The plugging was likely due to tar or coking. It implies that too high operating temperature caused failure in operation especially in the low and medium feed rate cases. It can be concluded that the medium feed rate offers suitable residence times for operating temperature between 798 (23 s) and 823 (21 s) K. The problem of carbon formation can be explained by Boudouard and cracking reactions. It was

probably caused by the promotion of Boudouard reaction (Equation (2.12)) as observed by the decrease in CO (Figure 8.3b) and increase in CO<sub>2</sub> (Figure 8.3c). It could also be caused by the endothermic methane cracking (Equation (2.13)) as observed by slight increase in CH<sub>4</sub> yield at low and medium feed rates (Figure 8.3d). Other previous works also suggested that C<sub>2</sub>H<sub>4</sub> was a precursor of carbon formation (Equation (2.16)) (Tuan, 2009; Therdthianwong et al., 2011a).

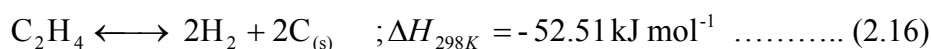
Boudouard reaction:



Methane cracking:



C<sub>2</sub>H<sub>4</sub> cracking:

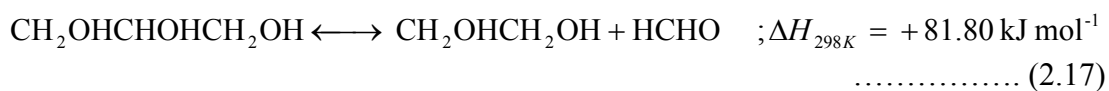


It was observed that the decrease of C<sub>2</sub>H<sub>4</sub> occurred at 575°C for the low and medium feed rates in Figure 8.3f. The results agreed with Therdthianwong et al. (2011a) who found that carbon formation occurred at low H<sub>2</sub>O to feedstock (ethanol) ratio and/or high operating temperature ( $\geq 823 \text{ K}$ ) for a reaction in Inconel 625 reactor.

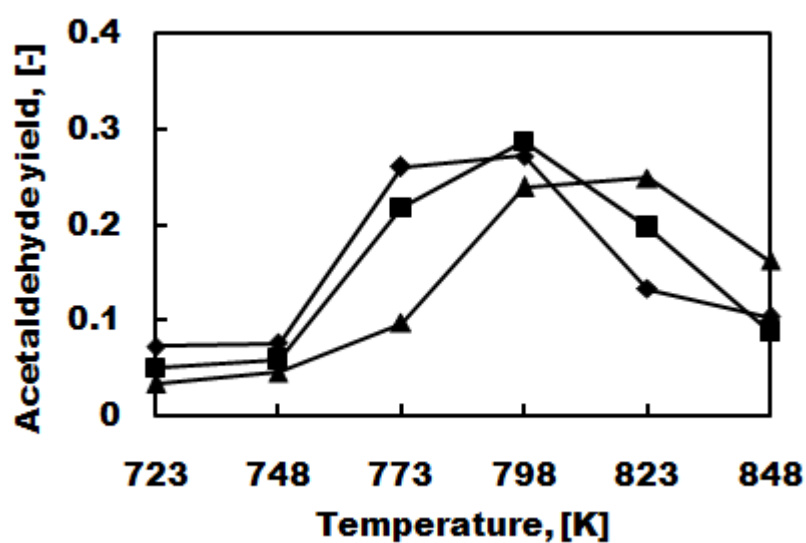
Analysis of liquid product distributions revealed a variety of components including acetaldehyde (CH<sub>3</sub>CHO), acetol (CH<sub>3</sub>COCH<sub>2</sub>OH), methanol (CH<sub>3</sub>OH), acetic acid (CH<sub>3</sub>COOH), propionaldehyde (CH<sub>3</sub>CH<sub>2</sub>CHO), and allyl alcohol (CH<sub>2</sub>CHCH<sub>2</sub>OH) as shown in Figure 8.4a-f. However, the product yields for acetone (CH<sub>3</sub>COCH<sub>3</sub>), acrolein (CH<sub>2</sub>CHCHO), ethanol (CH<sub>3</sub>CH<sub>2</sub>OH), ethylene glycol (CH<sub>2</sub>OHCH<sub>2</sub>OH), and acrylic acid (CH<sub>2</sub>CHCOOH) were less than 0.01, which can be considered negligible. All the components detected correspond to those found by Buhler et al. (2002) and May et al. (2010) except ethylene glycol that was not reported in their product distributions. It might be due to its too low concentration and/or the difference in operating parameters i.e. 622-748 K with the empty reactor

(Buhler et al., 2002), and 350 bars with 1%Ru/Al<sub>2</sub>O<sub>3</sub> (May et al., 2010). However, ethylene glycol was observed as a product via the fragmentation reaction (Equation (2.17)) as reported by Xu et al. (2009).

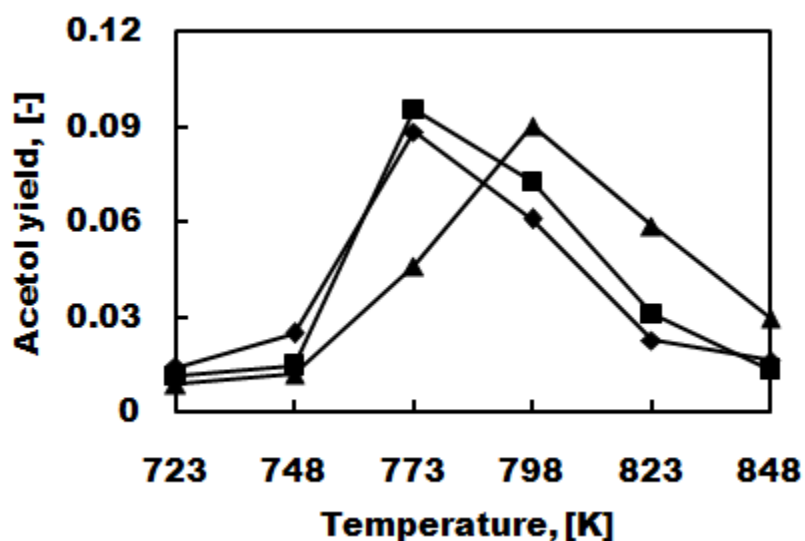
Fragmentation reaction of glycerol



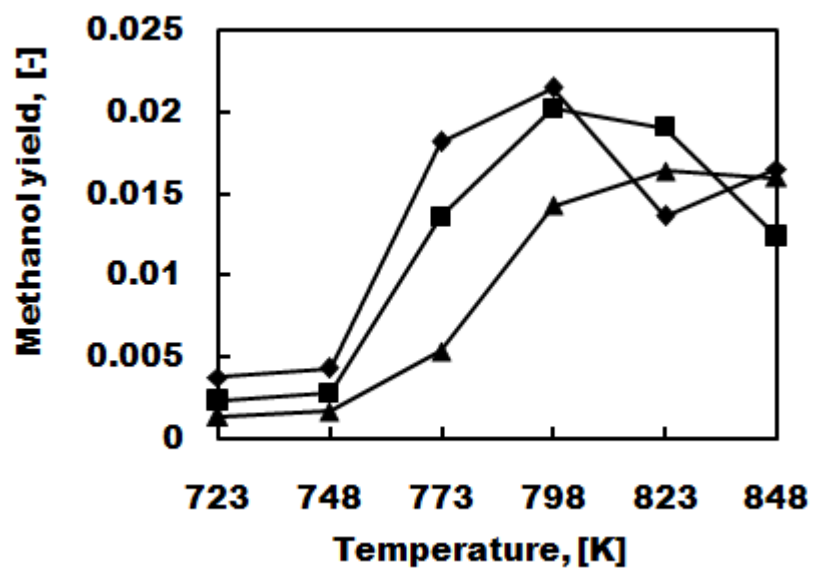
a



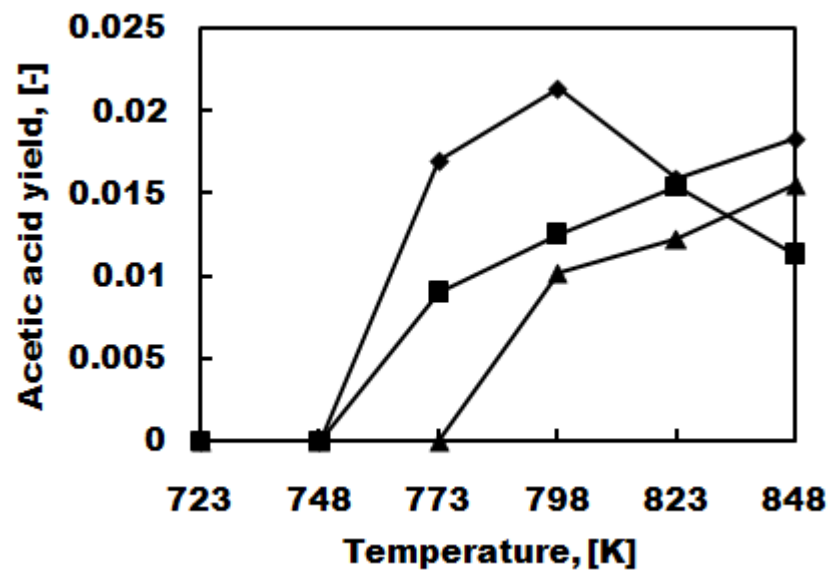
b



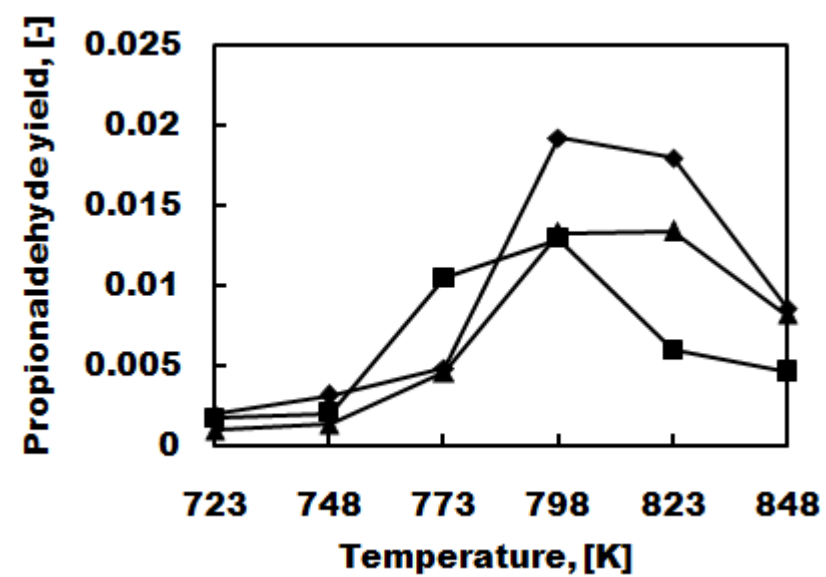
c



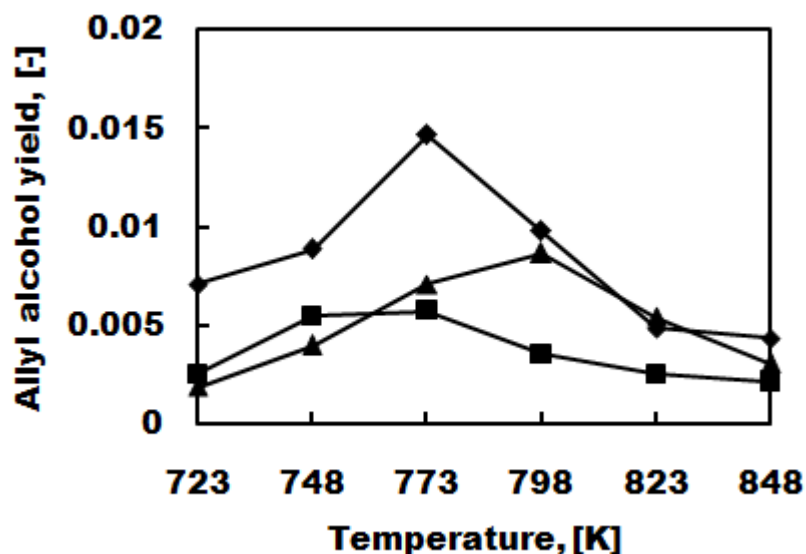
d



e



f



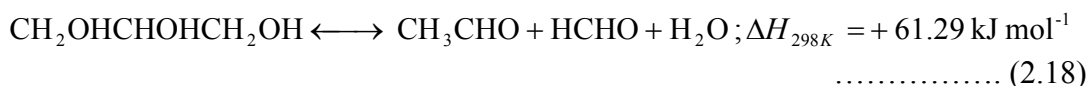
**Figure 8.4** Liquid yields of (a) acetaldehyde (b) acetol (c) methanol (d) acetic acid (e) propionaldehyde (f) allyl alcohol at different values of feed rate and operating temperature ( $P = 25$  MPa, 5 wt.% of feed glycerol concentration) —◆— Low feed rate (1.05 g/min), —■— Medium feed rate (2.15 g/min), —▲— High feed rate (3.60 g/min).

As shown in Figure 8.4a-f, it was observed that the liquid product yields initially increased with increasing operating temperature, and then became constant or decreased at high operating temperatures. Low glycerol conversion at low operating temperature resulted in low liquid product yields as well as low gas product yields as discussed previously. At higher operating temperatures (798-848 K), the reduction in liquid product yields was observed as they could be further reacted to gas products.

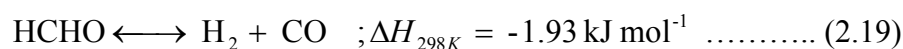
Acetaldehyde is the main liquid product with a yield up to 0.29 (medium feed rate) at 848 K by Equation (2.18) (Antal et al., 1985; Ramayya et al., 1987; Buhler et al., 2002), and then drastically decreased by about 70% (0.09) at operating temperatures approaching to 848 K. However, formaldehyde was also formed in this reaction, but could be subsequently reacted to  $H_2$ , CO, and  $CO_2$  by Equations (2.19) (Bröll et al., 1999; Xu et al., 2009; May et al., 2010), and (2.10) (Utaka et al., 2003), resulting in no formaldehyde in the gas and liquid phases. Decrease in acetaldehyde could be explained by its partial reaction with water and decomposition to gas

products in the 798-848 K temperature range, as shown by Equations (2.20) and (2.21) (Therdthianwong et al., 2011b).

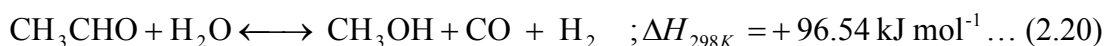
Decomposition of glycerol:



Decomposition of formaldehyde:



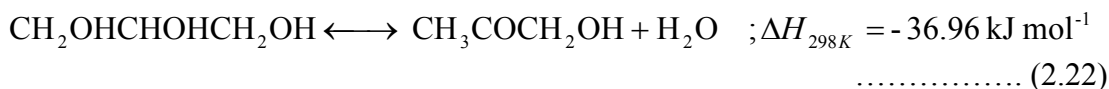
Acetaldehyde steam reforming:



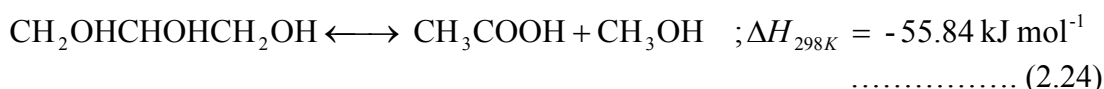
Methanol steam reforming:



Dehydration of glycerol:



Decomposition of glycerol:



Minor liquid products including acetol, methanol, and acetic acid were detected with maximum yields of around 0.10, 0.02, and 0.02, respectively. Acetol, normally formed by the dehydration of glycerol (Equation (2.22)) (Chiu et al., 2006; May et al., 2010), reached a maximum around 773-798 K and then dramatically decreased when increasing the operating temperature (Figure 8.4b). Methanol probably arose from the partial steam reforming reaction of acetaldehyde (Equation (2.20)) (Therdthianwong et al., 2011b) and/or from the decomposition of glycerol (Equation (2.24)) (Luo et al., 2008). The highest yield of methanol was obtained

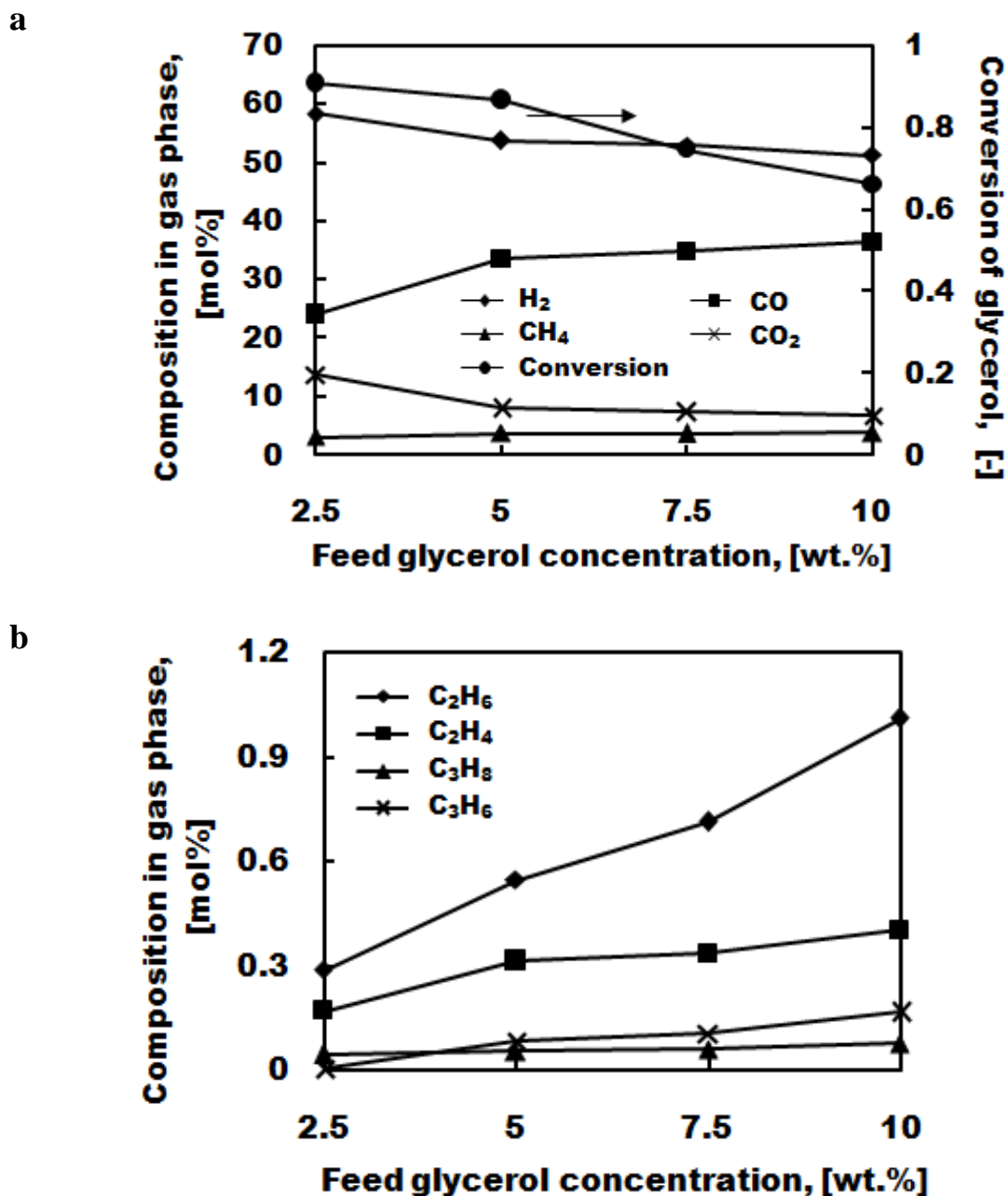


around 798 K (Figure 8.4c). Moreover, acetic acid was also formed as a product from Equation (2.24); however, it was totally suppressed at low operating temperatures (450-475°C) (Figure 8.4d). Luo et al. (2008) proposed a reaction pathway of acetic acid formation by reforming glycerol to  $\bullet\text{CH}_2\text{-OH}$  and  $\bullet\text{CH-OH-CH}_2\text{OH}$  (rearrangement with dehydrogenation) intermediates by C-C cleavage. Propionaldehyde, and allyl alcohol were also detected in our study with yields of less than 0.02. May et al. (2010) proposed that their formations occurred from the similar  $\bullet\text{CH}_2\text{-CHOH-CH}_2\text{OH}$  intermediate. The dependence of the product distribution on operating temperature has been known by the differences in activation energies, and as well as the density dependence of the reaction pathways (Buhler et al., 2002).

### 8.3.2 Effect of feed glycerol concentration

The optimum feed rate which offers the maximum  $\text{H}_2$  yield from the previous section was 2.15 g/min (medium feed rate). At 798-848 K, conversion of glycerol was slightly increased as shown in Figure 8.1. Thus 798 K was chosen for further study in this section as it has the lowest energy requirement and no carbon formation.

Figures 8.5a-b show the effect of feed glycerol concentration (2.5, 5, 7.5, and 10 wt.%) at 798 K and 250 bar on glycerol conversion and compositions of gas products. Conversion of glycerol was substantially decreased by increasing of feed glycerol concentration as shown in Figure 8.5a. It was explained that because higher feed glycerol concentration had more glycerol molecules per unit volume, it formed more gas product molecules in the fluid stream, resulting in reduction of the residence time (Taylor et al, 2003) and consequently decreasing the glycerol conversion



**Figure 8.5** (a) Conversion of glycerol, compositions of gas products (H<sub>2</sub>, CO, CO<sub>2</sub>, and CH<sub>4</sub>), (b) Compositions of gas products (C<sub>2</sub>H<sub>6</sub>, C<sub>2</sub>H<sub>4</sub>, C<sub>3</sub>H<sub>8</sub>, and C<sub>3</sub>H<sub>6</sub>) as a function of feed glycerol concentration (medium feed rate of 2.15 g/min,  $P = 25$  MPa,  $T = 798$  K).

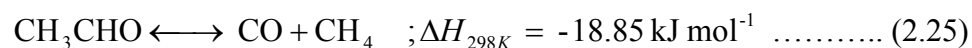
Increasing the feed glycerol concentration from 2.5 to 5 wt.% decreased H<sub>2</sub> and CO<sub>2</sub> concentrations but increased CO concentration, following the thermodynamics of reverse water gas shift reaction (RWGS, Equation (2.10)).

However, for 5-10 wt%, compositions in gas phase of H<sub>2</sub>, CO and CO<sub>2</sub> were slightly changed with a similar trend as the RWGS influence. Feed glycerol concentrations from 2.5, 5.0, 7.5, 10.0 wt.% represent water to glycerol molar ratios of 199.37, 97.13, 63.05, and 46.01, respectively. Boukis et al. (2006) stated that the higher water content in methanol supercritical water reforming without addition of a catalyst (Inconel 625 reactor) promoted the WGS reaction (Equation (2.10)). Another reason was the residence time; CO was produced at shorter residence time (higher feed glycerol concentration), and then subsequently converted to CO<sub>2</sub> and H<sub>2</sub> at longer residence time (lower feed glycerol concentration), according to the trend of H<sub>2</sub>, CO<sub>2</sub>, and CO (Taylor et al., 2003). Other gas products concentration, including C<sub>2</sub>H<sub>6</sub>, C<sub>2</sub>H<sub>4</sub>, C<sub>3</sub>H<sub>8</sub>, and C<sub>3</sub>H<sub>6</sub> increased with increasing feed glycerol concentration. This might be due to the fact that increasing feed glycerol concentration (decreasing molar water to glycerol ratio) reduces the reforming of carbon intermediates to light gaseous products (H<sub>2</sub>, CO, CO<sub>2</sub>, and CH<sub>4</sub>) and also reduces the residence time in the reactor, thus the conversion of carbon intermediates are decreased; however, the maximum C<sub>2</sub>-C<sub>3</sub> hydrocarbons were observed as C<sub>2</sub>H<sub>6</sub> for only 1.01% as a maximum value as shown in Figure 8.5b. A similar behavior was reported in the supercritical water from bioethanol reforming as WGS and the reforming of carbon intermediates were enhanced by higher water to organic molar ratios (Therdthianwong et al., 2011a).

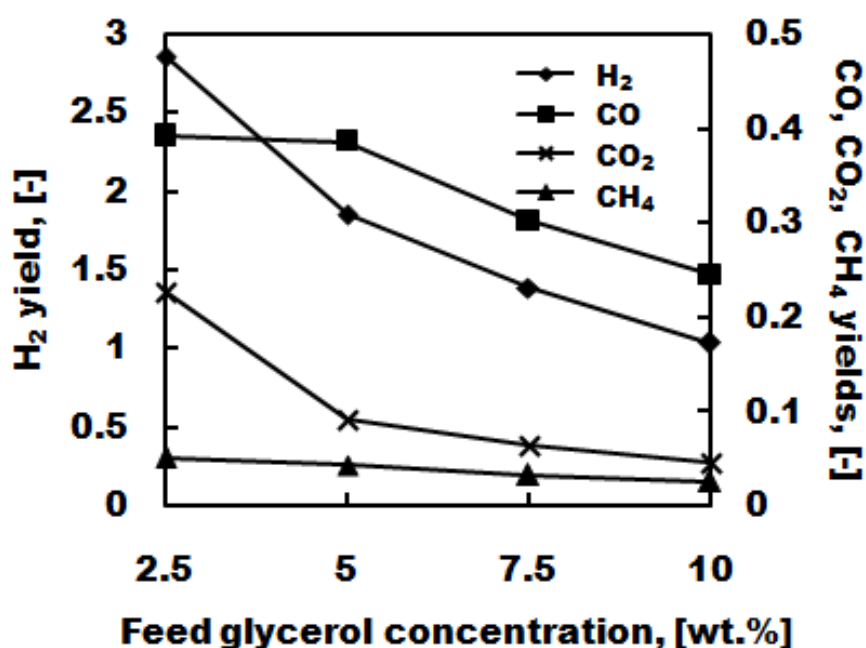
It was seen that a decrease in glycerol conversion lowered all major gas product yields. Since glycerol conversion decreases when increasing feed glycerol concentration, it is not surprising that this is also accompanied by a decrease in the main gas product yields, including H<sub>2</sub>, CO, CO<sub>2</sub>, and CH<sub>4</sub> as shown in Figure 8.6a. For example, the H<sub>2</sub> yield decreased from 2.86 to 1.04 when the feed glycerol concentration increased from 2.5 to 10 wt.%. The similar behavior was observed in some of previous works (Boukis et al., 2003b; Taylor et al., 2003; Byrd et al., 2008; Therdthianwong et al., 2011a). The CO yield decreased with the increasing feed glycerol concentration, following to the decreased glycerol conversion. However, the CO yield became constant during 2.5-5 wt.%. This might be due to the RWGS reaction (Equation (2.10)), and/or acetaldehyde steam reforming (Equation (2.20)), and/or the decomposition of acetaldehyde (Equation (2.25)), which produced more

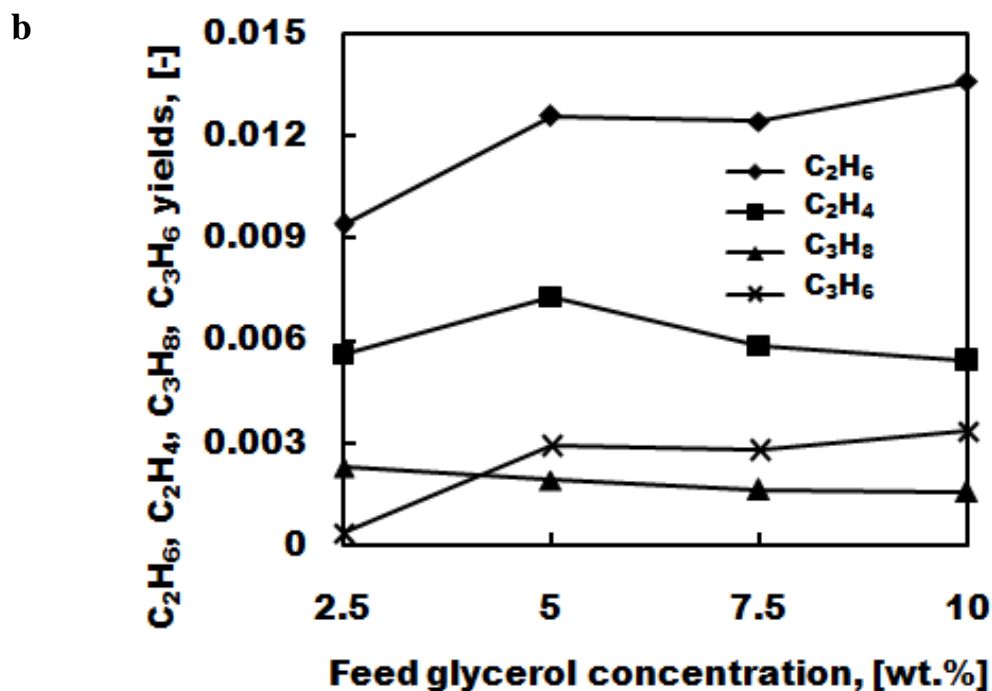
CO at higher feed glycerol concentration. CH<sub>4</sub> yield was very low and consistent with the increasing feed glycerol concentration in this process, indicating that methane formation was kinetically limited (against thermodynamic result) in the Inconel 625 reactor (Taylor et al., 2003). Gas yield was also confirmed by the measurement of volumetric gas flow rate as shown in Table 8.1 and which indicates that an increase in feed glycerol concentration significantly decreased the product gas yield. For C<sub>2</sub>H<sub>6</sub>, C<sub>2</sub>H<sub>4</sub>, C<sub>3</sub>H<sub>8</sub>, and C<sub>3</sub>H<sub>6</sub> yields, they were observed to be less than 0.02 as shown in Figure 8.6b.

Decomposition of acetaldehyde:



a





**Figure 8.6** Gas yields of (a) H<sub>2</sub>, CO, CO<sub>2</sub>, and CH<sub>4</sub>, (b) C<sub>2</sub>H<sub>6</sub>, C<sub>2</sub>H<sub>4</sub>, C<sub>3</sub>H<sub>8</sub>, and C<sub>3</sub>H<sub>6</sub> as a function of feed glycerol concentration (medium feed rate of 2.15 g/min,  $P = 25$  MPa,  $T = 798$  K).

**Table 8.1** Total gas products flow rate as a function of feed glycerol concentration (medium feed rate of 2.15 g/min,  $P = 25$  MPa,  $T = 798$  K)

Feed glycerol concentration (wt.%)	Total gas products flow rate (L/mol of glycerol fed)
2.5	121.3
5.0	85.6
7.5	64.8
10.0	50.1

**Table 8.2** Liquid yields as a function of feed glycerol concentration (medium feed rate of 2.15 g/min,  $P = 25$  MPa,  $T = 798$  K)

Component	Yield of different feed glycerol concentration (wt.%)			
	2.5	5	7.5	10
<b>acetaldehyde</b>	0.24	0.29	0.23	0.12
<b>acetol</b>	0.04	0.07	0.08	0.08
<b>methanol</b>	0.01	0.02	0.02	0.02
<b>acetic acid</b>	0.01	0.01	0.01	0.01
<b>propionaldehyde</b>	0.01	0.01	0.01	0.01
<b>acrolein</b>	0.02	trace	trace	trace
<b>ethylene glycol</b>	trace	0.01	0.01	n.d.
<b>allyl alcohol</b>	trace	trace	0.01	trace
<b>acetone</b>	trace	trace	trace	0.01

trace is a small amount less than 0.01

n.d. is not detected

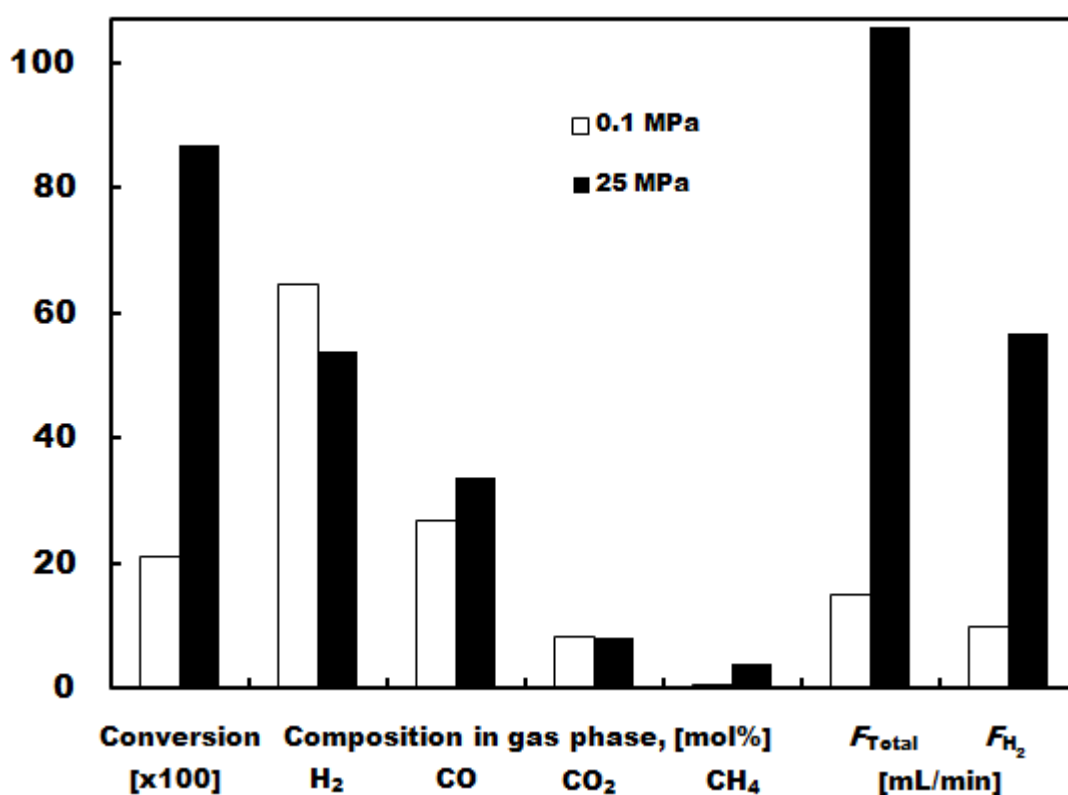
For the liquid analysis, it was shown in Table 8.2 that acetaldehyde was the major product in the liquid phase. Acetaldehyde yield increased from 0.24 to 0.29 with increasing feed glycerol concentration from 2.5 to 5 wt.%, and then it decreased when further increasing feed glycerol concentration. The decrease of acetaldehyde yield with increasing feed glycerol concentration obviously followed the trend of decreasing glycerol conversion with increasing feed glycerol concentration (Figure 8.5a); however, the decrease of the acetaldehyde yield when decreasing the feed glycerol concentration from 5 to 2.5 wt.% is likely due to the further reactions of acetaldehyde to gas phase products (Equations (2.20),(2.25)). On the other hand, acetol yield was increased when increasing glycerol concentration until 5 wt.%, and

then kept almost constant for feed glycerol concentration in the range 5-10 wt.%. The initial increase can be explained by the dehydration of glycerol (Equation (2.22)) which is preferred at lower extent of water. Chiu et al. (2006) stated that using a small amount of water promoted acetol formation. In contrast, increasing the feed glycerol concentration inhibited acrolein formation, as observed from acrolein yield of 0.02 at only 2.5% feed glycerol concentration. Methanol, propionaldehyde, acetone, allyl alcohol, acetic acid, and ethylene glycol yields were detected in very low amounts.

### **8.3.3 Comparison between “Conventional steam reforming” and “Supercritical water reforming”**

Although this paper focused on the supercritical water condition at 250 bar, it was also interesting to compare the performance of the reactions under conventional steam reforming and under supercritical steam reforming (medium feed rate 2.15 g/min, 798 K, and 5 wt.% feed glycerol concentration) carried out in the same empty Inconel 625 reactor. Broll et al. (1999) compared the physicochemical properties of water at 673 K between supercritical water (25 MPa) and superheated steam (0.1 MPa) and observed that the thermal conductivity, specific heat capacity and density of supercritical water were higher than those of superheated steam by around 3, 3 times and 4 orders of magnitude, respectively. The higher thermal conductivity of supercritical water than superheated steam is very favorable to promote endothermic reactions, in particular steam reforming (Equation (2.1)) that promotes production of more hydrogen gas. Moreover, higher density leads to a higher space-time yield in supercritical water condition (Boukris et al., 2006; Gadhe et al., 2007). Figure 8.7 illustrates the performance comparison between steam reforming and supercritical water reforming. Conversion of glycerol at high pressure reached 0.87, which was much higher than at ambient pressure (0.21). The trends in total and H<sub>2</sub> flow rates also corresponded to those with glycerol conversion. Furthermore, with steam reforming at 0.1 MPa, the reactions could proceed for only 2 h, after which it had to be stopped because of plugging by carbon at the bottom screen, while no problem was found in the supercritical water case presented here. CH<sub>4</sub> formation was inhibited at ambient pressure, therefore leading to higher H<sub>2</sub> and lower CO contents. However, it should be noted that addition of some catalysts and/or higher operating temperatures might be

necessary to achieve higher conversion at ambient pressure. Many effort on catalyst studies e.g. ruthenium catalysts (Hirai et al., 2005), ceria-supported metal catalysts (Zhang et al., 2007), Ni/MgO (Adhikari et al., 2007b), alumina-supported metal catalysts (Adhikari et al., 2007c) have been reported. Zhang et al. (2007), Adhikari et al. (2007c), and Slinn et al. (2008) reported that suitable conditions to produce hydrogen from glycerol steam reforming (0.1 MPa) were at 823 K (Ir/CeO<sub>2</sub>), 900 K (Rh/CeO<sub>2</sub>/Al<sub>2</sub>O<sub>3</sub>), 1133 K (Pt/Al<sub>2</sub>O<sub>3</sub>) for which glycerol conversion of 1.00, 0.94, and 1.00 could be obtained, respectively.



**Figure 8.7** Effect of pressure on glycerol conversion, composition of main gas products (H<sub>2</sub>, CO, CO<sub>2</sub>, and CH<sub>4</sub>), total flow rate and H<sub>2</sub> flow rate (medium feed rate of 2.15 g/min, 5 wt.% of feed glycerol concentration,  $T = 798$  K).



**Table 8.3** Gas yields as a function of pressure (medium feed rate of 2.15 g/min, 5 wt.% of feed glycerol concentration,  $T = 798$  K).

Pressure (MPa)	Yield							
	H <sub>2</sub>	CO	CO <sub>2</sub>	CH <sub>4</sub>	C <sub>2</sub> H <sub>6</sub>	C <sub>2</sub> H <sub>4</sub>	C <sub>3</sub> H <sub>8</sub>	C <sub>3</sub> H <sub>6</sub>
0.1	0.32	0.04	0.01	trace	trace	trace	trace	trace
25	1.85	0.39	0.09	0.04	0.01	0.01	trace	trace

**Table 8.4** Liquid yields as a function of pressure (medium feed rate of 2.15 g/min, 5 wt.% of feed glycerol concentration,  $T = 798$  K).

Pressure (MPa)	Yield					
	acetal- dehyde	acetol	methanol	acetic acid	propional- dehyde	ethylene glycol
0.1	0.06	0.01	trace	n.d.	trace	trace
25	0.29	0.07	0.02	0.01	0.01	0.01

Yields of gas and liquid products are shown in Tables 8.3 and 8.4. H<sub>2</sub>, CO, CO<sub>2</sub>, and acetaldehyde were observed as the main products in both conditions. However, in supercritical water conditions their yields were higher. It is worth noting that in the case of reforming at 0.1 MPa, others components, including CH<sub>4</sub>, C<sub>2</sub>H<sub>6</sub>, C<sub>2</sub>H<sub>4</sub>, C<sub>3</sub>H<sub>8</sub>, C<sub>3</sub>H<sub>6</sub> in the gas phase, and methanol, acetol, propionaldehyde, acetic acid, and ethylene glycol in liquid phase were found in only trace amounts.

## 8.4 Conclusion

Hydrogen production from glycerol reforming was investigated in an Inconel 625 reactor under supercritical water conditions at 25 MPa. With 5 wt.% of feed

glycerol concentration, conversion of glycerol and hydrogen yield increased when increasing the operating temperature from 723 to 848 K. However, carbon formation was found as a serious problem for low (1.05 g/min) and medium (2.15 g/min) feed rates at high operating temperature of 823-848 K and 848 K, respectively. WGS plays important role at operating temperature higher than 798 K and only a slightly increasing of glycerol conversion was found at high operating temperature (798-848 K). From the liquid analysis, acetaldehyde and acetol were the main liquid products with compositions up to 74, and 20 mol%, respectively. The effect of feed glycerol concentration was investigated and it was found that lower concentration at 2.5 wt.% supported the hydrogen production in term of glycerol conversion (0.91) and yield of H<sub>2</sub> (2.86) for operation at 798 K, and residence time of 23 s without carbon formation. Moreover, comparison between steam reforming at 0.1 MPa and supercritical water reforming at 25 MPa indicated that supercritical water reforming was superior in term of hydrogen production and inhibition of carbon formation.

# CHAPTER IX

## HYDROGEN PRODUCTION FROM CATALYTIC SUPERCRITICAL WATER REFORMING OF GLYCEROL WITH COBALT BASED CATALYSTS

This chapter presents the catalytic supercritical water reforming of glycerol over cobalt based catalysts for hydrogen production. Five commercial supports including  $\text{La}_2\text{O}_3$ ,  $\alpha\text{-Al}_2\text{O}_3$ ,  $\gamma\text{-Al}_2\text{O}_3$ ,  $\text{ZrO}_2$ , and YSZ are chosen for the study in the Inconel 625 reactor, the same one used in the previous chapter, at various operating temperatures (723-848 K). Then only one best support is chosen to study the effects of feed rate (low, medium, and high feed rates) and cobalt loading (0, 5, 10, and 15 wt.%). The results are considered in terms of glycerol conversion, yield of  $\text{H}_2$  and product distributions.

### 9.1 Introduction

Cobalt is a non-noble metal which has been well known to use with a variety of metal oxide supports in ethanol reforming (Haga et al., 1997; Llorca et al., 2002; Song et al., 2007; Profeti et al., 2009; Bayram et al., 2011). The cobalt based catalysts were found to provide similar activity to the noble metals in the C-C bond cleavage even at low operating temperatures (Llorca et al., 2002; Song et al., 2007; Moura et al., 2011). The encouragements of using cobalt based catalysts have been studied as below:

Haga et al. (1997a) conducted the ethanol SR process at 673 K by varying different supported transition metal catalysts on  $\gamma\text{-Al}_2\text{O}_3$ . The results showed that  $\text{Co} \gg \text{Ni} > \text{Rh} > \text{Pt}$ , Ru, Cu was the order of the reaction selectivity – this is in the reversed order with methanol SR.

Llorca et al. (2002) found that cobalt based catalysts performed a considerable improvement of catalytic activity in the SR of ethanol.

Zhang et al. (2007) observed that Ir/CeO<sub>2</sub> was the most active catalyst in ethanol and glycerol SR processes. However, the complete conversion of glycerol was also found by using Co/CeO<sub>2</sub> at 698 K, showing the hydrogen selectivity of 88% and much lowering values of CO, and CH<sub>4</sub>.

Cheng et al. (2010) produced the hydrogen-rich synthesis gas by using of Co/ $\gamma$ -Al<sub>2</sub>O<sub>3</sub> in glycerol SR process. Glycerol conversion ranging between 0.30 and 0.65 was obtained with H<sub>2</sub>: CO (6 to 12) and H<sub>2</sub>:CO<sub>2</sub> (2 to 2.30) and only small amount of CH<sub>4</sub> was observed. Increasing of glycerol partial pressure caused carbon formation on the catalyst.

Banach et al. (2011) found the 24 wt.% of cobalt on alumina-stabilized zinc oxide support at 693 K in ethanol SR process was the optimum condition for hydrogen production. Conversion of ethanol was completed and CO formation was depressed to 2-3%

However, Haga et al. (1997), Llorca et al. (2002), and Song et al. (2007) concluded that the reforming reactions greatly depended on the properties of support for cobalt metal including activity, stability and selectivity in that operating temperature. Thus, the advantages of individual support have been reviewed from literatures as follows.

La<sub>2</sub>O<sub>3</sub> is an interesting support in the reforming process (Zhang et al., 1996; Sun et al., 2005; Carrara et al., 2008). Tsipouriari and Verykios (1999) found that La<sub>2</sub>O<sub>3</sub> support acted as a dynamic oxygen pool in the reforming process over Ni/La<sub>2</sub>O<sub>3</sub> catalyst. Matsui et al. (1999) found that ruthenium on La<sub>2</sub>O<sub>3</sub> exhibited the good results in CO<sub>2</sub> reforming of methane. Fatsikostas et al. (2002) investigated SR of ethanol process by using of nickel based catalysts including La<sub>2</sub>O<sub>3</sub>,  $\gamma$ -Al<sub>2</sub>O<sub>3</sub>, YSZ, and MgO supports for hydrogen production. It was found that Ni/La<sub>2</sub>O<sub>3</sub> catalyst performed the excellent performance with high activity toward hydrogen rich gas, and long term stability. Especially, the improved stability was probably from the

scavenging of carbon formation on the Ni surface by intermediate formation of  $\text{La}_2\text{O}_2\text{CO}_3$  ( $\text{La}_2\text{O}_3 + \text{CO}_2$ ). This similar behavior was earlier reported by Zhang et al. (1996), Tsipouriari and Verykios (1999). Carrara et al. (2008) also reported that lanthana participated in cleaning the catalyst surface which reacted with the carbon formation in the methane reforming. Sun et al. (2005) found that Ni/ $\text{La}_2\text{O}_3$  was the best catalyst among Ni/ $\text{Y}_2\text{O}_3$ , and Ni/ $\text{Al}_2\text{O}_3$  in the hydrogen production from SR of ethanol at low temperature (523-623 K) for fuel cell application, indicating high catalytic activity, high stability, and high hydrogen selectivity. Sutthumporn and Kawi (2011) stated that Ni/ $\text{La}_2\text{O}_3$  exhibited the improvement of catalytic performance by lanthanide group elements. The rapid deactivation from carbon formation was not found.

$\alpha$ - $\text{Al}_2\text{O}_3$  is the most stable phase of alumina support according to its crystalline structure, chemical and physical stabilities (Pompeo et al., 2005). This support also offers the high mechanical resistance (Pompeo et al., 2005; Alberton et al., 2007) and its low cost (Buffoni et al., 2009). The poor properties include low reactivity and surface area which caused low metallic dispersion and metal-support interaction (Casella et al., 1998; Buffoni et al., 2009). Buffoni et al. (2009) modified  $\alpha$ - $\text{Al}_2\text{O}_3$  to Ni/ $\text{CeO}_2/\alpha$ - $\text{Al}_2\text{O}_3$  which catalyzed the SR of glycerol to obtain high selectivity of hydrogen at 823 K (minimum temperature). The high basic characteristics of Ni/ $\text{CeO}_2/\alpha$ - $\text{Al}_2\text{O}_3$  clearly inhibited the reactions, causing carbon formation.

$\gamma$ - $\text{Al}_2\text{O}_3$  is the most common support in the reforming process (Haga et al., 1997; Liguras et al., 2003; Batista et al., 2004; Liberatori et al., 2007; Cheng et al., 2010). It contains highly acidic sites and has the high surface area (especially when compared with  $\alpha$ - $\text{Al}_2\text{O}_3$ ). Their advantageous properties also include its high thermal and chemical stabilities (Paglia et al., 2006; Profeti et al., 2009; Tuan 2009). In SR of ethanol, the dehydration of ethanol took an important role to produce undesired products including ethylene from the acidic property (Vaidya et al., 2006; Profeti et al., 2009). Ethylene was reported to be a major precursor of carbon formation in polymerization reactions which caused catalyst deactivation (Vaidya et al., 2006; Moura et al., 2011) especially with the small metal loading (Batista et al., 2004). Alberton et al. (2007) compared two phases of  $\text{Al}_2\text{O}_3$  between  $\alpha$ - $\text{Al}_2\text{O}_3$ ,  $\gamma$ - $\text{Al}_2\text{O}_3$  with

the nickel loading. It was found that the activity of nickel based for hydrogen production on  $\gamma$ -Al<sub>2</sub>O<sub>3</sub> was higher than  $\alpha$ -Al<sub>2</sub>O<sub>3</sub> by providing better nickel particle dispersion. Comparing with other supports, Haga et al. (1997) reported that hydrogen production activity followed the order: Co/ $\gamma$ -Al<sub>2</sub>O<sub>3</sub> > Co/ZrO<sub>2</sub> > Co/MgO > Co/SiO<sub>2</sub> > Co/C.

ZrO<sub>2</sub> is the famous support for CO<sub>2</sub> reforming of methane to generate synthesis gas (Bitter et al., 1997; Stagg-Williams et al., 2000; Nagaoka et al., 2001; Mattos et al., 2003; Xu et al., 2003; Garcia et al., 2009; Barroso-Quiroga and Castro-Luna 2010; Gonzalez-Delacruz et al., 2011) especially for Pt/ZrO<sub>2</sub>. It has excellent properties in thermal stability, electrical conductivity, oxygen vacancies and strong resistance against carbon formation (Bellido et al., 2008; Youn et al., 2008a,b), and also performs as a stable support even at high operating temperature (Goud et al., 2007). Song et al. (2007) studied the SR of bio-ethanol over three cobalt based catalysts consisting of  $\gamma$ -Al<sub>2</sub>O<sub>3</sub>, TiO<sub>2</sub>, and ZrO<sub>2</sub>. It was found that 10 wt.% Co/ZrO<sub>2</sub> performed as the best catalyst at 823 K with the highest metal dispersion and hydrogen yields. Nguyen et al. (2008) investigated that 15 wt.% Ni/ZrO<sub>2</sub> achieved the highest activity and performed the good stability in SR of methane at 873 K. Barroso-Quiroga and Castro-Luna (2010) compared seven catalysts for the CO<sub>2</sub> reforming of methane. The results showed that 10 wt.% Ni/ZrO<sub>2</sub> exhibited the best performance in terms of high catalytic activity and stability. In addition, deactivation was not found during the reaction period.

Yttria-stabilized zirconia or YSZ is the zirconium oxide which is added with yttrium oxide in order to improve its properties such as the surface area, thermal stability, and electrical conductivity. The excellent properties of YSZ offer some advantages and it has extensively been used in the Solid oxide fuel cell (Hecht et al., 2005; Grgicak et al., 2005; Laosiripojana and Assabumrungrat, 2007; Resini et al., 2008; Momma et al., 2009). Laosiripojana and Assabumrungrat (2007) conducted the SR of methane, methanol, and ethanol processes with Ni/YSZ which acted as the anode of SOFC. It was observed that it is possible to directly feed methane and methanol Ni/YSZ anode without the carbon formation problem. However, ethanol needed to be pre-reformed using Ni/Ce-ZrO<sub>2</sub> and then properly fed to Ni/YSZ without

the carbon formation problem. Resini et al. (2008) investigated SR of ethanol process by using of YSZ supported Ni-Co alloys. Ni-Co(25:25)/YSZ performed as the best catalyst for which the ethanol conversion was completed at 670 K and offered the hydrogen yield of 65%. They explained that cobalt inhibited dehydration reaction, methane production and enhanced the hydrogen yield. Bellido et al. (2008) found that the hydrogen selectivity in the SR of ethanol process was improved when ZrO<sub>2</sub> was modified to YSZ support. However, it gave the poor results when ZrO<sub>2</sub> was modified to CSZ support (CaO) explaining that other interactions involved with the oxygen vacancies leading to different catalytic behavior of nickel species.

A number of catalysts have been developed and tested to enhance the hydrogen production and also to suppress undesired by-products in the glycerol reforming process, for examples, Ni/Al<sub>2</sub>O<sub>3</sub> (Czernik et al, 2002; Adhikari et al., 2007c; Zhang et al, 2007; Valliyappan et al, 2008), Ni/MgO (Hirai et al., 2005; Adhikari et al., 2007b, 2008), Ni/CeO<sub>2</sub> (Zhang et al., 2007; Adhikari et al., 2008), Ni/TiO<sub>2</sub> (Zhang et al., 2007; Adhikari et al., 2008) , Pd/Ni/Cu/K (Swami et al., 2006; Sharma et al., 2008), Ni/CeO<sub>2</sub>/Al<sub>2</sub>O<sub>3</sub> (Adhikari et al., 2007c, 2008; Profeti et al., 2009), La<sub>1-x</sub>Ce<sub>x</sub>NiO<sub>3</sub> (Cui et al., 2009), Ru/Y<sub>2</sub>O<sub>3</sub> (Hirai et al., 2005), Ir, Co/CeO<sub>2</sub> (Zhang et al., 2007), Rh, Pt, Pd, Ir, Ru, Ce/Al<sub>2</sub>O<sub>3</sub> (Adhikari et al., 2007c) for steam reforming (SR), Raney-NiSn (Shabaker et al., 2004), Pt/Al<sub>2</sub>O<sub>3</sub> (Shabaker et al., 2004; Lehnert et al., 2008; Wen et al., 2008), Ni/Al<sub>2</sub>O<sub>3</sub> (Wen et al., 2008; Iriondo et al., 2008) for aqueous phase reforming (APR), RhCeWc/Al<sub>2</sub>O<sub>3</sub> (Dauenhauer et al., 2006), Pd/Ni/Cu/K (Swami et al., 2006; Sharma et al., 2008) for autothermal reforming (ATR), Ru/Al<sub>2</sub>O<sub>3</sub> (Byrd et al., 2008), and Ru/ZrO<sub>2</sub> (May et al., 2010) for supercritical water reforming (SWR). Note that catalysts for hydrogen production in SWR of glycerol have not widely been studied.

## 9.2 Results and discussion

These results from all experiments were collected after 230 min of time on stream which was long enough to give stable product compositions except experiments with some catalysts at high operating temperatures. The reasons for

unstable behavior are due to catalyst fragility, carbon formation, catalyst deactivation, etc.

### 9.2.1 Effect of support and operating temperature

The commercial supports were characterized to indicate the surface area, pore size (volume, and diameter) as shown in Table 9.1.  $\gamma$ -Al<sub>2</sub>O<sub>3</sub> represented the highest surface, and pore volume which was the bulkiest among the others. The values of surface area follow the order of  $\gamma$ -Al<sub>2</sub>O<sub>3</sub> >> YSZ >  $\alpha$ -Al<sub>2</sub>O<sub>3</sub> > ZrO<sub>2</sub>, La<sub>2</sub>O<sub>3</sub>. After cobalt impregnation on the supports, the order was changed to  $\gamma$ -Al<sub>2</sub>O<sub>3</sub> >> La<sub>2</sub>O<sub>3</sub> > YSZ >  $\alpha$ -Al<sub>2</sub>O<sub>3</sub> > ZrO<sub>2</sub> as shown in Table 9.2. However, except  $\gamma$ -Al<sub>2</sub>O<sub>3</sub> support, all support were reported as very low surface area supports. Figure 9.1 shows the XRD patterns of commercial supports compared with those of the supports after cobalt impregnation and calcination. It is clear that Co<sub>3</sub>O<sub>4</sub> phase (31.3, 36.8, 45.1, 59.4, and 65.4°) is the cobalt phase in all supports. Llorca et al. (2003b, 2004) explained that a calcined form of cobalt based catalysts normally contained Co<sub>3</sub>O<sub>4</sub> phase which was transformed to CoO and metallic cobalt (Co<sup>0</sup>) at high operating temperature of SR process.

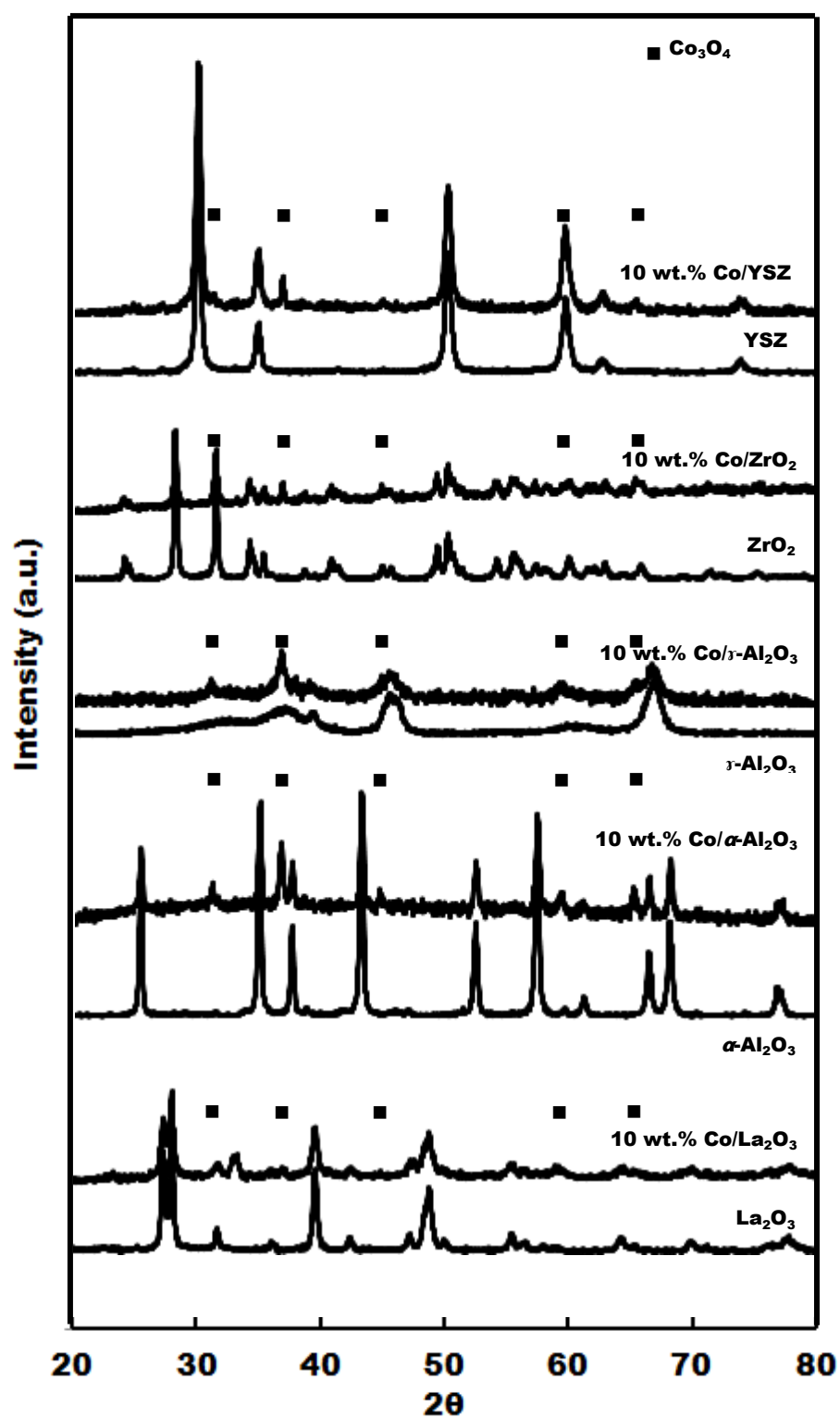
**Table 9.1** Physical properties of commercial supports

Commercial supports	BET surface area (m <sup>2</sup> /g)	Pore volume (cm <sup>3</sup> /g)	Pore diameter (nm)
La <sub>2</sub> O <sub>3</sub>	5.10	0.016	9.67
$\alpha$ -Al <sub>2</sub> O <sub>3</sub>	9.46	0.038	13.01
$\gamma$ -Al <sub>2</sub> O <sub>3</sub>	80.11	0.207	9.71
ZrO <sub>2</sub>	5.92	0.015	6.31
YSZ	13.18	0.061	14.60

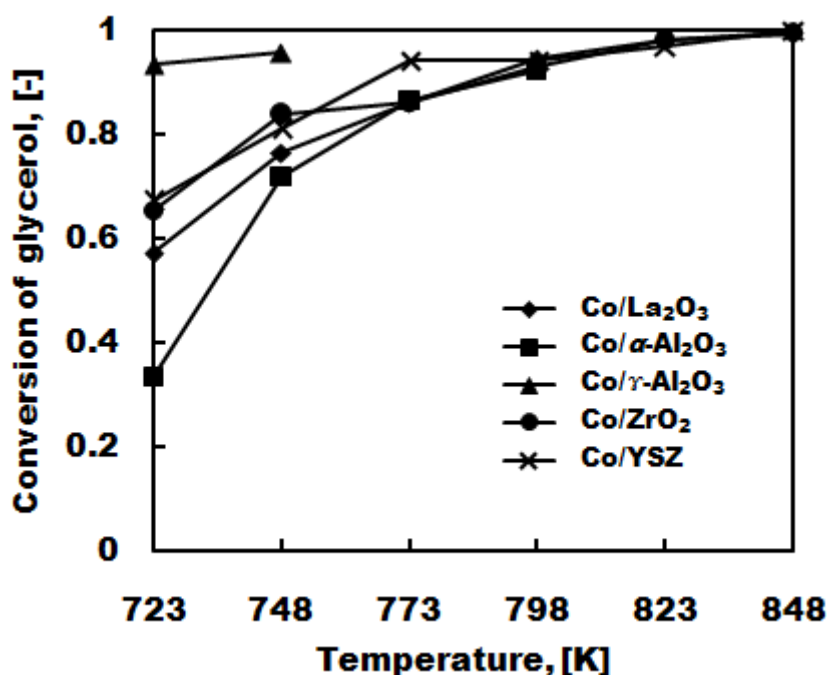


**Table 9.2** Physical properties of 10 wt.% of cobalt based catalysts

<b>Cobalt based catalysts</b>	<b>BET surface area (m<sup>2</sup>/g)</b>	<b>Pore volume (cm<sup>3</sup>/g)</b>	<b>Pore diameter (nm)</b>
<b>Co/La<sub>2</sub>O<sub>3</sub></b>	14.51	0.059	13.30
<b>Co/<math>\alpha</math>-Al<sub>2</sub>O<sub>3</sub></b>	6.70	0.030	14.80
<b>Co/<math>\gamma</math>-Al<sub>2</sub>O<sub>3</sub></b>	55.30	0.250	15.44
<b>Co/ZrO<sub>2</sub></b>	5.82	0.017	8.23
<b>Co/YSZ</b>	9.64	0.044	15.61



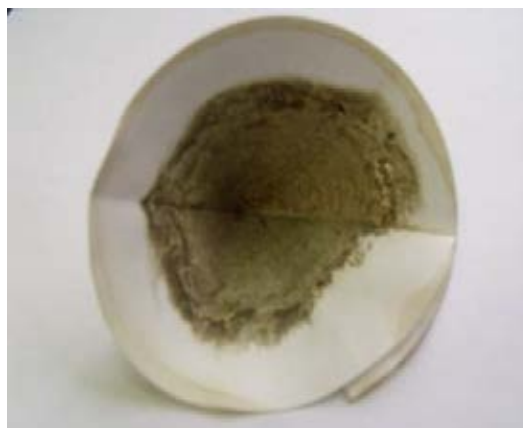
**Figure 9.1** XRD patterns of commercial supports and 10 wt.% of cobalt based catalysts.



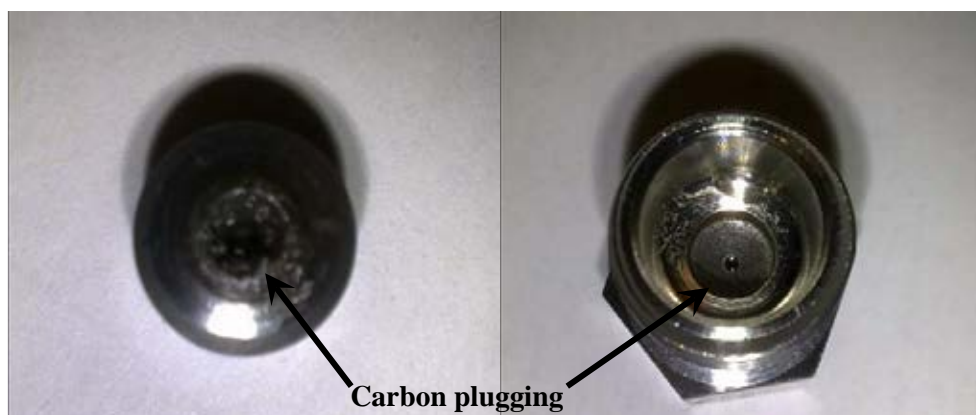
**Figure 9.2** Glycerol conversion at different cobalt based catalysts and operating temperature ( $P = 25$  MPa, medium feed rate of 2.15 g/min, 5 wt.% of feed glycerol concentration, 10 wt.% of cobalt loading)

Figure 9.2 indicates that glycerol conversion is increased by increasing of operating temperature and dependent on the type of metal oxide support. Compared with the results under empty Inconel 625 conditions (Figure 8.1), all the catalysts clearly enhanced the conversion of glycerol especially at low operating temperatures (723-773 K). It was found that  $\text{Co}/\alpha\text{-Al}_2\text{O}_3$  and  $\text{Co}/\gamma\text{-Al}_2\text{O}_3$  catalysts had the carbon formation problem causing the failure of the reaction system. For that reason, 773 and 723 K were the highest operating temperatures which could operate the system longer than 230 min of time on stream, respectively. The acidic sites of  $\text{Al}_2\text{O}_3$  supports caused the carbon formation problem, many literatures reported about this behavior in the reforming process (Casella et al., 1998; Vaidya et al., 2006; Taun, 2009; Buffoni et al., 2009; Profeti et al., 2009; Moura et al., 2011). The lowest glycerol conversion was found in  $\text{Co}/\alpha\text{-Al}_2\text{O}_3$  catalyst at 723, and 748 K which corresponded to the disadvantage of this support including low reactivity, and metallic dispersion (Casella et al., 1998; Buffoni et al., 2009). In  $\text{Co}/\gamma\text{-Al}_2\text{O}_3$  catalyst, it offered the highest glycerol conversion (0.93-0.96) at low operating temperatures; however, the plugging of carbon formation

caused the termination of the experiment before 230 min and could not increase the operating temperature higher than 748 K. Note that, higher operating temperature caused more dramatically carbon formation problem. Figure 9.3 shows the dark yellow liquid sample mixed with dark solid carbon from the supercritical water reforming of glycerol with  $\text{Co}/\gamma\text{-Al}_2\text{O}_3$  catalyst at 748 K. After filtration, solid carbon was found on the filtrated paper that caused the failure system by carbon plugging at the screenings (inside reactor), tubes, and back pressure regulator (BPR seat and nut) as shown in Figure 9.4. Only slight difference in glycerol conversion was observed during the high operating temperatures of 798-848 K for  $\text{Co}/\text{La}_2\text{O}_3$ ,  $\text{Co}/\text{ZrO}_2$ , and  $\text{Co}/\text{YSZ}$  catalysts. The complete glycerol conversion was obtained at the highest operating temperature of 848 K in these three catalysts.

**a****b**

**Figure 9.3** (a) liquid product sample from the supercritical water reforming of glycerol with 10 wt.%  $\text{Co}/\gamma\text{-Al}_2\text{O}_3$  catalyst at 748 K (b) solid products after filtration



**Figure 9.4** Carbon plugging at the back pressure regulator seat (left) and nut (right)

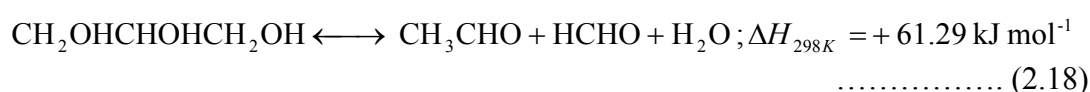
From Figure 9.5a, it was found that the order of  $H_2$  yield is  $Co/YSZ > CO/La_2O_3 = Co/ZrO_2 > Co/\alpha-Al_2O_3 > Co/r-Al_2O_3$ . The explanations for all catalysts were described as follows (Figures 9.5 and 9.6).

In  $Co/r-Al_2O_3$  catalyst, the high glycerol conversion offered very low  $H_2$  yield, and also all gas product yields except for CO yield as shown in Figures 9.5b-d. From liquid analysis, the product contained mostly in acetaldehyde and the rests were methanol and acrolein. It was explained that glycerol was decomposed to acetaldehyde and formaldehyde by Equation (2.18) The proposed mechanisms were suggested by Antal et al. (1985) and Buhler et al. (2002). It has been known that formaldehyde is subsequently decomposed to  $H_2$ , CO, and  $CO_2$  via Equations (2.19),(2.10) (Bröll et al., 1999; Xu et al., 2009; May et al., 2010). Methanol and acrolein were found probably via reactions show in Equations (2.20) (Therdthianwong et al., 2011a,b), (2.23) (Antal et al. (1985); Buhler et al. (2002); Rennard et al. (2009)), respectively. Some methanol was also probably reformed to  $H_2$ , CO, and  $CO_2$  by Equations (2.21) (Therdthianwong et al., 2011a,b) and (3). The proposed carbon formation pathways were due to Boudouard reaction (Equation (2.12)), methane cracking (Equation (2.13)), and ethylene cracking (Equation (2.16)) (Tuan, 2009; Therdthianwong et al., 2011a,b).

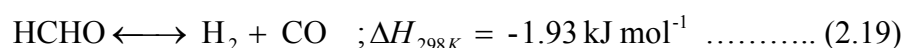
In  $Co/\alpha-Al_2O_3$  catalyst, low conversion caused low yields in the product distribution. However, the acidic sites of  $\alpha-Al_2O_3$  similar to  $r-Al_2O_3$  caused high

production of acetaldehyde and carbon. For this support, methane and carbon monoxide were produced more than the other supports ( $\text{La}_2\text{O}_3$ ,  $\alpha\text{-Al}_2\text{O}_3$ ,  $\gamma\text{-Al}_2\text{O}_3$ , and  $\text{ZrO}_2$ ). Equation (10) is the further reaction of acetaldehyde to generate methane and carbon monoxide (Arita et al., 2003; Therdtianwong et al., 2011a,b). Higher  $\text{CH}_4$  yield at low operating temperatures was the reason to have lower  $\text{H}_2$  yield in the product stream.

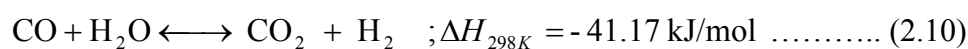
Decomposition of glycerol:



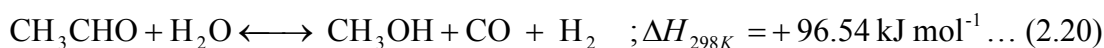
Decomposition of formaldehyde:



Water Gas Shift (WGR or reverse of this is called RWGS):



Acetaldehyde steam reforming:



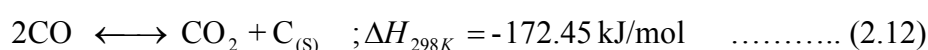
Dehydration of glycerol:



Methanol steam reforming:



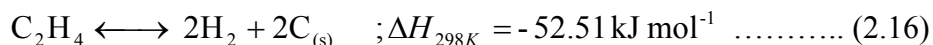
Boudouard reaction:



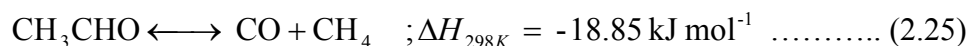
Methane cracking:



C<sub>2</sub>H<sub>4</sub> cracking:

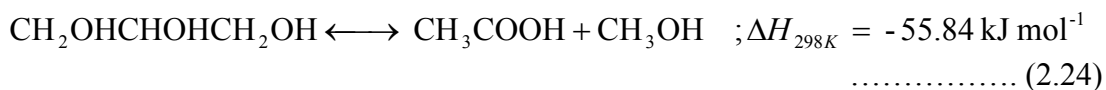


Decomposition of acetaldehyde:

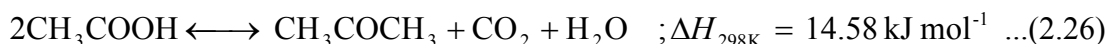


In Co/La<sub>2</sub>O<sub>3</sub>, and Co/ZrO<sub>2</sub> catalysts, the trends of their product distribution look similar when changing operating temperature. The highest of H<sub>2</sub> yields were 2.24 and 2.43, respectively at 848 K. The main liquid product was acetaldehyde which initially was increased by increasing of operating temperature, and then decreased until the highest operating temperature by further reactions (Equations (2.25),(2.20),(2.10)) to gas phase products mainly in carbon dioxide and hydrogen. Other liquid products included methanol, acetic acid, acetone, acetol, and ethylene glycol. Acetic acid was occurred by the decomposition of glycerol, indicating more methanol formation (Equation (2.14)) (Luo et al., 2008). However, acetic acid was selectively converted to acetone by decarboxylation at higher operating temperatures (Equation (2.26)). This behavior was reported by Watanabe et al. (2003). They explained that ZrO<sub>2</sub> supports contained almost equal acid and base sites which catalyzed the acetone formation in supercritical water condition. Acetol was the dehydration product from glycerol (Equation (2.22)) that was reduced by increasing operating temperature (Chiu et al., 2006; Rennard et al. (2009); May et al., 2010). Another liquid product was ethylene glycol which was formed the fragmentation reaction of glycerol (Equation (2.17)) (Xu et al. (2009)).

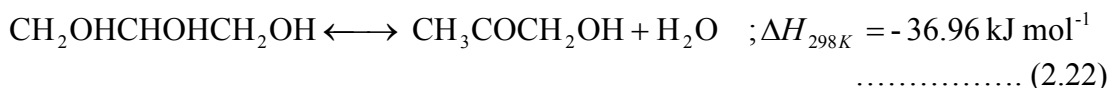
Decomposition of glycerol:



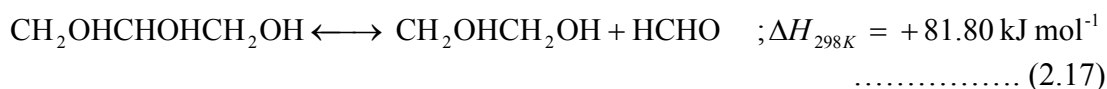
Decarboxylation of acetic acid:



Dehydration of glycerol:



Fragmentation reaction of glycerol

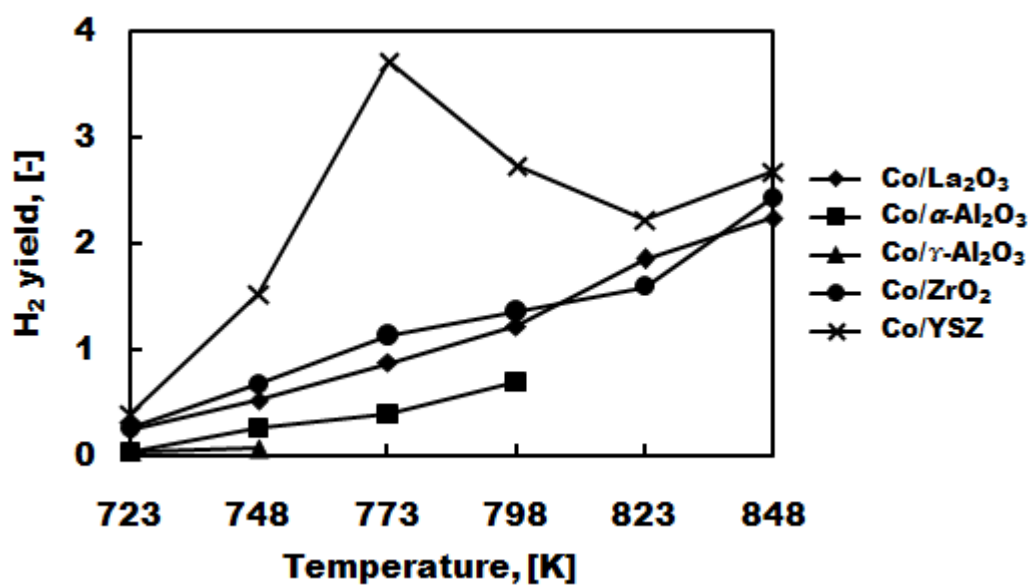


In Co/YSZ catalyst, it offered the highest H<sub>2</sub> yields in all ranges of operating temperature when compared with the other catalysts. The H<sub>2</sub> yield was increased by increasing operating temperature until 773 K, and then the unclear decreasing of H<sub>2</sub> yield was observed above 773 K. This behavior was due to unstable process; it will be discussed in the next paragraph. By-products in gas phase were mostly CO<sub>2</sub> with some CH<sub>4</sub> and CO. However, CO formation was increased by increasing operating temperature. In liquid phase, the selectively products followed with Co/La<sub>2</sub>O<sub>3</sub>, and Co/ZrO<sub>2</sub> catalysts including acetaldehyde, methanol, acetone, acetic acid, and ethylene glycol. The similar liquid products were influenced from zirconia containing in YSZ support. In addition, acetaldehyde was minimized comparing to other catalysts, causing of H<sub>2</sub> yield enhancement. Therefore, it can be concluded that Co/YSZ catalyst is the suitable catalyst to produce hydrogen in supercritical water conditions.

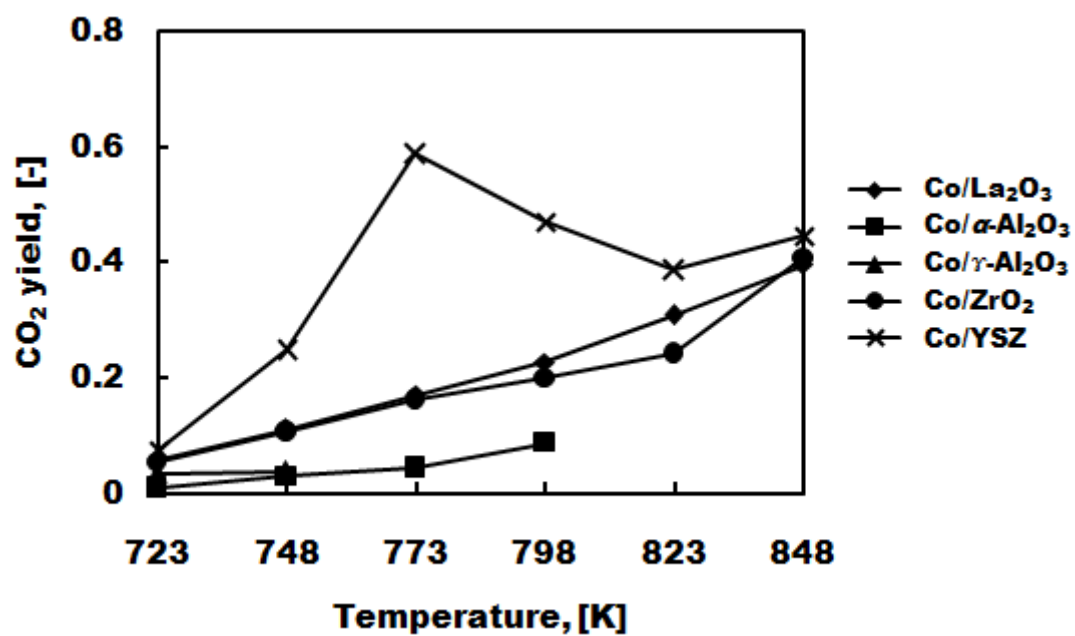
Focusing on H<sub>2</sub> yield of Co/YSZ catalyst as a function of time on stream (Figure 9.7a), it was observed that H<sub>2</sub> yield was largely diminished during of 70-230 min when increasing time on stream at the operating temperatures of 798, 823 K, respectively. At 30 min, H<sub>2</sub> yields were at the highest values of 4.23, and 4.03 corresponding with minimum acetaldehyde yields (Figure 9.7b). It can be concluded that the high performance in H<sub>2</sub> yields (798, 823 K) of Co/YSZ catalyst were continuously decreased with the observed acetaldehyde in liquid product when time on stream was longer than 70 min. Note that 773 K was the highest operating temperature to operate without stability problem.



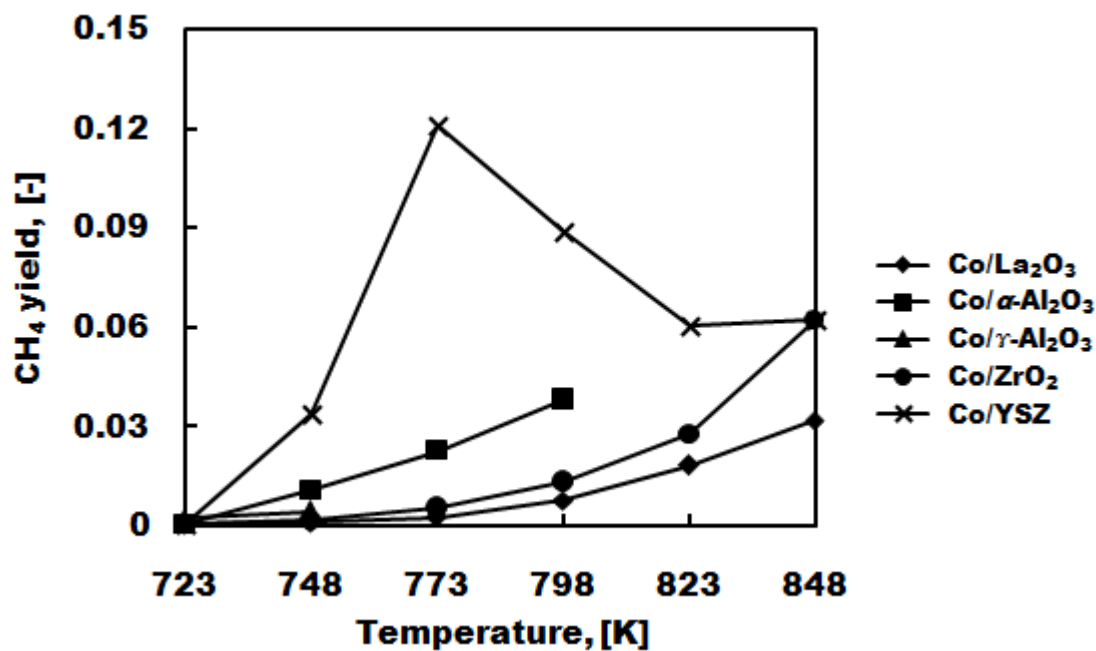
a



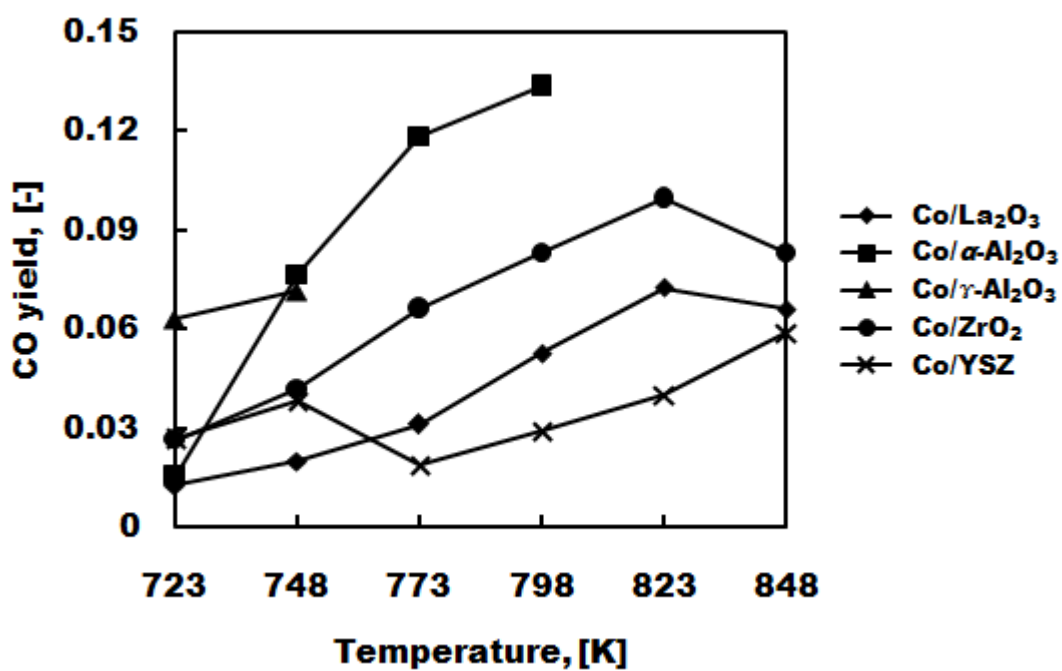
b



c

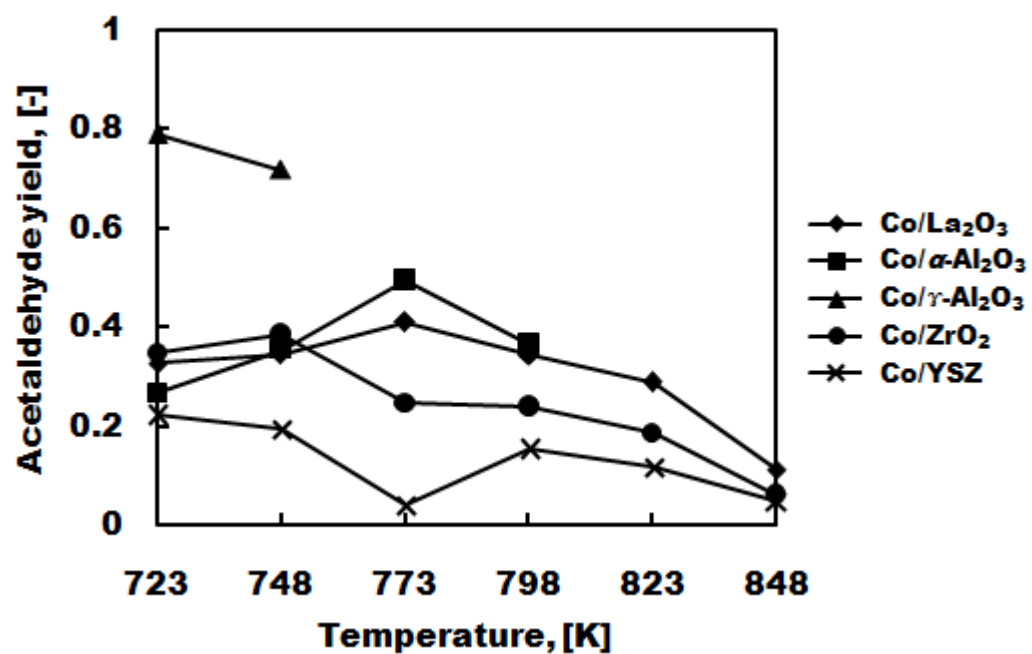


d

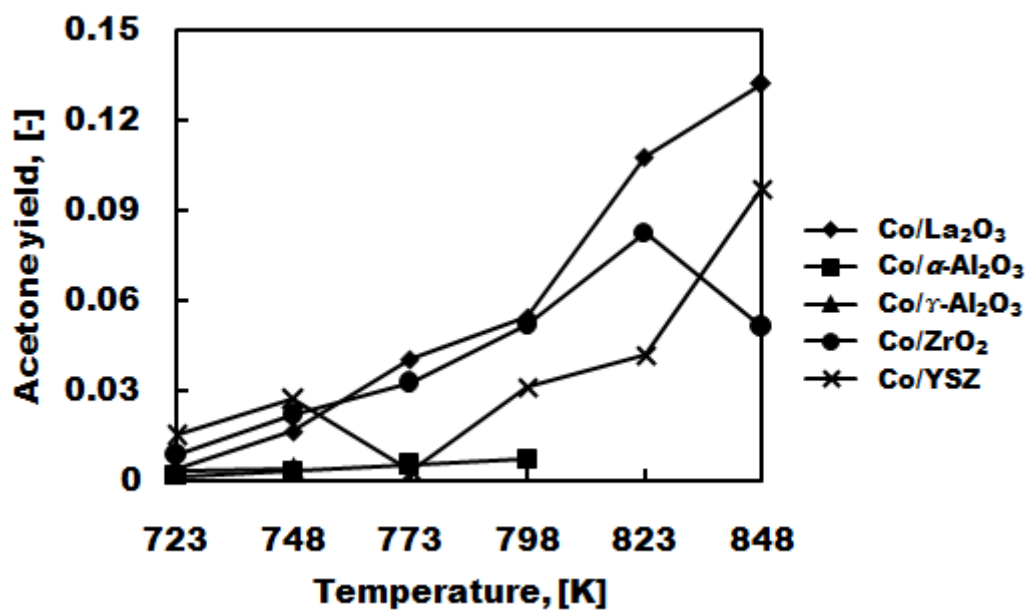


**Figure 9.5** Gas yields of (a) H<sub>2</sub>, (b) CO<sub>2</sub>, (c) CH<sub>4</sub>, (d) CO at different cobalt based catalysts and operating temperatures ( $P = 25$  MPa, medium feed rate of 2.15 g/min, 5 wt.% of feed glycerol concentration, 10 wt.% of cobalt loading)

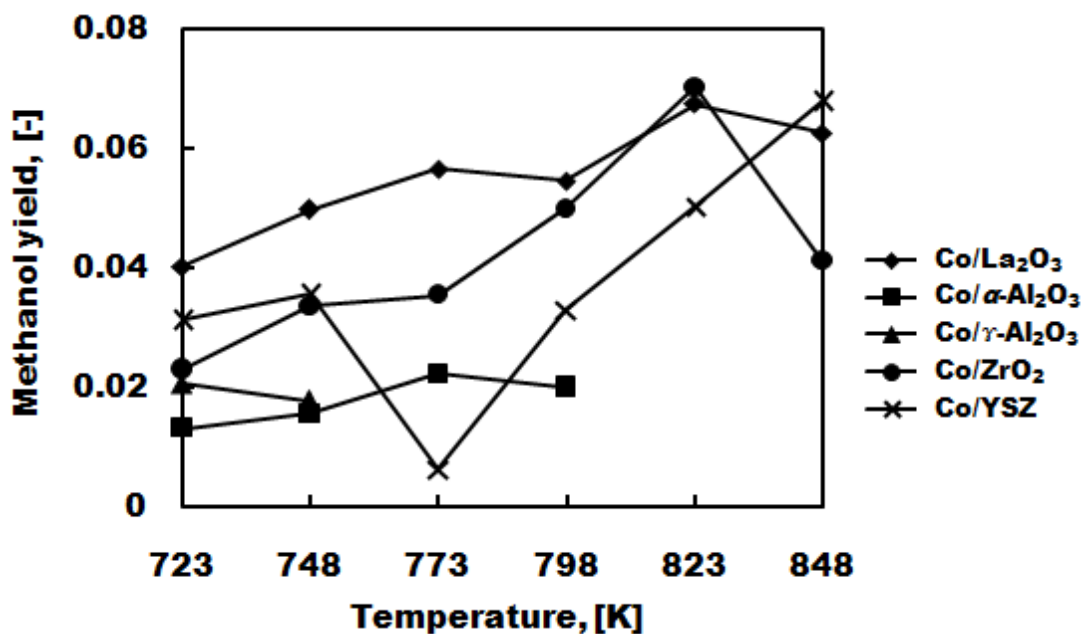
a



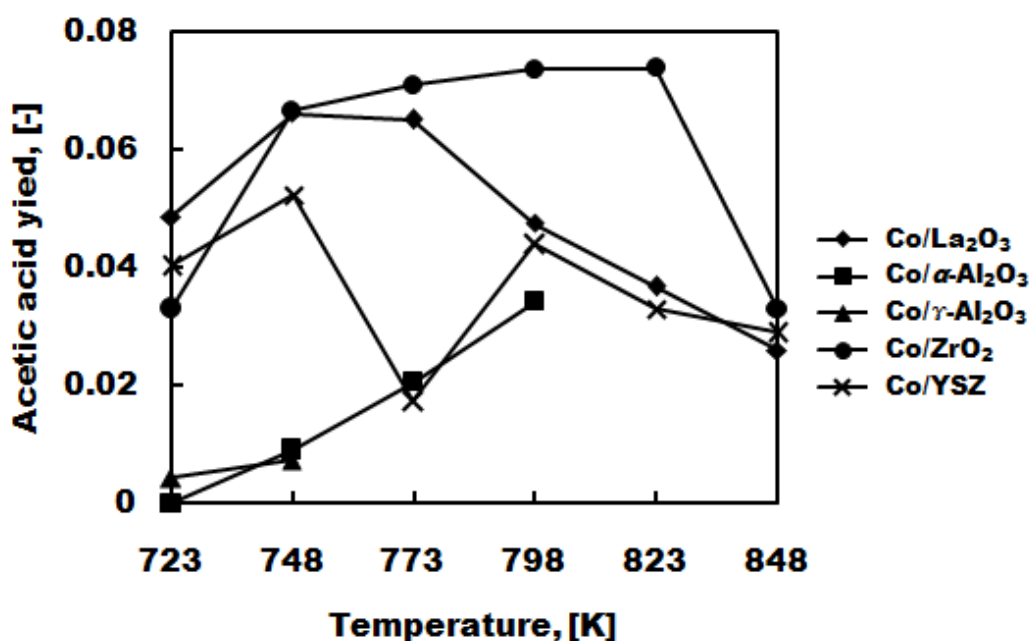
b



c

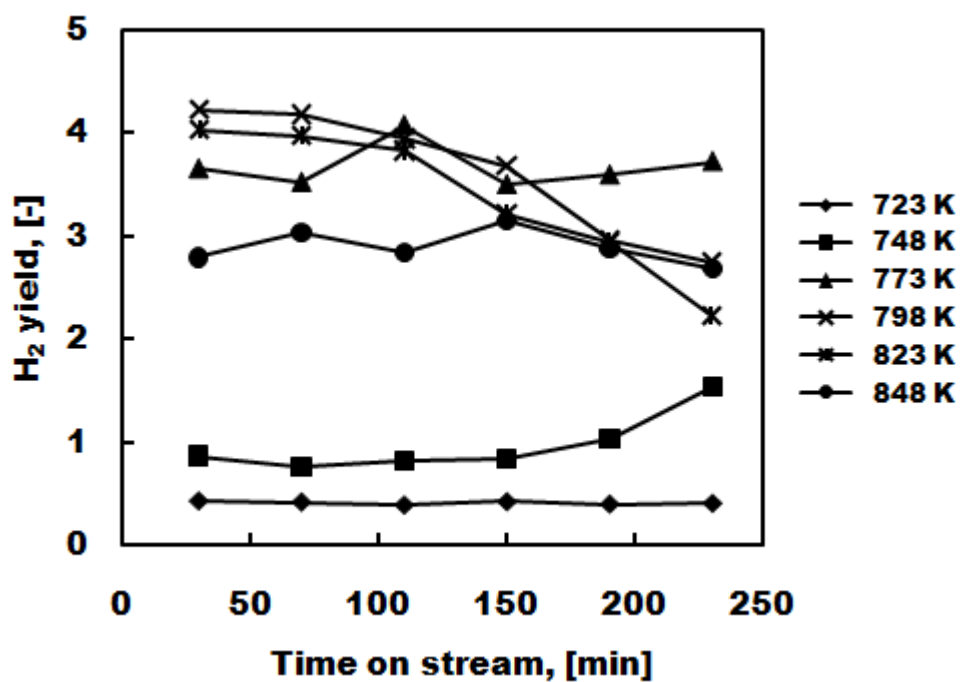


d

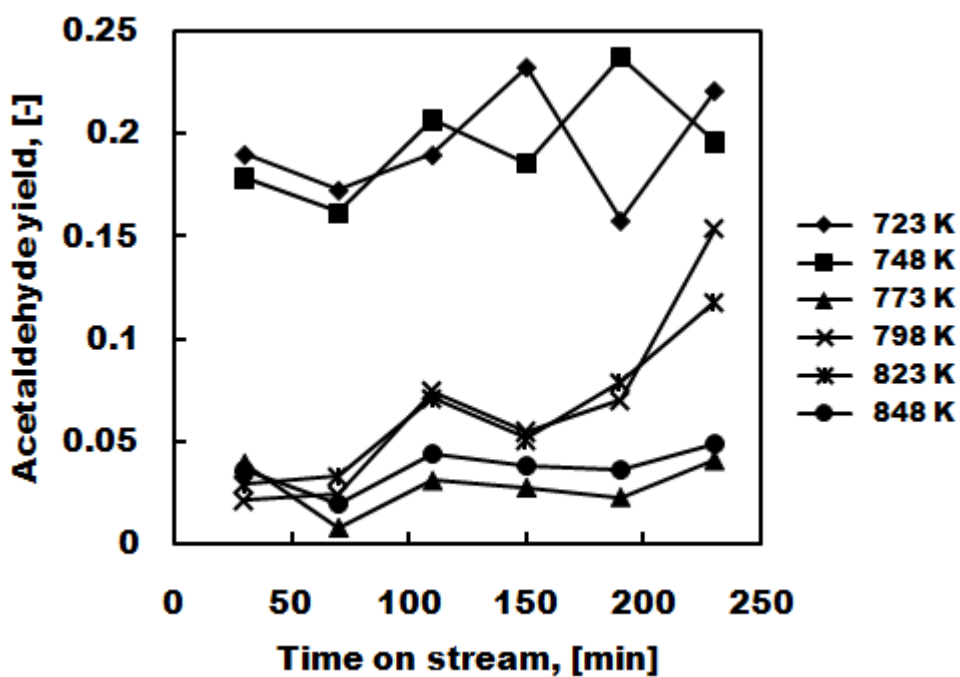


**Figure 9.6** Liquid yields of (a) acetaldehyde, (b) acetone, (c) methanol, (d) acetic acid at different cobalt based catalysts and operating temperatures ( $P = 25$  MPa, medium feed rate of 2.15 g/min, 5 wt.% of feed glycerol concentration, 10 wt.% of cobalt loading)

a

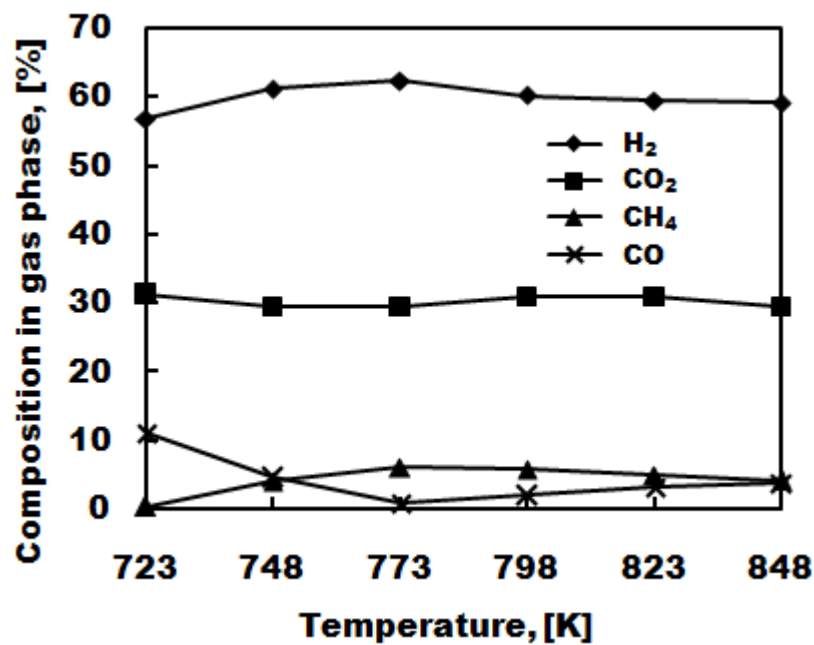


b

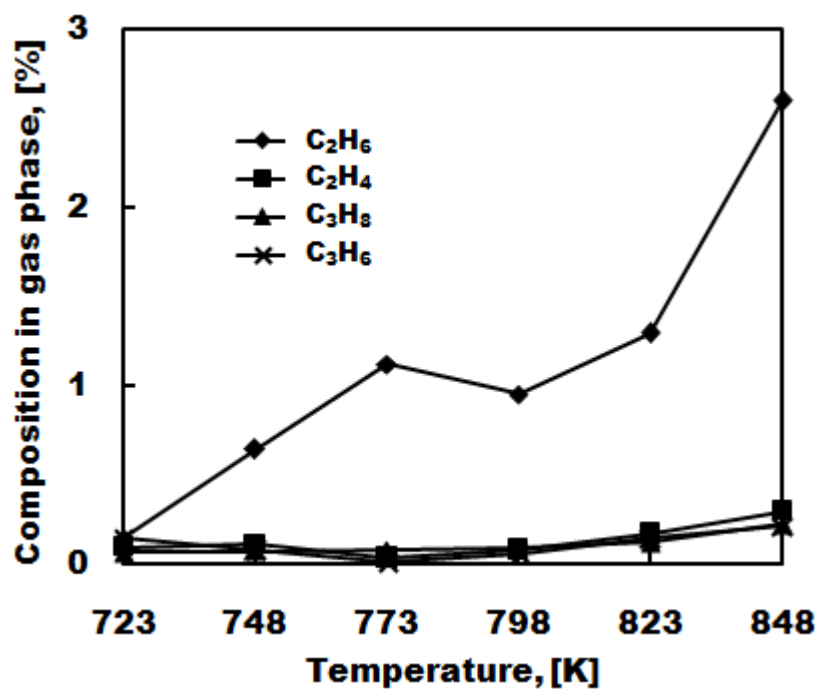


**Figure 9.7** Yield of (a) H<sub>2</sub>, (b) acetaldehyde as a function of time on stream and operating temperature by using of 10 wt.% Co/YSZ catalyst ( $P = 25$  MPa, medium feed rate of 2.15 g/min, 5 wt.% of feed glycerol concentration)

a



b



**Figure 9.8** Compositions of gas products (a) H<sub>2</sub>, CO<sub>2</sub>, CH<sub>4</sub>, and CO (b) C<sub>2</sub>H<sub>6</sub>, C<sub>2</sub>H<sub>4</sub>, C<sub>3</sub>H<sub>8</sub>, C<sub>3</sub>H<sub>6</sub> as a function of operating temperature by using of 10 wt.% Co/YSZ catalyst ( $P = 25$  MPa, medium feed rate of 2.15 g/min, 5 wt.% of feed glycerol concentration)

Considering the product distributions in gas phase when using Co/YSZ catalyst (Figures 9.8a,b), only slight changes of  $H_2$ ,  $CO_2$ ,  $C_2H_4$ ,  $C_3H_8$ , and  $C_3H_6$  were found with increasing operating temperature. The trend of  $CH_4$  was in contrast with  $CO$  during all operating temperatures. Below 773 K, acetaldehyde yield was converted to  $CO$ , and  $CH_4$  (Equation (2.25)) at increased operating temperature. However,  $CO$  could be further reacted (Equation (2.10)) to selectively produce higher  $H_2$  concentration. This type of water gas shift is called “fast type water gas shift reaction” which has been explained in the previous chapter. Above 773 K, increasing of  $CO$  concentration was obtained at increasing operating temperature (Methanations : Equations (2.7,2.8), RWGS, Equation (2.10)) along with the slight decreasing of  $H_2$ ,  $CH_4$ , and  $CO_2$ . On the other hand,  $C_2H_6$  was always increased by increasing operating temperature as same as the supercritical water condition without presence of a catalyst (empty reactor). It probably means that  $C_2H_6$  is the most stable compound among  $C_{2-3}$  gas product compounds. Bennekom et al. (2011) stated that it was not clear whether  $C_2H_6$  was a primary gas product in supercritical water reforming of glycerol – it was probably occurred from hydrogenation of  $C_2H_4$  or combination by proposed reaction pathways in Figure 3.5.

### 9.2.2 Effect of feed rate

From the previous part, the highest  $H_2$  yield was obtained around 4.23 at time on stream of 30 min and operating temperature of 798 K. So this operating temperature was represented to study the effect of feed rate by means of residence time in the reactor. Three feed rates were considered including low feed rate (1.05 g/min), medium feed rate (2.50 g/min), and high feed rate (3.60 g/min).

Table 3 shows that the glycerol conversion, and total gas product flow were decreased by increasing feed rate. It indicates that glycerol required time to stay inside the reactor (residence time), increasing of time enhanced the conversion of glycerol to products. These results correspond to the studying on the supercritical water reforming without addition a catalyst in the previous chapter. Lower feed rates (higher residence times) promoted more amounts of gas product yields, especially for  $H_2$ , and  $CO_2$ . It was clear when the liquid analysis was determined as shown in Table 9.4. The

main liquid product, acetaldehyde, was decreased from 0.10-0.15 to 0.04 of yield in low feed rate condition. Note that lower feed rate favors the further reactions to terminate products in gas phase.

H<sub>2</sub> yield was significantly decreased by increasing time on stream for medium feed rate at this operating temperature. Figures 9.9a,b shows H<sub>2</sub> and acetaldehyde yields at 30-230 min of time on stream. The similar result was obtained for high feed rate condition. The highest H<sub>2</sub> yield was reached to the maximum value of 5.15 at 70 min of time on stream, and then a dramatic decrease was observed to 2.57 at 230 min. The decreasing in H<sub>2</sub> yield performance could possibly be reduced in the lower feed rate, indicating only slightly change in low feed rate. The reason might involve with the productivity and the catalyst reduction (self reduction). This behavior corresponded to the increasing of acetaldehyde yield when increasing of time on stream (Figure 9.9b). Nevertheless, no significant gas product distribution was found by changing of feed rate. Note that, higher gas flow rate products condition always appears in fluctuating of gas and liquid flow rates, causing uncontrollable pressure at BPR.

**Table 9.3** Glycerol conversion, total gas products flow rate, and gas yields as a function of feed rates (low feed rate=1.05 g/min, medium feed rate=2.50 g/min, and high feed rate=3.60 g/min) by using of 10 wt.% Co/YSZ catalyst ( $T=798$  K,  $P = 25$  MPa, medium feed rate of 2.15 g/min, 5 wt.% of feed glycerol concentration)

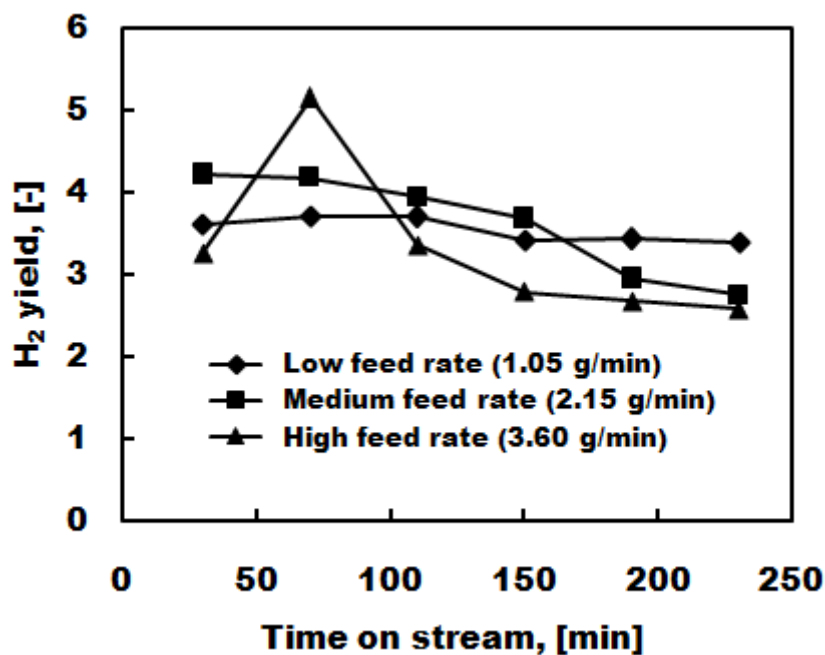
Feed rate	Conversion, (-)	Total gas products flow rate (L/mol of glycerol fed)	Yield of				
			H <sub>2</sub>	CO <sub>2</sub>	CH <sub>4</sub>	CO	C <sub>2</sub> H <sub>6</sub>
low	0.97	144.0	3.40	0.58	0.15	0.04	0.06
medium	0.94	113.2	2.75	0.47	0.09	0.03	0.03
high	0.87	105.3	2.57	0.42	0.09	0.03	0.03

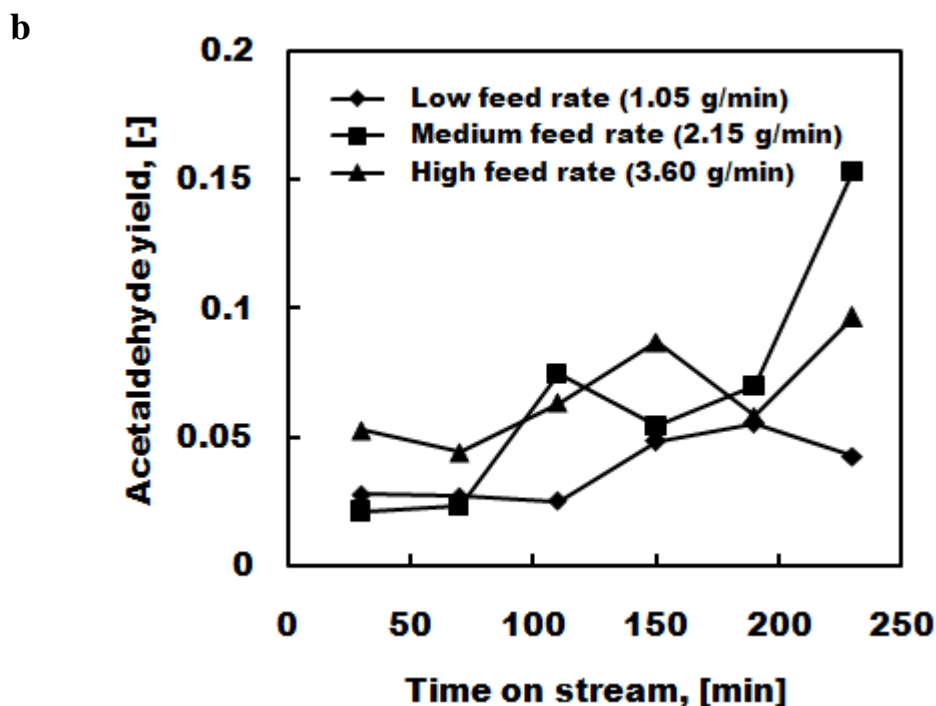


**Table 9.4** Liquid yields as a function of feed rates (low feed rate=1.05 g/min, medium feed rate=2.50 g/min, and high feed rate=3.60 g/min) by using of 10 wt.% Co/YSZ catalyst ( $T=798$  K,  $P = 25$  MPa, medium feed rate of 2.15 g/min, 5 wt.% of feed glycerol concentration)

Feed rates	Yield of, (-)			
	acetaldehyde	acetic acid	methanol	acetone
low	0.04	0.02	0.01	0.01
medium	0.15	0.04	0.03	0.03
high	0.10	0.03	0.01	0.01

a





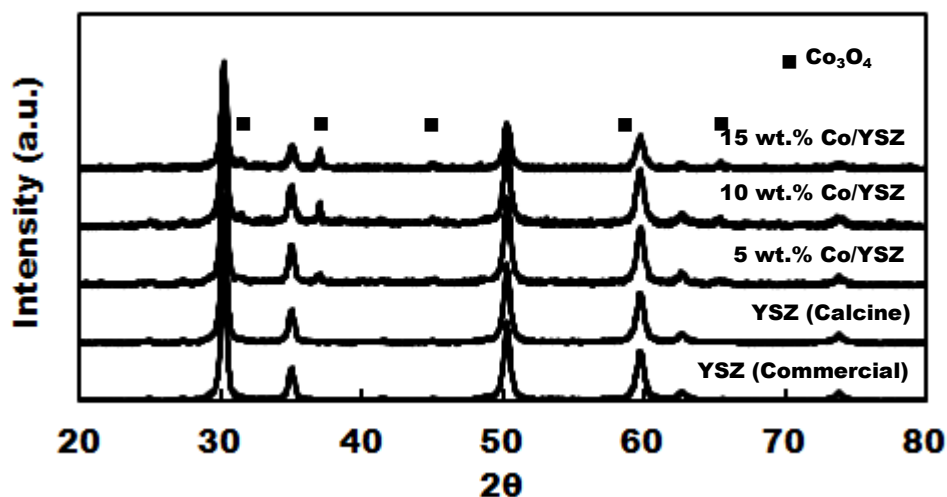
**Figure 9.9** Yield of (a)  $H_2$ , (b) acetaldehyde as a function of time on stream and feed rate by using of 10 wt.% Co/YSZ catalyst ( $T=798$  K,  $P = 25$  MPa, medium feed rate of 2.15 g/min, 5 wt.% of feed glycerol concentration)

### 9.2.3 Effect of metal loading

From the previous parts, the condition of operating temperature of 773 K and medium feed rate was chosen to study in this part for the reason that high  $H_2$  yield was produced and stayed in stability for 230 min. This part focuses on the effect of percent of cobalt loading on YSZ as the catalysts in the supercritical water reforming process. Table 9.5 shows the physical properties of YSZ support and various percents of cobalt loading on YSZ. The slightly lower surface area was shown by increasing percents of cobalt loading as well as the pore volume and pore diameter. XRD patterns confirmed the increasing of cobalt loading in Co/YSZ catalyst, indicating the higher  $Co_3O_4$  peaks as shown in Figure 9.10. It is confirmed that  $Co_3O_4$  is the most stable of cobalt form in this study.

**Table 9.5** Physical properties of YSZ support and different cobalt loading for Co/YSZ catalysts

Cobalt on YSZ support	BET surface area (m <sup>2</sup> /g)	Pore volume (cm <sup>3</sup> /g)	Pore diameter (nm)
YSZ	12.39	0.067	18.23
5 wt.% Co/YSZ	11.42	0.048	14.93
10 wt.% Co/YSZ	9.64	0.044	15.61
15 wt.% Co/YSZ	9.65	0.046	15.94



**Figure 9.10** XRD patterns of YSZ support and different cobalt loading for Co/YSZ catalysts

Conversion of glycerol (0.88-0.94) was not significantly different by increasing cobalt loading as shown in Table 9.6. It means that YSZ support (0 wt.%) was also active to conversion of glycerol to other products in supercritical water condition. However, the gas product yields including H<sub>2</sub>, CO<sub>2</sub>, and CH<sub>4</sub> were considerably increased by increasing cobalt loading until 10 wt.%. In contrast, CO yield was decreased when cobalt metal appeared in the catalyst. In the liquid analysis (Table 9.7), acetaldehyde was the main component which is perfectly decreased to produce more amounts of gas products as same as other liquid products including methanol, acetone, acetic acid, ethylene glycol, and ethylene glycol. Comparing

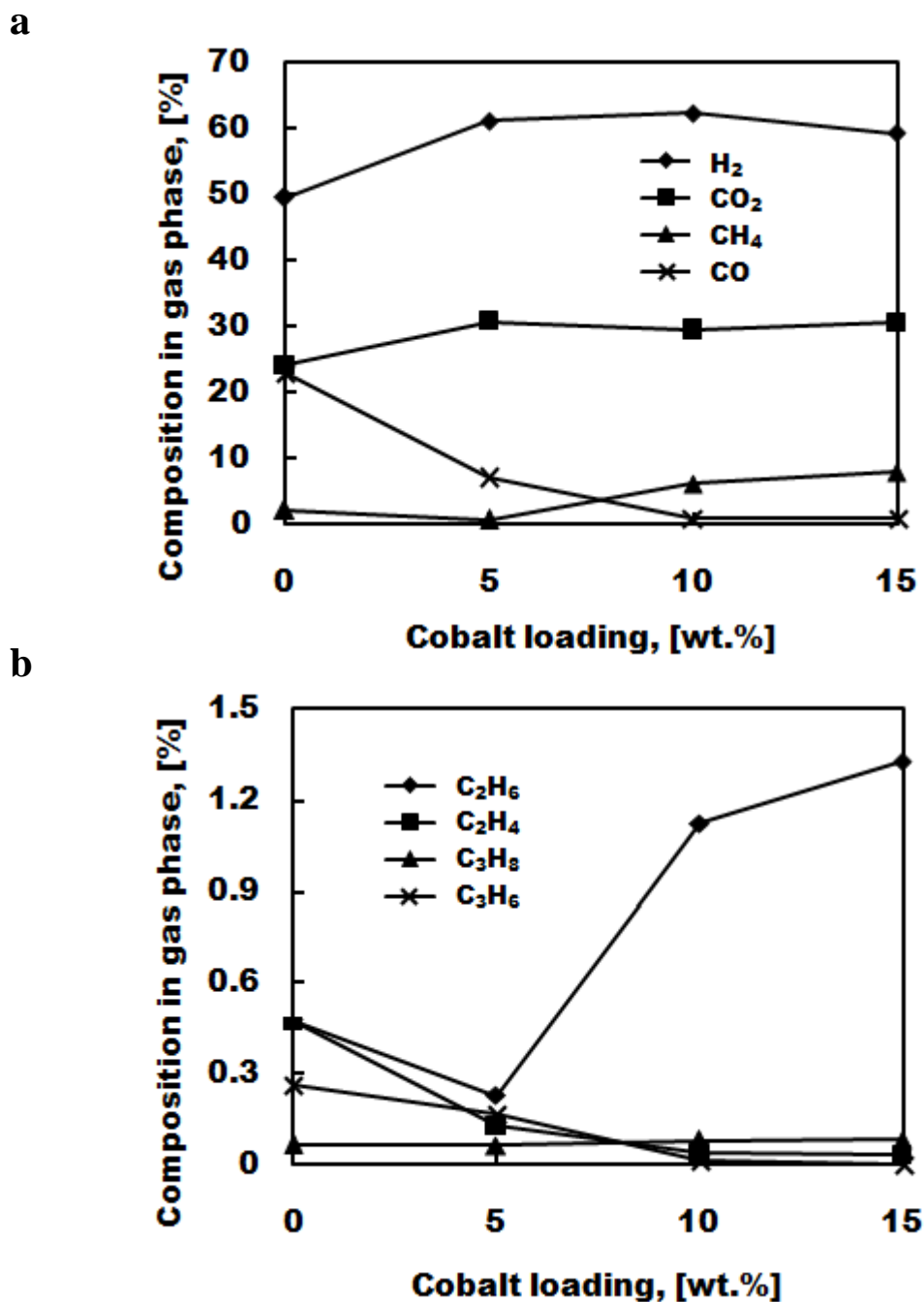
between 10 and 15 wt.% loadings, no significant difference was observed in term of gas and liquid product yields. Therefore, 10 wt.% of cobalt loading was the optimum metal loading.

**Table 9.6** Glycerol conversion, and gas yields as a function of cobalt loading for Co/YSZ catalysts ( $T=773$  K,  $P = 25$  MPa, medium feed rate of 2.15 g/min, 5 wt.% of feed glycerol concentration)

Cobalt loading, [wt%]	Conversion, (-)	Yield of, (-)					
		H <sub>2</sub>	CO <sub>2</sub>	CH <sub>4</sub>	CO	C <sub>2</sub> H <sub>6</sub>	C <sub>3</sub> H <sub>8</sub>
0	0.90	0.64	0.10	0.01	0.12	trace	trace
5	0.88	1.29	0.22	trace	0.05	trace	trace
10	0.94	3.72	0.59	0.12	0.02	0.04	trace
15	0.92	3.66	0.63	0.16	0.02	0.05	0.01

**Table 9.7** Liquid yields as a function of cobalt loading for Co/YSZ catalysts ( $T=773$  K,  $P = 25$  MPa, medium feed rate of 2.15 g/min, 5 wt.% of feed glycerol concentration)

Cobalt loading, [wt%]	Yield of					
	acetaldehyde	methanol	acetone	acetic acid	ethanol	ethylene glycol
0	0.38	0.08	0.07	0.04	0.04	0.02
5	0.19	0.08	0.09	0.06	0.01	0.03
10	0.04	0.01	trace	0.02	trace	0.01
15	0.06	0.01	trace	0.02	trace	0.01



**Figure 9.11** Compositions of gas products (a) H<sub>2</sub>, CO<sub>2</sub>, CH<sub>4</sub>, and CO (b) C<sub>2</sub>H<sub>6</sub>, C<sub>2</sub>H<sub>4</sub>, C<sub>3</sub>H<sub>8</sub>, C<sub>3</sub>H<sub>6</sub> as a function of cobalt loading for Co/YSZ catalysts ( $T=773$  K,  $P = 25$  MPa, medium feed rate of 2.15 g/min, 5 wt.% of feed glycerol concentration)

About the gas product distribution (Figures 9.11a,b), high CO concentration was detected when using YSZ support (0 wt.%) as observed in the empty reactor condition from the previous chapter. The appearance of cobalt metal in the catalyst

had influence on inhibiting the CO formation by promotion of WGS reaction (Equation (2.10)). On the other hand, the increasing of CH<sub>4</sub> concentration was explained by the decomposition of acetaldehyde in Equation (2.25). For C<sub>2-3</sub> gas product compounds, C<sub>2</sub>H<sub>6</sub> was the most stable compound, as observed by the increasing of C<sub>2</sub>H<sub>6</sub> at higher cobalt loading.

### 9.3 Conclusion

For all the cobalt base catalysts, glycerol conversion was highly dependent on the operating temperature. Complete conversion was achieved at the highest operating temperature of 848 K for Co/La<sub>2</sub>O<sub>3</sub>, Co/ZrO<sub>2</sub>, and Co/YSZ catalysts. However, the plugging of carbon formation occurred by using of Co/ $\alpha$ -Al<sub>2</sub>O<sub>3</sub>, Co/ $\gamma$ -Al<sub>2</sub>O<sub>3</sub> catalysts which is corresponding to high acidic sites in their support properties. Comparing all the catalysts, Co/YSZ catalyst performed the best activity in term of H<sub>2</sub> yield. It promoted the highest H<sub>2</sub> yield at 773 K and then the decreasing of H<sub>2</sub> yield was observed with the increasing of operating temperature. Note that higher operating temperatures (798, 823 K) led to decrease of the H<sub>2</sub> yield by increasing of time on stream (30-230 min), appearing more amount of acetaldehyde. In the study of Co/YSZ catalyst, increasing of feed rate significantly decreased the glycerol conversion and H<sub>2</sub> yield, but increased the liquid products including acetaldehyde, acetic acid, methanol, and acetone. Regarding the effect of metal loading, the appearance of cobalt in YSZ support influenced the suppression of the CO formation. It was found that 10 wt.% Co/YSZ catalyst was the optimum cobalt loading during 0-15 wt.% Co/YSZ catalysts.

# **CHAPTER X**

## **HYDROGEN PRODUCTION FROM CATALYTIC SUPERCRITICAL WATER REFORMING OF GLYCEROL WITH NICKEL BASED CATALYSTS**

This chapter follows the catalyst screening from the previous chapter by replacing cobalt with nickel metal and testing the reaction at the operating temperature of 723-848 K. Similar to the study with the cobalt based catalysts, a suitable support is chosen to study an in-depth analysis about the effects of feed rate (low, medium, and high feed rates) and nickel loading (0, 2.5, 5, 10, and 15 wt.%). Additionally, the effect of feed glycerol concentration (2.5, 5, 7.5, 10 wt.%) is determined in this chapter.

### **10.1 Introduction**

Nickel is a well-known metal which has been employed in the various reforming processes for example, CO<sub>2</sub> reforming of methane (Slagtern et al., 1997; Liu et al., 2008; Garcia et al., 2009; Sutthiumporn and Kawi, 2011), methane reforming (Matsumura and Nakamori, 2004; Rakass et al., 2006; Nguyen et al., 2008; Jen Huang and Chin Huang, 2008), ethanol reforming (Marino et al., 2001; Frusteri et al., 2004a, 2004b, 2004c; Sun et al., 2005; Resini et al., 2008), and glycerol reforming (Hirai et al., 2005; Swami and Abraham, 2006; Adhikari et al., 2007a, 2007b, 2008; Zhang et al., 2007; Cui et al., 2009). It has been substituted for noble metal since nickel is more reasonably priced, and highly active toward the hydrogen rich gas (Rakass et al., 2006; Youn et al., 2008; Garcia et al., 2009). Ability of nickel was reported as the excellent C-C bond rupture (Marino et al., 2001; Youn et al., 2008). Frusteri et al., (2004a) obtained that nickel performed the best performance

comparing to Pd, Pt, Rh, and Co with the support MgO in the steam reforming of ethanol. Hirai et al., (2005) compared the metal activity based on the hydrogen production:  $Ru \approx Rh > Ni > Ir > Co > Pt > Pd > Fe$ . In addition, Adhikari et al., (2007a) observed the order of hydrogen selectivity at 1173 K was  $Ni > Ir > Ru > Pt > Rh, Pd$ . It can be concluded that nickel showed very high activity among the others. On the other hand, the deactivation of nickel catalyst is mainly caused from carbon formation and metal sintering (Frusteri et al., 2004a, 2004c; Rakass et al., 2006; Liu et al., 2008; Wen et al., 2008). Therefore, nickel based catalysts is an interesting choice for investigation of the performance of hydrogen production in supercritical water conditions.

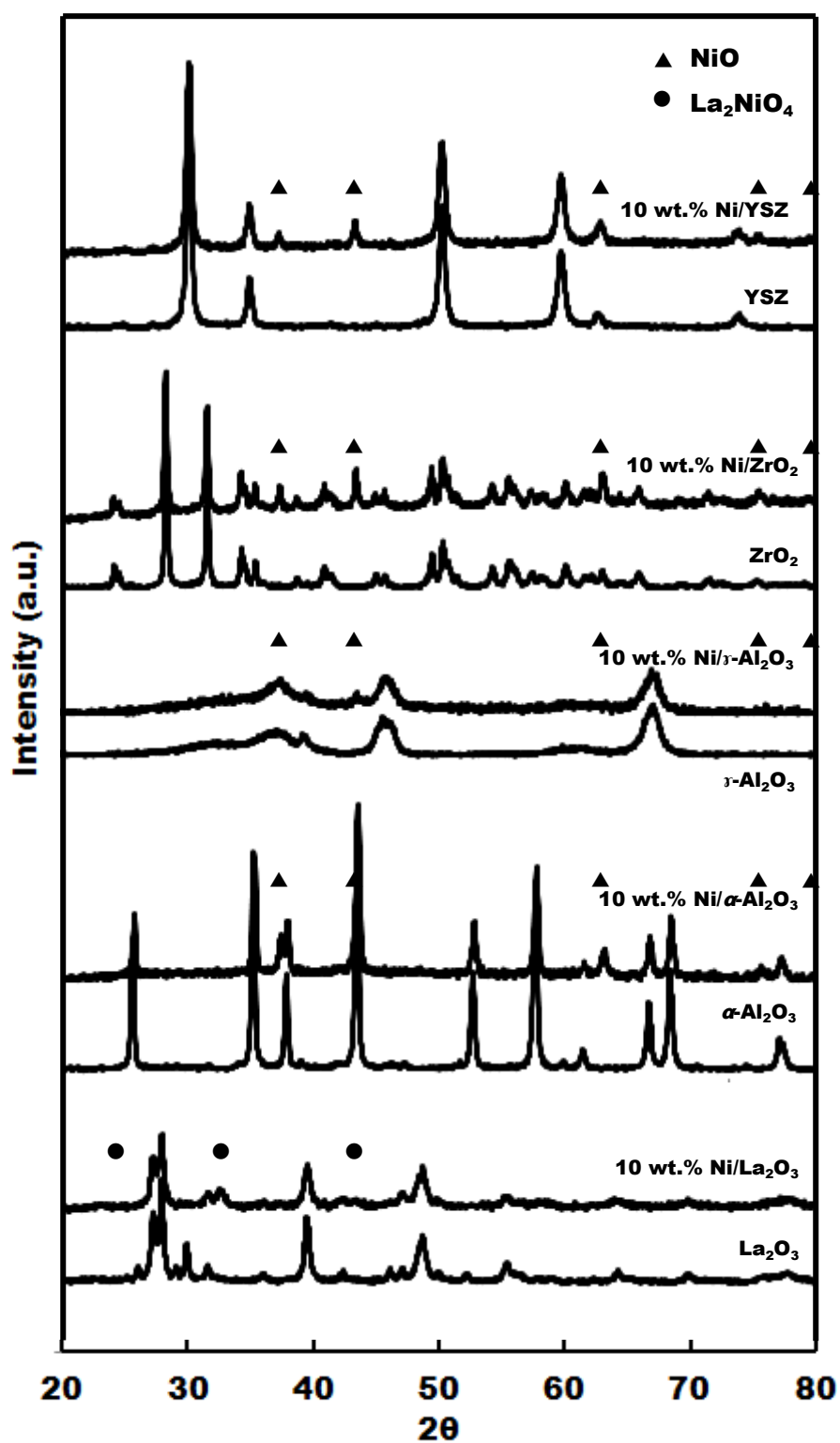
## 10.2 Results and discussion

These results from all experiments were collected until 230 min of time on stream (every 40 min). They were always stable except for some catalysts at high operating temperatures. The reasons included the catalyst fragility, carbon formation, catalyst deactivation, etc.

### 10.2.1 Effect of support and operating temperature

The physical properties of commercial supports were reported in the previous chapter. Table 10.1 shows that surface area values are approximately equivalent to those of cobalt based catalysts:  $Ni/\gamma-Al_2O_3 \gg Ni/La_2O_3 > Ni/YSZ > Ni/\alpha-Al_2O_3 > Ni/ZrO_2$ . Furthermore, pore volume is corresponding to surface area.  $Ni/\gamma-Al_2O_3$  catalyst offers the highest value among the other catalysts. However, 14.9-16.8 nm is the range of pore diameter found in all catalysts excluding of  $Ni/ZrO_2$  catalyst which has the lowest surface area, the lowest pore volume, and the smallest pore diameter compared to the other catalysts. Figure 10.1 provides XRD patterns for different nickel based catalysts after calcination at 973 K. The nickel phase is observed as NiO phase in the  $\alpha-Al_2O_3$ ,  $\gamma-Al_2O_3$ ,  $ZrO_2$ , and YSZ supports. However,  $La_2NiO_4$  phase was found in  $La_2O_3$  support as also reported in the literatures (Slagtern et al. (1997), Luo et al. (1999), Cui et al. (2007)). It probably had some NiO phase when using  $La_2O_3$  support but it was detected at very low signal.

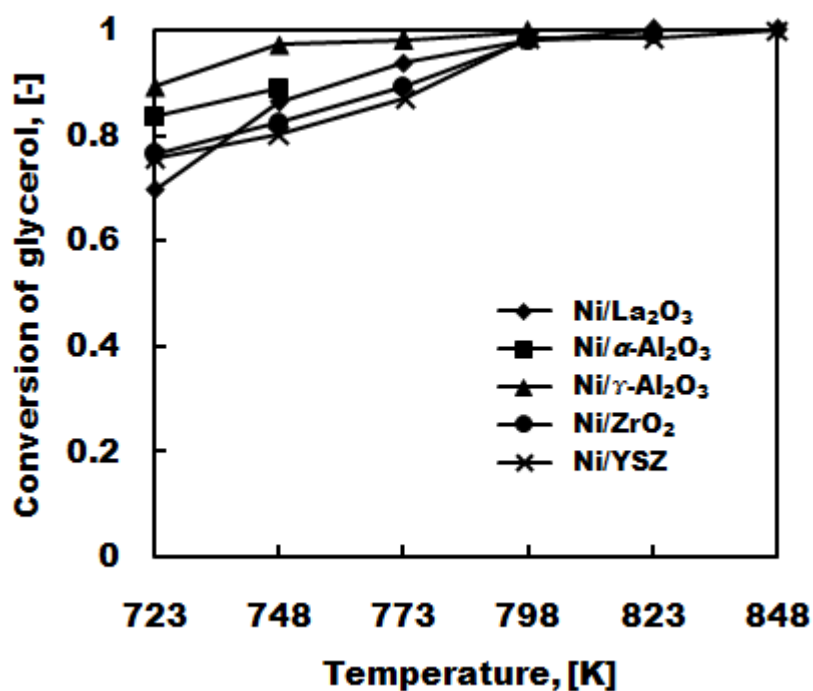




**Figure 10.1** XRD patterns of commercial supports and 10 wt.% of nickel based catalysts

**Table 10.1** Physical properties of 10 wt.% of nickel based catalysts

Nickel catalysts	BET surface area (m <sup>2</sup> /g)	Pore volume (cm <sup>3</sup> /g)	Pore diameter (nm)
Ni/La <sub>2</sub> O <sub>3</sub>	13.49	0.0609	14.936
Ni/ $\alpha$ -Al <sub>2</sub> O <sub>3</sub>	8.58	0.0400	15.886
Ni/ $\gamma$ -Al <sub>2</sub> O <sub>3</sub>	53.60	0.2527	15.789
Ni/ZrO <sub>2</sub>	7.20	0.0211	9.494
Ni/YSZ	10.71	0.0540	16.753



**Figure 10.2** Glycerol conversion at different nickel based catalysts and operating temperatures ( $P = 25$  MPa, medium feed rate of 2.15 g/min, 5 wt.% of feed glycerol concentration, 10 wt.% of nickel loading)

The glycerol conversion was enhanced by increasing of operating temperature as shown in Figure 10.2. Compared to the results in the empty reactor and cobalt based catalysts, nickel based catalysts showed the highest glycerol conversion especially at low operating temperatures. The nearly complete glycerol conversions

were observed for all catalysts since 798 K. On the other hand, Ni/ $\alpha$ -Al<sub>2</sub>O<sub>3</sub>, Ni/ $\gamma$ -Al<sub>2</sub>O<sub>3</sub>, Ni/ZrO<sub>2</sub> and Ni/YSZ catalysts suffered severe coke problem which they could not be operated longer than 230 min at 748, 798, 823, and 848 K, respectively. The high acidic property of Al<sub>2</sub>O<sub>3</sub> supports clearly contributes to the failure system by catalyzing of carbon formation pathways as same as the cobalt based catalysts. However, ZrO<sub>2</sub>, and YSZ also had the similar problem, causing high fluctuated product flow rates at high operating temperatures. The highest glycerol conversion of Ni/ $\gamma$ -Al<sub>2</sub>O<sub>3</sub> catalyst was obtained during low operating temperatures corresponding with the highest glycerol conversion from Co/ $\gamma$ -Al<sub>2</sub>O<sub>3</sub> catalyst. In contrast, Ni/ $\alpha$ -Al<sub>2</sub>O<sub>3</sub> performed the good activity in glycerol conversion. Unfortunately, carbon formation played a role for this catalyst even at the low operating temperature (748 K). For Ni/La<sub>2</sub>O<sub>3</sub>, Ni/ZrO<sub>2</sub> and Ni/YSZ catalysts, they illustrate the similar increased trends by increasing of operating temperature.

Gas and liquid yields are shown in Figures 10.3 and 10.4 for all catalysts. The explanations for all catalysts were described as follows.

Ni/ $\alpha$ -Al<sub>2</sub>O<sub>3</sub> catalyst was conducted only at two operating temperatures of 723 and 748 K due to the carbon formation problem. Gas products consisted of H<sub>2</sub>, CO<sub>2</sub>, CH<sub>4</sub>, and low amount of CO components. It offered the highest H<sub>2</sub> yield compared to the other catalysts at low operating temperatures. It was found that only small liquid yields contained acetaldehyde (Equations (2.18)) and acetol (Equation (2.21)). It indicated that liquid products could be further reacted (Equations (2.19),(2.10),(2.20),(2.21),(2.25)) forming gas products. Carbon formation which was a major cause for the breakdown system is like to occur via Equations (2.12),(2.13),(2.16) especially when increasing of the operating temperature.

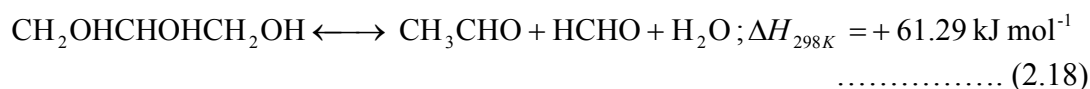
Ni/ $\gamma$ -Al<sub>2</sub>O<sub>3</sub> catalyst was found to be a poor catalyst for hydrogen production in the supercritical water conditions. Low H<sub>2</sub> yield was obtained for all ranges of operating temperature. The main product was acetaldehyde in the liquid phase (Equation (2.18)). However, acetaldehyde yield was decreased from 0.81 to 0.59 by increasing of operating temperature. It was clear that more amount of CO was produced from the decomposition of acetaldehyde (Equation (2.25)) and CH<sub>4</sub> was

probably reformed to H<sub>2</sub>, CO and CO<sub>2</sub> by methane steam reforming (Equations (11),(12)). Other liquid products included acetic acid, methanol, ethanol and acetol.

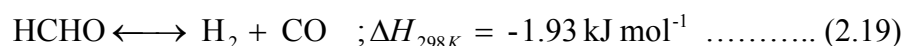
Ni/YSZ catalyst was found to favor the hydrogen production even at low operating temperatures. H<sub>2</sub> yield was increased from 1.89 to 3.63 by increasing operating temperature from 723 to 848 K. Unfortunately, the carbon formation was obtained at 848 K, resulting in the failure system before 230 min. CO<sub>2</sub> and CH<sub>4</sub> yields were also increased following H<sub>2</sub> gas yield but CO yield was detected with a small content. In addition, liquid products were minimized with this catalyst during all operating temperatures and particularly low acetaldehyde yield was observed at low operating temperature. It can be concluded that Ni/YSZ catalyst performed a good ability in gasification of liquid glycerol to gas products.

Ni/ZrO<sub>2</sub> and Ni/La<sub>2</sub>O<sub>3</sub> catalysts offered almost the similar product distributions. About the gas yields, around 0.29-0.40 of H<sub>2</sub> yield was obtained at 723 K but the values were significantly increased by increasing operating temperature until 773 K and then lesser increase was detected at higher operating temperatures. The similar trends of CO<sub>2</sub>, and CH<sub>4</sub> yields were exhibited by increasing of operating temperature with suppression of CO yields at high operating temperatures. For liquid yields, acetaldehyde, acetic acid, methanol, acetol, and ethanol were found at high yields at low operating temperature. The increasing of operating temperature strongly resulted in decreasing liquid yields and totally gasified at 823-848 K. It was clear that higher operating temperature was favored to produce more products in gas phase such as H<sub>2</sub>, CO<sub>2</sub>, and CH<sub>4</sub>. For example, acetaldehyde, and acetic acid were decomposed to gas products by Equations (2.25),(2.27), respectively. Marino et al. (2001) explained that nickel based catalysts favored to both reactions. Only Ni/ZrO<sub>2</sub> catalyst was found to suffer from serious carbon formation, leading to early system shut down at high operating temperature (823K).

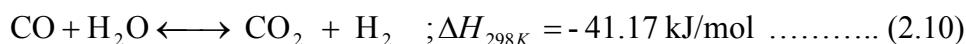
Decomposition of glycerol:



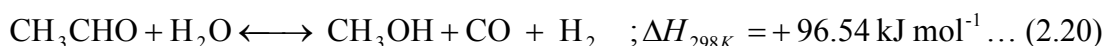
Decomposition of formaldehyde:



Water Gas Shift (WGR or reverse of this is called RWGS):



Acetaldehyde steam reforming:



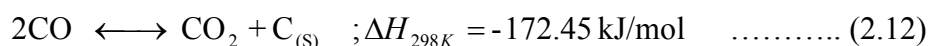
Dehydration of glycerol:



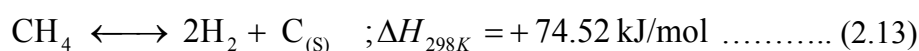
Methanol steam reforming:



Boudouard reaction:



Methane cracking:



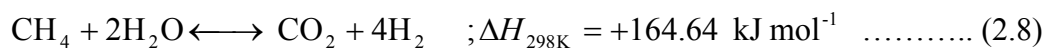
C<sub>2</sub>H<sub>4</sub> cracking:

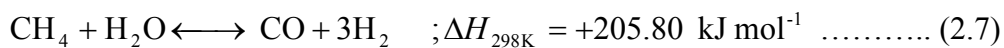


Decomposition of acetaldehyde:

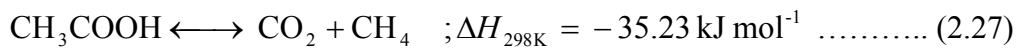


Methane steam reforming:

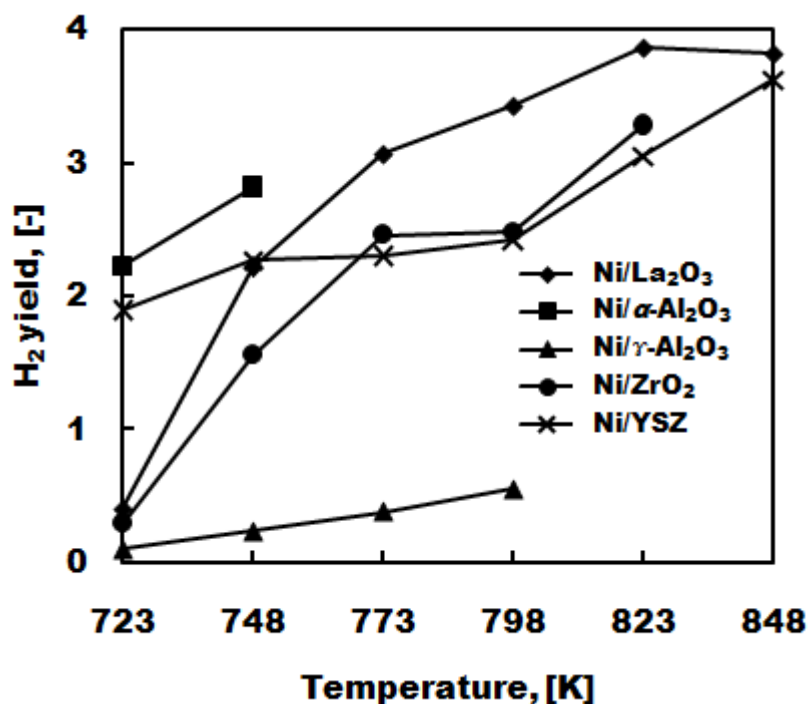




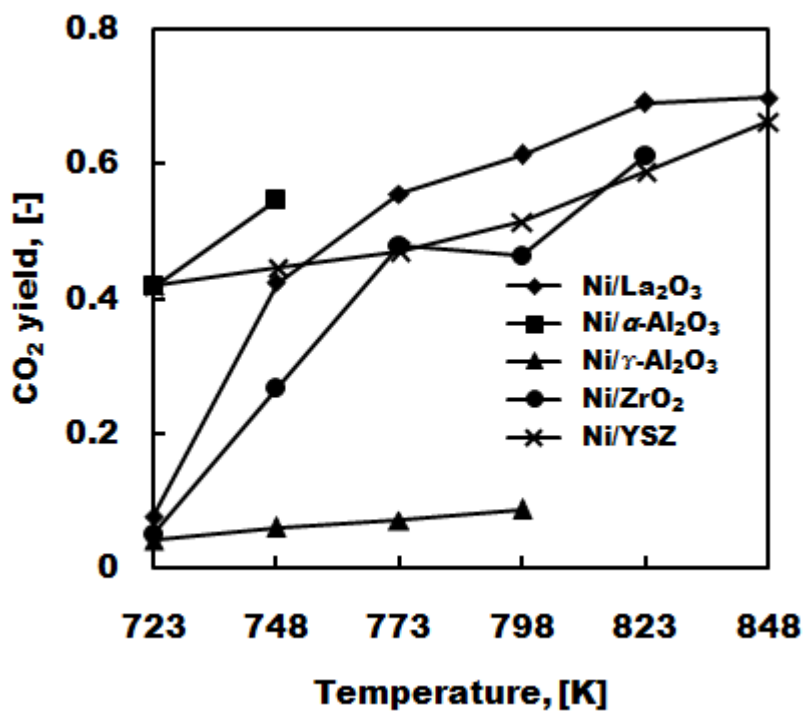
Decomposition of acetic acid:



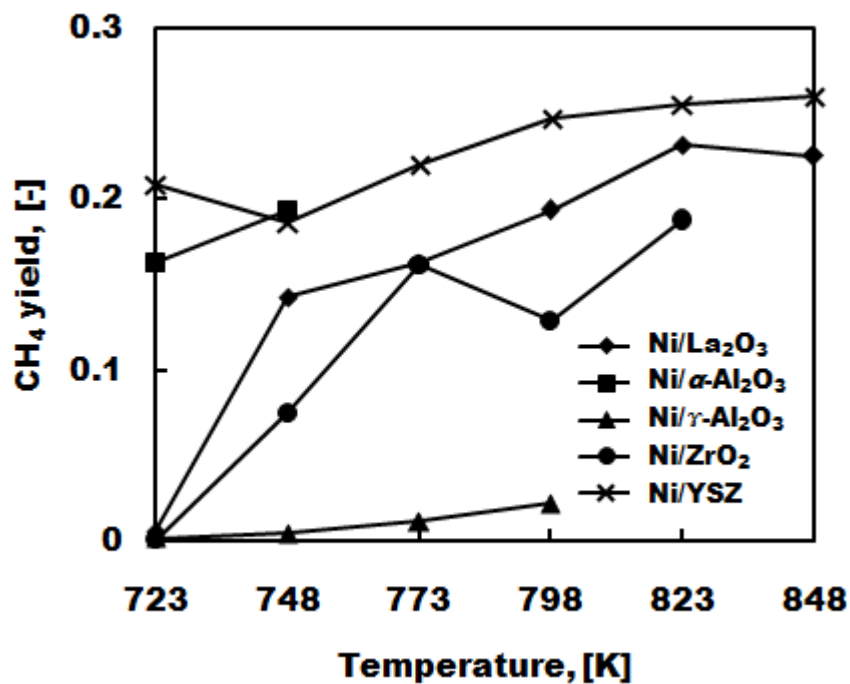
a



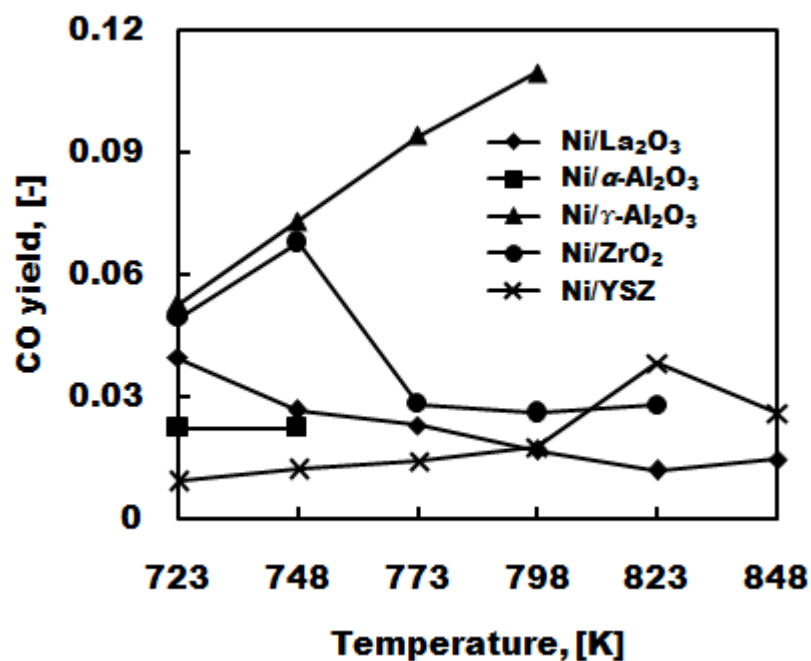
b



c

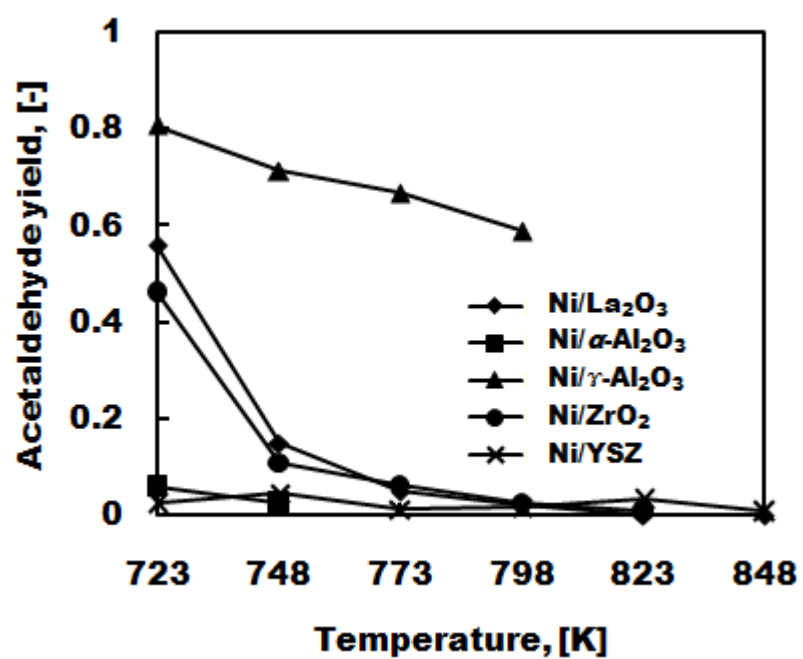


d

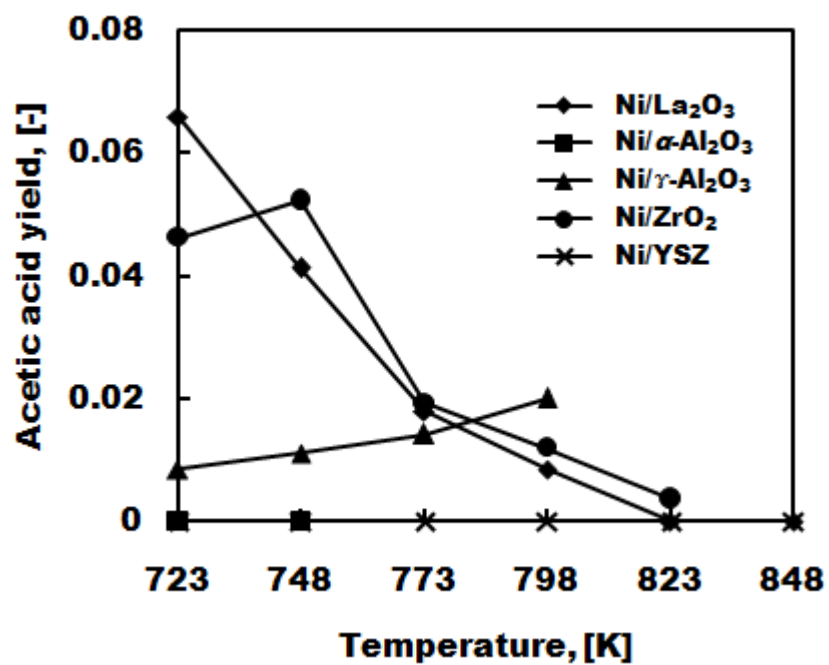


**Figure 10.3** Gas yields of (a) H<sub>2</sub>, (b) CO<sub>2</sub>, (c) CH<sub>4</sub>, (d) CO at different nickel based catalysts and operating temperatures ( $P = 25$  MPa, medium feed rate of 2.15 g/min, 5 wt.% of feed glycerol concentration, 10 wt.% of nickel loading)

a

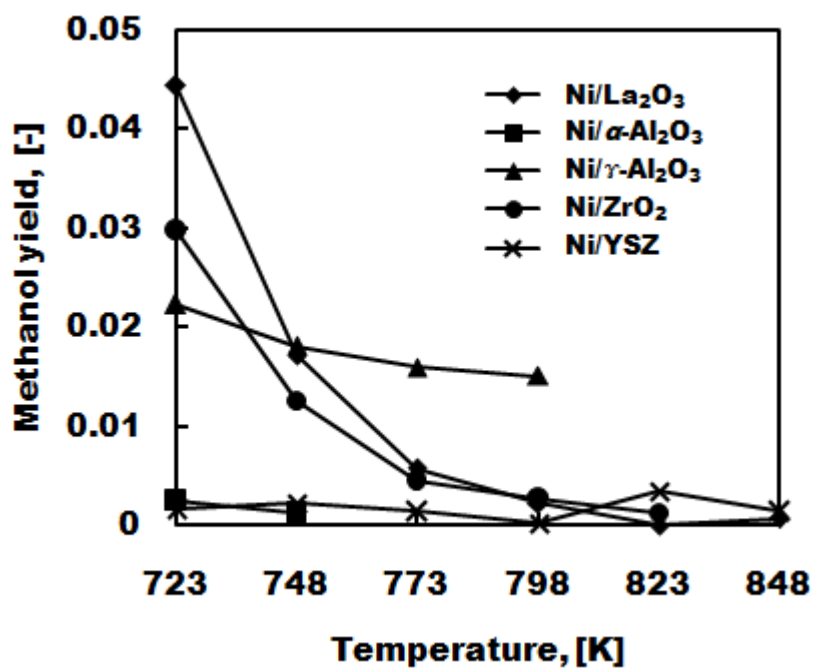


b

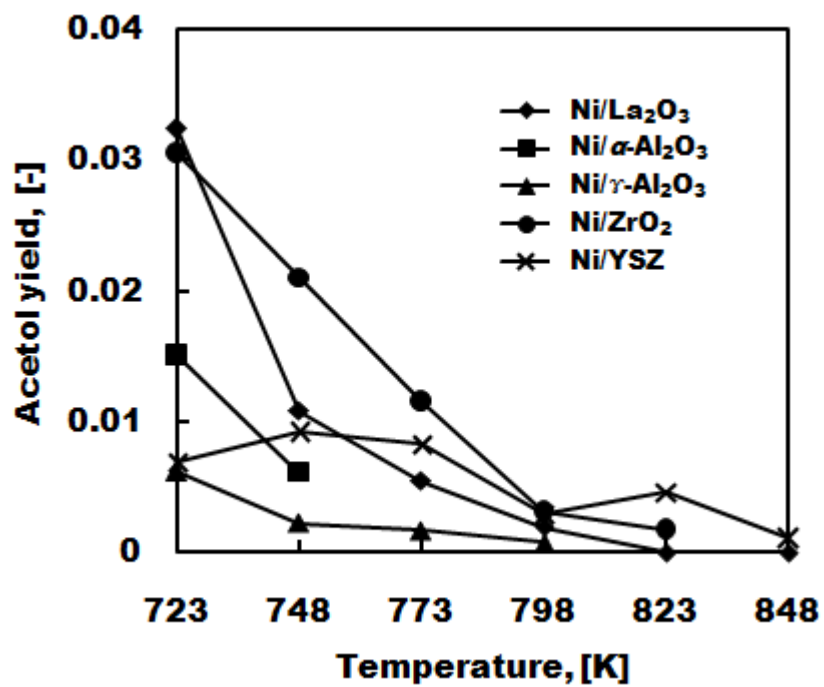


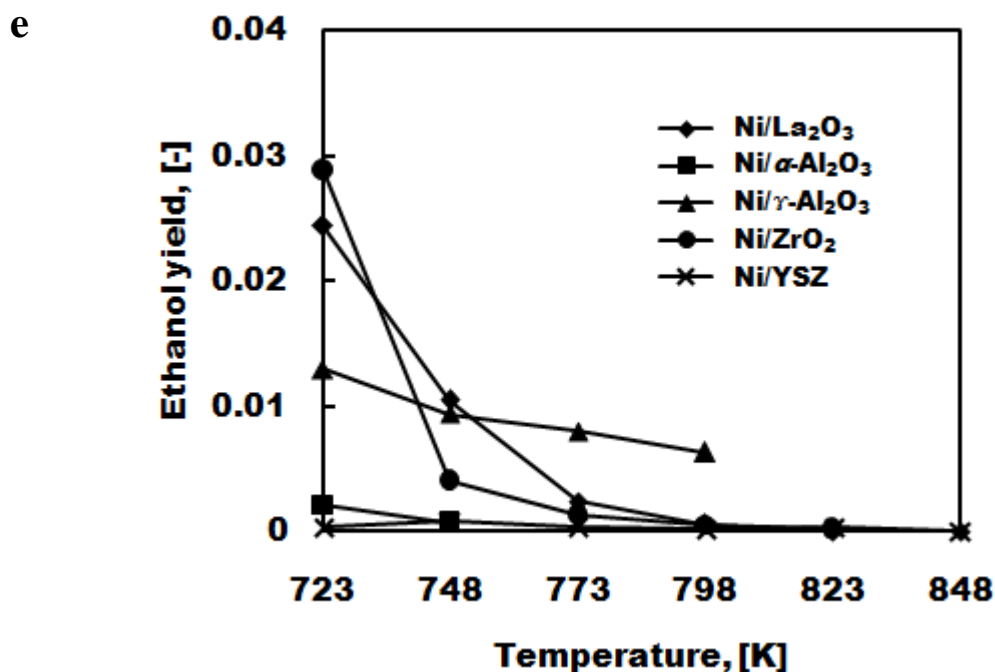


c



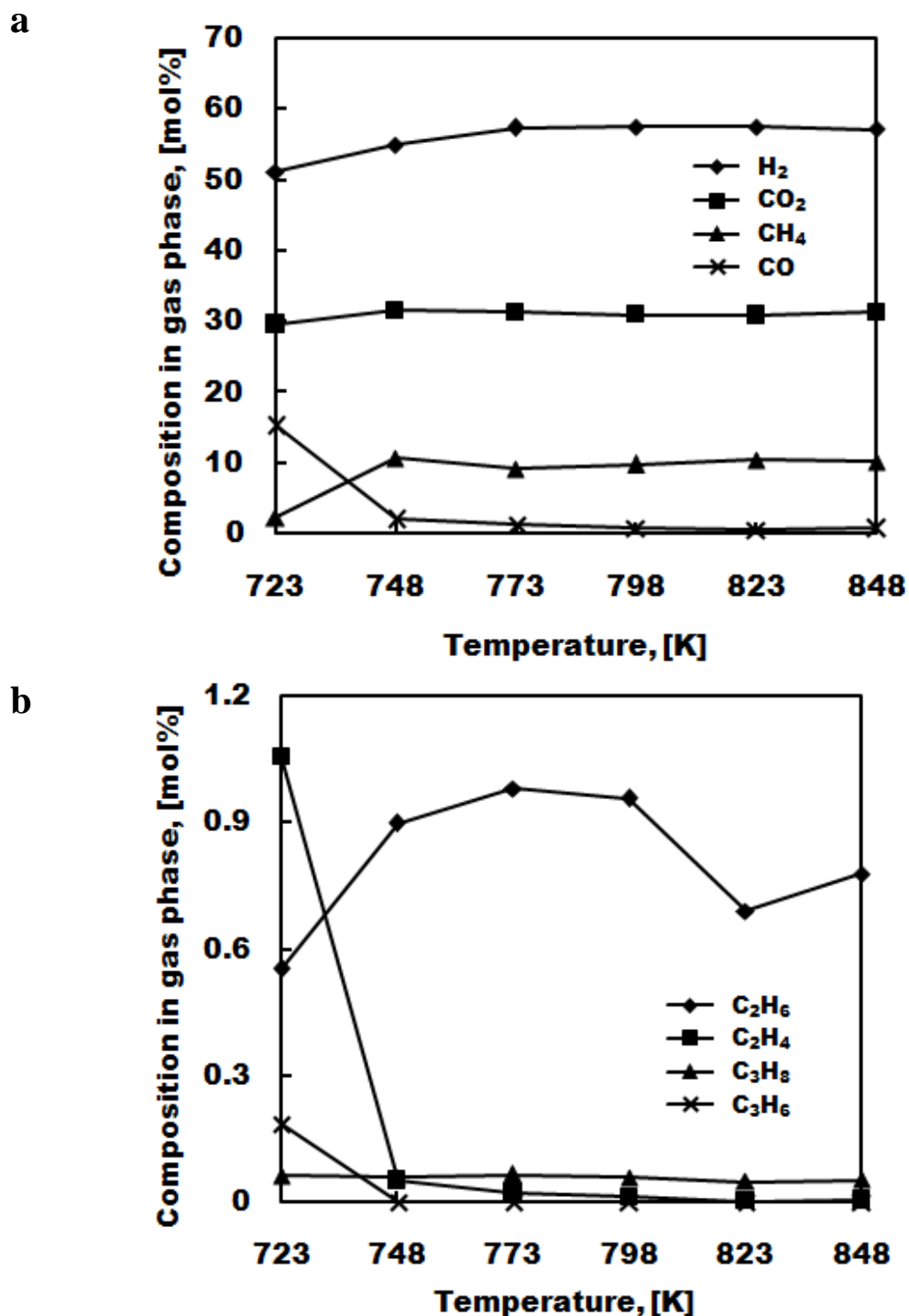
d





**Figure 10.4** Liquid yields of (a) acetaldehyde, (b) acetic acid, (c) methanol, (d) acetol, (e) ethanol at different nickel based catalysts and operating temperatures ( $P = 25$  MPa, medium feed rate of 2.15 g/min, 5 wt.% of feed glycerol concentration, 10 wt.% of nickel loading)

Among all the catalysts, Ni/La<sub>2</sub>O<sub>3</sub> catalyst performed the best performance in hydrogen production without severe carbon formation problem. Therefore, the further study on Ni/La<sub>2</sub>O<sub>3</sub> catalyst was chosen to investigate the effect of other parameters such as feed rate, feed glycerol concentration, and nickel loading. However, the compositions in gas phase depending on the operating temperature were shown in Figures 10.5(a),(b). Carbon monoxide was inhibited by increasing of operating temperature from 723 to 748 K. In contrast, methane was the promoted product instead of carbon monoxide. No significant change in main gas components (H<sub>2</sub>, CO<sub>2</sub>, CH<sub>4</sub>, and CO) was observed above 748 K of operating temperature. For C<sub>2-3</sub> gas products, high amount of C<sub>2</sub>H<sub>6</sub> (< 1%) was observed for all ranges of operating temperature but C<sub>2</sub>H<sub>4</sub>, C<sub>3</sub>H<sub>8</sub>, and C<sub>3</sub>H<sub>6</sub> were depressed after 748 K similar to that of CO.



**Figure 10.5** Compositions of gas products (a) H<sub>2</sub>, CO<sub>2</sub>, CH<sub>4</sub>, and CO (b) C<sub>2</sub>H<sub>6</sub>, C<sub>2</sub>H<sub>4</sub>, C<sub>3</sub>H<sub>8</sub>, C<sub>3</sub>H<sub>6</sub> as a function of operating temperature by using of 10 wt.% Ni/La<sub>2</sub>O<sub>3</sub> catalyst ( $P = 25$  MPa, medium feed rate of 2.15 g/min, 5 wt.% of feed glycerol concentration)

### 10.2.2 Effect of feed rate

From the previous part, the highest H<sub>2</sub> yield was obtained at 823 K. This operating temperature was higher than the case with using cobalt based catalysts for 25 K. Considering the operating temperature of 798 K, it also produced high H<sub>2</sub> yield (3.42) with a small acetaldehyde yield (0.02) – the H<sub>2</sub> yield was slightly less than at 823 K. Thus, 798 K was chosen as an operating temperature in the subsequent study. Three feed rates were investigated including low feed rate (1.05 g/min), medium feed rate (2.15 g/min), and high feed rate (3.60 g/min) to represent different residence time in the reactor.

Table 10.2 shows the effect of feed rate on glycerol conversion, total gas products flow rate, and gas yields. Note that the carbon formation problem was observed at low feed rate condition after 70 min of time on stream. This condition was reproducible at least twice and exhibited the similar results in carbon formation. It was corresponded to the low feed rate condition in the empty reactor (Chapter VIII) whose carbon formation problem was observed at high operating temperatures. Glycerol conversion was decreased by increasing of feed rate. High feed rate caused the decreasing of glycerol conversion down to 0.93. It was explained that higher residence time in the reactor was required for converting more glycerol to other products. However, the results from using total gas products flow rate at the medium and high feed rates were not significantly different as same as the gas product yields. Figure 10.6 indicates that higher feed rate favored higher concentration of H<sub>2</sub>, and CO but lesser in CO<sub>2</sub> and CH<sub>4</sub>. It was because that higher residence time in the reactor favored methane formation by depressing of CO. H<sub>2</sub> concentration was found to decrease with increasing of CH<sub>4</sub>. For liquid analysis, lower feed rate (higher residence time) was favorable to production of gas phase products. A large acetaldehyde yield was possibly converted to gas products by decreasing feed rate as shown in Table 10.3. However, the drawback of Ni/La<sub>2</sub>O<sub>3</sub> catalyst was the hardness which could easily destroy the catalyst (fragility) at high flowrate of product stream (real gas product flow rate) especially gas product. The fragile catalyst could possible plug at the BPR, leading to failure system. Therefore, the medium feed rate was considered

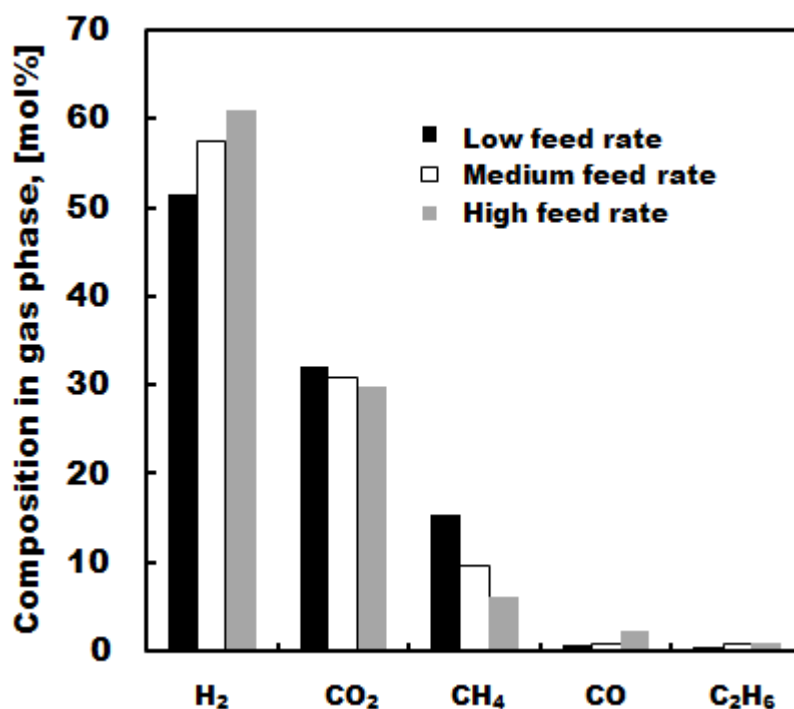
to represent the optimum feed rate with the highest total gas products flow rate (per mol of glycerol fed) and without plugging of carbon formation in 230 min.

**Table 10.2** Glycerol conversion, total gas products flow rate, and gas yields as a function of feed rates (low feed rate=1.05 g/min, medium feed rate=2.15 g/min, and high feed rate=3.60 g/min) by using of 10 wt.% Ni/La<sub>2</sub>O<sub>3</sub> catalyst ( $T=798$  K,  $P = 25$  MPa, medium feed rate of 2.15 g/min, 5 wt.% of feed glycerol concentration)

Feed rate	Conversion, (-)	Total gas products flow rate (L/mol of glycerol fed)	Yield of				
			H <sub>2</sub>	CO <sub>2</sub>	CH <sub>4</sub>	CO	C <sub>2</sub> H <sub>6</sub>
low	1.00	131.6	2.73	0.57	0.27	0.01	0.01
medium	0.98	147.6	3.42	0.61	0.19	0.02	0.04
high	0.93	146.5	3.60	0.59	0.12	0.04	0.04

**Table 10.3** Liquid yields as a function of feed rates (low feed rate=1.05 g/min, medium feed rate=2.15 g/min, and high feed rate=3.60 g/min) by using of 10 wt.% Ni/La<sub>2</sub>O<sub>3</sub> catalyst ( $T=798$  K,  $P = 25$  MPa, medium feed rate of 2.15 g/min, 5 wt.% of feed glycerol concentration)

Feed rate	Yield of, (-)			
	acetaldehyde	acetic acid	methanol	Acetol
low	0.01	n.d.	trace	trace
medium	0.02	0.01	trace	trace
high	0.10	0.02	0.01	0.01



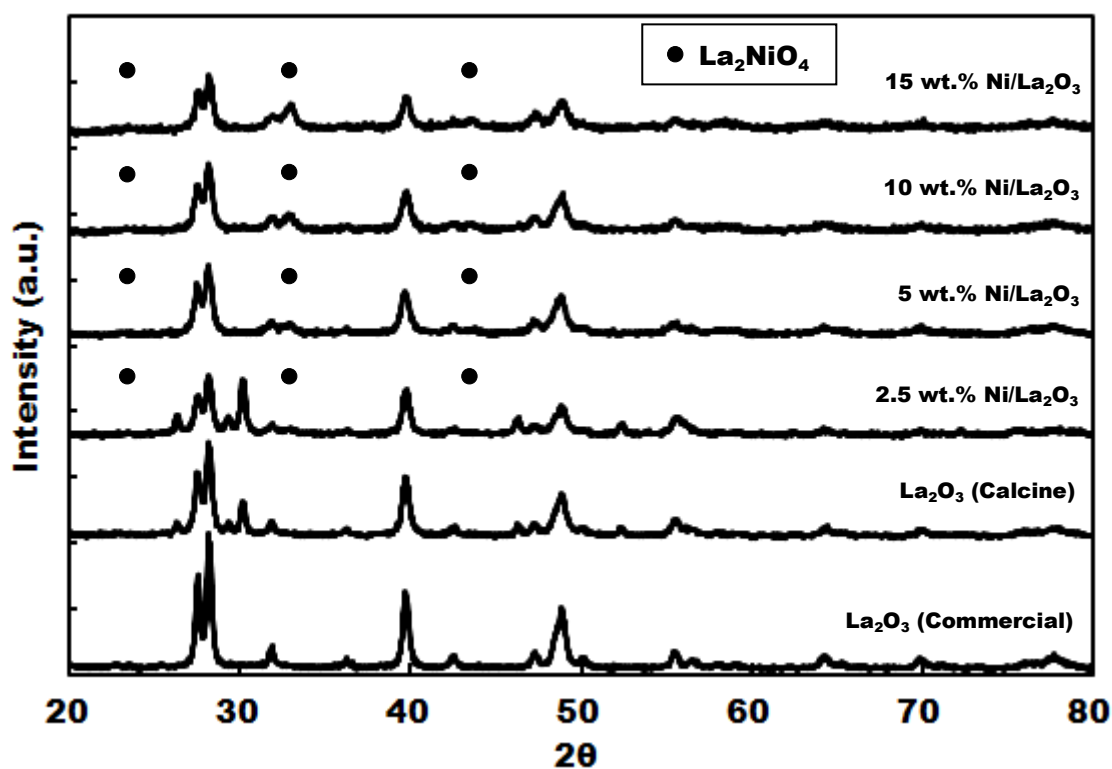
**Figure 10.6** Compositions of gas products as a function of feed rates (low feed rate=1.05 g/min, medium feed rate=2.50 g/min, and high feed rate=3.60 g/min) by using of 10 wt.% Ni/La<sub>2</sub>O<sub>3</sub> catalyst ( $T=798$  K,  $P = 25$  MPa, medium feed rate of 2.15 g/min, 5 wt.% of feed glycerol concentration)

### 10.2.3 Effect of metal loading

The medium feed rate with the operating temperature of 798 K, and 5 wt.% feed glycerol concentration was chosen to investigate the effect of amount of nickel on the La<sub>2</sub>O<sub>3</sub> support. Figure 10.7 confirmed the presence of nickel on the La<sub>2</sub>O<sub>3</sub> by XRD pattern. It was found that the main peaks of La<sub>2</sub>NiO<sub>4</sub> phase were getting higher when more amount of nickel was loaded to the La<sub>2</sub>O<sub>3</sub> support. For the physical properties of La<sub>2</sub>O<sub>3</sub>, and Ni/La<sub>2</sub>O<sub>3</sub> catalysts, surface area was increased by increasing of nickel loading (0-5 wt.%) on La<sub>2</sub>O<sub>3</sub> support which contrasted to the Co/YSZ catalysts as shown in Table 10.4. It probably means that the new phase La<sub>2</sub>NiO<sub>4</sub> (La<sub>2</sub>O<sub>3</sub>+Ni) instead of NiO phase caused to change the surface area of La<sub>2</sub>O<sub>3</sub> support. Approximately higher pore volume and lower in pore diameter were also obtained by increasing of nickel loading. However, surface area was slightly decreased by increasing a large amount nickel loading (5-15 wt.%) corresponding with the Co/YSZ catalysts.

**Table 10.4** Physical properties of  $\text{La}_2\text{O}_3$  support and different nickel loading for  $\text{Ni}/\text{La}_2\text{O}_3$  catalysts

Nickel on $\text{La}_2\text{O}_3$ support	BET surface area ( $\text{m}^2/\text{g}$ )	Pore volume ( $\text{cm}^3/\text{g}$ )	Pore diameter (nm)
$\text{La}_2\text{O}_3$	6.69	0.0291	15.646
2.5 wt.% $\text{Ni}/\text{La}_2\text{O}_3$	10.74	0.0491	15.490
5 wt.% $\text{Ni}/\text{La}_2\text{O}_3$	14.04	0.0572	13.236
10 wt.% $\text{Ni}/\text{La}_2\text{O}_3$	13.49	0.0609	14.936
15 wt.% $\text{Ni}/\text{La}_2\text{O}_3$	12.82	0.0515	12.971



**Figure 10.7** XRD patterns of  $\text{La}_2\text{O}_3$  support and different nickel loading for  $\text{Ni}/\text{La}_2\text{O}_3$  catalysts

The increasing nickel loading on the  $\text{La}_2\text{O}_3$  catalysts slightly enhanced the glycerol conversion whose complete glycerol conversion was achieved at 15 wt.% of nickel loading as shown in Table 10.5. It was observed that increasing of nickel

loading significantly enhanced the H<sub>2</sub>, CO<sub>2</sub>, CH<sub>4</sub> yields but inhibited CO yield excluding the H<sub>2</sub>, and CO<sub>2</sub> yields at 10 wt.% of nickel loading (to be discussed in the next paragraph). Only La<sub>2</sub>O<sub>3</sub> support without nickel loading expressed very high CO yield as same as the empty reactor condition from Chapter VIII. It can be concluded that nickel has an important role to improve the hydrogen production and suppress the carbon monoxide formation. Furthermore, it was found that gas product distribution instantly corresponded to the gas yield. Figures 10.8(a) shows that CO concentration was continuously decreased by increasing of nickel loading; completely distinguished to the CH<sub>4</sub> concentration. However, the increasing of H<sub>2</sub> and CO<sub>2</sub> concentrations were obtained during of 0-5 wt.% of nickel loading, then the similar concentrations were remained rather constant (58 mol% H<sub>2</sub>, 30 mol% of CO<sub>2</sub>) by increasing of nickel loading. Among C<sub>2-3</sub> hydrocarbon gas products, C<sub>2</sub>H<sub>6</sub> was observed as the highest content as same as the previous reports from empty reactor and cobalt based catalysts. Nevertheless, all of them were decreased by increasing of nickel loading as shown in Figure 10.8(b). In the liquid analysis, acetaldehyde yield was totally decreased by increasing nickel loading as same as other liquid products including methanol, acetone, acitic acid, ethanol, and acrylic acid. Note that various liquid products were found without nickel appearance.

**Table 10.5** Glycerol conversion, and gas yields as a function of nickel loading for Ni/La<sub>2</sub>O<sub>3</sub> catalysts ( $T=798$  K,  $P=25$  MPa, medium feed rate of 2.15 g/min, 5 wt.% of feed glycerol concentration)

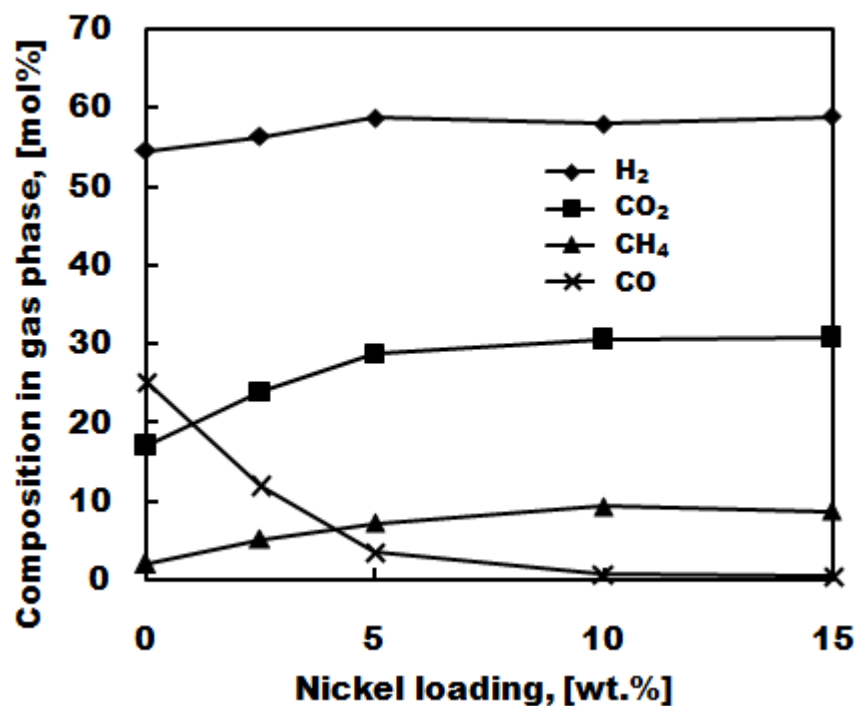
Nickel loading, (wt.%)	Conversion, (-)	Yield of, (-)					
		H <sub>2</sub>	CO <sub>2</sub>	CH <sub>4</sub>	CO	C <sub>2</sub> H <sub>6</sub>	C <sub>2</sub> H <sub>4</sub>
0	0.96	1.52	0.16	0.02	0.23	0.01	trace
2.5	0.97	2.36	0.33	0.07	0.17	0.06	0.01
5	0.98	3.69	0.60	0.15	0.08	0.06	trace
10	0.98	3.42	0.61	0.19	0.02	0.04	trace
15	1.00	4.26	0.74	0.21	0.01	0.04	trace



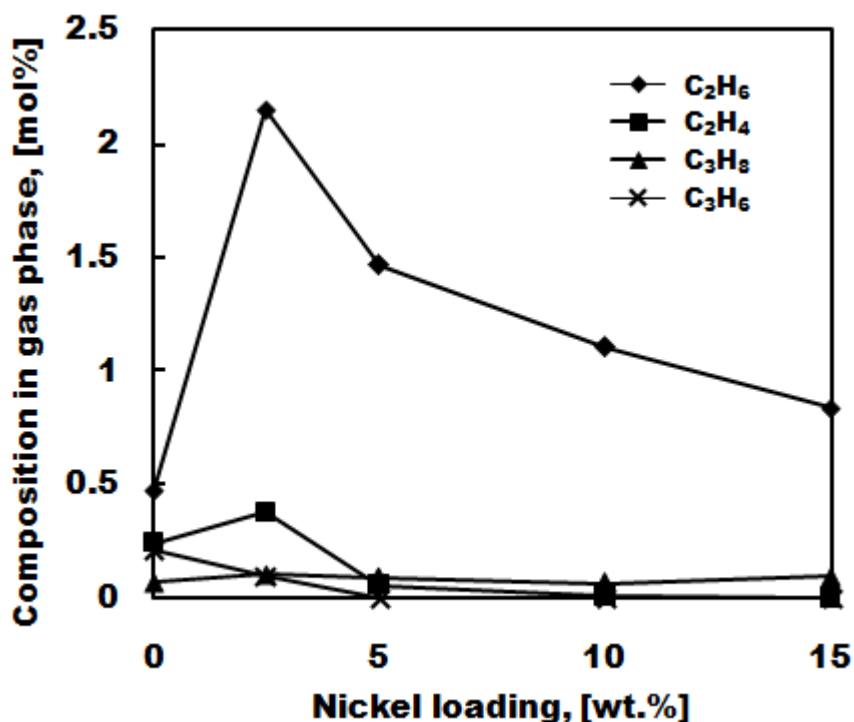
**Table 10.6** Liquid yields as a function of nickel loading for Ni/La<sub>2</sub>O<sub>3</sub> catalysts ( $T=773$  K,  $P = 25$  MPa, medium feed rate of 2.15 g/min, 5 wt.% of feed glycerol concentration)

Nickel loading, (wt.%)	Yield of, (-)					
	acetaldehyde	methanol	acetone	acetic acid	ethanol	acrylic acid
0	0.46	0.07	0.05	0.03	0.03	0.03
2.5	0.12	0.03	0.02	0.03	0.01	trace
5	0.07	0.01	0.01	0.02	trace	trace
10	0.02	trace	trace	0.01	trace	trace
15	trace	trace	trace	trace	trace	Trace

a



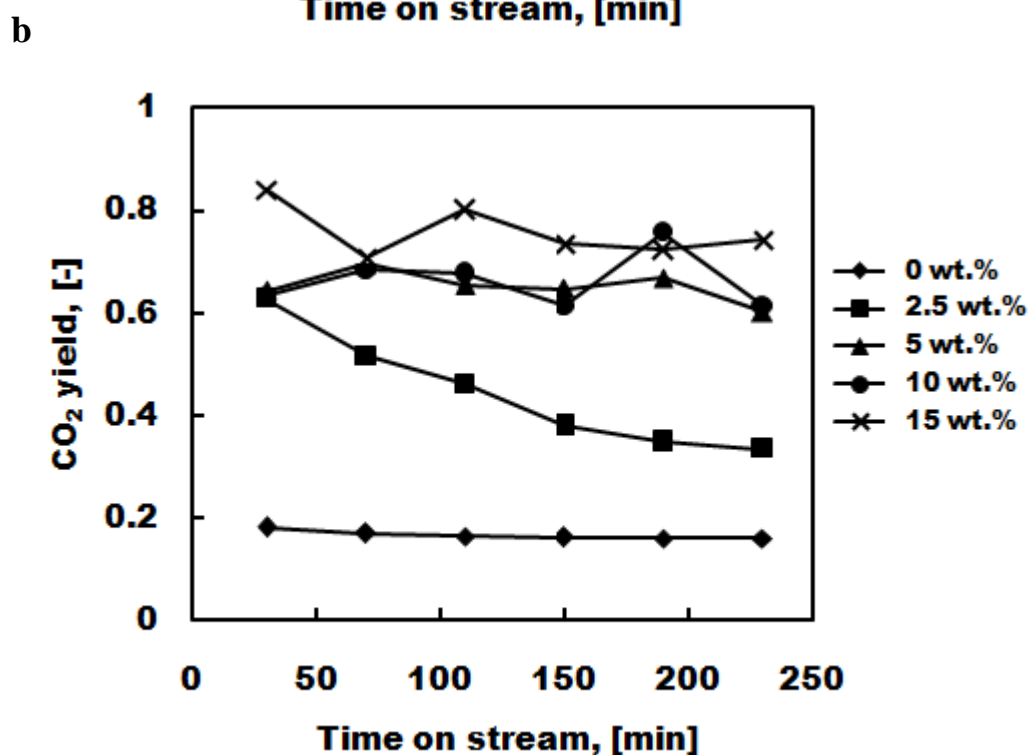
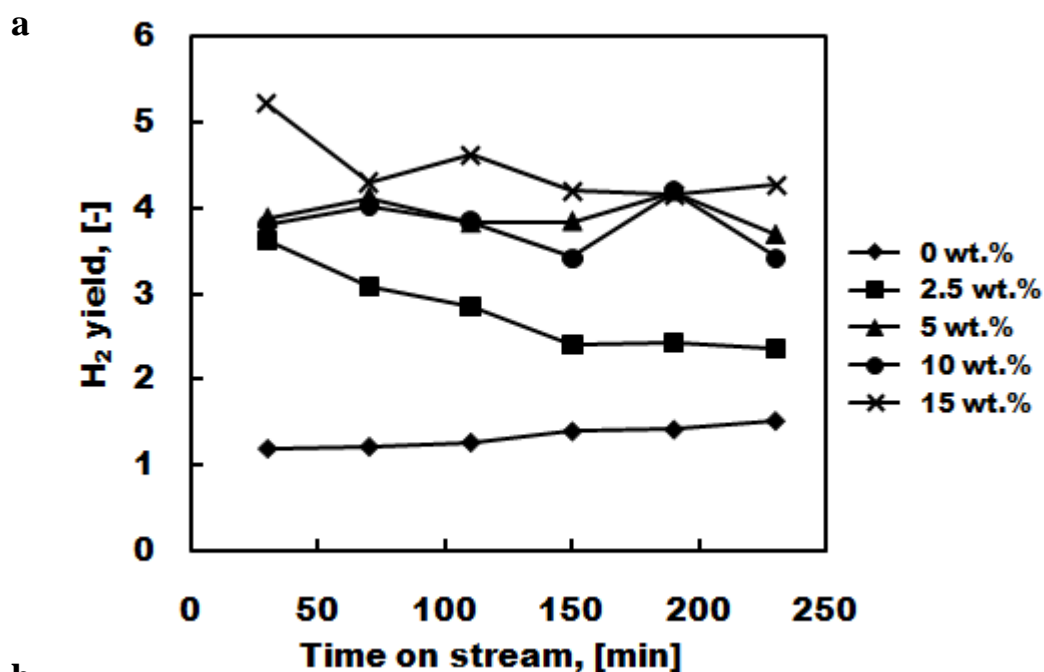
b



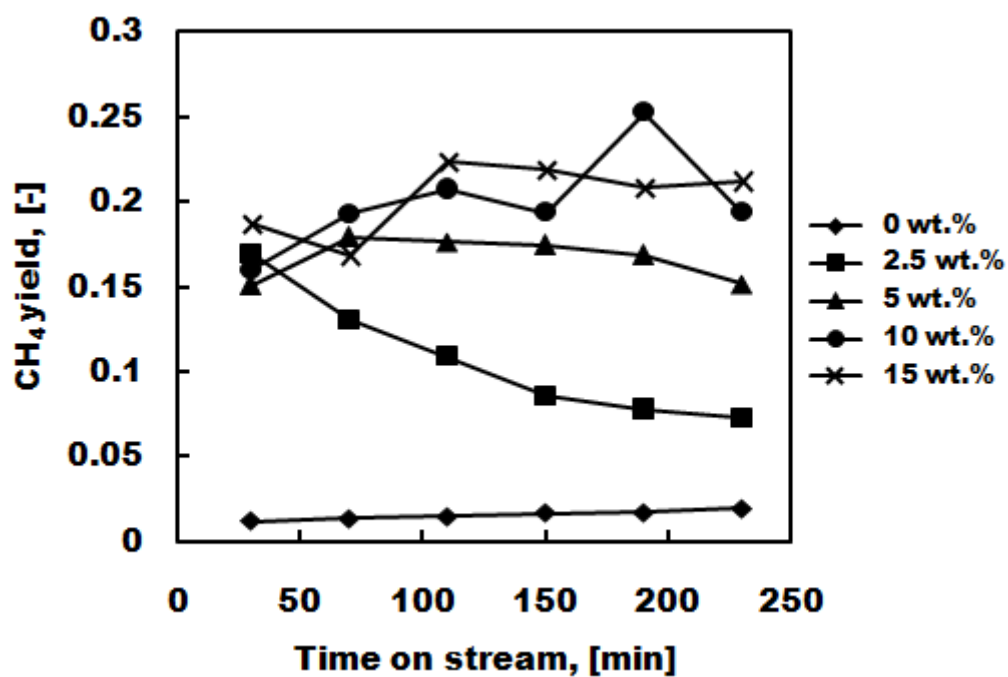
**Figure 10.8** Compositions of gas products (a) H<sub>2</sub>, CO<sub>2</sub>, CH<sub>4</sub>, and CO (b) C<sub>2</sub>H<sub>6</sub>, C<sub>2</sub>H<sub>4</sub>, C<sub>3</sub>H<sub>8</sub>, C<sub>3</sub>H<sub>6</sub> as a function of nickel loading for Ni/La<sub>2</sub>O<sub>3</sub> catalysts ( $T=798$  K,  $P = 25$  MPa, medium feed rate of 2.15 g/min, 5 wt.% of feed glycerol concentration)

The catalytic stability was also considered with the individual amount of nickel loading on La<sub>2</sub>O<sub>3</sub> support by varying of time on stream parameter from 30 to 230 min (Figures 10.9a-e). For 2.5 wt.% Ni/La<sub>2</sub>O<sub>3</sub> catalyst, the H<sub>2</sub>, CO<sub>2</sub>, CH<sub>4</sub> yields were dramatically decreased especially when increasing time on stream within 30-150 min. It was clear that the catalyst lost the catalytic stability by observing more CO and acetaldehyde yields in the product stream. For 5-15 wt.% Ni/La<sub>2</sub>O<sub>3</sub> catalysts, the average H<sub>2</sub> yields were slightly increased especially between 5 and 10 wt.% of nickel loading. It explained that the more favorable CH<sub>4</sub> formation was found to make almost the similar H<sub>2</sub> yields even increasing of nickel loading from 5 to 15 wt.%. The increasing of CO, and acetaldehyde yields were found by increasing time on stream with 0-5 wt.% of nickel loadings. However, this behavior was not occurred with 10, and 15 wt.% of nickel loading. In addition, acetaldehyde and other liquid yields were completely suppressed for all ranges of time on stream when increasing nickel loading

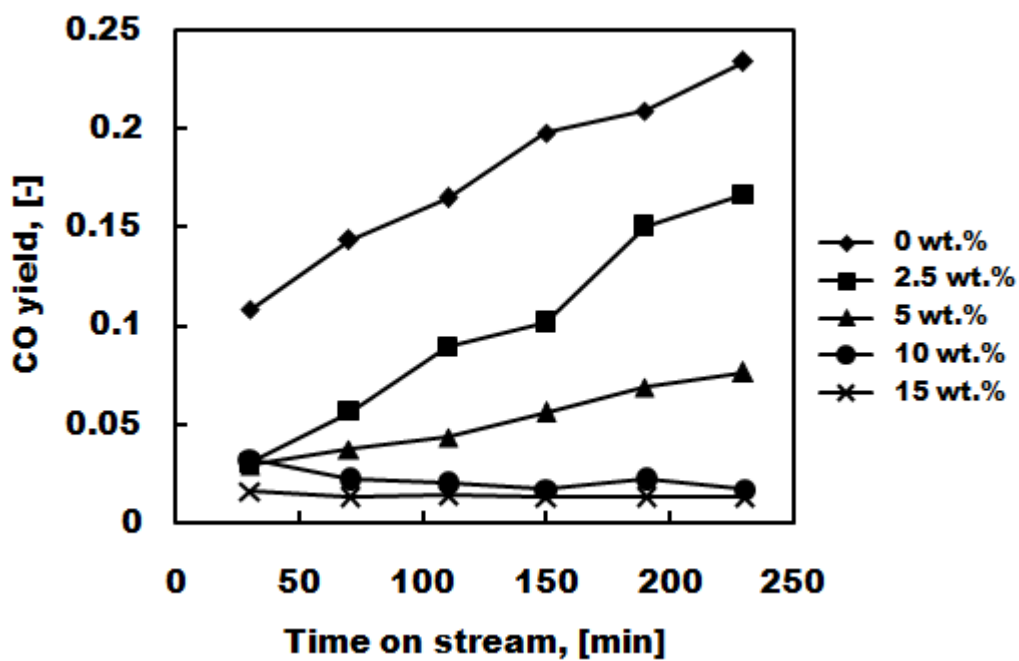
to 15 wt.%. Therefore, without liquid products from this condition, H<sub>2</sub> yield could be slightly improved even high CH<sub>4</sub> yield was observed. It can be concluded that 15 wt.% Ni/La<sub>2</sub>O<sub>3</sub> catalyst performed the high stability in 230 min of time on stream and the best results by offering the highest H<sub>2</sub> yield about 4.26, and complete gasification of glycerol. Note that high amount of nickel loading helped to extend the catalytic stability of catalyst in supercritical water condition.



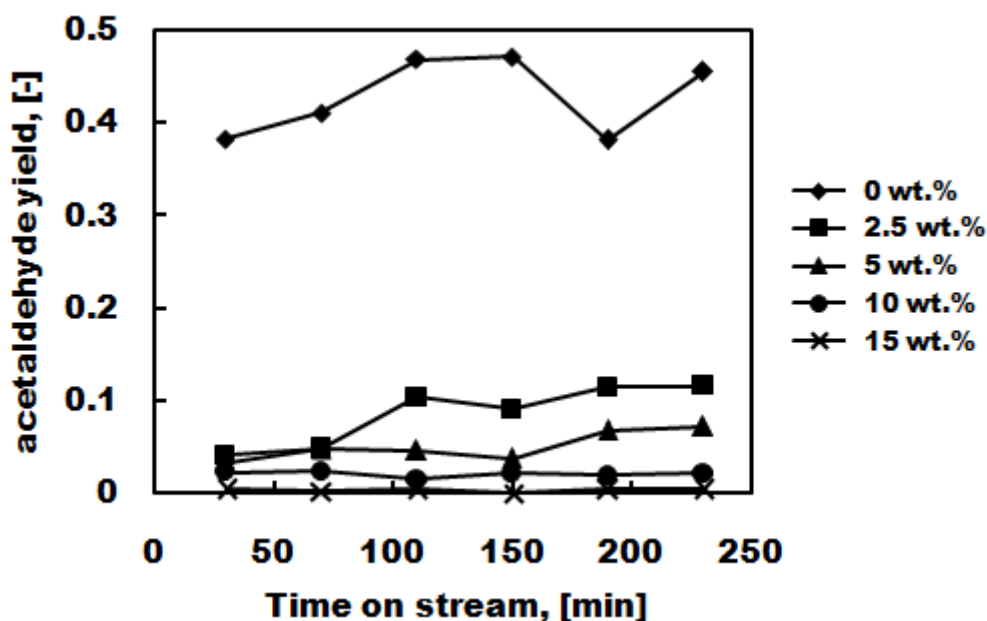
c



d



e

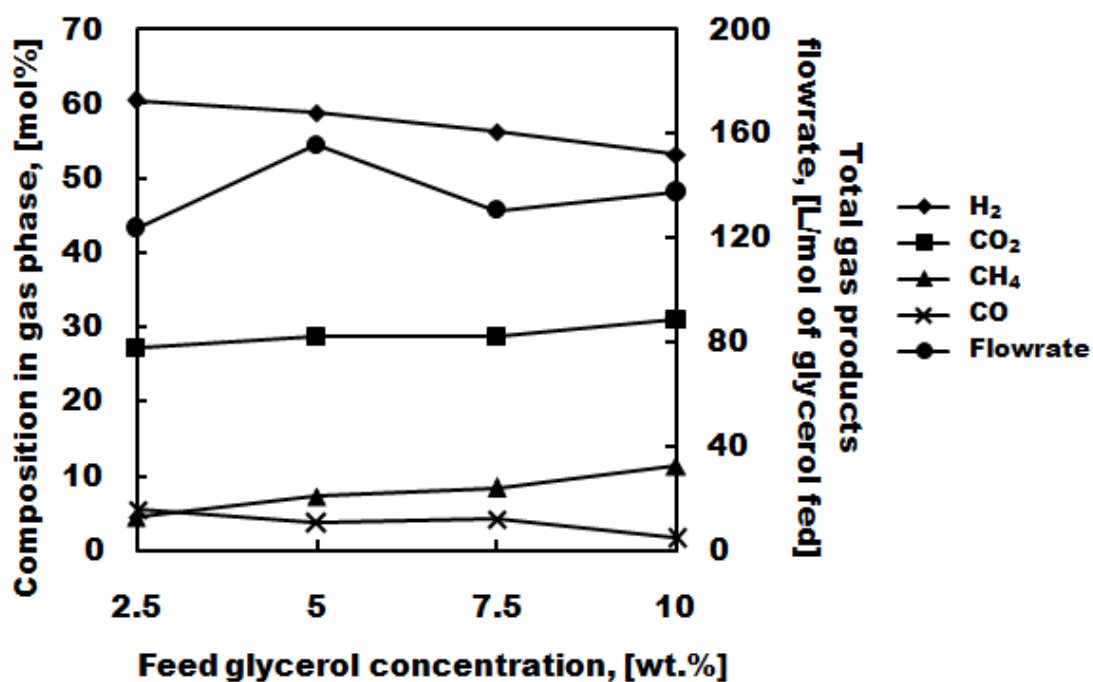


**Figure 10.9** Gas yields of (a) H<sub>2</sub>, (b) CO<sub>2</sub>, (c) CH<sub>4</sub>, (d) CO and liquid yield of (e) acetaldehyde at different percent nickel loading for Ni/La<sub>2</sub>O<sub>3</sub> catalysts and time on stream ( $T = 708$  K,  $P = 25$  MPa, medium feed rate of 2.15 g/min, 5 wt.% of feed glycerol concentration)

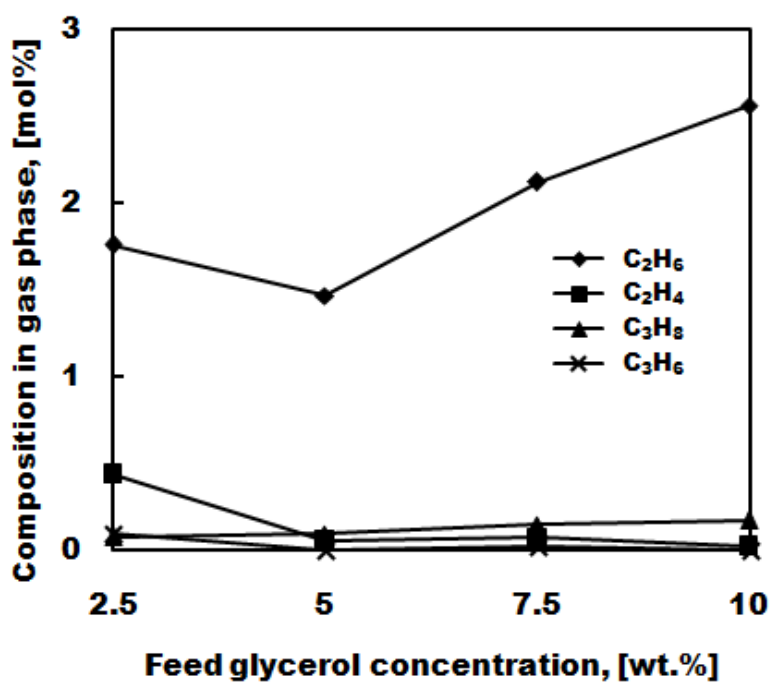
#### 10.2.4 Effect of feed glycerol concentration

Feed glycerol concentration is an important parameter to affect the productivity in supercritical water as reported in the previous study in the empty reactor condition. Taylor et al. (2003) explained that this parameter involved changing of the residence time in the reactor. Figure 10.10 indicates that H<sub>2</sub> and CO concentrations were decreased but CH<sub>4</sub> concentration was increased with increasing feed glycerol concentration. It was explained that higher feed glycerol concentration favored the methane formation (Equation (2.7)) by reducing of H<sub>2</sub> and CO concentrations. It also corresponded to the equation that less amount of water (higher feed glycerol concentration) shifted the equilibrium backward to the left hand side. However, this behavior is in contrast with the empty reactor condition at which the CO formation was promoted to the CO formation by increasing feed glycerol concentration, resulting in decreasing of CO<sub>2</sub> concentration but constant in CH<sub>4</sub> concentration.

a



b



**Figure 10.10** Compositions of gas products (a) H<sub>2</sub>, CO<sub>2</sub>, CH<sub>4</sub>, CO, and total gas products flow rate (b) C<sub>2</sub>H<sub>6</sub>, C<sub>2</sub>H<sub>4</sub>, C<sub>3</sub>H<sub>8</sub>, C<sub>3</sub>H<sub>6</sub> as a function of feed glycerol concentration for Ni/La<sub>2</sub>O<sub>3</sub> catalysts ( $T=798$  K,  $P = 25$  MPa, medium feed rate of 2.15 g/min, 5 wt.% of feed glycerol concentration, 5 wt.% of nickel loading)

Figure 10.10a shows that the highest total gas products flowrate was obtained at 5 wt.% feed glycerol concentration. Focusing on the gas yields, the highest H<sub>2</sub> yield was found at 5 wt.% feed glycerol concentration. In addition, trends of CO, CH<sub>4</sub>, and C<sub>2</sub>H<sub>6</sub> yields seemed to follow the gas products distribution as shown in Table 10.7. No significant change was found in term of glycerol conversion by increasing of feed glycerol concentration, However, all liquid yields including acetaldehyde, methanol, acetic acid and acetone did not have a obvious trend with increasing feed glycerol concentration but the highest liquid yields was clearly appeared at 2.5 wt.% feed glycerol concentration as shown in Table 10.8.

**Table 10.7** Glycerol conversion, and gas yields as a function of feed glycerol concentration for Ni/La<sub>2</sub>O<sub>3</sub> catalysts ( $T=798$  K,  $P = 25$  MPa, medium feed rate of 2.15 g/min, 5 wt.% of feed glycerol concentration, 5 wt.% of nickel loading)

Feed glycerol conc, (wt%)	Conver- sion, (-)	Yield of, (-)						
		H <sub>2</sub>	CO <sub>2</sub>	CH <sub>4</sub>	CO	C <sub>2</sub> H <sub>6</sub>	C <sub>2</sub> H <sub>4</sub>	C <sub>3</sub> H <sub>8</sub>
2.5	0.99	3.02	0.45	0.07	0.09	0.06	0.01	trace
5	0.98	3.69	0.60	0.15	0.08	0.06	trace	0.01
7.5	0.98	2.96	0.50	0.15	0.07	0.07	trace	0.01
10	0.98	2.96	0.57	0.21	0.03	0.09	trace	0.01

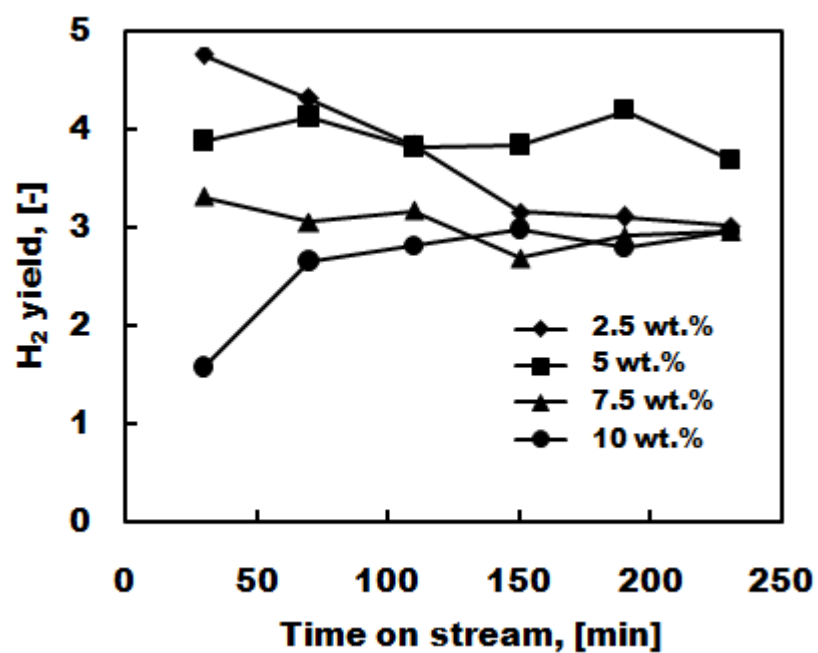
**Table 10.8** Liquid yields as a function of feed glycerol concentration for Ni/La<sub>2</sub>O<sub>3</sub> catalysts ( $T=798$  K,  $P = 25$  MPa, medium feed rate of 2.15 g/min, 5 wt.% of feed glycerol concentration, 5 wt.% of nickel loading)

Feed glycerol conc, (wt.%)	Yield of, (-)			
	acetaldehyde	methanol	acetic acid	acetone
2.5	0.10	0.04	0.04	0.03
5	0.07	0.01	0.02	0.01
7.5	0.09	0.01	0.02	0.01
10	0.04	0.01	0.01	0.01

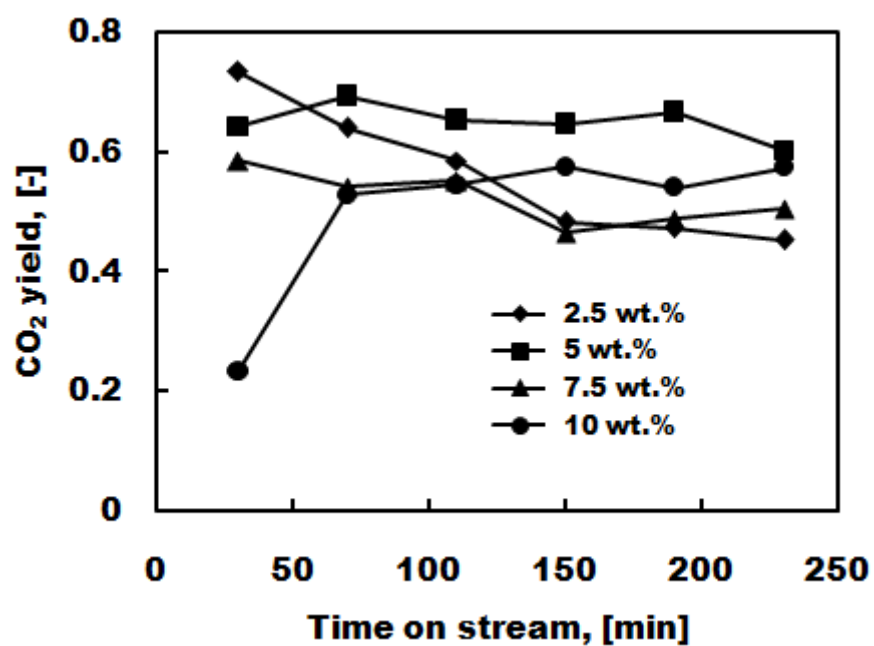
Time on stream is another parameter to be considered for the catalytic stability which was arisen from the effect of feed glycerol concentration as shown in Figure 10.11a-f. For 2.5 wt.% glycerol concentration, the catalyst totally lost the catalytic stability in hydrogen production with producing of CO and acetaldehyde. It was described that the amount of hydrogen production was not high enough to make a catalyst reduction for all sites (self-reduction). It was the reason to lose the activity with the increasing of time on stream. In contrast, H<sub>2</sub> yield was initially increased, and then stable by increasing of time on stream at 10 wt.% of feed glycerol concentration. A large amount of CO and acetaldehyde yields were dramatically suppressed after H<sub>2</sub> yield reached the highest value. It is because higher feed glycerol concentration required a longer time to make a catalyst reduction at the start; however, it seemed to be stable after that. For 5 and 7.5 wt.% of feed glycerol concentrations, H<sub>2</sub> yields were stable for all ranges of time on stream but 5 wt.% offered higher H<sub>2</sub> yield than 7.5 wt.%. Higher C<sub>2</sub>H<sub>6</sub> and acetaldehyde yields were observed along with the lower H<sub>2</sub> yield for 7.5 wt.%. Note that the increasing of CO, C<sub>2</sub>H<sub>6</sub>, and acetaldehyde yields were the reason to lose the catalytic stability for hydrogen production. Finally, it can be concluded that 5 wt.% feed glycerol concentration was the optimum condition for H<sub>2</sub> production as it offered high stability over the reaction period of 230 min.



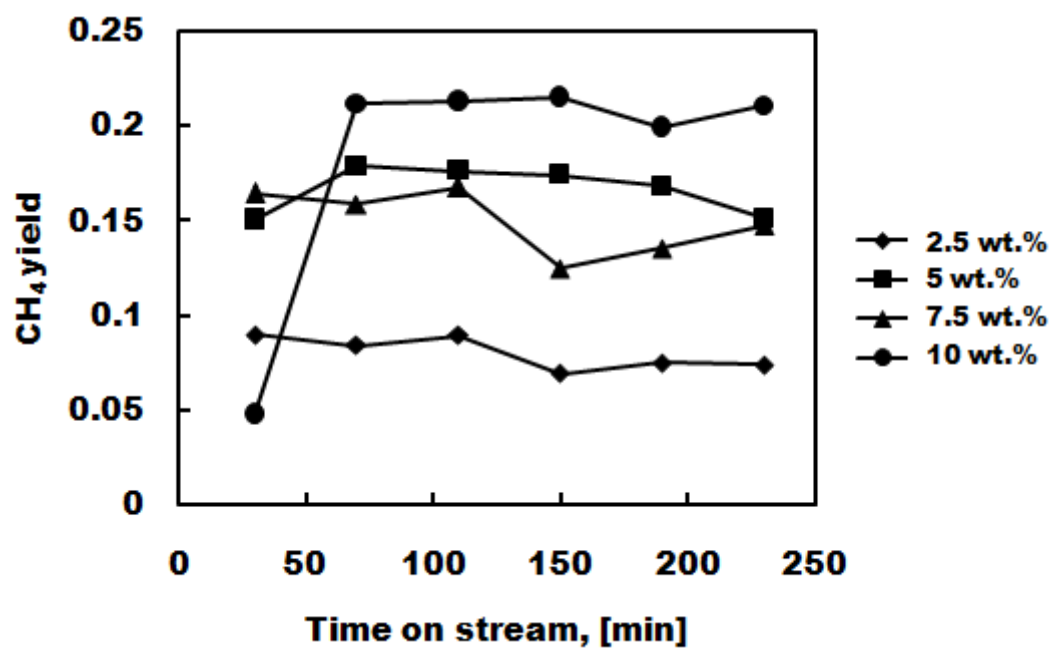
a



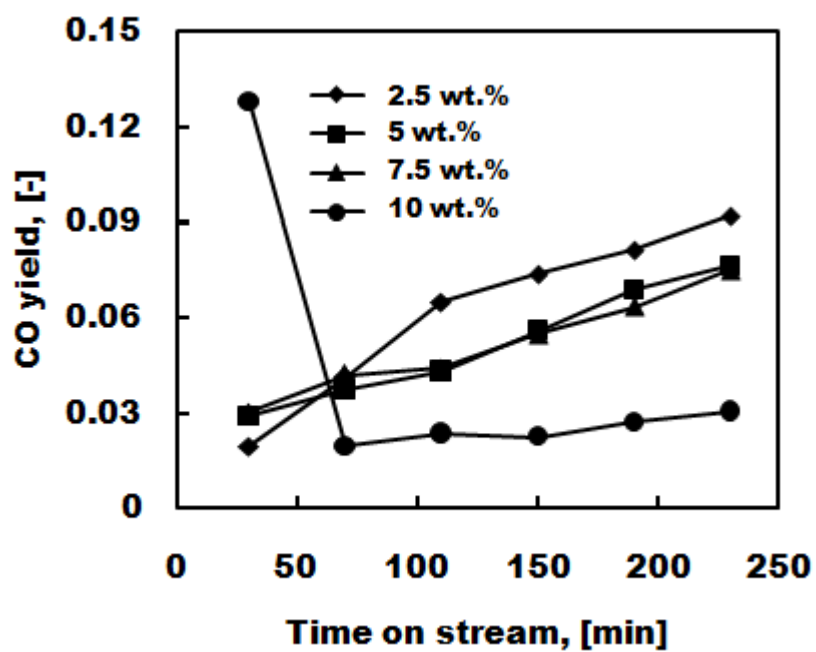
b



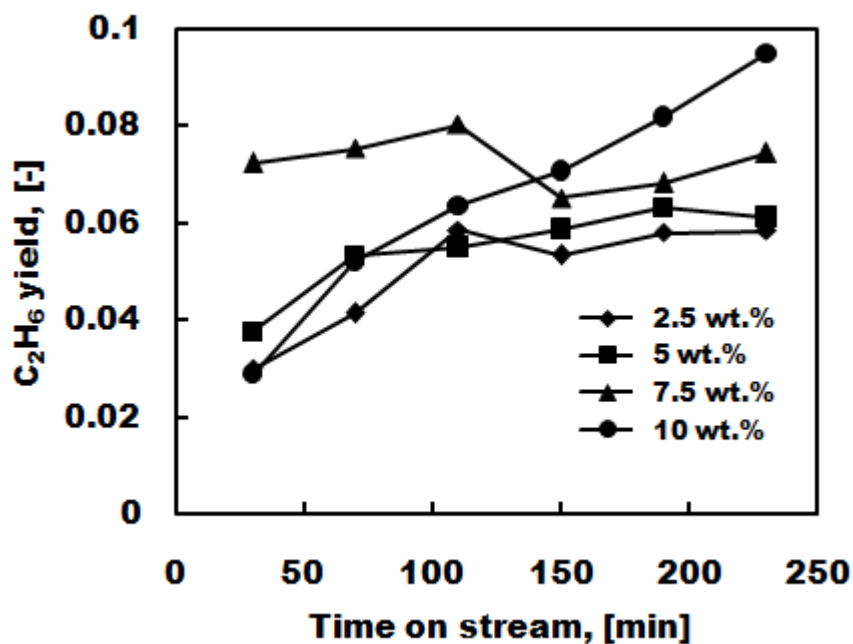
c



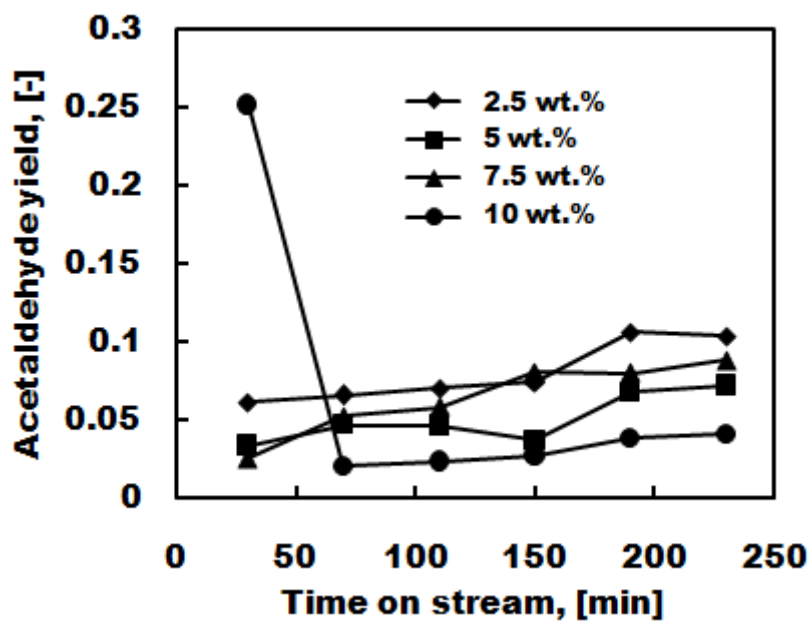
d



e



f



**Figure 10.11** Gas yields of (a) H<sub>2</sub>, (b) CO<sub>2</sub>, (c) CH<sub>4</sub>, (d) CO, (e) C<sub>2</sub>H<sub>6</sub>, and liquid yields of (f) acetaldehyde as a function of feed glycerol concentration and time on stream for Ni/La<sub>2</sub>O<sub>3</sub> catalysts ( $T=798$  K,  $P = 25$  MPa, medium feed rate of 2.15 g/min, 5 wt.% of feed glycerol concentration, 5 wt.% of nickel loading).

### 10.3 Conclusion

Glycerol conversion was highly dependent on the operating temperature for all nickel based catalysts. Complete conversion was achieved by increasing operating temperature to 823 and 848 K for Ni/La<sub>2</sub>O<sub>3</sub>, and Ni/YSZ catalysts, respectively. However, carbon formation was suffered with all nickel based catalysts except the use of La<sub>2</sub>O<sub>3</sub> support. Note that nickel based catalysts are more susceptible to carbon formation than cobalt based catalysts. Comparing with all catalysts, Ni/La<sub>2</sub>O<sub>3</sub> catalyst was the suitable catalyst in term of hydrogen production which promoted higher H<sub>2</sub> yield by increasing of operating temperature.

In the Ni/La<sub>2</sub>O<sub>3</sub> catalyst study, lower feed rate (higher residence time) promoted higher glycerol conversion; however the carbon formation caused to shut down the system at low feed rate (1.05 g/min) condition. Therefore, medium feed rate (2.15 g/min) became an optimum feed rate by considering the glycerol conversion, carbon formation, and catalyst hardness for which fragile catalyst probably happened easier with high feed rate (3.60 g/min). With the effect of nickel loading, 15 wt.% was the suitable percent of nickel loading. It performed the highest hydrogen production (H<sub>2</sub> yield=4.26) and also high catalytic stability with complete gasification. Regarding the effect of feed concentration for 5 wt.% of nickel loading, 5 wt.% feed glycerol concentration was found as the optimum percent feed in term of H<sub>2</sub> yield, and stability. The catalyst significantly lost the catalytic stability with 2.5 wt.% feed glycerol concentration by considering on time on stream in 230 min.

# CHAPTER XI

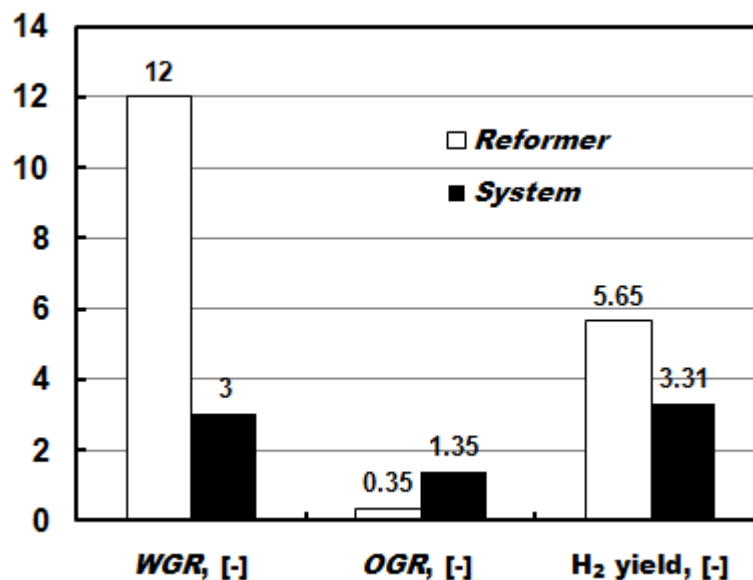
## CONCLUSION AND RECOMMENDATIONS

This chapter summarizes the works done on hydrogen production from different processes of glycerol reforming. It starts with technical comparison of all processes, and their advantages and disadvantages then, suitable catalysts for supercritical water reforming of glycerol are provided. Finally, the recommendations of future work are suggested.

### 11.1 Conclusion

#### 11.1.1 Comparison of all processes

For isothermal operation, increasing water to glycerol ratio (*WGR*) enhances the hydrogen production but it requires large extent of external heat source. However, an increase of oxygen to glycerol (*OGR*) reduces the hydrogen production but decreases the energy requirement of the operation.

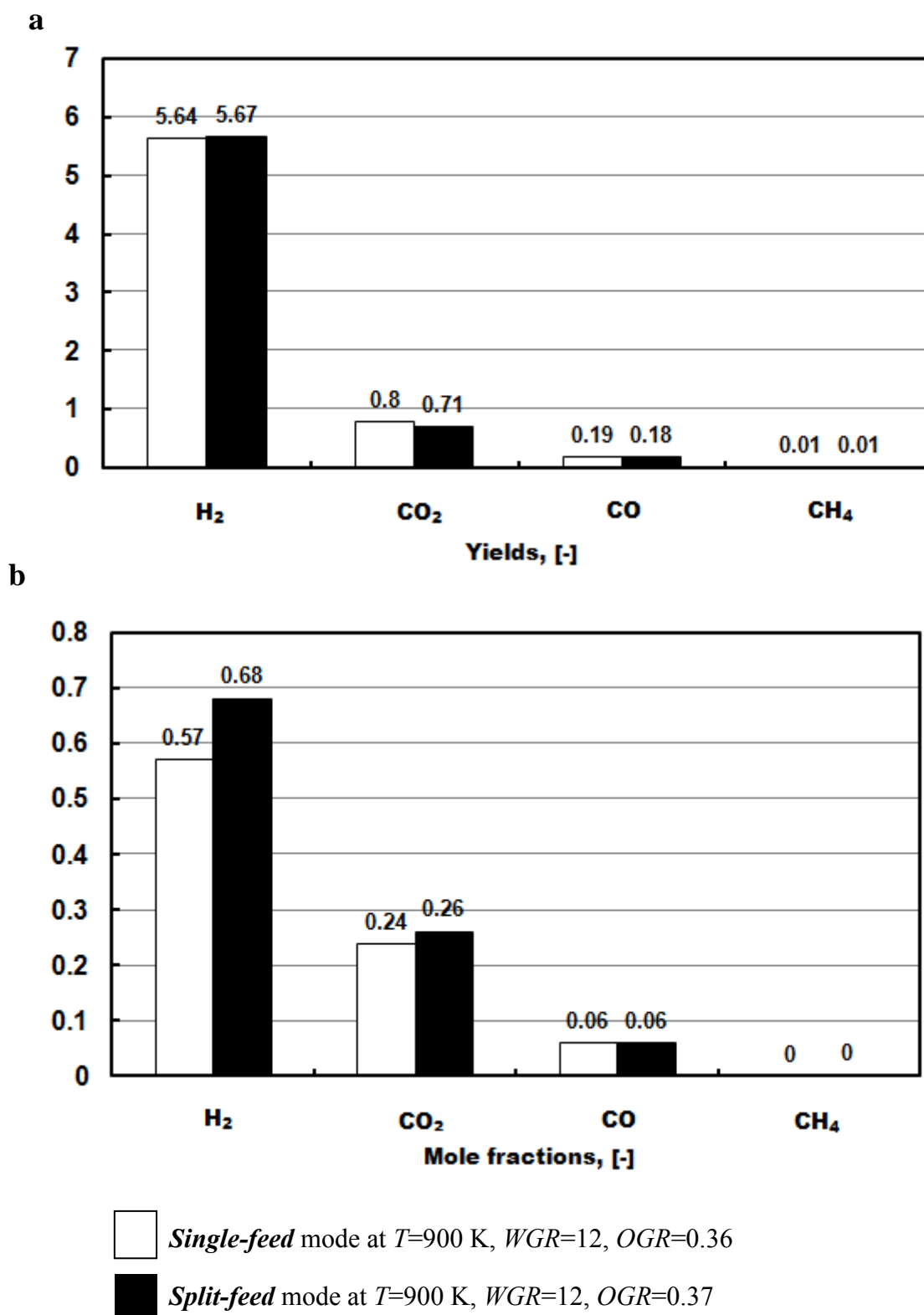


**Figure 11.1** Comparison of *Reformer* (880 K) and *System* (875 K) levels by providing of *WGR*, *OGR*, and maximum H<sub>2</sub> yield at thermal neutral condition ( $Q_{\text{net}}=0$ ,  $P=0.101325$  MPa)

The thermal neutral condition can be achieved when *WGR*, *OGR*, and operating temperature are carefully selected. For *Reformer* level, only a small amount of *OGR* is required in the operation. Much higher *OGR* is required to provide sufficient energy especially for the feed preheating in *System* level as shown in Figure 11.1.

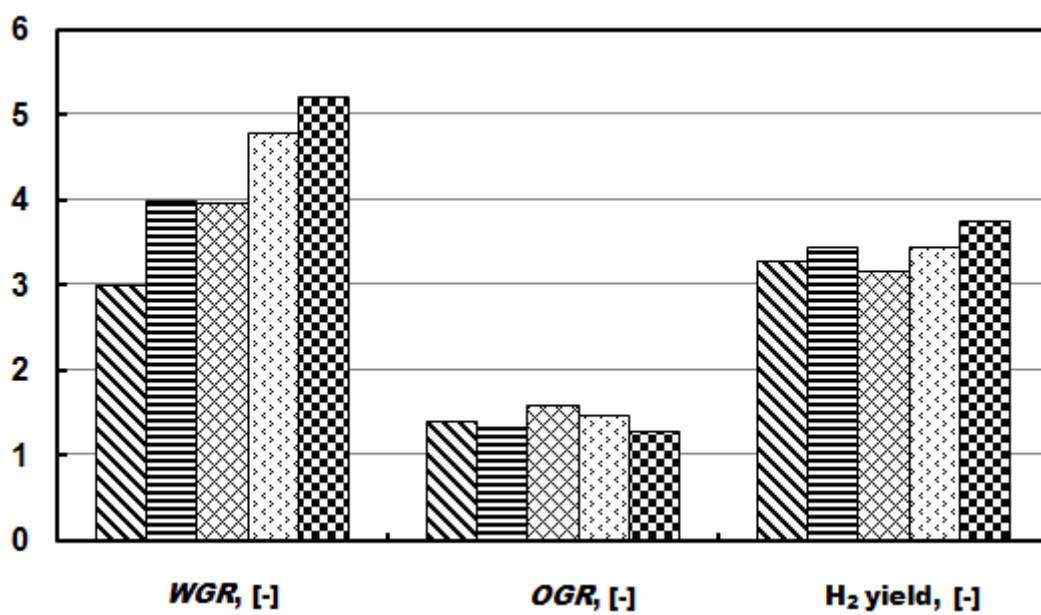
*Single-feed* and *Split-feed* of air feeding modes are considered in *Reformer* and *System* levels. The H<sub>2</sub> yield from both modes is not significantly different at the *Reformer* level due to the small energy requirement from the heat of reactions as shown in Figure 11.2a. Figure 11.2b indicates that *Split-feed* mode offers higher H<sub>2</sub> concentration in the product gas because N<sub>2</sub> from air and part of CO<sub>2</sub> are not present in the gas product. For the *System* level (Figures 11.3a-c), the *Single-feed* mode is favorable to H<sub>2</sub> generation at low temperatures (600-900 K), whereas in the *Split-feed* mode, more H<sub>2</sub> are generated at high temperatures (900-1200 K). The *Single-feed* mode is a superior mode in term of suppressing carbon formation – no carbon formation is observed when operating at temperature above 900 K. Using pure O<sub>2</sub> is considered to be a good choice for H<sub>2</sub> production from glycerol at the thermal neutral conditions especially in the *Single-feed* mode. However, using air or O<sub>2</sub> does not make a significant difference in term of H<sub>2</sub> mole fraction in *Split-feed* mode. In addition, using the ABP stream to supply heat is beneficial to increase the H<sub>2</sub> yield in the *Split-feed* mode as it decreases the fuel requirement (glycerol and air).

Comparison of thermodynamic analysis and experiment results are shown in Figures 11.4a-b. Catalysts (Co/YSZ and Ni/La<sub>2</sub>O<sub>3</sub>) promote the hydrogen production in the supercritical water condition. Their H<sub>2</sub> yields are provided higher than thermodynamic analysis, and empty reactor (Inconel 625 reactor) cases. It is clear that empty reactor at ambient pressure offers the lowest H<sub>2</sub> yield, glycerol conversion, and other gas yields. Results from thermodynamic analysis seem to favor the CH<sub>4</sub> formation. In contrast, methane is suppressed by promoting of CO formation in the empty reactor condition; observing very high CO yield. Addition of a catalyst has duties to inhibit CO formation, and enhance the H<sub>2</sub> production. The large amount of CO<sub>2</sub> yield is obtained instead of CH<sub>4</sub> yield unlike in thermodynamic analysis.

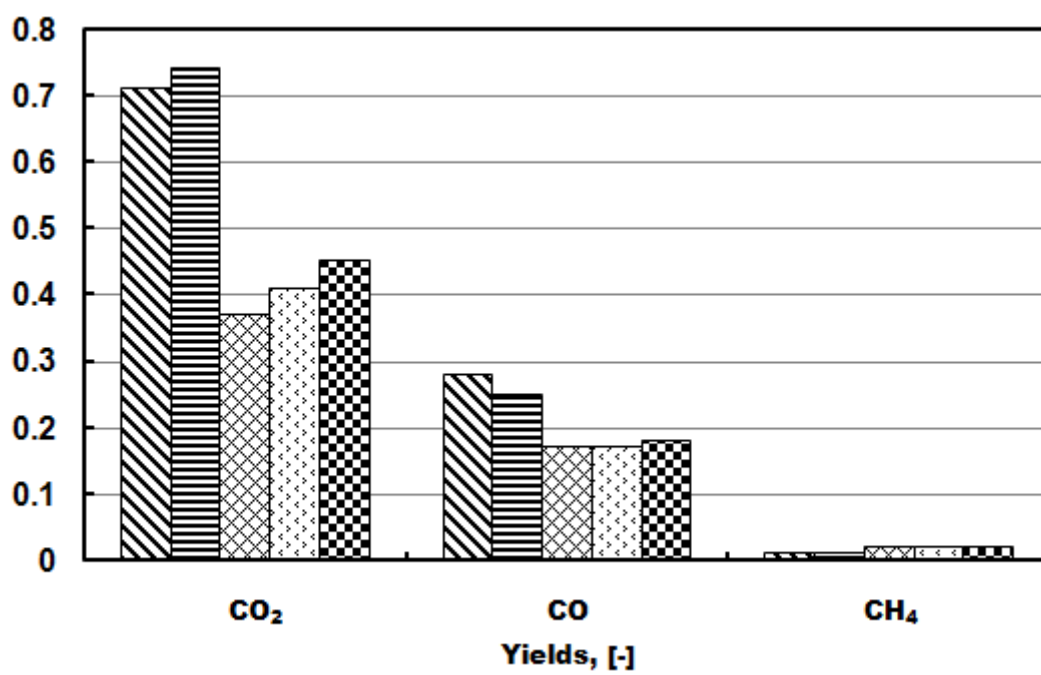


**Figure 11.2** Effect of mode at maximum H<sub>2</sub> yield condition in the *Reformer* level (a) gas product yields (b) mole fraction of gas products ( $Q_{\text{net}}=0$ ,  $P=0.101325$  MPa)

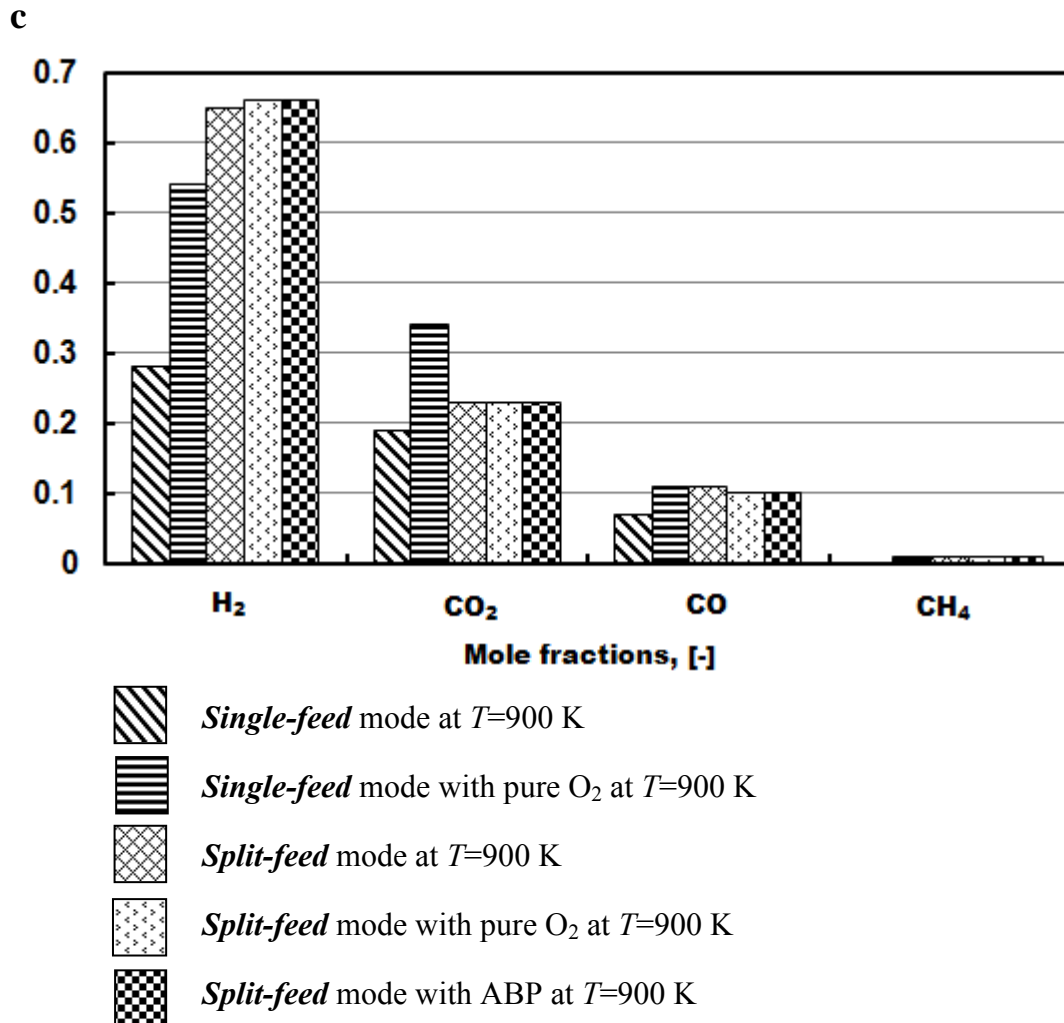
a



b

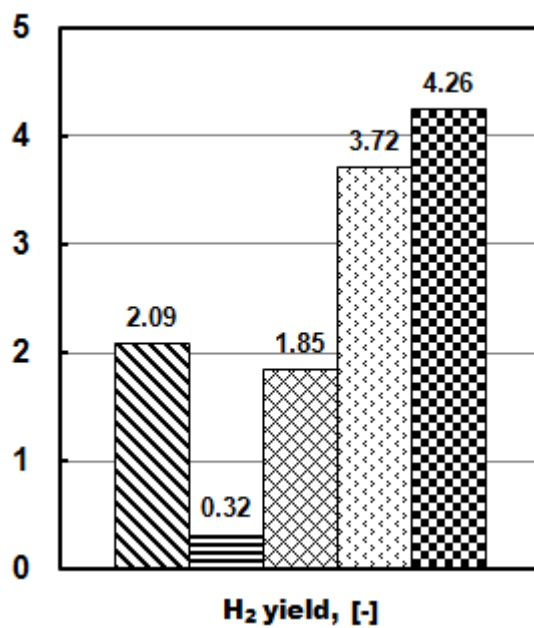




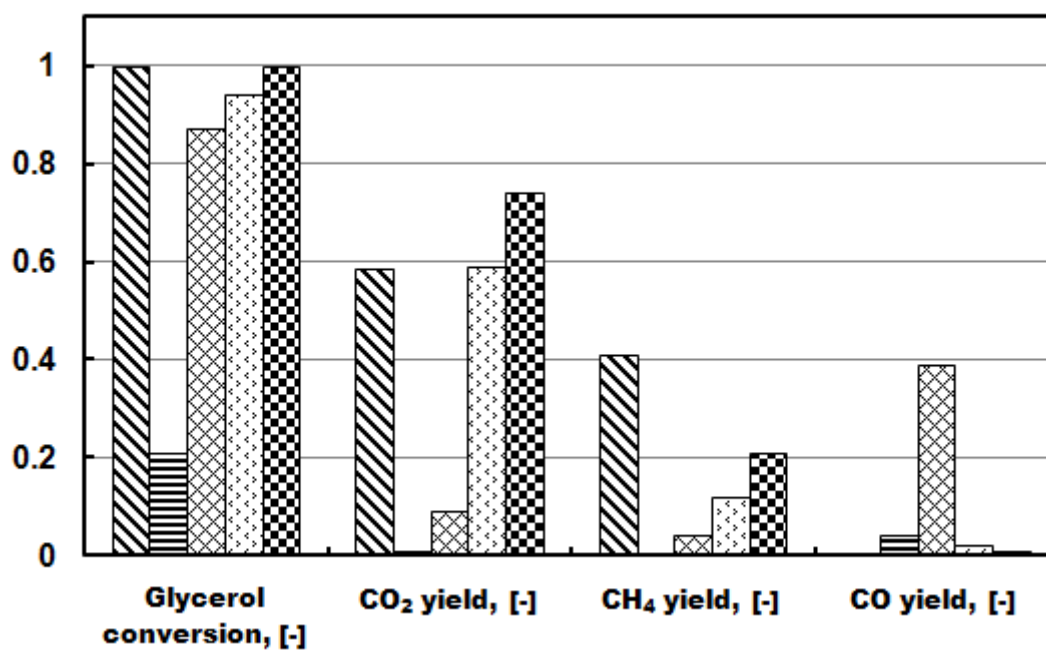



**Figure 11.3** Effect of mode and using of pure  $O_2$ , and ABP at maximum  $H_2$  yield condition in the *System* level (a)  $WGR$ ,  $OGR$ ,  $H_2$  yield (b) gas product yields (c) mole fraction of gas products ( $Q_{net}=0$ ,  $P=0.101325$  MPa)


a

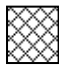
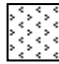



b



 Thermodynamic analysis at  $T=798$  K,  $P = 25$  MPa, medium feed rate of 2.15 g/min, 5 wt.% of feed glycerol concentration

 Empty reactor at  $T=798$  K,  $P = 0.1$  MPa (ambient pressure), medium feed rate of 2.15 g/min, 5 wt.% of feed glycerol concentration

-  **Empty reactor** at  $T=798$  K,  $P = 25$  MPa, medium feed rate of 2.15 g/min, 5 wt.% of feed glycerol concentration
-  **10 wt.% Co/YSZ catalyst** at  $T=773$  K,  $P = 25$  MPa, medium feed rate of 2.15 g/min, 5 wt.% of feed glycerol concentration
-  **15 wt.% Ni/La<sub>2</sub>O<sub>3</sub> catalyst** at  $T=798$  K,  $P = 25$  MPa, medium feed rate of 2.15 g/min, 5 wt.% of feed glycerol concentration

**Figure 11.4** Comparison of thermodynamic analysis, empty reactor (0.1 MPa), empty reactor (25 MPa), Co/YSZ catalyst, and Ni/La<sub>2</sub>O<sub>3</sub> catalyst in the supercritical water reforming of glycerol (a) H<sub>2</sub> yield (b) glycerol conversion, gas product yields

### 11.1.2 Selection of the suitable catalyst

For the catalytic supercritical water reforming, cobalt and nickel metals with the La<sub>2</sub>O<sub>3</sub>,  $\gamma$ -Al<sub>2</sub>O<sub>3</sub>,  $\alpha$ -Al<sub>2</sub>O<sub>3</sub>, ZrO<sub>2</sub>, and YSZ supports are investigated. 10 wt.% Co/YSZ catalyst represented the best catalyst among the cobalt based catalysts. The suitable conditions are the medium operating temperature, lower feed rate, and 10 wt.% of cobalt loading. In addition, high catalytic stability in 230 min was provided at this operating temperature (H<sub>2</sub> yield = 3.72 at 230 min) without carbon formation problem. On the other hand, 10 wt.% Ni/La<sub>2</sub>O<sub>3</sub> catalyst performed the best results in nickel based catalysts. It favored high operating temperature, medium feed rate, high amount of nickel loading (15 wt.%), and medium feed glycerol concentration (5 wt.%) at 798 K with high catalytic stability during reaction times (H<sub>2</sub> yield = 4.26 at 230 min). The weakness of this catalyst was its lower hardness when compared to Co/YSZ catalyst which could easily damage the catalyst under fluctuating product flowrate. Comparison between both metal catalysts, it was clear that nickel based catalysts provided higher glycerol conversion, higher H<sub>2</sub> yield but more susceptible to carbon formation problem which eventually results in the failure system.

## 11.2 Recommendation for future works

- As it has been known that supercritical water phase is very different from gas and liquid phase. Hence, more complicated equation of state should be used in the thermodynamic analysis in order to obtain more accurate product distribution.

- In the empty reactor condition, the treatment with oxidizing agent (i.e.  $\text{H}_2\text{O}_2$ ) should be provided for cleaning the reactor wall after a long operation period. Then, the effect after treatment should be studied.
- The free radical and ionic pathways have been reported to take place in supercritical water condition. Therefore, basic metals such as Li, Na, K, Mg, Ca, etc would be interesting choices for further study.
- For metal oxide catalysts, the addition of promoter (i.e.  $\text{CeO}_2$ ), 2 mixed metal support (i.e.  $\text{La}_2\text{O}_3+\alpha\text{-Al}_2\text{O}_3$ ), bimetallic (i.e. Ni+Co), noble metal (i.e. Rh, Ru) probably help to minimize the carbon formation and encourage the hydrogen production.
- Improve the catalyst hardness of Ni/ $\text{La}_2\text{O}_3$  catalyst is the interesting topic to extend the catalyst life. The catalyst preparation would be improved.
- Crude glycerol feeding is interesting to investigate and compare with pure glycerol.
- Set up the new equipments such as high pressure pump, and back pressure regulator in order to keep the system stable. They will provide the constant feed rate, pressure, and product flowrates in the supercritical water condition.
- Two BPRs should be installed in order to make a precision for controlling pressure and clean the plugging particles at the BPR seat without shutting down the process.
- Regenerate the catalyst should be considered.

## REFERENCES

- Adhikari, S., Fernando, S., Gwaltney, S.R., To, S.D.F., Bricka, R.M., Steele, P.H., and Haryanto, A. A thermodynamic analysis of hydrogen production by steam reforming of glycerol. International Journal of Hydrogen Energy 32 (2007a): 2875 – 2880.
- Adhikari, S., Fernando, S., and Haryanto, A. A Comparative Thermodynamic and Experimental Analysis on Hydrogen Production by Steam Reforming of Glycerin Energy & Fuels 21 (2007b): 2306-2310.
- Adhikari, S., Fernando, S., and Haryanto, A. Production of hydrogen by steam reforming of glycerin over alumina-supported metal catalysts. Catalysis Today 129(2007c): 355–364.
- Adhikari, S., Fernando, S.D., To, S.D.F., Bricka, R.M., Steele, P.H., and Haryanto, A. Conversion of glycerol to hydrogen via a steam reforming process over nickel catalysts. Energy & Fuels 22(2008): 1220–1226.
- Adhikari, S., Fernando, S.D., and Haryanto, A. Hydrogen production from glycerol: An update, Energy Conversion and Management 50 (2009): 2600–2604.
- Ahmed, S., and Krumpelt, M., Hydrogen from hydrocarbon fuels for fuel cells. International Journal of Hydrogen Energy 26 (2001): 291–301.
- Alberton, A., Souza, M.M.V.M., and Schmal, M. Carbon formation and its influence on ethanol steamreforming over Ni/Al<sub>2</sub>O<sub>3</sub> catalysts. Catalysis Today 123 (2007): 257-264.
- Anand, K.A., Anisia, K.S., Agarwal, A.K. and Kumar, A. Hydrogenolysis of glycerol with FeCo macrocyclic complex bonded to raney nickel support under mild reaction conditions, The Canadian Journal of Chemical Engineering 88(2010): 208-216.

- Antal, Jr.M.J., Allen, S.G., Schulman, D., Xu, Xiaodong, and Divilio, R.J. Biomass Gasification in supercritical water. Industrial Engineering Chemistry Research 39(2000): 4040-4053.
- Antal, Jr.M.J., Mok, W.S.L., Roy, J.C., Raissi, A.T., Anderson, D.G.M. Pyrolytic sources of hydrocarbons from biomass. Journal of Analytical and Applied Pyrolysis 8(1985): 291-303.
- Arita, T., Nakahara, K., Nagami, K., and Kajimoto, O. Hydrogen generation from ethanol in supercritical water without catalyst. Tetrahedron Letters 44(2003):1083-1086.
- Aspen Plus<sup>®</sup> Version 2006, Aspen Technology, Inc. Massachusetts, USA:Cambridge.
- Authayanun, S., Arpornwichanop, A., Patcharavorachot, Y., Wiyaratn, W., and Assabumrungrat, S. Hydrogen production from glycerol steam reforming for low- and high-temperature PEMFCs. International Journal of Hydrogen Energy 36(2011): 267-275.
- Banach, B., Machocki, A., Rybak, P., Denis, A., and Grzegorzczuk, W. Selective production of hydrogen by steam reforming of bio-ethanol. Catalysis Today 176(2011): 28-35.
- Barroso-Quiroga, M.M., and Castro-Luna, A.E. Catalytic activity and effect of modifiers on Ni-based catalysts for the dry reforming of methane. International Journal of Hydrogen Energy 35(2010): 6052-6056.
- Batista, M.S., Santos, R.K.S., Assaf, E.M., and Assaf, J.M., Ticianelli, E.A. High efficiency steam reforming of ethanol by cobalt-based catalysts. Journal of Power Sources 134(2004):27-32.
- Bayram, B., Soykal, I.I., Deak, D.V., Miller, J.T., and Ozkan, U.S. Ethanol steam reforming over Co-based catalysts: Investigation of cobalt coordination environment under reaction conditions. Journal of Catalysis 284(2011): 77-89.

- Beaver, M.G., Caram, H.S. and Sircar, S. Sorption enhanced reaction process for direct production of fuel-cell grade hydrogen by low temperature catalytic steam–methane reforming, Journal of Power Sources 195(2010): 1998-2002.
- Bellido, J.D.A., and Assaf, E.M. Nickel catalysts supported on ZrO<sub>2</sub>, Y<sub>2</sub>O<sub>3</sub>-stabilized ZrO<sub>2</sub> and CaO-stabilized ZrO<sub>2</sub> for the steam reforming of ethanol: Effect of the support and nickel load. Journal of Power Sources 177(2008): 24-32
- Bennekom, J.G., Venderbosch, R.H., Assink, D., Heeres, H.J. Reforming of methanol and glycerol in supercritical water. Journal of Supercritical Fluids 58(2011): 99– 113.
- Bernesson, S., Nilsson, D., and Hansson, P.A. A limited LCA comparing large- and small-scale production of rape methyl ester (RME) under Swedish conditions, Biomass & Bioenergy 26(2004): 545–559.
- Biodiesel 2020: Global Market Survey, Feedstock Trends and Forecasts, Multi-Client Study, 2<sup>nd</sup> Edition, Emerging Markets Online (2008):1-685.
- Bitter, J.H., Seshan, K. and Lercher, J.A. The state of zirconia supported platinum catalysts for CO<sub>2</sub>/CH<sub>4</sub> reforming. Journal of Catalysis 171(1997): 279-286.
- Bondioli, P. From oilseeds to industrial products: Present and near future of oleochemistry. Italian Journal of Agronomy 7 (2003): 129–135.
- Boukis, N., Diem, V., Habicht, W., and Dinjus, E. Methanol reforming in supercritical water. Industrial Engineering Chemistry Research 42 (2003a): 728-735.
- Boukis N, Habicht W, Franz G, and Dinjus E. Behavior of Ni-base alloy 625 in methanol supercritical water systems. Materials and Corrosion 54(2003b): 326–330.
- Boukis N, Diem V, U. Galla, and Dinjus E. Methanol reforming in supercritical water for hydrogen production. Combustion Science and Technology 178(2006): 467-485.

- Bröll, D., Kaul, C., Krämer, A., Krammer, P., Richter, T., Jung, M., Vogel, H., and Zehner, P. Chemistry in supercritical water. Angewandte Chemie International Edition 38(1999): 2998-3014.
- Buffoni, I.N., Pompeo, F., Santori, G.F., and Nichio, N.N. Nickel catalysts applied in steam reforming of glycerol for hydrogen production. Catalysis Communications 10(2009): 1656-1660.
- Buhler, W., Dinjus, E., Ederer, H.J., Kruse, A., and Mas, C. Ionic reactions and pyrolysis of glycerol as competing reaction pathways in near- and supercritical water. Journal of Supercritical Fluids 22(2002): 37–53.
- Busca, G., Costantino, U., Montanari, T., Ramis, G., Resini, C., and Sisani, M. Nickel versus cobalt catalysts for hydrogen production by ethanol steam reforming: Ni-Co-Zn-Al catalysts from hydrotalcite-like precursors. International Journal of Hydrogen Energy 35(2010): 5356-5366.
- Byrd, A.J., and Gupta, R.B. Stability of cerium-modified  $\gamma$ -alumina catalysts support in supercritical water. Applied Catalysis A: General 381(2010): 177-182.
- Byrd, A.J. Kumar, S., Kong, L., Ramsurn, H., and Gupta, R.B. Hydrogen production from catalytic gasification of switchgrass biocrude in supercritical water. International Journal of Hydrogen Energy 36(2011): 3426-3433.
- Byrd, A. J., Pant, K.K., and Gupta R.B. Hydrogen Production from Ethanol by Reforming in Supercritical Water Using Ru/Al<sub>2</sub>O<sub>3</sub> Catalyst. Energy & Fuels 21 (2007a): 3541–3547
- Byrd, A. J., Pant, K.K., and Gupta R.B. Hydrogen Production from Glucose Using Ru/Al<sub>2</sub>O<sub>3</sub> Catalyst in Supercritical Water. Industrial Engineering Chemistry Research 46 (2007b): 3574-3579.
- Byrd, A. J., Pant, K.K., and Gupta R.B. Hydrogen production from glycerol by reforming in supercritical water over Ru/Al<sub>2</sub>O<sub>3</sub> catalyst. Fuel 87 (2008): 2956–2960.



- Cansell, F., Rey, S., and Beslin, P. Thermodynamic aspects of supercritical fluids processing: Applications to polymer and wastes treatment. Oil Gas Science Technology 53 (1998): 71-98.
- Carrara, C., Munera, J., Lombardo, E.A., and Cornaglia, L.M. Kinetic and stability studies of Ru/La<sub>2</sub>O<sub>3</sub> used in the dry reforming of methane. Topic in Catalysis 51(2008): 98-106
- Chakinala, A.G.C., Brilman, D.W.F., Swaaij, W.P.M., and Kersten, S.R.A. Catalytic and Non-catalytic supercritical water gasification of microalgae and glycerol. Industrial Engineering Chemistry Research 49(2010):1113-1122.
- Chen, H., Zhang, T., Dou, B., Dupont, V., Williams, P., Ghadiri, M., and Ding, Y. Thermodynamic analyses of adsorption-enhanced steam reforming of glycerol for hydrogen production. International Journal of Hydrogen Energy 34(2009): 7208–7222.
- Cheng, C.K., Foo, A.Y., and Adesina, A.A. H<sub>2</sub>-rich synthesis gas production over Co/Al<sub>2</sub>O<sub>3</sub> catalyst via glycerol steam reforming. Catalysis Communications 12(2010): 292-298
- Chiu, C.W., Dasari, M.A., Suppes, G.J., and Sutterlin, W.R. Dehydration of glycerol to acetol via catalytic reactive distillation. AIChE Journal 52(2006): 3543-3548.
- Cortright, R.D., Davda, R.R., and Dumesic, J.A. Hydrogen from catalytic reforming of biomass-derived hydrocarbons in liquid water. Nature 418 (2002): 964–966.
- Cui, Y., Galvita, V., Rihko-Struckmann, L., Lorenz, H., and Sundmacher, K. Steam reforming of glycerol: The experimental activity of La<sub>1-x</sub>Ce<sub>x</sub>NiO<sub>3</sub> catalyst in comparison to the thermodynamic reaction equilibrium. Applied Catalysis B: Environmental 90 (2009): 29–37.

- Czernik, S., French, R., Feik, C., and Chornet, E. Hydrogen by Catalytic Steam Reforming of Liquid Byproducts from Biomass Thermoconversion Processes. Industrial Engineering Chemistry Research 41 (2002): 4209-4215.
- Das, N.K., Dalai, A.K., and Ranganathan, R. Hydrogen yield from low temperature steam reforming of ethanol. The Canadian Journal of Chemical Engineering 85(2007): 92-100.
- Dasari, M.A., Kiatsimkul, P., Sutterlin, W.R., and Suppes, G.J. Low-pressure hydrogenolysis of glycerol to propylene glycol. Applied Catalysis A: General 281 (2005): 225-231.
- Dasari, M.A., Catalytic conversion of glycerol and sugar alcohols to value-added products. A dissertation presented to the faculty of the graduate school. University of Missouri-Columbia (2006).
- Dauenhauer, P.J., Salge, J.R., and Schmidt, L.D. Renewable hydrogen by autothermal steam reforming of volatile carbohydrates. Journal of Catalysis 244 (2006): 238–247.
- Davda, R.R., Shabaker, J.W., Huber, G.W., Cortright, R.D., and Dumesic, J.A. Aqueous-phase reforming of ethylene glycol on silica-supported metal catalysts. Applied Catalysis B: Environmental 43 (2003): 13–26
- Deutsch, J., Martin, A., and Lieske, H. Investigations on heterogeneously catalysed condensations of glycerol to cyclic acetals. Journal of Catalysis 245 (2007): 428-435.
- Dicks, A.L. Hydrogen generation from natural gas for the fuel cell systems of tomorrow. Journal of Power Sources 61 (1996): 113-124.
- Dieuzeide, M.L., and Amadeo, N. Thermodynamic analysis of glycerol steam reforming. Chemical Engineering Technology 33(2010): 89–96.
- DiLeo, G.J., Savage, P.E. Catalysis during methanol gasification in supercritical water. Journal of Supercritical Fluids 39(2006): 228-232.

- Docter, A., and Lamm, A. Gasoline fuel cell systems. Journal of Power Sources 84 (1999): 194-200.
- Douette, A.M.D., Turn, S.Q., Wang, W., and Keffer, V.I. Experimental investigation of hydrogen production from glycerin reforming. Energy & Fuels 21 (2007): 3499-3504.
- Fatsikostas, A.N., Kondarides, D.I., Verykios, X.E. Production of hydrogen for fuel cells by reformation of biomass-derived ethanol. Catalysis Today 75(2002): 145-155.
- Faungnawakij, K., Kikuchi, R. and Eguchi, K. Thermodynamic evaluation of methanol steam reforming for hydrogen production, Journal of Power Sources 161(2006): 87-94.
- Fishtik, I., Alexander, A., Datta, R., and Geana D. A thermodynamic analysis of hydrogen production by steam reforming of ethanol via response reactions. International Journal of Hydrogen Energy 25(2000): 31-45.
- Furusawa, T., Sato, T., Sugito, H., Miura, Y., Ishiyama, Y., Sato, M., Itoh, N., and Suzuki, N. Hydrogen production from the gasification of lignin with nickel catalysts in supercritical water, International Journal of Hydrogen Energy 32(2007): 699-704.
- Gadhe, J.B., and Gupta, R.B. Hydrogen Production by Methanol Reforming in Supercritical Water: Suppression of Methane Formation, Industrial Engineering Chemistry Research 44 (2005): 4577-4585.
- Gadhe, J.B., and Gupta, R.B. Hydrogen production by methanol reforming in supercritical water: Catalysis by in-situ-generated copper nanoparticles. International Journal of Hydrogen Energy 32 (2007): 2374 – 2381.
- Garcia E.Y., and Laborde M.A. Hydrogen production by the steam reforming of ethanol: thermodynamic analysis. International Journal of Hydrogen Energy 16 (1991): 307–312.

- Garcia, V., Fernandez, J.J., Ruiz, W., Mondragon, F., and Moreno, A. Effect of MgO addition on the basicity of Ni/ZrO<sub>2</sub> and on its catalytic activity in carbon dioxide reforming of methane. Catalysis Communications 11(2009): 240-246.
- Goodwin, A.K., and Rorrer, G.L. Conversion of xylose and xylose-phenol mixtures to hydrogen-rich gas by supercritical water in an isothermal microtube flow reactor. Energy & Fuels 23(2009): 3818-3825.
- Gonzalez-Delacruz, V.M., Pereniguez, R., Ternero, F., Holgado, J.P., and Caballero, A. Modifying the size of nickel metallic particles by H<sub>2</sub>/CO treatment in Ni/ZrO<sub>2</sub> methane dry reforming catalysts. ACS Catalysis 1(2011): 82-88.
- Grgicak, C.M., Green, R.G., and Giorgi, J.B. Control of microstructure, sinterability and performance in Co-precipitated NiYSZ, CuYSZ and CoYSZ SOFC anodes. Journal of Materials Chemistry 16(2006): 885-897.
- Guo, Y., Wang, S.Z., Xu, D.H., Gong, Y.M., Ma, H.H., and Tang, X.Y. Review of catalytic supercritical water gasification for hydrogen production from biomass. Renewable & Sustainable Energy Reviews 14(2010): 334-343.
- Haga, F., Nakajima, T., Miya, H., and Mishima, S. Catalytic properties of supported cobalt catalysts for steam reforming of ethanol. Catalysis Letters 48(1997): 223-227.
- Hao, X.H., Guo, L.J., Mao, X., Zhang, X.M., and Chen, X.J. Hydrogen production from glucose used as a model compound of biomass gasified in supercritical water, International Journal of Hydrogen Energy 28(2003): 55-64.
- Hecht, E.S., Gupta, G.K., Zhu, H., Dean, A.M., Kee, R.J., Maier, L., and Deutschmann, O. Methane reforming kinetics within a Ni-YSZ SOFC anode support. Applied Catalysis A: General 295(2005): 40-51.
- Hernandez, L., and Kafarov, V., Thermodynamic evaluation of hydrogen production for fuel cells by using bio-ethanol steam reforming: Effect of carrier gas addition. Journal of Power Sources 192(2009): 195-199.

- Hirai, T., Ikenaga, N., Miyake, T., and Suzuki, T. Production of Hydrogen by Steam Reforming of Glycerin on Ruthenium Catalyst. Energy & Fuels 19 (2005): 1761-1762.
- Holgate, H.R., Meyer, J.C., and Tester, J.W. Glucose hydrolysis and oxidation in supercritical water. AIChE Journal 41(1995): 637-648.
- Holladay, J.D., Hu, J., King, D.L., and Wang, Y. An overview of hydrogen production technologies. Catalysis Today 139 (2009): 244-260
- Iriondo, A., Barrio, V.L., Cambra, J. F., Arias, P. L., Guemez, M. B., Navarro, R. M., Sanchez-Sanchez, M. C., and Fierro, J. L. G. Hydrogen Production from Glycerol Over Nickel Catalysts Supported on Al<sub>2</sub>O<sub>3</sub> Modified by Mg, Zr, Ce or La. Topic in Catalysis 49(2008): 46-58.
- Johnsona, D.T., and Taconib, K.A. The Glycerin Glut: Options for the Value-Added Conversion of Crude Glycerol Resulting from Biodiesel Production. Wiley InterScience (2007).
- Ketchie, W. C., Murayama, M., and Davis, R. J. Selective oxidation of glycerol over carbon-supported AuPd catalysts. Journal of Catalysis 250 (2007): 264-273.
- Kiatkittipong, W., Intarachoen, P., Laosiripojana, N., Chaisuk, C., Prasertthdam, P., and Assabumrungrat, S. Glycerol ethers synthesis from glycerol etherification with tert-butyl alcohol in reactive distillation, Computers & Chemical Engineering 35 (2010):2034-2043.
- Kiatkittipong, W., Suwanmanee, S., Laosiripojana, N., Prasertthdam, P., and Assabumrungrat, S. Cleaner gasoline production by using glycerol as fuel extender, Fuel Processing Technology 91(2010): 456-460.
- Klepacova, K., Mravec, D., Kaszonyi, A., and Bajus, M. Applied Catalysis A: General 328 (2007): 1-13.

- Kruse, A., and Gawlik, A. Biomass conversion in water at 330-410°C and 30-50 MPa. Identification of key compounds for indicating different chemical reaction pathways, Industrial Engineering Chemistry Research 42(2003): 267-279.
- Laosiripojana, N., and Assabumrungrat, S. Catalytic steam reforming of methane, methanol, and ethanol over Ni/YSZ: The possible use of these fuels in internal reforming SOFC. Journal of Power Sources 163(2007): 943-951.
- Lechon, Y., Cabal, H., Rua, C., Caldes, N., Santamaria, M., and Saez, R. Energy and greenhouse gas emission savings of biofuels in Spain's transport fuel. The adoption of the EU policy on biofuels, Biomass & Bioenergy 33(2009): 920-932.
- Lee, I.G., Kim, M.S., and Ihm, S.K. Gasification of glucose in supercritical water. Industrial Engineering Chemistry Research 41(2002): 1182-1188.
- Lehnert, K., and Claus, P. Influence of Pt particle size and support type on the aqueous-phase reforming of glycerol. Catalysis Communications 9 (2008): 2543-2546.
- Li, A., Lim, C.J., Boyd, T., and Grace, J.R. Simulation of autothermal reforming in a stage-separation membrane reactor for pure hydrogen production, The Canadian Journal of Chemical Engineering 86(2008): 387-394.
- Li, Sha., Lu, Yu., Guo, L., and Zhang, X. Hydrogen production by biomass gasification in supercritical water with bimetallic Ni-M/ $\gamma$ -Al<sub>2</sub>O<sub>3</sub> catalysts (M=Cu, Co and Sn). (2011) Article in Press.
- Li, Y., Wang, Y., Zhang, X., and Mi, Z. Thermodynamic analysis of autothermal steam and CO<sub>2</sub> reforming of methane, International Journal of Hydrogen Energy 33 (2008): 2507 - 2514.
- Liberatori, J.W.C., Ribeiro, R.U., Zanchet, D., Noronha, F.B., and Bueno, J.M.C. Steam reforming of ethanol on supported nickel catalysts. Applied Catalysis A: General 327(2007): 197-204.

- Liguras, D.K., Kondarides, D.I., Verykios, X.E., Production of hydrogen for fuel cells by steam reforming of ethanol over supported noble metal catalysts. Applied Catalysis B: Environmental 43(2003): 345-354.
- Llorca, J., Dalmon, J.A., Piscina, P.R., and Homs, N. In situ magnetic characterization of supported cobalt catalysts under steam-reforming of ethanol. Applied Catalysis A:General 243(2003) 261-269
- Llorca, J., Homs, N., Sales, J. and Piscina P.R. Efficient production of hydrogen over supportedcobalt catalysts from ethanol steam reforming. Journal of Catalysis 209(2002): 306-317.
- Llorca, J., Piscina, P.R., Dalmon, J.A., and Homs, N. Transformation of  $\text{Co}_3\text{O}_4$  during ethanol steam-re-forming. Activation process for hydrogen production. Chemistry Materials 16(2004): 3573-3578.
- Loppinet-Serani, A, Aymonier, C., and Cansell, F. Current and foreseeable applications of supercritical water for energy and the environment. Chem Sus Chem 1(2008): 486–503.
- Lu, Y., Guo, L., Zhang, X., and Yan, Q. Thermodynamic modeling and analysis of biomass gasification for hydrogen production in supercritical water, Chemical Engineering Journal 131 (2007): 233–244.
- Luo, N., Fu, X., Cao, F., Xiao, T. and Edwards, P.P. Glycerol aqueous phase reforming for hydrogen generation over Pt catalyst – Effect of catalyst composition and reaction conditions. Fuel 87 (2008): 3483–3489.
- Luo, N., Zhao, X., Cao, F., Xiao, T., and Fang, D. Thermodynamic study on hydrogen generation from different glycerol reforming processes. Energy & Fuels 21(2007): 3505–3512.
- Maia, T.A., Assaf, J.M., and Assaf, E.M. Steam reforming of ethanol for hydrogen production on  $\text{Co/CeO}_2\text{-ZrO}_2$  catalysts prepared by polymerization method. Materials Chemistry and Physics 132(2012): 1029-1034.

- Malca, J. and Fausto, F. Life-cycle studies of biodiesel in Europe: A review addressing the variability of results and modeling issues, Renewable & Sustainable Energy Reviews 15(2011): 338–351.
- Maris, E.P., and Davis, R.J. Hydrogenolysis of glycerol over carbon-supported Ru and Pt catalysts. Journal of Catalysis 249(2007): 328–37.
- Matsumura, Y., Minowa, T., Potic, B., Kersten, S.R.A., Prins, W., Swaaij, W.P.M.V., Beld, B.V.D., Elliott, D.C., Neuenschwander, G.G., Kruse, A., and Antal Jr, M.J. Biomass gasification in near- and super-critical water: Status and prospects. Biomass & Bioenergy 29(2005): 269-292.
- Mattos, L.V., Rodino, E., Resasco, D.E., Passos, F.B., and Noronha, F.B. Partial oxidation and CO<sub>2</sub> reforming of methane on Pt/Al<sub>2</sub>O<sub>3</sub>, Pt/ZrO<sub>2</sub>, and Pt/Ce-ZrO<sub>2</sub> catalysts. Fuel Processing Technology 83(2003): 147-161.
- May, A., Salvado, J., Torras, C., and Montane, D. Catalytic gasification of glycerol in supercritical water. Chemical Engineering Journal 160(2010):751–759.
- Mink, K.A. Purifying crude biodiesel glycerol. Industrial Bioprocessing 30 (2008): 2.
- Momma, A. Takano, K., Tanaka, Y., Negishi, A., Kato, K., Nozaki, K., Kato, T., Ichigi, T., Matsuda, K., and Ryu, T. Internal reforming characteristics of cermet supported solid oxide fuel cell using yttria stabilized zirconia fed with partially reformed methane. Journal of Power Sources 193(2009): 65-71.
- Moser, B.R., Biodiesel production, properties, and feedstocks. In Vitro Cell.Dev.Biol.-Plant (2009) 45: 229–266.
- Moura, J.S., Souza, M.O.G., Bellido, J.D.A., Assaf, E.M., Opprtus, M., Reyes, P., and Rangel, M.C. Ethanol steam reforming over rhodium and cobalt-based catalysts: Effect of the support. International Journal of Hydrogen Energy (Article in Press)



- Nagaoka, K., Seshan, K., Aika, K., and Lercher, J.A. Carbon decomposition during carbon dioxide reforming of methane-comparison between Pt/Al<sub>2</sub>O<sub>3</sub> and Pt/ZrO<sub>2</sub>. Journal of Catalysis 197(2001): 34-42.
- Nguyen, L.Q., Abella, L.C., Gallardo, S.M., and Hinode, H. Effect of nickel loading on the activity of Ni/ZrO<sub>2</sub> for methane steam reforming at low temperature. Reaction Kinetic Catalysis Letter 93(2008): 227-232.
- Niederl-Schmidinger, A. and Narodoslowsky, M. Life Cycle Assessment as an engineer's tool?, Journal of Cleaner Production 16(2008): 245-252.
- Oliveira, E.L.G., Grande, C.A., and Rodrigues, A.E. Steam methane reforming in a Ni/Al<sub>2</sub>O<sub>3</sub> catalyst: kinetics and diffusional limitations in extrudates, The Canadian Journal of Chemical Engineering 87(2009): 945-956.
- Ott, L., Bicker, M., and Vogel, H. Catalytic dehydration of glycerol in sub- and supercritical water: a new chemical process for acrolein production, Green Chemistry 8(2006): 214-220.
- Paglia, G., Bozin, E.S., and Billinge, J.L. Fine-scale nanostructure in  $\gamma$ -Al<sub>2</sub>O<sub>3</sub>. Chemistry Materials 18(2006): 3242-3248.
- Perry, R.H., and Green, D.W. Perry's chemical engineers' handbook, seventh edition, McGraw-Hill (1997).
- Pinkwart, K., Bayha, T., Lutter, W., and Krausa, M. Gasification of diesel oil in supercritical water for fuel cells. Journal of Power Sources 136(2004): 211-214.
- Pompeo, F., Nichio, N.N., Ferretti, O.A., and Resasco, D. Study of Ni catalysts on different supports to obtain synthesis gas. International Journal of Hydrogen Energy 30(2005): 1399-1405.
- Profeti, L.P.R., Ticianelli, E.A., and Assaf, E.M. Production of hydrogen via steam reforming of biofuels on Ni/CeO<sub>2</sub>-Al<sub>2</sub>O<sub>3</sub> catalysts promoted by noble metals. International Journal of Hydrogen Energy 34(2009): 5049-5060.

- Qadariyah, L., Sumarno, M., Machmudah, S., Wahyudiono, Sasaki, M., Goto, M., Degradation of glycerol using hydrothermal process. Bioresource Technology 102(2011): 9267-9271.
- Qi, C., Amphlett, J.C., and Peppley, B.A. Hydrogen production by methanol reforming on NiAl layered double hydroxide derived catalyst: Effect of the pretreatment of the catalyst. International Journal of Hydrogen Energy 32 (2007): 5098 – 5102.
- Rabenstein, G., and Hacker, V. Hydrogen for fuel cells from ethanol by steam-reforming, partial-oxidation and combined auto-thermal reforming: A thermodynamic analysis. Journal of Power Sources 185 (2008): 1293–1304.
- Rakib, M.A., Grace, J.R., S. Elnashaie, S.S.E.H., Lim, C.J., and Bolkan, Y.G. Kinetic simulation of a compact reactor system for hydrogen production by steam reforming of higher hydrocarbons, The Canadian Journal of Chemical Engineering 86(2008): 403-412.
- Ramayya, S., Brittain, A., DeAlmeida, C., Mok, W., and Antal, Jr.M.J. Acid-catalysed dehydration of alcohols in supercritical water. Fuel 66(1987):1364-1371.
- Reese, M.A., Turn, S.Q., and Cui, H. High pressure autothermal reforming in low oxygen environments, Journal of Power Sources 187(2009): 544-554.
- Reese, M.A., Turn, S.Q., and Cui, H. Kinetic modeling of high pressure autothermal reforming, Journal of Power Sources 195(2010): 553-558.
- Rossi, C.C.R.S., Alonso, C.G., Antunes, O.A.C., Guirardello, R., and Cardozo-Filho, L. Thermodynamic analysis of steam reforming of ethanol and glycerine for hydrogen production. International Journal of Hydrogen Energy 34 (2009): 323-332.
- Rennard, D.C., Kruger, J.S., and Schmidt, L.D. Autothermal catalytic partial oxidation of glycerol to syngas and to non-equilibrium products. Chem Sus Chem 2(2009): 89–98.

- Resini, C., Delgado, M.C.H., Presto, S., Alemany, L.J., Riani, P., Marazza, r., Ramis, G., and Busca, G. Yttria-stabilized zirconia(YSZ) supported Ni-Co alloys (precursor of SOFC anodes) as catalysts for the steam reforming of ethanol. International Journal of Hydrogen Energy 33(2008): 3728-3735.
- Sato, T., Kurosawa, S., Smith, Jr.R.L., Adschiri, T., Arai, K. Water gas shift reaction kinetics under noncatalytic conditions in supercritical water. Journal of Supercritical Fluids 29(2004): 113-119.
- Schmieder, H., Abeln, J., Boukis, N., Dinjus, E., Kruse, A., Kluth, M., Petrich, G., Sadri, E., and Schacht, M. Hydrothermal gasification of biomass and organic wastes. Journal of Supercritical Fluids 17(2000): 145-153.
- Shabaker, J.W., Huber, G.W., and Dumesic, J.A. Aqueous-phase reforming of oxygenated hydrocarbons over Sn-modified Ni catalysts. Journal of Catalysis 222(2004):180–191.
- Sharma, P.O., Swami, S., Goud, S., and Abraham, M.A. Catalyst development for stable hydrogen generation during steam reforming of renewable and nonrenewable resources. Environment Progress 27(2008): 22-29.
- Soares, R.R., Simonetti, D.A., and Dumesic, J.A. Glycerol as a source for fuels and chemicals by low-temperature catalytic processing. Angewandte Chemie International Edition 45(2006): 3982–3985.
- Soimakallio, S., Makinen, T., Ekholm, T., Pahkala, K., Mikkola, H., and Paappanen, T. Greenhouse gas balances of transportation biofuels, electricity and heat generation in Finland—Dealing with the uncertainties, Energy Policy 37 (2009): 80–90.
- Song, H., Zhang, L., Watson, R.B., Braden, D., and Ozkan, U.S. Investigation of bio-ethanol steam reforming over cobalt-based catalysts. Catalysis Today 129(2007): 346-354.

- Slinn, M., Kendall, K., Mallon, C., and Andrews, J. Steam reforming of biodiesel by-product to make renewable hydrogen. Bioresource Technology 99 (2008): 5851-5858.
- Sun, J., Qiu, X.P., Wu, F., and Zhu, W.T. H<sub>2</sub> from steam reforming of ethanol at low temperature over Ni/Y<sub>2</sub>O<sub>3</sub>, Ni/La<sub>2</sub>O<sub>3</sub> and Ni/Al<sub>2</sub>O<sub>3</sub> catalysts for fuel-cell application. International Journal of Hydrogen Energy 30(2005): 437-445.
- Sutthiumporn, K. and Kawi, S. Promotional effect of alkaline earth over Ni/La<sub>2</sub>O<sub>3</sub> catalyst for CO<sub>2</sub> reforming of CH<sub>4</sub>: Role of surface oxygen species on H<sub>2</sub> production and carbon suppression. International Journal of Hydrogen Energy 36(2011): 14435-14446.
- Swami, S.M., and Abraham, M.A. Integrated catalytic process for conversion of biomass to hydrogen. Energy & Fuels 20 (2006): 2616–2622.
- Székely, E., Supercritical Fluid Extraction. Budapest University of Technology and Economics (2007): 11-20.
- Takeguchi, T., Kani, Y., Yano, T., Kikuchi, R., and Eguchi, K. Study on steam reforming of CH<sub>4</sub> and C<sub>2</sub> hydrocarbons and carbon deposition on Ni/YSZ cermets. Journal of Power Sources 112 (2002): 588-595.
- Tang, H., and Kitagawa, K. Supercritical water gasification of biomass: thermodynamic analysis with direct Gibbs free energy minimization, Chemical Engineering Journal 106 (2005): 261–267.
- Taylor, J.D., Herdman, C.M., Wu, B.C., Karl, W.K., and Rice, S.F. Hydrogen production in a compact supercritical water reformer. International Journal of Hydrogen Energy 28(2003):1171-1178.
- Thamsiroj, T., and Murphy, J.D. Can Rape Seed Biodiesel Meet the European Union Sustainability Criteria for Biofuels?, Energy & Fuels 24(2010): 1720–1730.

- Therdthianwong, S., Srisiriwat, N., Therdthianwong, A., and Croiset, E. Hydrogen production from bioethanol reforming in supercritical water. Journal of Supercritical Fluids 57(2011a): 58-65.
- Therdthianwong, S., Srisiriwat, N., Therdthianwong, A., and Croiset, E. Reforming of bioethanol over Ni/Al<sub>2</sub>O<sub>3</sub> and Ni/CeZrO<sub>2</sub>/Al<sub>2</sub>O<sub>3</sub> catalysts in supercritical water for hydrogen production. International Journal of Hydrogen Energy 36(2011b): 2877–2886.
- Trimm, D.L., Coke formation and minimisation during steam reforming reactions, Catalysis Today 37 (1997): 233-238.
- Tsipouriari, V.A., and Verykios, X.E., Carbon and oxygen reaction pathways of CO<sub>2</sub> reforming of methane over Ni/La<sub>2</sub>O<sub>3</sub> and Ni/Al<sub>2</sub>O<sub>3</sub> catalysts studied by isotopic tracing techniques. Journal of Catalysis 187(1999): 85-94.
- Tsolakis, A., Megaritis, A., and Wyszynski, M.L. Application of exhaust gas fuel reforming in compression ignition engines fueled by diesel and biodiesel fuel mixtures. Energy & Fuels 17 (2003): 1464–73.
- Tuan, T.A.A. Hydrogen production from catalytic ethanol reforming in supercritical water. A thesis presented to the University of Waterloo, Waterloo, Ontario, Canada, 2009.
- Turpeinen, E., Raudaskoski, R., Pongracz, E., and Keiski, R.L. Thermodynamic analysis of conversion of alternative hydrocarbon-based feedstocks to hydrogen. International Journal of Hydrogen Energy 33 (2008): 6635-6643.
- Utaka, T., Okanishi, T., Takeguchi, T., Kikuchi, R., and Eguchi, K. Water gas shift reaction of reformed fuel over supported Ru catalysts. Applied Catalysis A: General 245(2003): 343–351.
- Valliyappan, T., Ferdous, D., Bakhshi, N.N., and Dalai, A.K. Production of hydrogen and syngas via steam gasification of glycerol in a fixed-bed reactor. Topic in Catalysis 49(2008): 59–67.

- Vivanpatarakij, S., Laosiripojana, N., Arpornwichanop, A., and Assabumrungrat, S. Performance improvement of solid oxide fuel cell system using palladium membrane reactor with different operation modes. Chemical Engineering Journal 146 (2009): 112–119.
- Wagner, W., Kruse, A. Properties of Water and Steam. Springer-Verlag, Berlin, 1998.
- Wang, H., Wang, X., Li, M., Li, S., Wang, S., and Ma, X. Thermodynamic analysis of hydrogen production from glycerol autothermal reforming, International Journal of Hydrogen Energy 34 (2009): 5683-5690.
- Wang, X., Li, S., Wang, H., Liu, B., and Ma, X. Thermodynamic Analysis of Glycerin Steam Reforming. Energy & Fuels 22 (2008): 4285–4291.
- Watanabe, M., Iida, T., Aizawa, Y., Aida, T.M., Inomata, H. Acrolein synthesis from glycerol in hot-compressed water. Bioresource Technology 98(2007): 1285-1290.
- Watanabe, M., Iida, T., Aizawa, Y., Ura, H., Inomata, H., and Arai, K. Conversions of some small organic compounds with metal oxides in supercritical water at 673 K. Green Chemistry. 5(2003a): 539-544.
- Watanabe, M., Inomata, H., and Arai, K. Catalytic hydrogen generation from biomass (glucose and cellulose) with ZrO<sub>2</sub> in supercritical water. Biomass Bioenergy 22(2002): 405-410.
- Watanabe, M., Inomata, H., Smith, Jr.R.L.S., and Arai, K. Catalytic decarboxylation of acetic acid with zirconia catalyst in supercritical water. Applied Catalysis A: General 219(2001):149-156.
- Watanabe, M., Osada, M., Inomata, H., Arai, K., and Kruse, A. Acidity and basicity of metal oxide catalysts for formaldehyde reaction in supercritical water at 673 K. Applied Catalysis A: General 245(2003b): 333-341.

- Wen, G., Xu, Y., Ma, H., Xu, Z., and Tian, Z. Production of hydrogen by aqueous-phase reforming of glycerol. International Journal of Hydrogen Energy 33(2008): 6657-6666.
- Wicke, B., Dornburg, V., Junginger, M., and Faaij, A. Different palm oil production systems for energy purposes and their greenhouse gas implications, Biomass & Bioenergy 32(2008): 1322–1337.
- Williams, P.T., and Onwudili, J. Subcritical and supercritical water gasification of cellulose, starch, glucose, and biomass waste. Energy & Fuels 20 (2006): 1259-1265.
- Xu, B.Q., Wei, J.M., Yu, Y.T., Li, J.L., and Zhu, Q.M. Carbon dioxide reforming of methane over nanocomposite Ni/ZrO<sub>2</sub> catalysts. Topic in Catalysis 22(2003): 77-85.
- Xu, X., and Antal, Jr.M.J. Gasification of sewage sludge and other biomass for hydrogen production in supercritical water. Environment Progress 17(1998): 215-220.
- Xu, X., Matsumura, Y., Stenberg, J., and Antal, Jr.M.J. Carbon-catalyzed gasification of organic feedstocks in supercritical water. Industrial Engineering Chemistry Research 35(1996): 2522-2530.
- Xu, D., Wang, S., Hu, X., Chen, C., Zhang, Q., and Gong, Y. Catalytic gasification of glycine and glycerol in supercritical water. International Journal of Hydrogen Energy 34(2009): 5357-5364.
- Xuan, J., Leung, M.K.H., Leung, D.Y.C., and Ni, M. A review of biomass-derived fuel processors for fuel cell systems. Renewable and Sustainable Energy Reviews (2008): Article in press.
- Yanbing, L., Baosheng, J., and Rui, X. Carbon dioxide reforming of methane with a free energy minimization approach. Korean Journal Chemical Engineering 24 (2007): 688-692.

- Yang, L., Joo, J.B., Kim, Y.J., Oh, S., Kim, N.D., and Yi, j. Synthesis of superacidic mesoporous alumina and its application in the dehydration of glycerol. Korean Journal Chemical Engineering 25 (2008): 1014-1017.
- Youn, M. H., Seo, J. G., Cho, K. M., Jung, J. C., Kim, H., La, K. W., Park, D. R., Park, S., Lee, S. H., and Song, I. K. Effect of support on hydrogen production by auto-thermal reforming of ethanol over supported nickel catalysts. Korean Journal Chemical Engineering 25 (2008a): 236-238.
- Youn, M.H., Seo, J.G., Park, S., Jung, J.C.H., Park, D.R., and Song, I.K. Hydrogen production by auto-thermal reforming of ethanol over Ni catalysts supported on ZrO<sub>2</sub>: Effect of preparation method of ZrO<sub>2</sub> support. International Journal of Hydrogen Energy 33(2008b): 7457-7463.
- Yu, D., Aihara, M., Antal Jr, M.J. Hydrogen production by steam reforming glucose in supercritical water. Energy & Fuels 7(1993): 574-577.
- Zhang, B., Tang, X., Li, Y., Xu, Y., and Shen, W. Hydrogen production from steam reforming of ethanol and glycerol over ceria-supported metal catalysts. International Journal of Hydrogen Energy 32 (2007): 2367 – 2373.



## **APPENDICES**

# APPENDIX A

## GAS CHROMATOGRAPHY

### CALIBRATION CURVES

#### A.1 Gas calibration curves for gas chromatography (GC, Varian CP-3800)

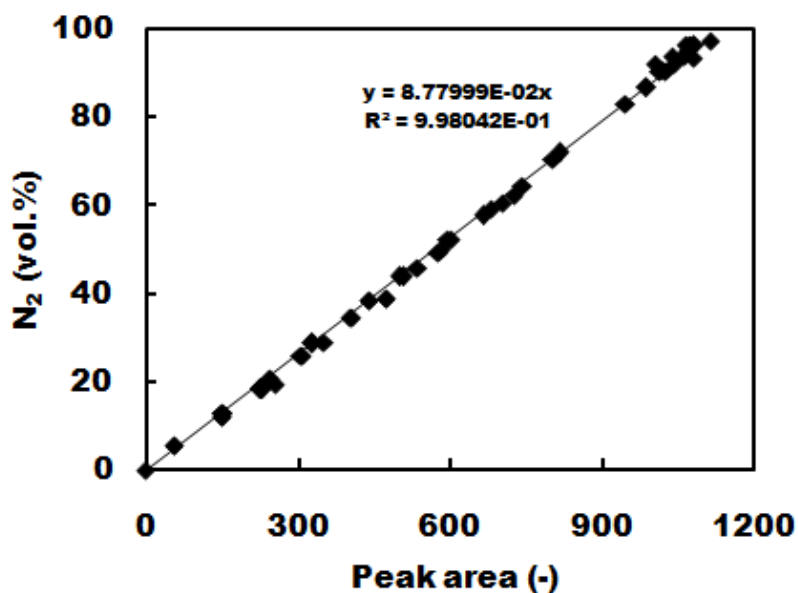
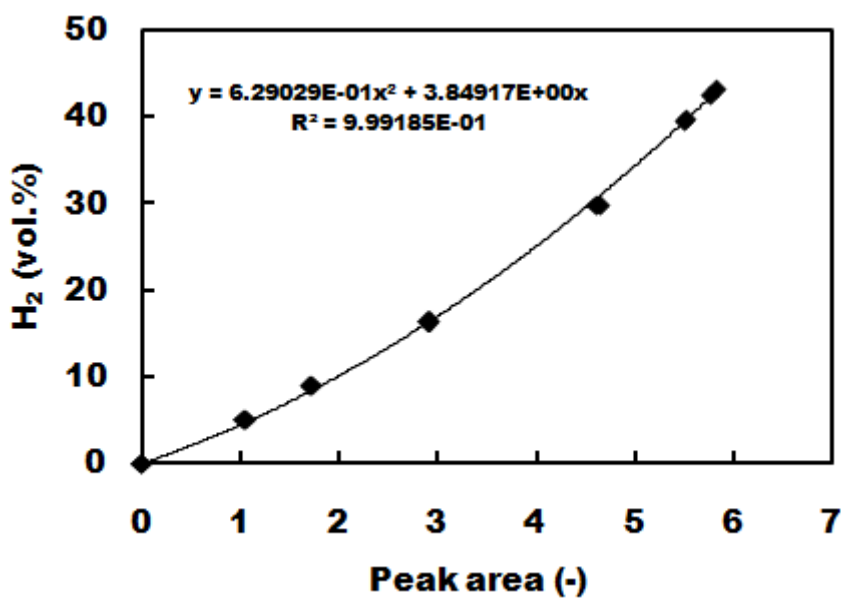


Figure A.1 N<sub>2</sub> calibration curve in the range of 0-100 vol.%

a



b

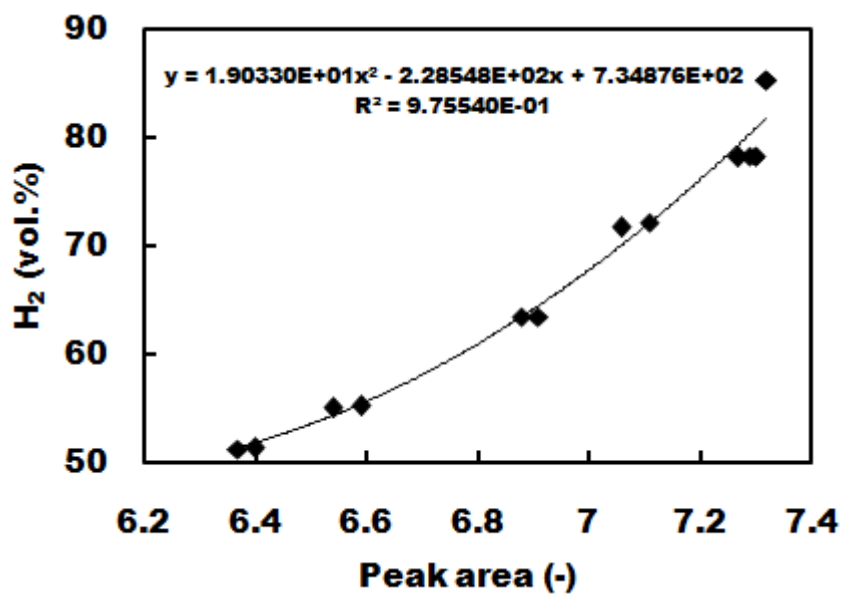


Figure A.2 H<sub>2</sub> calibration curves in the range of (a) 0-50 vol.% (b) 50-90 vol.%

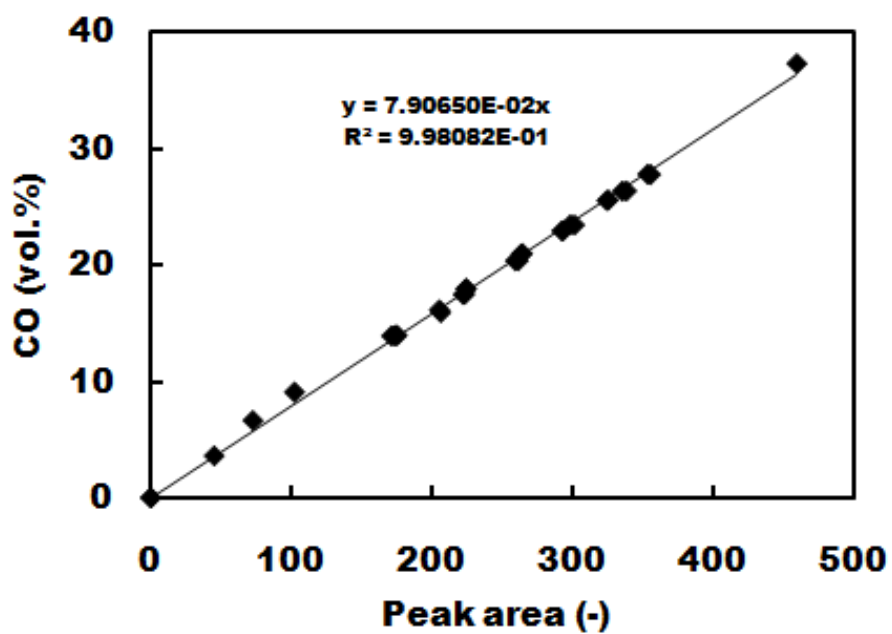


Figure A.3 CO calibration curve in the range of 0-40 vol.%

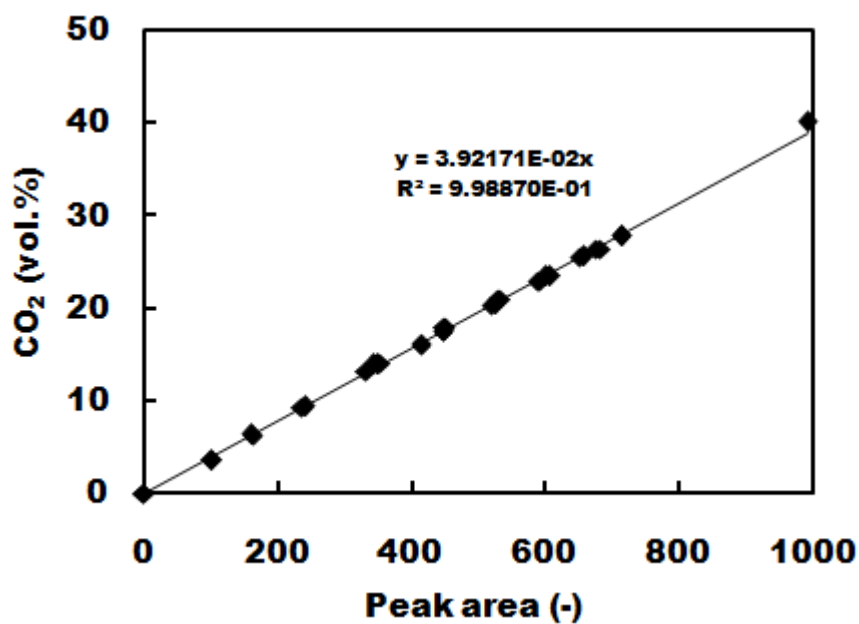


Figure A.4 CO<sub>2</sub> calibration curve in the range of 0-45 vol.%

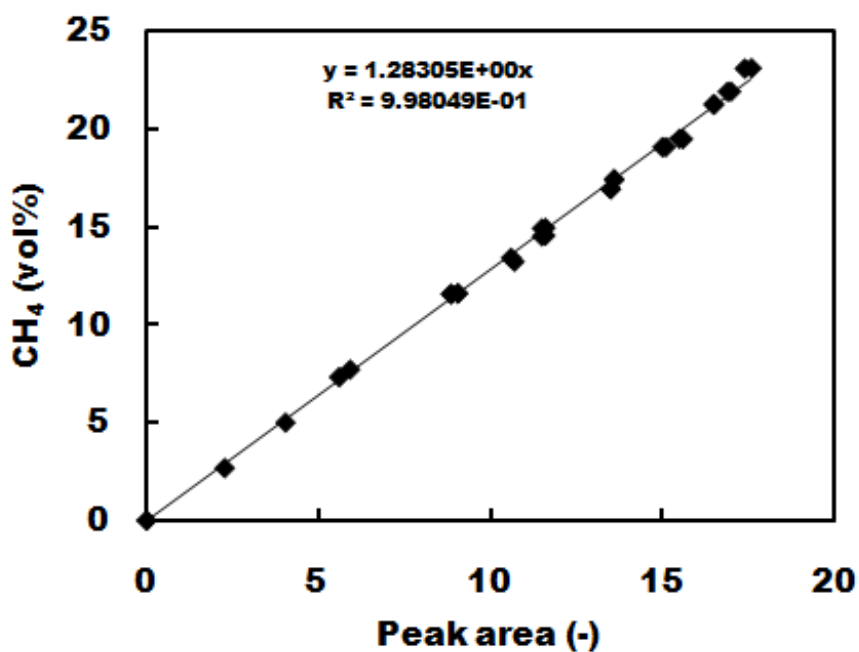


Figure A.5 CH<sub>4</sub> calibration curve in the range of 0-25 vol.%

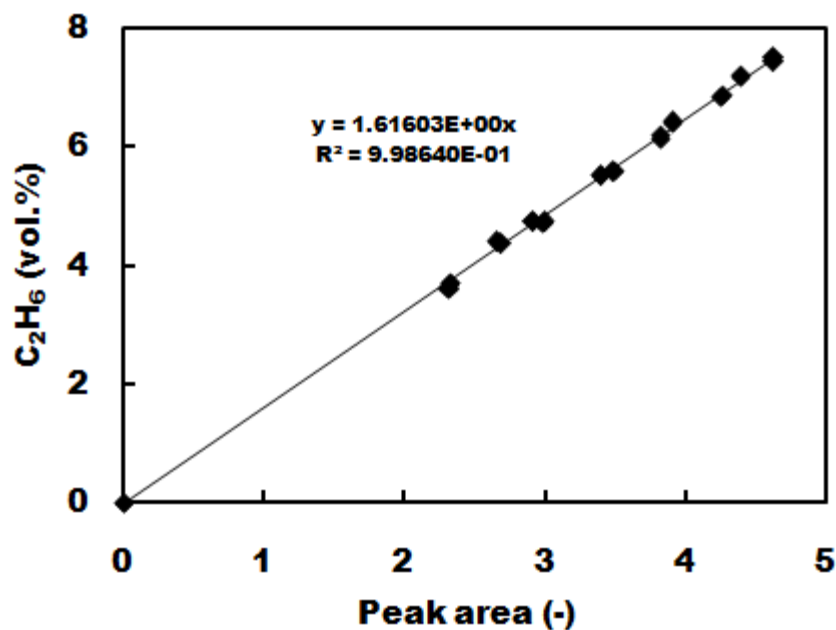


Figure A.6 C<sub>2</sub>H<sub>6</sub> calibration curve in the range of 0-8 vol.%

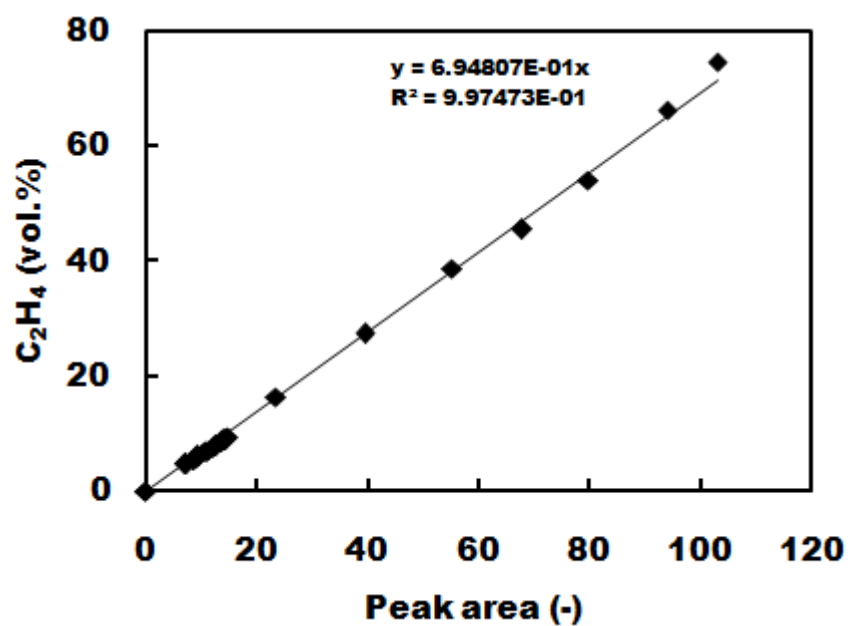
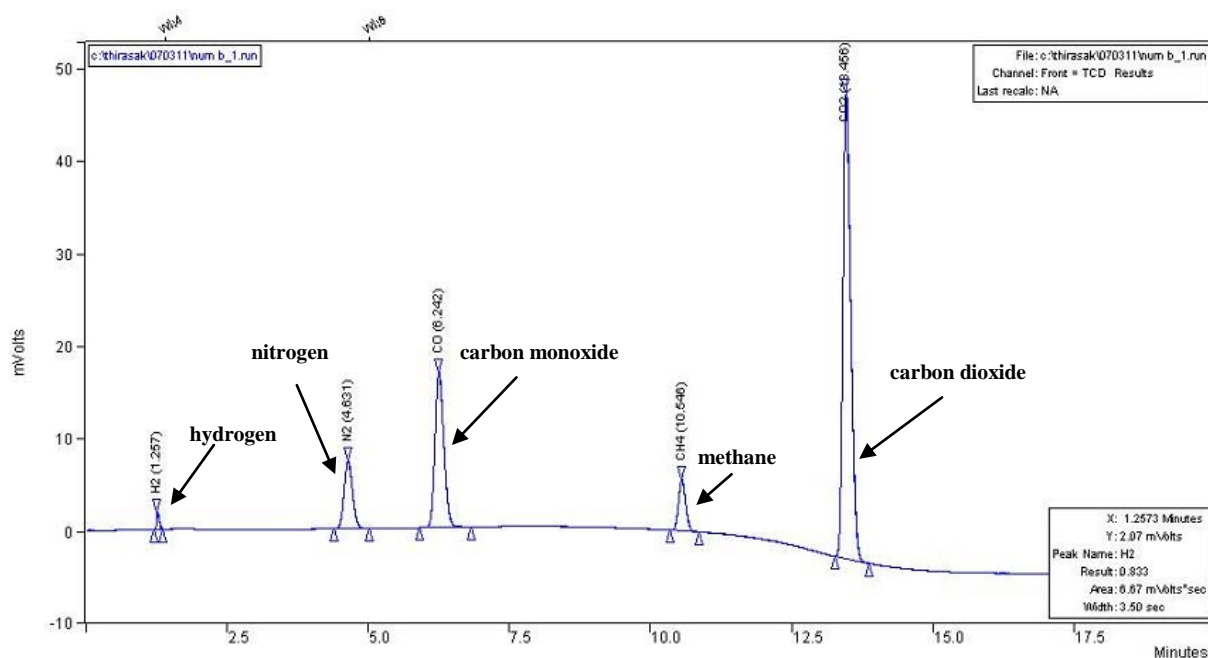
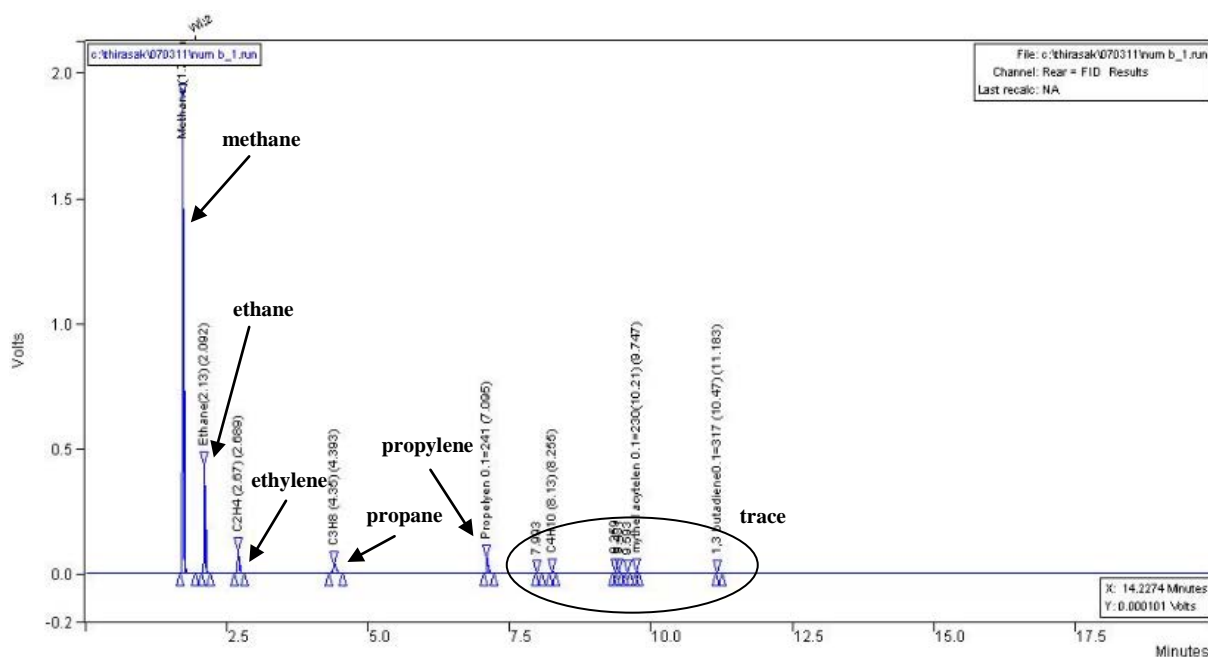


Figure A.7 C<sub>2</sub>H<sub>4</sub> calibration curve in the range of 0-80 vol.%

*Remark:* The other gas analysis including C<sub>3</sub>H<sub>8</sub>, C<sub>3</sub>H<sub>6</sub>, and O<sub>2</sub> were given as C<sub>3</sub>H<sub>8</sub>,  $y=3.70E-01x+3.30$ ; C<sub>3</sub>H<sub>6</sub>,  $y=4.494E-01x-3.81$ ; O<sub>2</sub>,  $y=1.06E-01x+2.06E-01$ .



**Figure A.8** Gas products diagram (TCD, 15' x 1/8" stainless steel 60/80 mesh Carboxen- 1000 column) of gas chromatographic analysis for empty reactor studying (2.15 g/min,  $T=848$  K (575°C),  $P=25$  MPa)



**Figure A.9** Gas products diagram (FID, 50 m x 0.53 mm Al<sub>2</sub>O<sub>3</sub>/KCl fused silica PCOT column) of gas chromatographic analysis for empty reactor studying (2.15 g/min,  $T=848$  K (575°C),  $P=25$  MPa)

**Table A.1** Retention time of gas components in gas chromatographic analysis

<b>Component</b>	<b>Retention time (min)</b>
<b>TCD</b>	
<b>H<sub>2</sub></b>	1.257
<b>N<sub>2</sub></b>	4.631
<b>CO</b>	6.242
<b>CH<sub>4</sub></b>	10.546
<b>CO<sub>2</sub></b>	13.456
<b>FID</b>	
<b>CH<sub>4</sub></b>	1.672
<b>C<sub>2</sub>H<sub>6</sub></b>	2.167
<b>C<sub>2</sub>H<sub>4</sub></b>	2.791
<b>C<sub>3</sub>H<sub>8</sub></b>	4.573
<b>C<sub>3</sub>H<sub>6</sub></b>	7.187

## A.2 Liquid calibration curves for Gas chromatography (GC, Agilent 6890)

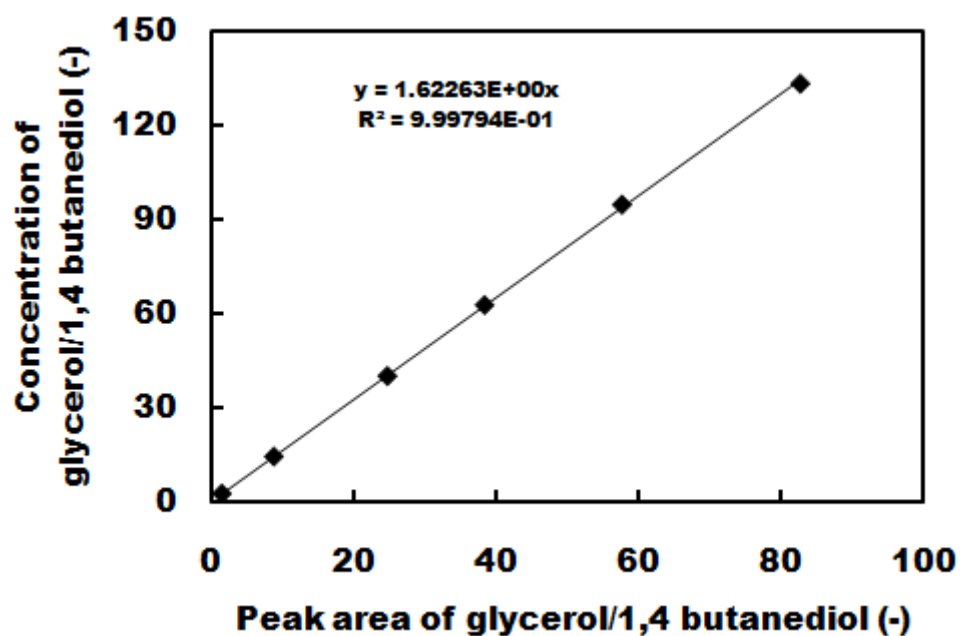


Figure A.10 Glycerol calibration curve in the range of 0-11 wt.%

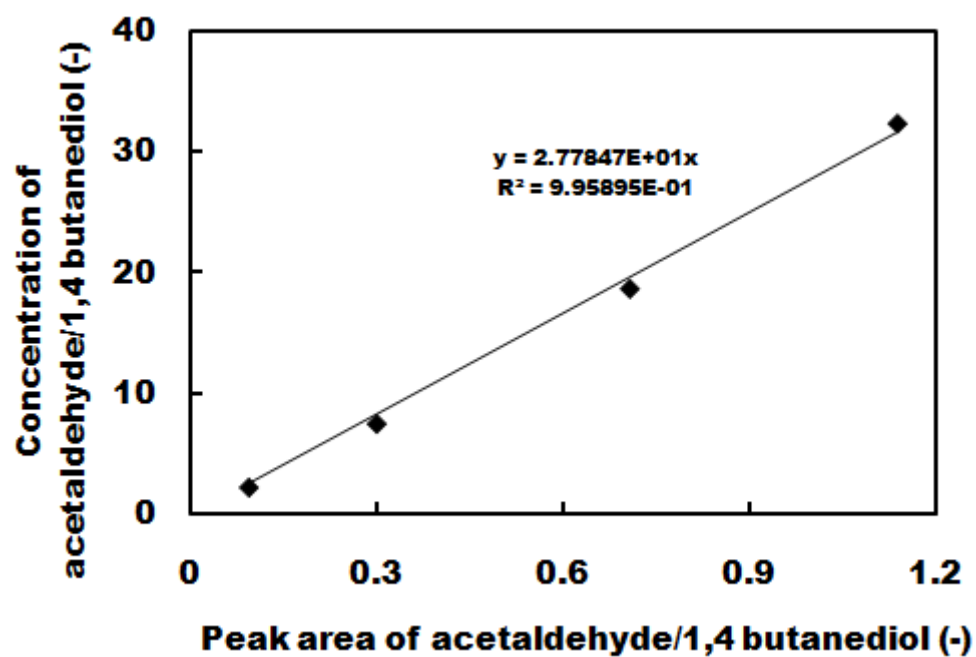


Figure A.11 Acetaldehyde calibration curve in the range of 0-1.1 wt.%



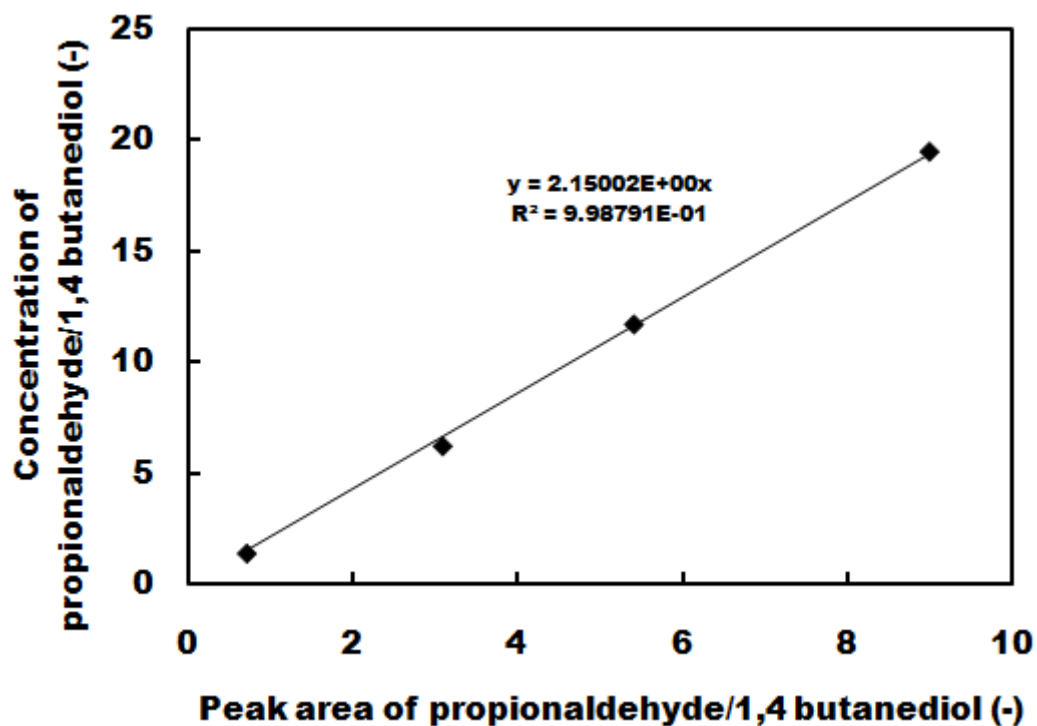


Figure A.12 Propionaldehyde calibration curve in the range of 0-1.0 wt.%

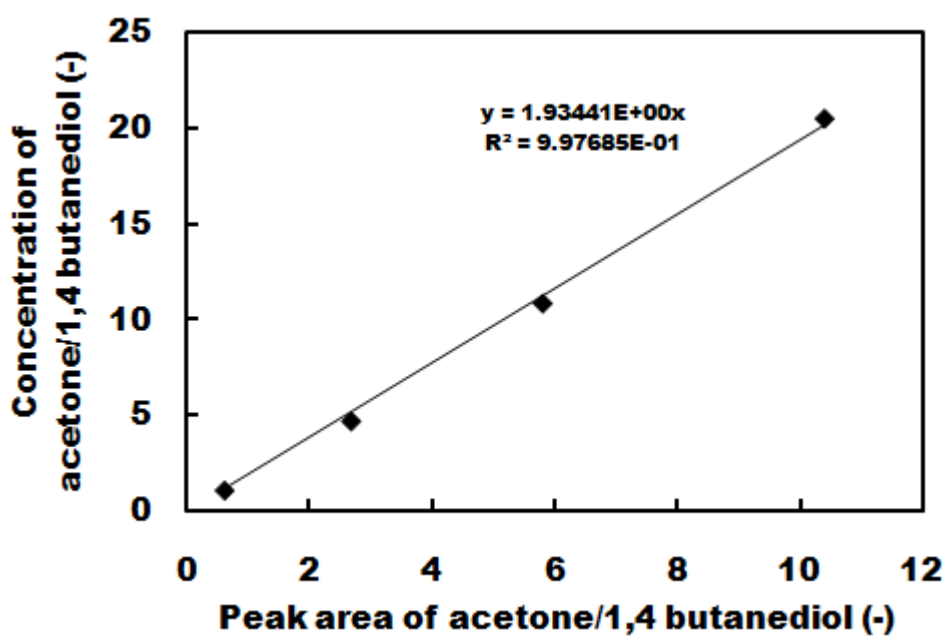


Figure A.13 Acetone calibration curve in the range of 0-1.0 wt.%

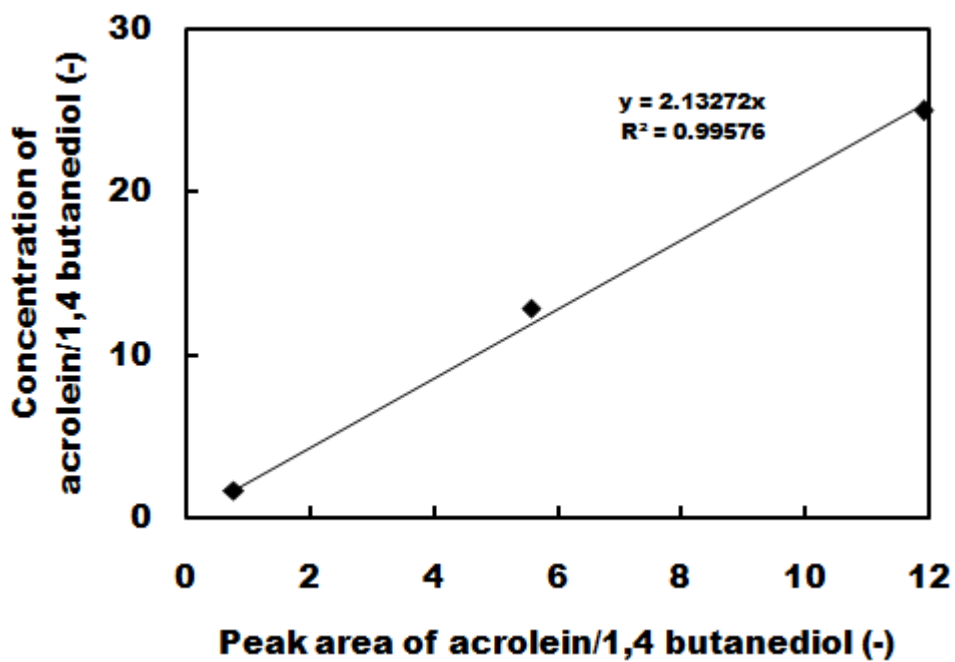


Figure A.14 Acrolein calibration curve in the range of 0-1.1 wt.%

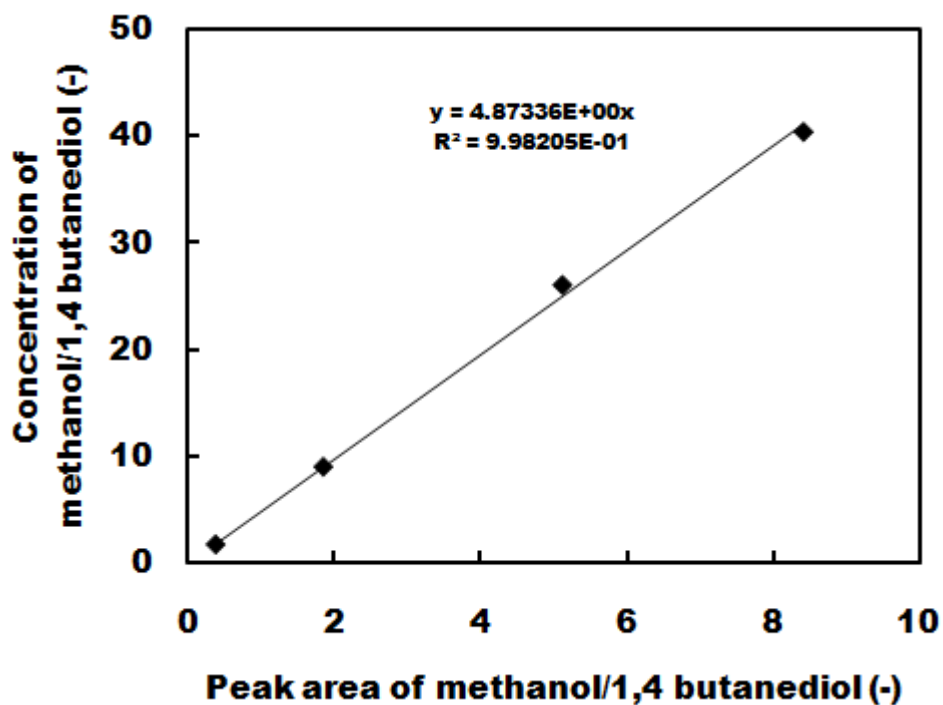


Figure A.15 Methanol calibration curve in the range of 0-1.1 wt.%

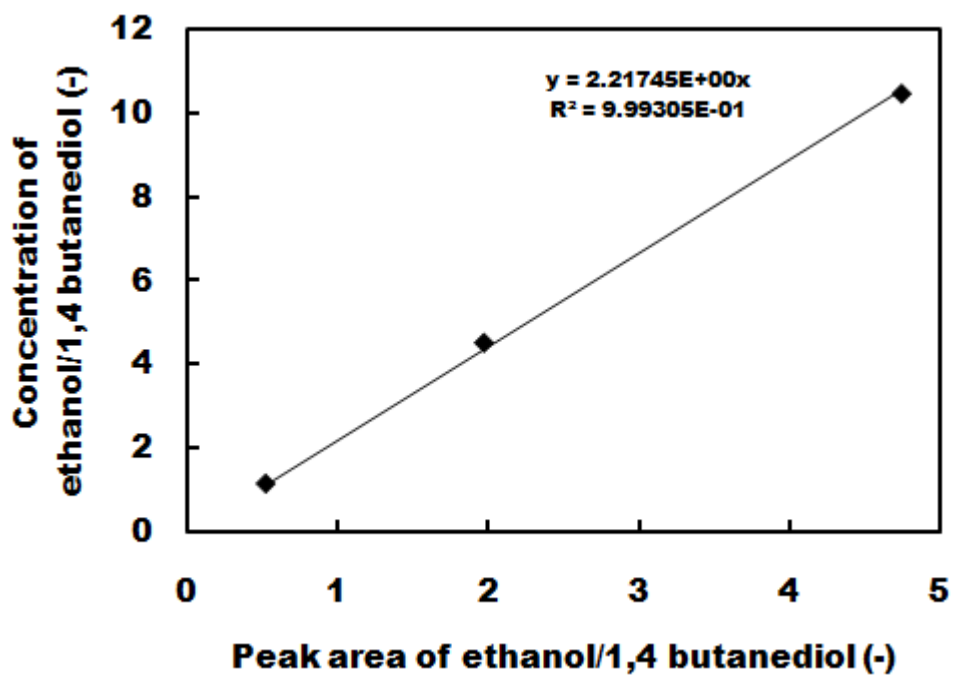


Figure A.16 Ethanol calibration curve in the range of 0-0.5 wt. %

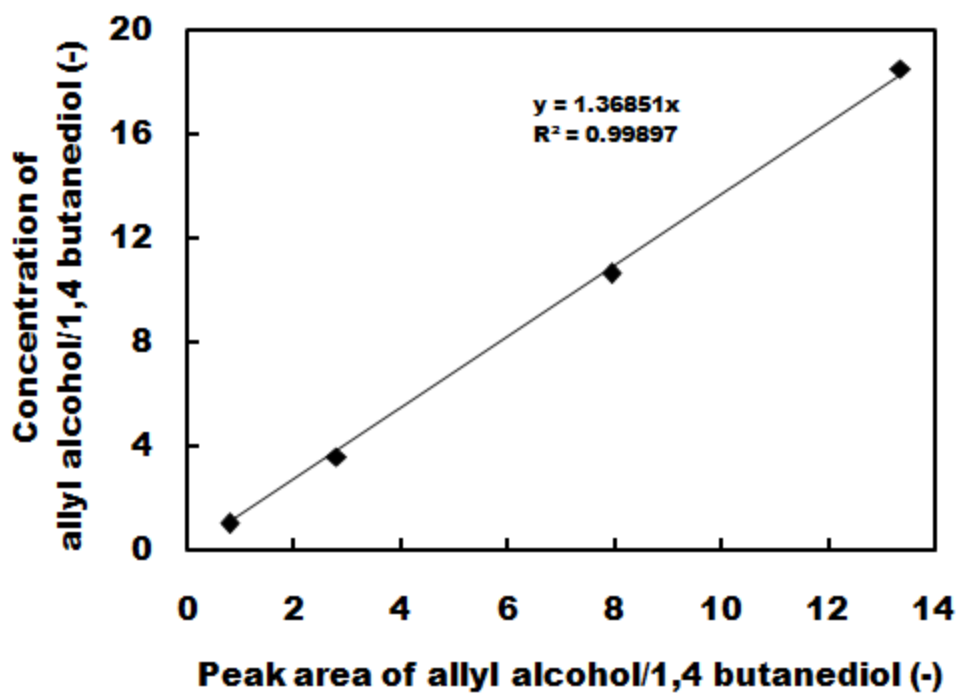


Figure A.17 Allyl alcohol calibration curve in the range of 0-0.9 wt. %

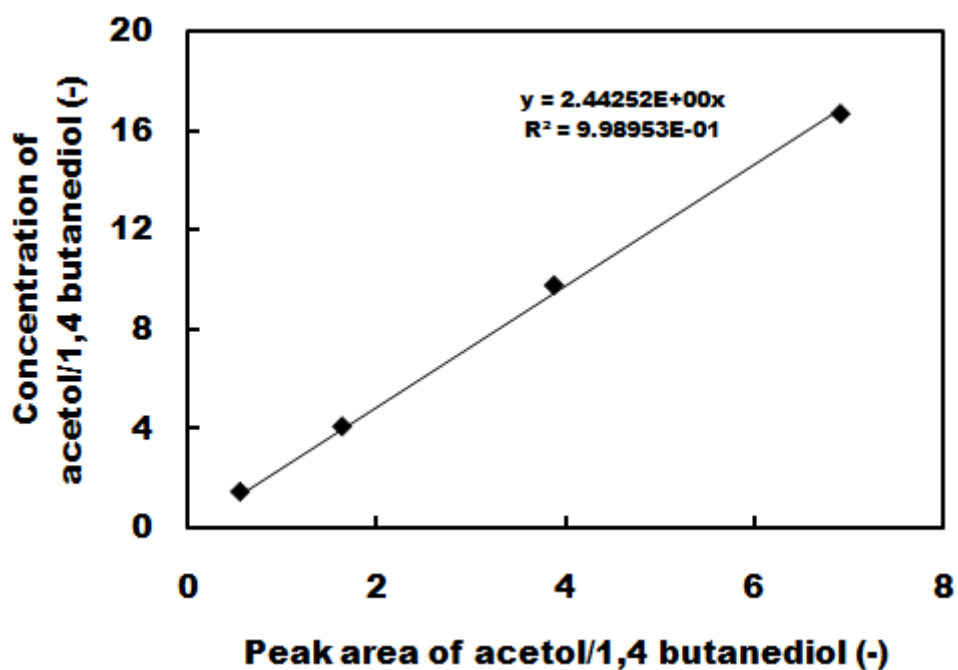


Figure A.18 Acetol calibration curve in the range of 0-1.2 wt.%

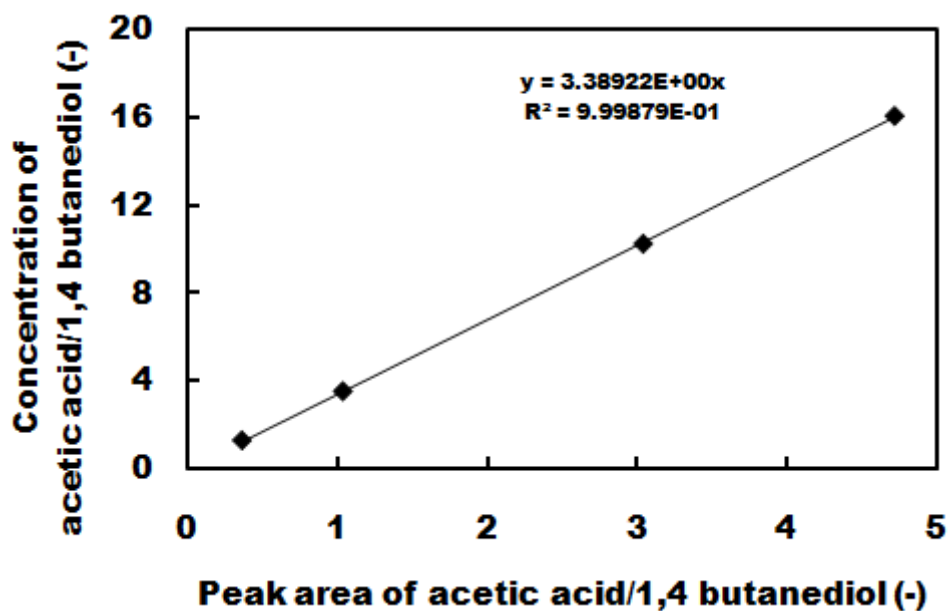


Figure A.19 Acetic acid calibration curve in the range of 0-0.9 wt.%

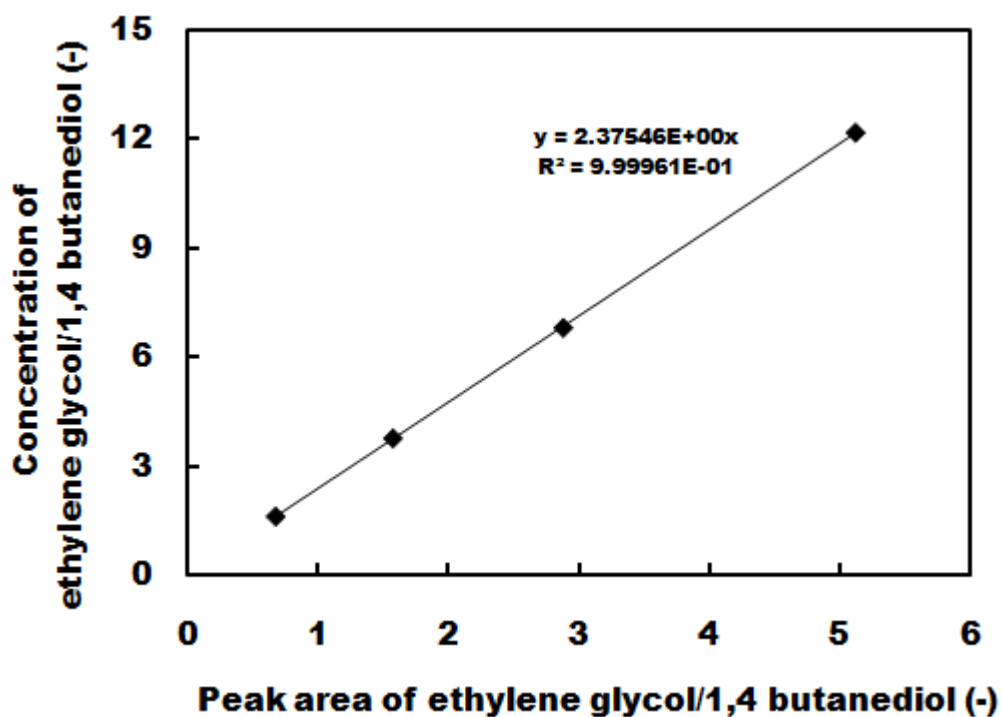


Figure A.20 Ethylene glycol calibration curve in the range of 0-0.8 wt.%

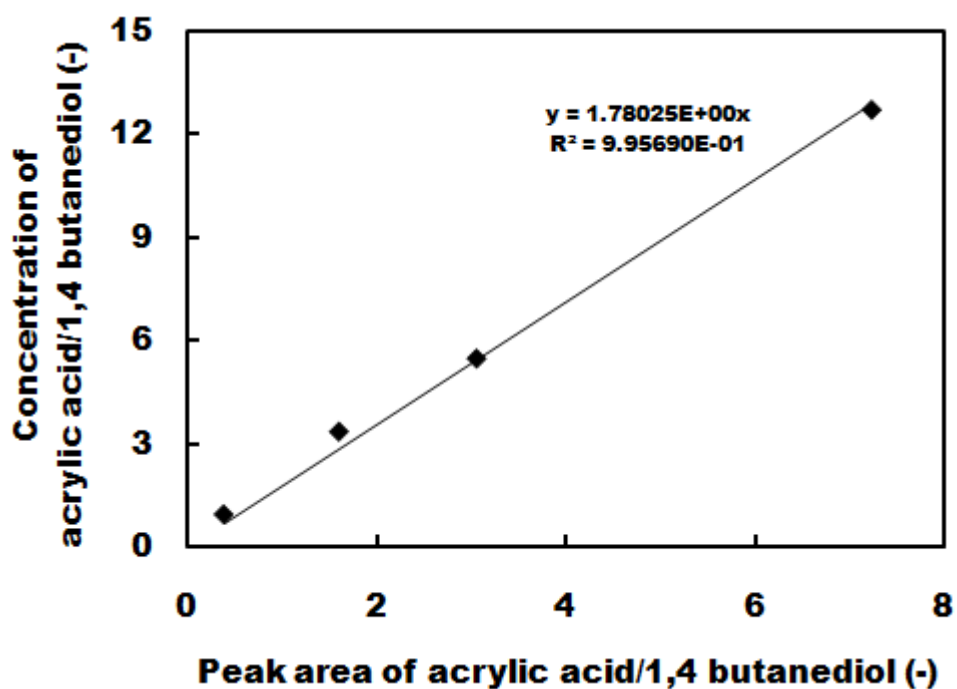


Figure A.21 Acrylic acid calibration curve in the range of 0-0.9 wt.%

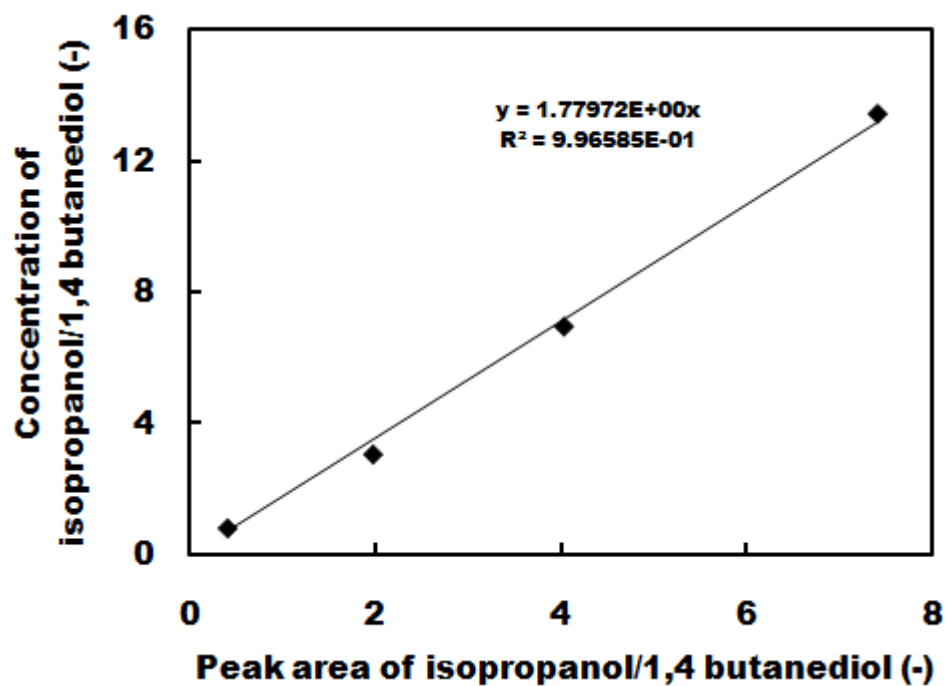


Figure A.22 Isopropanol calibration curve in the range of 0-0.9 wt.%

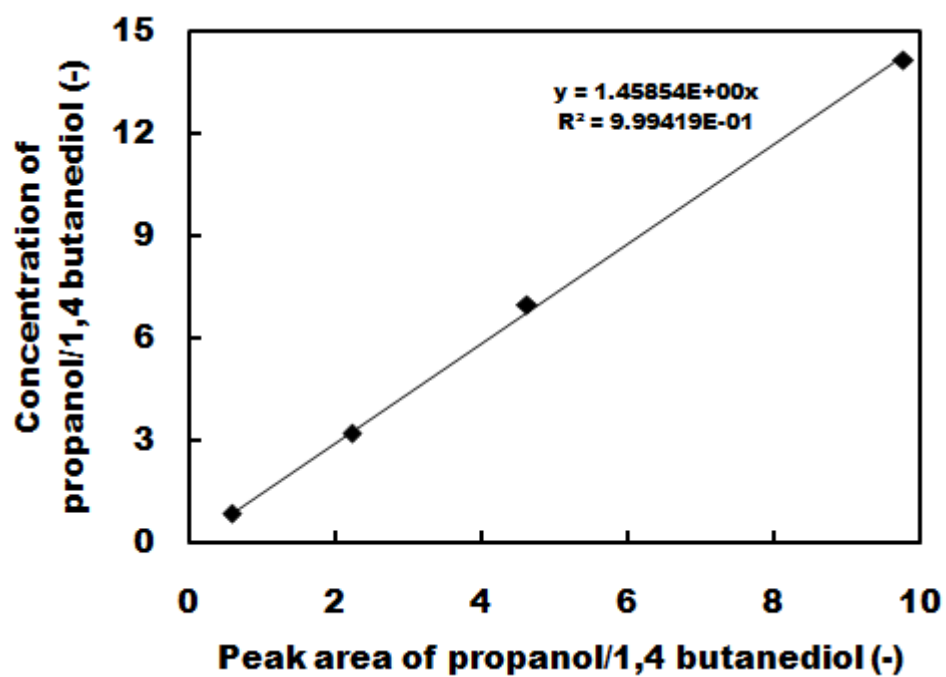


Figure A.23 Propanol calibration curve in the range of 0-0.9 wt.%

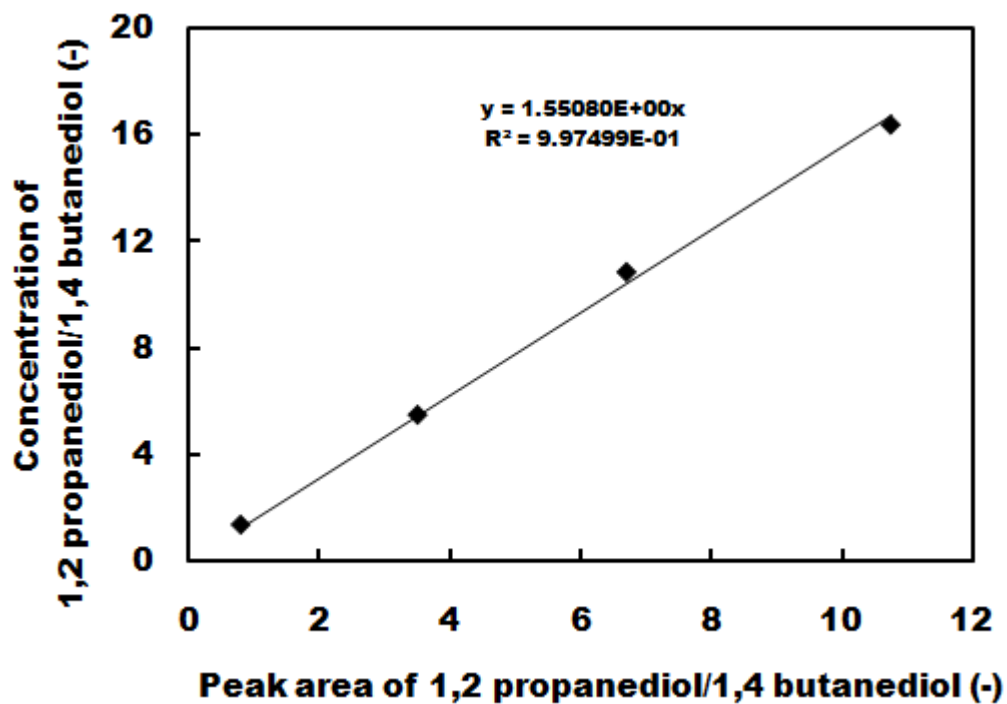


Figure A.24 1,2 propanediol calibration curve in the range of 0-1.0 wt.%

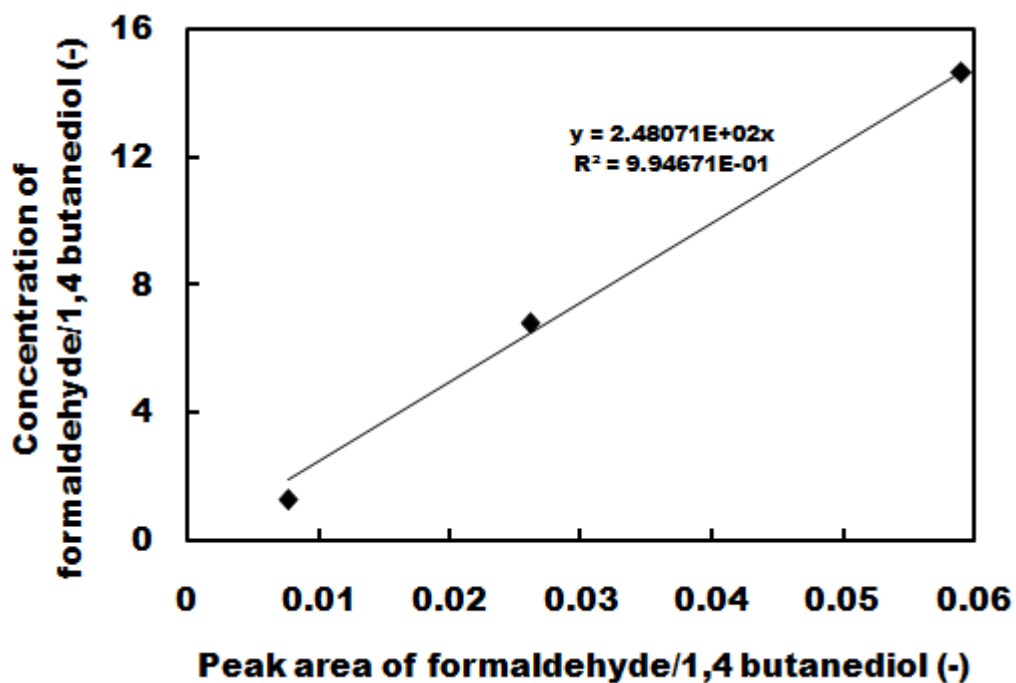
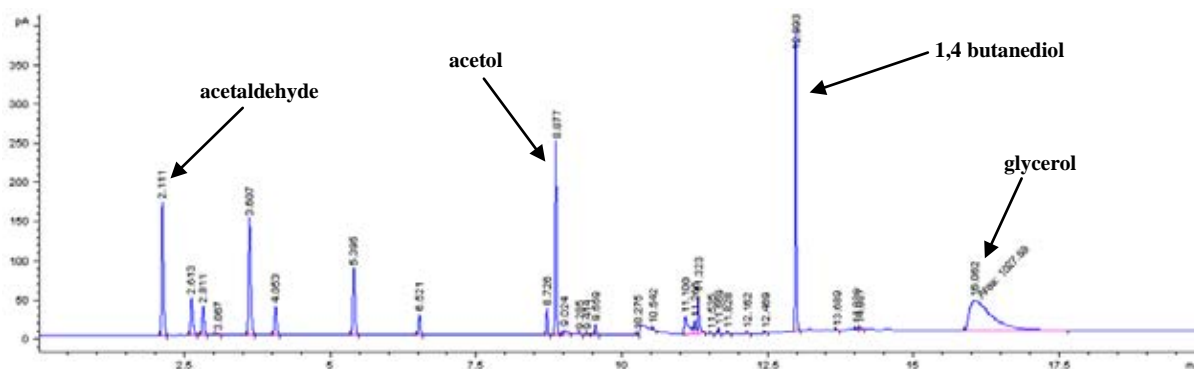
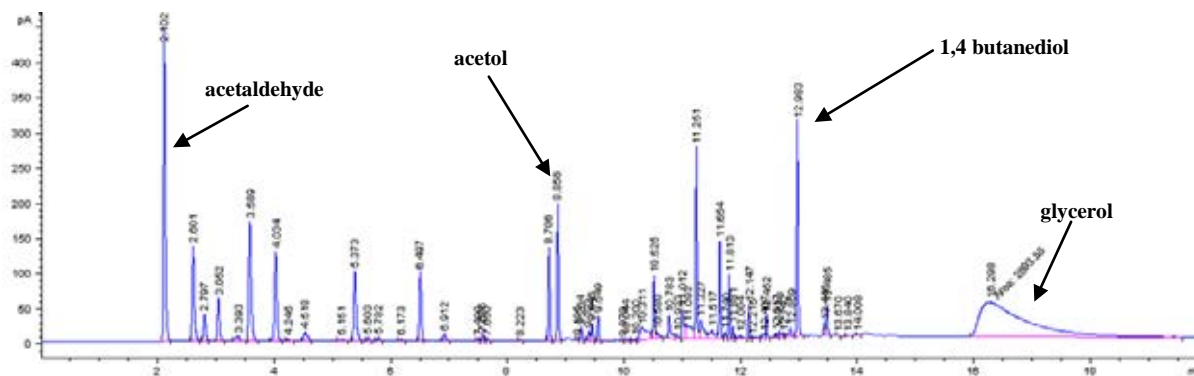


Figure A.25 Formaldehyde calibration curve in the range of 0-0.4 wt.%



**Figure A.26** Diagram of gas chromatographic analysis (FID, DB-WAX column) for empty reactor studying (2.15 g/min,  $T=823$  K (550°C),  $P=25$  MPa)



**Figure A.27** Diagram of gas chromatographic analysis (FID, DB-WAX column) for catalyst studying (10 wt.% Co/ $\alpha$ -Al<sub>2</sub>O<sub>3</sub>, 2.15 g/min,  $T=773$  K (500°C),  $P=25$  MPa)



**Table A.2** Retention time of liquid components in gas chromatographic analysis

<b>Component</b>	<b>Retention time (min)</b>
<b>acetaldehyde</b>	2.107
<b>formaldehyde</b>	2.275
<b>propionaldehyde</b>	2.61
<b>acetone</b>	2.807
<b>acrolein</b>	3.062
<b>methanol</b>	3.604
<b>ethanol</b>	4.03
<b>propanol</b>	5.394
<b>allyl alcohol</b>	6.521
<b>acetol</b>	8.88
<b>acetic acid*</b>	10.084
<b>1,2 propanediol</b>	11.085
<b>ethylene glycol</b>	11.311
<b>acrylic acid*</b>	11.5
<b>1,4 butanediol</b>	12.992
<b>glycerol*</b>	16

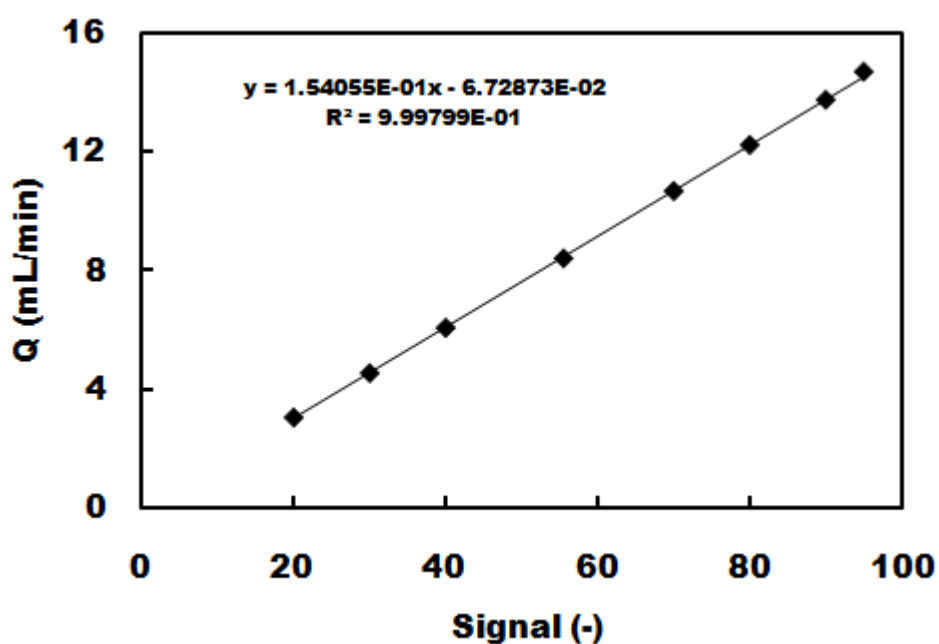
\* Acetic acid, acrylic acid, and glycerol are broad peaks in this analysis.

# APPENDIX B

## MASS FLOW CONTROLLER VS GAS FLOW RATE

### B.1 UFC-1200A (range: 12 SCCM)

This mass flow controller was used for only N<sub>2</sub> gas. The calibration was shown in Figure B.1.



**Figure B.1** Volume metric flow rate of N<sub>2</sub> (3.1-14.5 mL/min) as a function of signal.

### B.2 UFC-1100A (range: 125 SCCM)

This mass flow controller was used for H<sub>2</sub>, CO<sub>2</sub>, CO, and mixed gases. The calibrations were shown in Figures B.2-B.5.

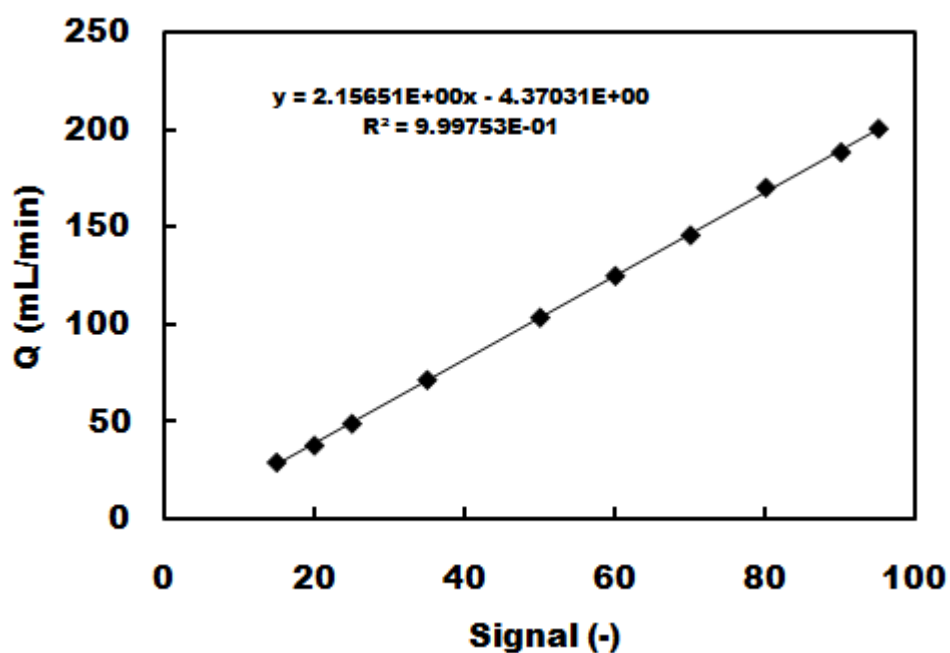


Figure B.2 Volume metric flow rate of H<sub>2</sub> (30-190 mL/min) as a function of signal.

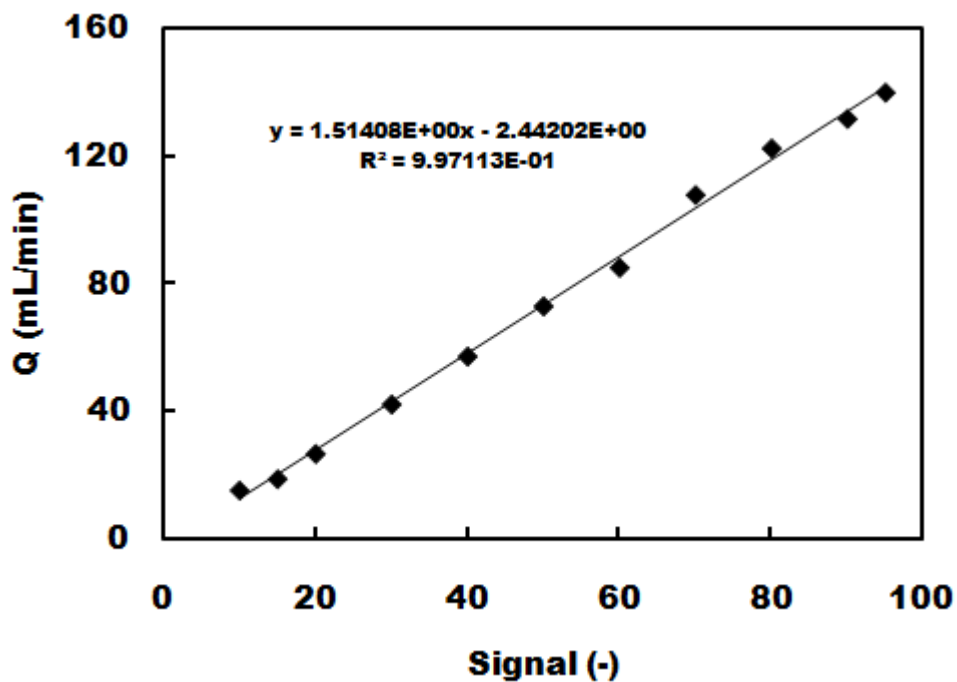


Figure B.3 Volume metric flow rate of CO<sub>2</sub> (15-140 mL/min) as a function of signal.

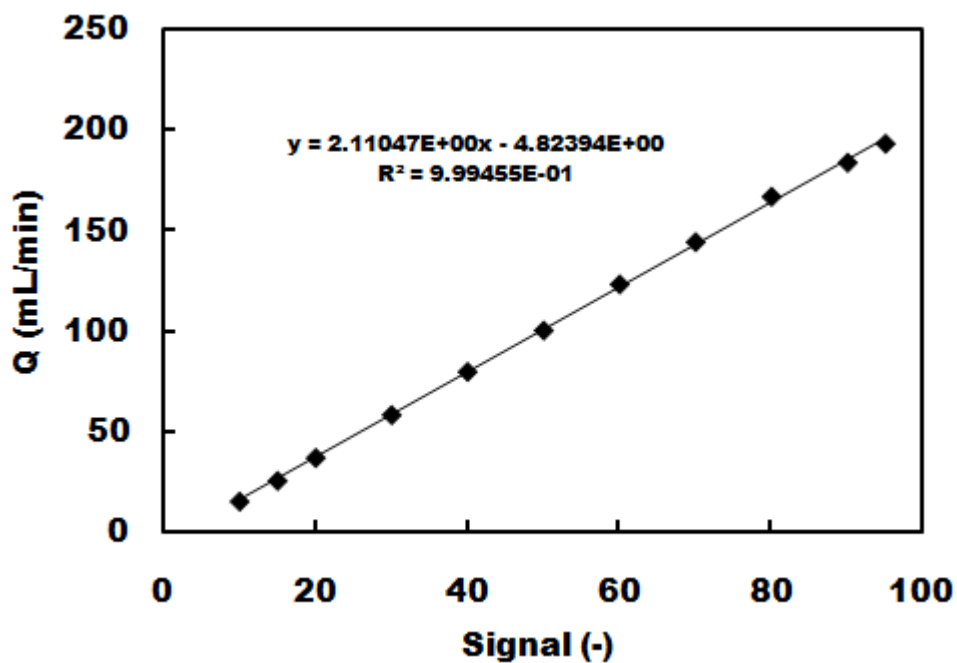


Figure B.4 Volume metric flow rate of CO (15-190 mL/min) as a function of signal.

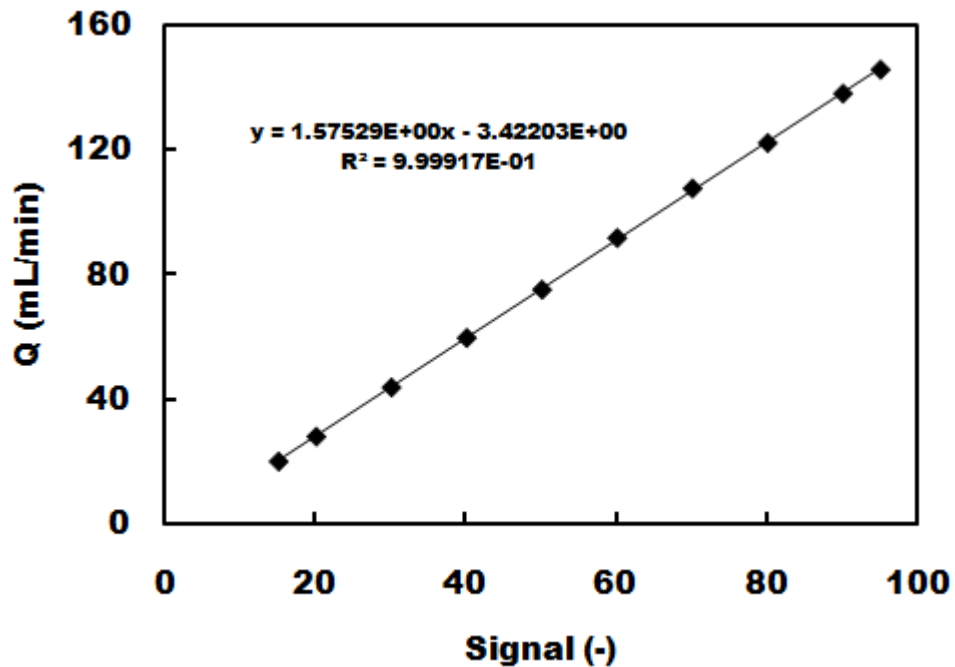


Figure B.5 Volume metric flow rate of mixed gas (30 vol.%  $\text{CO}_2$ , 30 vol.% CO, 25 vol.%  $\text{CH}_4$ , 10 vol.%  $\text{C}_2\text{H}_4$ , and 5 vol.%  $\text{C}_2\text{H}_6$ ) (20-140 mL/min) as a function of signal.

# APPENDIX C

## CALCULATION FOR CATALYST PREPARATION

### C.1 The calculation for the preparation of cobalt based catalyst

For example, 10 wt.% Co/YSZ catalyst by the wetness impregnation method is given as follow:

*Reagent:* Cobalt (II) nitrate hexahydrate ( $\text{Co}(\text{NO}_3)_2 \cdot 6\text{H}_2\text{O}$ )  $\implies$  Molecular weight of 291.03

*Support:* Ytria-stabilized zirconia (YSZ) by a commercial support

*Calculation (based on the support = 15 g):*

$$\text{YSZ} = 15 \text{ g}$$

$$\frac{\text{Co}}{\text{Co} + 15.0000} \times 100 = 10$$

$$\text{Co} = 1.6667 \text{ g}$$

$\therefore$  Cobalt was required 1.6667 g #

Molecular weight of Cobalt = 58.9332

$$\text{Co}(\text{NO}_3)_2 \cdot 6\text{H}_2\text{O} = \frac{1.6667}{58.9332} \times 291.03$$

$$= 8.2305 \text{ g}$$

$\therefore$   $\text{Co}(\text{NO}_3)_2 \cdot 6\text{H}_2\text{O}$  was required 8.2305 g #

## C.2 The calculation for the preparation of nickel based catalyst

For example, 5 wt.% Ni/La<sub>2</sub>O<sub>3</sub> catalyst by the wetness impregnation method is given as follow:

*Reagent:* Nickel (II) nitrate hexahydrate (Ni(NO<sub>3</sub>)<sub>2</sub>.6H<sub>2</sub>O) ==> Molecular weight of 290.79

*Support:* Lanthanum oxide (La<sub>2</sub>O<sub>3</sub>) by a commercial support

*Calculation (based on the support = 15 g):*

$$\text{La}_2\text{O}_3 = 15 \text{ g}$$

$$\frac{\text{Ni}}{\text{Ni} + 15.0000} \times 100 = 5$$

$$\text{Ni} = 0.7895 \text{ g}$$

∴ Nickel was required 0.7895 g #

Molecular weight of Nickel = 58.6934

$$\text{Ni}(\text{NO}_3)_2 \cdot 6\text{H}_2\text{O} = \frac{0.7895}{58.6934} \times 290.79$$

$$= 3.9114 \text{ g}$$

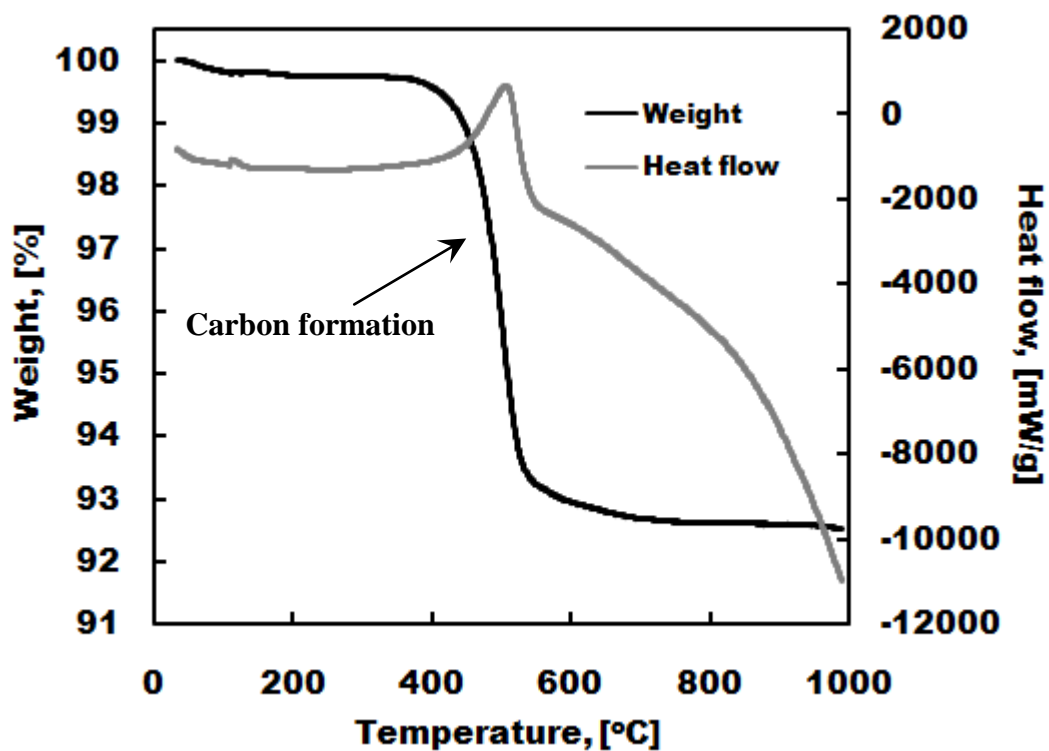
∴ Ni(NO<sub>3</sub>)<sub>2</sub>.6H<sub>2</sub>O was required 3.9114 g #

# APPENDIX D

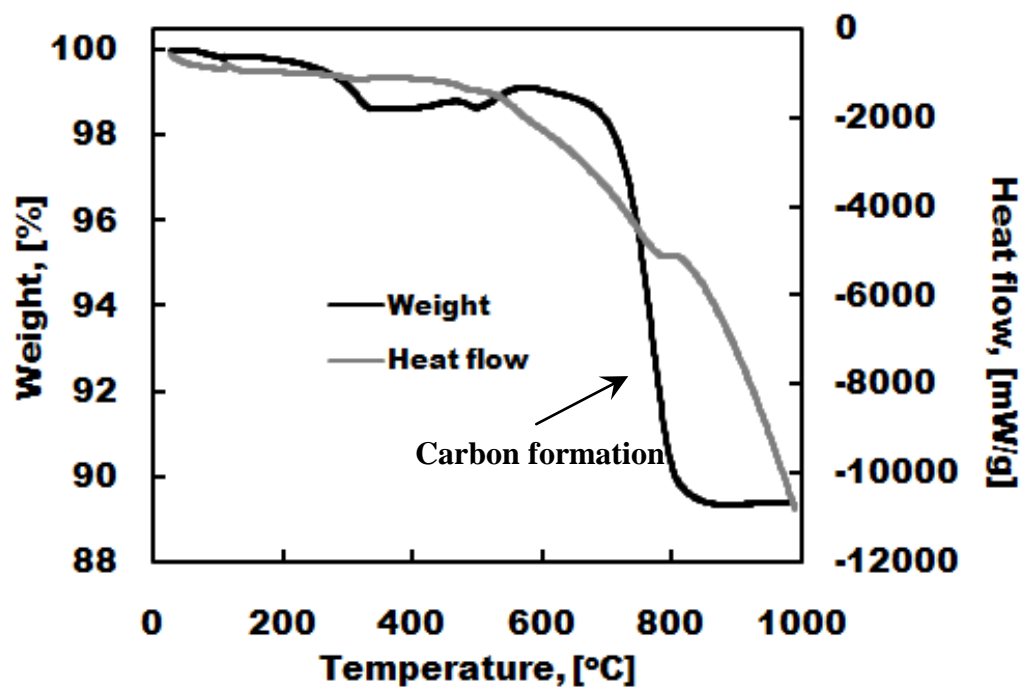
## THERMAL GRAVIMETRIC ANALYSIS

### DATA

For example, spent 10 wt.% Co/ $\gamma$ -Al<sub>2</sub>O<sub>3</sub> catalyst with 2.15 g/min,  $T=748$  K,  $P=25$  MPa, 5 wt.% feed glycerol concentration and spent 10 wt.% Ni/La<sub>2</sub>O<sub>3</sub> catalyst with 1.05 g/min,  $T=798$  K,  $P=25$  MPa, 5 wt.% feed glycerol concentration.



**Figure D.1** TGA curves for spent 10 wt.% Co/ $\gamma$ -Al<sub>2</sub>O<sub>3</sub> catalyst with 2.15 g/min,  $T=748$  K,  $P=25$  MPa, 5 wt.% feed glycerol concentration.



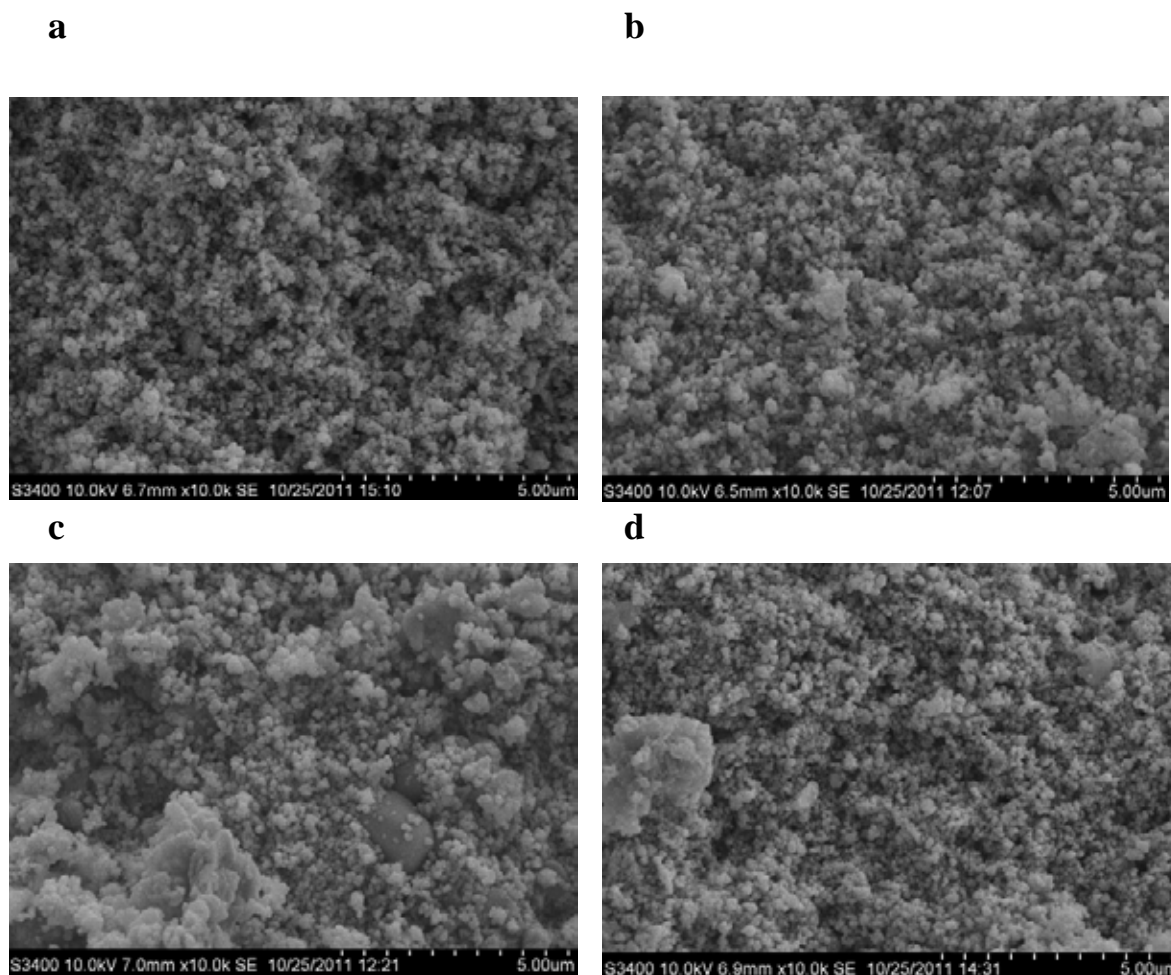
**Figure D.2** TGA curves for spent 10 wt.% Ni/La<sub>2</sub>O<sub>3</sub> catalyst with 1.05 g/min,  $T=798$  K,  $P=25$  MPa, 5 wt.% feed glycerol concentration.



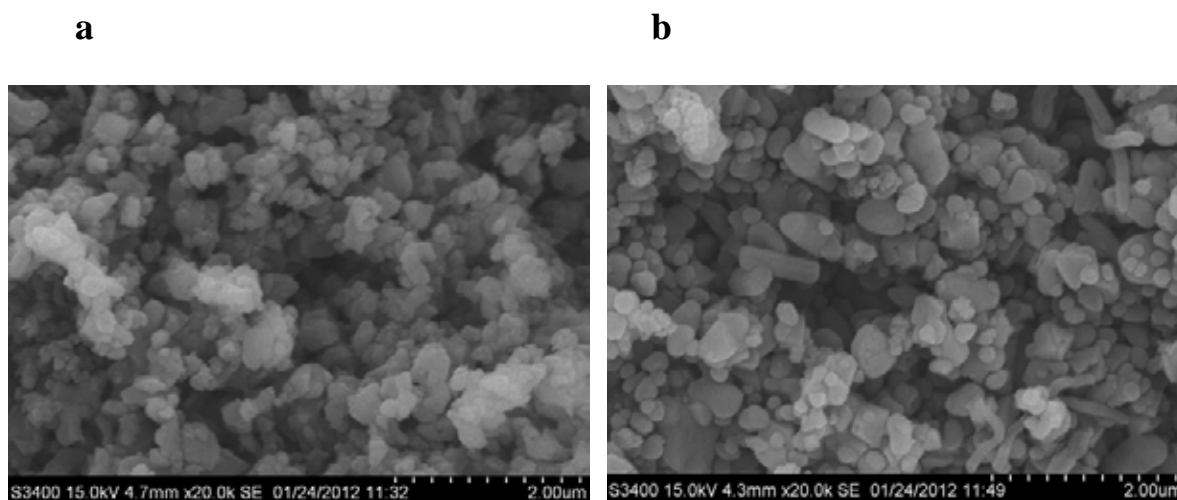
# APPENDIX E

## SCANNING ELECTRON MICROSCOPE DATA

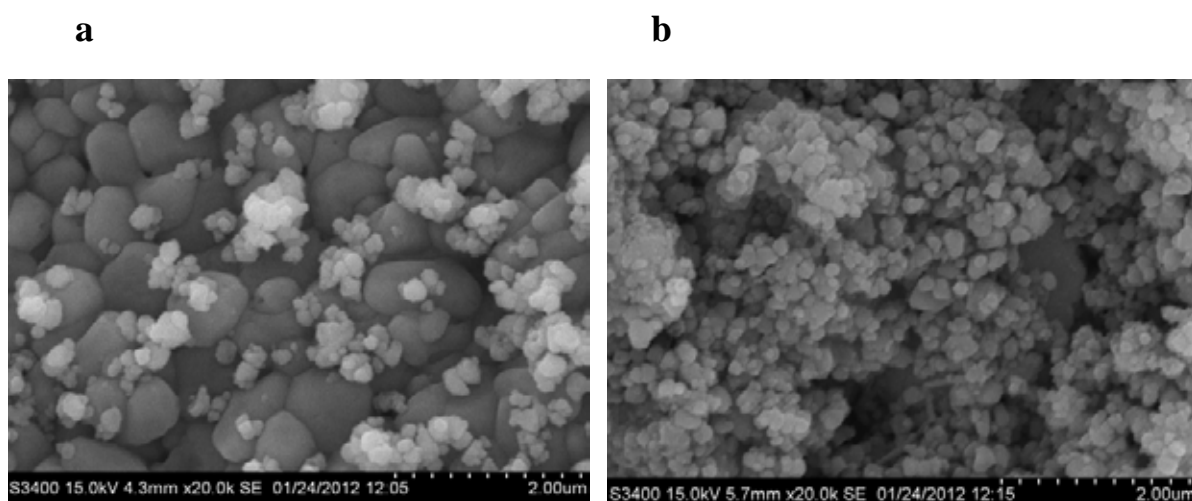
For example, fresh and spent 10 wt.% Co/YSZ catalysts, 10 wt.% Co/ $\alpha$ -Al<sub>2</sub>O<sub>3</sub> catalysts, and 10 wt.% Co/ZrO<sub>2</sub> with 2.15 g/min,  $P=25$  MPa, 5 wt.% feed glycerol concentration.



**Figure E.1** SEM photos for 10 wt.% Co/YSZ catalysts (a) fresh (b) spent at  $T=773$  K (c) 798 K (d) 823 K with 2.15 g/min,  $P=25$  MPa, 5 wt.% feed glycerol concentration.



**Figure E.2** SEM photos for 10 wt.% Co/ $\alpha$ -Al<sub>2</sub>O<sub>3</sub> catalysts (a) fresh (b) spent at  $T=798$  K with 2.15 g/min,  $P=25$  MPa, 5 wt.% feed glycerol concentration.



**Figure E.3** SEM photos for 10 wt.% Co/ZrO<sub>2</sub> catalysts (a) fresh (b) spent at  $T=823$  K with 2.15 g/min,  $P=25$  MPa, 5 wt.% feed glycerol concentration.

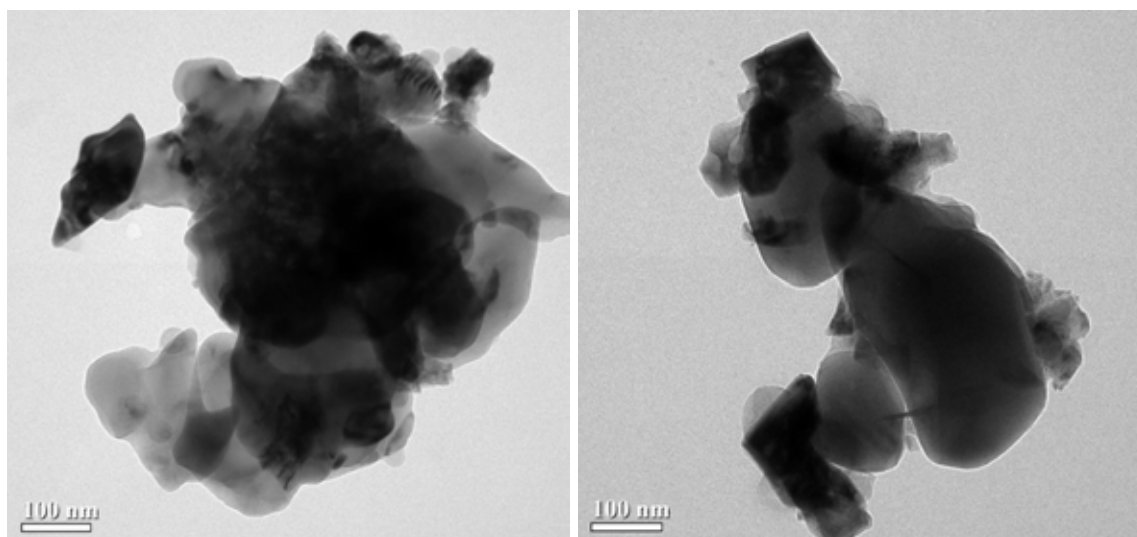
# APPENDIX F

## TRANSMISSION ELECTRON MICROSCOPY DATA

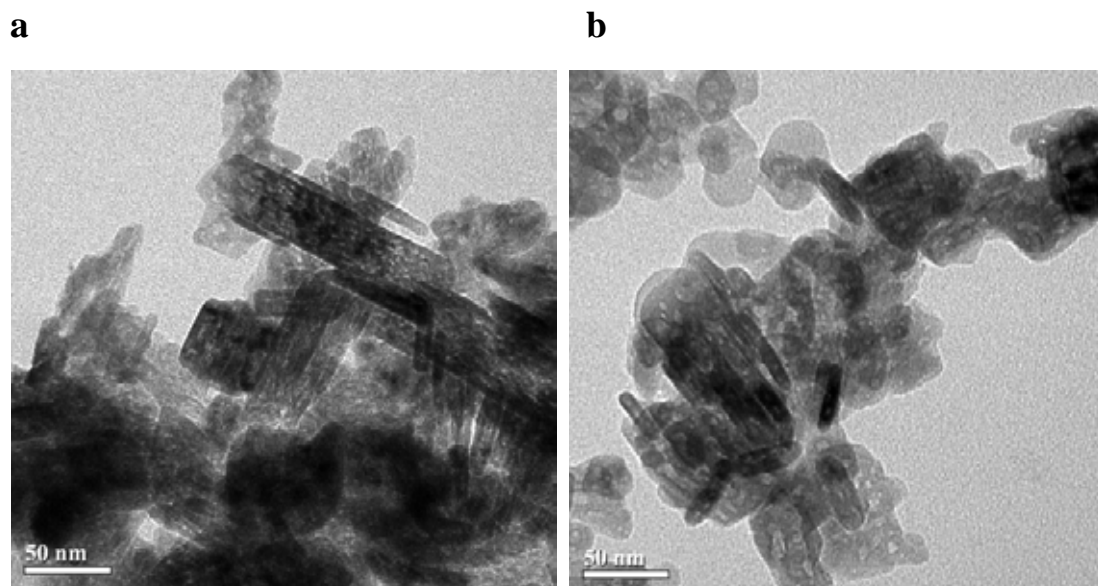
For example, fresh and spent 10 wt.% Co/ $\alpha$ -Al<sub>2</sub>O<sub>3</sub> catalysts, and 10 wt.% Ni/ $\gamma$ -Al<sub>2</sub>O<sub>3</sub> catalysts with 2.15 g/min,  $P=25$  MPa, 5 wt.% feed glycerol concentration.

**a**

**b**



**Figure F.1** TEM photos for 10 wt.% Co/ $\alpha$ -Al<sub>2</sub>O<sub>3</sub> catalysts (a) fresh (b) spent at  $T=798$  K with 2.15 g/min,  $P=25$  MPa, 5 wt.% feed glycerol concentration.



**Figure F.2** TEM photos for 10 wt.% Ni/ $\gamma$ -Al<sub>2</sub>O<sub>3</sub> catalysts (a) fresh (b) spent at  $T=798$  K with 2.15 g/min,  $P=25$  MPa, 5 wt.% feed glycerol concentration.

# APPENDIX G

## SUPERCritical WATER OPERATING PROCEDURE

### G.1 Loading the Reactor

1. Clean the inside of the reactor with a brush. Wash with water and dry it using compressed air.
2. Clean all threads with a brush.
3. Insert the stainless steel small tube. Make sure it is located at the bottom of the reactor (push with a rod – e.g. quartz rod, if necessary). The mesh will sit on top of this support. Note that when running several experiments with catalysts, no need to remove this support (unless very dirty in case of heavy coking).
4. Insert the bottom screen. There are two types of screen; for the bottom, use the one with the higher mesh size (60 mesh). Make sure the screen is flat; if necessary bang it with a hammer to flatten it. When inserting the screen, push with a rod to ensure that it remains flat and that it sits well on the support tube.
5. Load the catalyst (Skip to 6 for empty reactor studying).
6. Insert the top screen (smaller mesh size, 40 mesh). Do not push until the end, leave space between the top of the catalyst bed and the screen in order to be able to remove it at the end of the experiment.
7. Place the first O-ring (smaller one). This O-ring must be covered with high temperature grease (Jet-lube SS-30)
8. Insert the top piece (the longer side is the top).
9. Insert the bigger O-ring. Again, this O-ring must be greased.
10. Grease the thread of the big nut and tight this nut using a torque wrench @ 115 (No need to tight too strongly).
11. Put the ferrule inside the big nut.

12. Grease the small nut and tight it over the big nut by using a torque wrench @ 45.
13. Brush the bottom nut and put the grease on it, and then the top also.
14. Install the reactor assembly, first start on the bottom (Use the piece of wood under the furnace to push up).
15. Tight the bottom nuts and the top nuts (Do not tight too much) by using a smaller wrench 5/8-20 long. When tightening the top nut, hold the pre-heating coil with your thumb to prevent it to touch the wall).
16. Put cotton wool on the bottom nut to plug the hole and make sure the metal does not touch the heating element.
17. Put cotton wool on the top of furnace (for insulation purpose).
18. Currently the furnace temperature always indicates around 30 °C more! (But there is a second thermocouple to double check).

## **G.2 Removing and Opening the reactor**

1. Start to untwist (just make it a little bit move) two nuts at the top of reactor assembly by using a big long torque wrench (Inspection M6 and # 16 end) and an adjusting wrench (Mastercraft 58-8327) and untwist at the bottom of the reactor assembly too. Then, untwist until final round at both sides.  
\*\*\* At the top of reactor assembly: the top nut moves counter-clockwise, the below moves clockwise.
2. Bring cotton wool out from both sides, then push down at the reactor outlet and push up at the Cross until the reactor can be taken out. Be careful!!!
3. Bring a paper to close the hole at the reactor outlet for protecting from small particles and, then clean with a brush at all dirty area.
4. Use Power compress air gun to remove a smaller nut at the top (Untwist!!! Push reverse at the gun, we have to use the connection and a small head) and, then remove a bigger nut too.
5. Blow air to remove the small particles (from the grease).
6. Remove the top part and blow air above the screen.

7. Remove the O-ring and top screen.
8. Pour the catalyst to a small vial, and then remove the bottom screen.

### **G.3 The experiment procedure**

1. Turn on the water bath containing 30% (v/v) ethylene glycol/water and set the temperature at 7°C. Lower temperature is important to condense all vapors. Do not forget to turn on cooling system also.
2. Prepare water in the flask on a balance.
3. Turn on the furnace and set the experimental temperature (Warning: do not exceed 600°C unless adjust lowering the alarms for maximum working pressure). The default alarm (BPR and pump) is 350 bar for reaction temperatures below 600°C. (Test at 450°C)
4. Access the ICM software at the Computer 1 (C:\software\ICM\ICM.exe) and close valve #1. (MV1) (Close valve on the left, open valve on the right and place the flask under the drain near the needle valve).
5. Access the HyperTerminal software (Start/All Programs/Accessories/Communications/Hyperterminal, then open file balance inlet, and Outlet balance). It can be recorded to the Excel (Transfer/Capture text/save name .txt).
6. Set pump 2 (water) flow rate at 2 g/min in ICM software (above critical pressure of water, 221 bar) for the rapid filling of the liquid gas separator in order to remove any residual gas in the separator (Click pump2, type the flow rate at Change flow, and click start pump). We can see the water flow to the flask by adjusting the needle valve. Then open the left valve and close the right valve at MV1.
7. Set the temperature of the pre-heater (HE1) to 200°C.
8. Set temperature (Click TCM1 Panel and set up temperatures at any places. Do not forget to click on; you will see the green light and the furnace temperature is increased to the set point temperature).

9. Set the BPR using the handheld palm, to the experimental value (Warning: do not exceed 300 bar). Start with a lower pressure, by adjusting the BPR's needle. The starting pressure depends on the amount of the total gas products; higher gas products require lower starting pressure. This is an important step to reduce pressure fluctuation. The starting pressure is not necessary the same as the set pressure (Test at 250 bar: Push F2, A, "250", Enter). Some case for example, if we expect high conversion (a lot of gas are produced) pull the needle so that the pressure before glycerol injection is less than 100 bar. Time for only water feeding before glycerol injection should be around 2 hrs in order to clean all dirty in the experiment line. To pull: Using the handheld palm (Press F5, F4, "50", shift F1, "0", Enter, F2, A, "250", Enter), To push: Using the handheld palm (Press F5, shift F1, "50" (or other value), Enter, F4, "0", Enter, F2, A, "250", Enter). You will see the pressure at palm which keeps slightly increasing to the set point. When is near that point, you will hear the needle sound working.

#### **G.4 Shutdown procedure**

1. Set water flow rate of pump 2 equal 0 in ICM software.
2. Set the temperature of the furnace, and pre-heater temperature to 25°C.
3. Decrease the pressure gradually using the BPR until it reaches atmospheric pressure.
4. Open valve 3 slowly (Do not open valve 3 fully at once; by doing that it will damage the heating and cooling system).
5. Drying wet catalyst overnight by flowing nitrogen gas through the reactor.



# APPENDIX H

## LIST OF PUBLICATIONS

### H.1 International publications

1. **Pairojpiriyakul, P.**, Kiatkittipong, W., Wiyaratn, W., Soottitantawat, A., Arpornwichanop, A., Laosiripojana, N., Croiset, E. and Assabumrungrat, S. (2010). Effect of mode of operation on hydrogen production from glycerol at thermal neutral conditions: Thermodynamic analysis, *International Journal of Hydrogen Energy*, 35, 10257-10270. (*Impact factor: 4.053 (2010)*)
2. **Pairojpiriyakul, P.**, Kiatkittipong, W., Soottitantawat, A., Arpornwichanop, A., Laosiripojana, N., Wiyaratn, W., Croiset, E. and Assabumrungrat, S. (2012) Thermodynamic analysis of hydrogen production from glycerol at energy self-sufficient conditions, *The Canadian Journal of Chemical Engineering*, Article in Press. (*Impact factor: 0.707 (2011)*)
3. **Pairojpiriyakul, P.**, Kiatkittipong, W., Assabumrungrat, S. and Croiset, E. (2012). Hydrogen production from supercritical water reforming of glycerol in empty Inconel 625 reactor, Submitted to *International Journal of Hydrogen Energy*.

### H.2 International conferences

1. **Pairojpiriyakul, P.**, Kiatkittipong, W., Arpornwichanop, A., Soottitantawat, A., Wiyaratn, W., Laosiripojana, N., Croiset, E. and Assabumrungrat, S. (2010). Thermodynamic analysis of hydrogen production from glycerol at energy self-sufficiency conditions, The 21<sup>st</sup> International Symposium on Chemical Reaction Engineering, (ISCRE 21), Philadelphia, PA, USA, June 13-16, 2010 (Poster presentation).

2. **Pairojpiriyakul, P.**, Kiatkittipong, W., Assabumrungrat, S. and Croiset, E. (2011). Hydrogen production from non-catalytic supercritical water reforming of glycerol, The 6<sup>th</sup> Asia Pacific Chemical Reaction Engineering Symposium, (APCRE 11), Beijing, China, September 18-21, 2011 (Oral presentation).
3. **Pairojpiriyakul, P.**, Kiatkittipong, W., Assabumrungrat, S. and Croiset, E. (2012). Hydrogen production from catalytic supercritical water reforming of glycerol with cobalt based catalysts, The 22<sup>nd</sup> International Symposium on Chemical Reaction Engineering, (ISCRE 22), Maastricht, The Netherlands, September 2-5, 2012 (Poster presentation).

### **H.3 National conferences**

1. **Pairojpiriyakul, P.**, Kiatkittipong, W., Arpornwichanop, A., Soottitantawat, A., Wiyaratn, W., Laosiripojana, N., Croiset, E. and Assabumrungrat, S. (2009) Steam reforming, partial oxidation and autothermal operation of glycerol, The 19<sup>th</sup> Thai Institute of Chemical Engineering and Applied Chemistry, (TICHE 2009), Kanchanaburi, Thailand, October 26-27, 2009 (Oral presentation).

## VITAE

Mr. Thirasak Pairojpiriyakul was born in Bangkok, on May 24, 1985. He finished high school from Taweethapisek School, Bangkok in 2002. He received his Bachelor's Degree in Chemical Engineering from Kasetsart University in 2006. He subsequently continued studying Doctoral degree of Chemical Engineering, Chulalongkorn University since May 2007 and received Royal Golden Jubilee Scholarship from Thailand Research Fund (TRF). He had collaborated with Professor Eric Croiset and done the experiment parts of his research in University of Waterloo, Canada from January 16, 2010-May 22, 2011.